The Simulation and Experimental Characterisation of the Torque Converter Damper System

Aurora-Smith, Amyce

Award date:
2017

Awarding institution:
University of Bath

The Simulation and Experimental Characterisation of the Torque Converter Damper System

Amyce Aurora-Smith

A thesis submitted for the degree of Doctor of Philosophy

University of Bath

Department of Mechanical Engineering

June 2017

Abstract

In recent years, due to a need to reduce emissions, the automotive industry has focused on increasing vehicle efficiency. One of the areas being examined for potential improvement is the automatic transmission; specifically, the torque converter clutch damper. The better the performance of the damper, the more time the torque converter can be kept in the optimum locked position, thus increasing vehicle efficiency. Currently a large number of vehicle manufacturers use transmission technology sourced from external OEMs; due to a lack of available performance data or validated simulations, sometimes vehicle manufacturers are not able to fully understand the behaviour of the damper. If damper performance (or interactions with other components) cannot be fully assessed during the design development phase, key issues may become known too late in the development process. Thus a deeper understanding of the processes of experimentally characterising and simulating torque converter dampers is required. This thesis describes the development of an arc spring torque converter damper simulation, including the gathering of the experimental data required to validate the simulation. The simulation is used to draw conclusions on the impact of excitation signal form on damper behaviour, leading to new knowledge on the signals required to experimentally characterise a damper.

In this thesis a methodology for (and implementation of) the characterisation of torque converter dampers is detailed. It was found that existing available technologies (e.g. fired engines, electric dynamometers) were either too inflexible or prohibitively expensive; thus a novel high frequency mechanical pulsation generator was developed. This solution was developed from a 4 cylinder motored diesel engine; the cylinders are filled with compressed air and the crankshaft driven using an electric dynamometer. Simulation and experimental data has confirmed that mean torque can be controlled using the input dynamometer, with the compressed air producing fluctuations of up to 900Nm amplitude. However, it was found that the frequency of the output pulsations varied from a fired engine; this is due to reactions between the pulsation generator and the stiffness and inertias of other components on the rig. A review of the performance of the novel pulsation generation concept against other damper excitation methods was also conducted. It was determined that fired engines and electric motors are more suitable for durability testing; the flexibility of the electric motors and the low running costs of the pulsation generator suit damper performance tests.

The second phase of this project was to develop a simulation of a two-stage arc spring turbine damper. This damper consists of three inertias, separated by two spring sets; the outer spring set has 3 individual arc springs, while the inner spring set has 5 nested pairs. The principle of conservation of angular momentum is applied to each of the three inertias in order to calculate their individual accelerations. This method is also applied when calculating the acceleration and movement of the springs; the arc springs are discretised into mass and (massless) spring segments. Two features not previously seen in literature are included in the simulation; hardstops and nested springs. The physical hardstops limit the movement of the spring sets (relative movements of the inertias). In this study, the nested springs were simulated as a pair of parallel springs, rather than as a single stiffer arc spring; this is due to the friction that occurs between the springs (the inner race of the larger spring forms the housing for the inner spring). These two features highlight the need for hardware examination before simulation development; disassembling the hardware also allows the location of hardstops (and other features) to be measured rather than relying on the test data.

Once a damper simulation was designed, a methodology for simulation parameterisation was required; parameterisation is the process of improving simulation performance through iterations of estimated parameters. The simulated damper was excited using sampled experimental data; to maximise parameterisation process efficiency, each time a parameter change was made, a set of key test points were selected in order to assess simulation performance change. It is not recommended that single test points be examined individually; parameter changes may improve simulation performance at one test point but have an adverse reaction at another.

A clear causal relationship between simulation timestep and accuracy (as well as simulation run time) was found; a link between the number of discretised segments and simulation accuracy (and run time) was also confirmed. It was determined that 8 segments was optimal for the inner springs and 18 outer segments offered the best balance between computing power and simulation time. A variety of methods for analysing damper (and simulation) performance are presented in this thesis; it was found that for the 2.5 bar torque curve experimental data set the simulation performs excellently, with on average less than 5% error. Overall torque error is less than 10% across the tested speed range (900 to 2800rpm), with mean torque differences between simulated and tested order magnitudes of less than 5Nm. It has been determined that hysteresis loops are not an accurate predictor of real-world damper performance; while they can approximate general trends, they do not cover the normal operating condition.

In the final phase of this thesis, the validated simulation has been used to investigate excitation signal, areas of poor damper performance and the link between speed and damper stiffness. By subjecting the simulation to a variety of sinusoidal input signals, it was established that if a sinusoidal signal approximates the 3 most dominant frequencies in a real signal, the damper will behave in a representative manner. Additional orders that have lower frequencies than the dominant order will have a greater impact on the attenuation behaviour of the damper; the effect of additional orders on attenuation behaviour is also linked to their magnitude (relative to the dominant order).

A methodology for efficient damper mapping is proposed; the key aim is to produce a dataset that will minimise the length of the parameterisation process while capturing key damper behaviours. It was found that the magnitude of the torque oscillations used to excite the damper is linked to parameter adjustment impact, though this relationship is not linear for all parameters; an approximate level of 300Nm should be used for excitation. Parameters such as spring stiffness and plate inertias are more likely to have a substantial impact on damper performance at frequencies below 70Hz; friction tuning factors are impacted more by magnitude changes at frequencies above 150Hz. It has been demonstrated that while speed can have an effect on magnification ratio, this effect is far less significant at mean torques above the knee point and when sinusoidal input magnitude is kept at or above 300Nm. It was concluded that neither engine speed nor precise excitation magnitude must be replicated in order to predict approximate performance.

During the investigation into areas of poor damper performance, it was confirmed that the trend of increasing magnification ratio with lower frequencies (<30Hz) seen in experimental data continued. Simulation testing above 140Hz revealed that there is not a linear relationship between increased frequency and increased magnification ratio; these areas of magnification ratio spikes are likely due to system resonances. It has been confirmed that while fluctuation magnitude does impact magnification ratio, fluctuation frequency has the most significant (dominant) impact. Finally, the effect of speed on apparent damper stiffness was investigated for both hysteresis loop testing and across a range of outer spring vibration angles; it was confirmed that increasing speed does result in non-homogeneous compression of the springs. It was established that while speed can have an effect on spring stiffness, this effect will vary significantly depending on the movement range (vibration angle) of the spring. The largest increase in spring stiffness with speed is seen when segments of the spring become inactive (cease to move), hence why the effect of speed is more substantial at vibration angle of <10°. The simulation was used to confirm the theories linking speed and stiffness found in the literature; higher speeds increase frictional forces, slowing damper segments, resulting in reduced movement.

The findings of this thesis are relevant to damper simulation and testing engineers; by expanding knowledge of damper behavioural responses to high frequency excitation signals, as well as demonstrating an effective method for producing validated damper simulations, it is hoped that the vehicle design process will be more efficient and damper modifications more effective.

Acknowledgements

Firstly, I would like to express my appreciation and thanks to my advisors Professor Chris Brace and Dr Sam Akehurst; without their support, guidance, and encouragement I would not have been able to start, let alone complete, this thesis project. My thanks also to Dr Chris Bannister, who convinced me a PHD was a good idea, and to Dr Simon Pickering, whose mere presence sometimes fixed my simulation issues.

I must also thank Sean Biggs, Ben Wicksteed, Markus Hose and Michael Leese from Jaguar Land Rover; without the financial support they (and the EPSRC) provided this project would have not have been possible.

My special thanks to the technicians that made this project possible, especially to Bob; the advice and friendly ear provided by the old Scottish git were invaluable.

Thanks also to the wonderful department admins, Cheryl, Marion and Alison, who could make me laugh on even the most rubbish of days and made excellent substitute mothers/sisters. I would have been completely lost without this wonderful team and their practical and emotional help.

I would like to thank my mother, Caroline, for her emotional support and concern about my wellbeing during this (sometimes arduous) process; my thanks also to my step-father Ludovic for making sure my mother didn't annoy me too much!

Finally, my deepest thanks to Mortimer, Dave, Emer and Simon. Without their moral support, laughter and calming influence I would never have made it to the end.

My dearest Simon: I don't know how you managed to stick with me throughout this arduous, rollercoaster process, but I am eternally grateful that you have. Thank you for being an ear to babble at in the early hours of the morning and for reassuring me that it will all work out in the end.

Table of Contents

List of Figures

List of Tables

Nomenclature

2/4/AWD	*Two/Four/All Wheel Drive*
ABB	*ASEA Brown Boveri Ltd*
AC	*Alternating Current*
ATF	*Automatic transmission fluid*
BDC	*Bottom Dead Centre*
CAD	*Computer Aided Design*
CAE	*Computer Aided Engineering*
CAN	*Controller Area Network*
CO_2	*Carbon Dioxide*
CPA	*Centrifugal Pendulum Absorber*
CR	*Compression Ratio*
CVDT	*Circumferential Variable Differential Transformer*
CVT	*Continually Variable Transmission*
DC	*Direct Current*
DMF	*Dual Mass Flywheel*
ECU	*Engine/Electronic Control Unit*
EO	*Engine Order*
FEA	*Finite Element Analysis*
FFT	*Fast Fourier Transform*
GM	*General Motors*
HBM	*Hottinger Baldwin Messtechnik GmbH*
HIL	*Hardware In The Loop*
KLT	*Key life Test*
LDV	*Laser Doppler Vibrometers*
LTD	*Long Travel Dampers*
NVH	*Noise, Vibration and Harshness*
PCM	*Powertrain Control Module*
PID	*Proportional Integral Derivative*
PVRC	*Powertrain and Vehicle Research Centre*
RF	*Radio Frequency*
SI	*Spark Ignition*
SUV	*Sports Utility Vehicle*
SWI	*Southwest Research Institute*
TC	*Torque Converter*
TCC	*Torque Converter Clutch*
TCU	*Transmission Control Unit*
TDC	*Top Dead Centre*
TUM	*Technische Universität München*
WOT	*Wide Open Throttle*

Notation

B	*Internal damping factor*
D	*Cylinder Bore (Diameter)*
F_c	*Centrifugal force*
F_{Red}	*Redirection force*
F_p	*Preload force*
F_S	*Spring load*
G	*Shear modulus of the material*
h	*Piston height*
HS	*Hardstop*
J	*Inertia*
K	*Stiffness*
L	*Connecting Rod Length*
M	*Mass*
nS	*Number of Springs*
n_W	*Number of coils per segment*
P_a	*Ambient Pressure*
P_c	*Compressed air pressure*
P_i	*Indicated (instantaneous) air pressure*
P_{max}	*Maximum pressure*
r	*Crankshaft throw, Stroke*0.5*
R	*Radius*
rad_{PL}	*Radial Preload*
S	*Stroke of Piston*
T	*Torque*
V	*Cylinder Volume*
V_c	*Clearance Volume*
V_{max}	*Maximum Cylinder Volume*
$\dot{x}$	*Linear Speed*
$+ve$	*Positive*
-ve	*Negative*
α	*Friction weighting or tuning factor*
γ	*Ratio of constant-pressure to constant-volume specific heats*
$\gamma_{1\text{-}6}$	*Friction model coefficients*
θ	*Angle (of crank, inertia or segment)*
$\ddot{\theta}$	*Acceleration (inertia, mass or segment)*
μ	*Coefficient of Friction*
σ	*Spring-Inertia/Hardstop contact trigger*
φ	*Length of segment, spring, stopper or hardstop arc*

Subscripts

Fric	*Friction*
HS	*Hardstop*
I	*Inner*
In	*Input*
N	*Signifies the N^{th} segment*
O	*Outer*
Out	*Output*
P, pri	*Primary*
PS	*Primary stopper*
rel	*Relative*
res	*Resultant*
s	*Spring*
S, sec	*Secondary*
seg	*Segment*
sm	*Spring Mass*
SS	*Secondary stopper*
T, ter	*Tertiary*
Tot	*Total*
$X_{1,2}$	*Hardstop contact points*

Chapter 1 Introduction

1.1 Key motivations

Decreasing access to fossil fuels (through shortages and price fluctuations), in combination with new legislation to reduce the impact of vehicle emissions on the environment, has resulted in the automotive industry placing greater emphasis on emission reduction and fuel economy. This is primarily achieved by increasing the efficiency of all areas of the vehicle powertrain, including the transmission.

In automatic transmissions, one of the components being examined in this efficiency drive is the torque converter. The torque converter takes the place of a manual clutch in an automatic drivetrain. It is at its most efficient when the two halves of the torque converter are spinning at the same speed; maximum efficiency is achieved by locking-up the torque converter with a clutch. However, in this locked position, providing maximum power transfer, the torque converter also transfers a substantial amount of vibration from the engine to the driveline (and to the rest of the vehicle). This can result in a number of undesired NVH issues in the vehicle, from noise to reduced comfort. These NVH issues can be especially noticeable when using downsized engines (a common modern method of reducing environmental impact).

One of the methods used to attenuate powertrain oscillations is torque converter clutch slip. While slip does help damp disturbances between the transmission and the engine, its usage is limited, due to the friction related instabilities (e.g. shudder) it can introduce. Torque converter clutch driveability issues are also more likely to occur when engaging the TCC at higher speeds. To avoid these issues, and increase the time spent at maximum efficiency, the lock-up clutch system should be engaged as low down in the engine speed range as possible. To allow this to occur, and to reduce the reliance on clutch slip for vibration attenuation, the lock up clutch system is equipped with an isolator system – a torque converter clutch damper. The better the performance of the damper, the more time can be spent with the torque converter in the optimum locked position, increasing vehicle efficiency.

Currently a large number of vehicle manufacturers use transmission technology sourced from external partners; understandably, to protect intellectual property, the information shared between vehicle manufacturers and OEMs (Original Equipment Manufacturers) can be limited. This can result in vehicle manufacturers not fully understanding the behaviour of the components, due to the lack of validated simulations or performance data. Without accurate simulations, engineers are unable to fully assess the performance of a damper with other powertrain components (e.g. engines) during the design development phase, potentially resulting in key issues only becoming known late in the development process (i.e. during prototype testing). While the performance of the damper when paired with an existing engine can be assessed experimentally, this method of damper characterisation can be a long process, requiring substantial rig time.

Thus if an original, efficient, methodology for damper characterisation can be developed – ideally without requiring the use of a fired engine – the efficiency of the vehicle design process can be improved (reducing costs). The ability to accurately characterise an OEM's damper, in combination with a methodology for simulating a common damper type, will also allow manufacturers to test potential modifications to improve damper – and therefore vehicle – performance.

1.2 Aims and Objectives

The primary aim of this thesis is to produce a validated simulation of a torque converter clutch damper system. Part of this aim requires the damper to be experimentally characterised; this requires the development of a novel method for exciting a damper with a high frequency signal. The simulation of the torque converter damper system will be an original contribution to knowledge; very little published work is available on this subject.

A validated system simulation will also allow investigations into the effect of excitation signals on damper behaviour to take place. This is another area of original contribution; if knowledge on damper behaviour is improved, experimental excitation procedures can be made more efficient.

In order to achieve this primary aim, a set of more specific objectives has been defined:

1. Review current torque converter damper technology and literature relating to damper testing and simulation, including high frequency pulsation generation technology.
2. Develop a methodology for, and implement, an experimental programme to produce a results set that can be used to characterise and validate a damper simulation.
3. Develop a prototype pulsation generator concept for damper excitation.
4. Develop a simulation of a two-stage arc spring torque converter damper.
5. Characterise the torque converter damper through simulation parameterisation and experimental validation.
6. Use the validated simulation to establish excitation signal requirements and investigate some aspects of damper behaviour.

1.3 Summary of Chapters

A summary of the core chapters contained in this thesis can be found below.

In Chapter 2, a review of torque converter damper technology and the methods used to test and simulate dampers is carried out. Due to a lack of available literature on torque converter damper procedures, this review has been expanded to include testing and simulation methodologies for Dual Mass Flywheels (DMFs) and other driveline components.

In Chapter 3 the available testing facilities are described, as well as the procedures required to setup the transmission; experimental and analytical methodologies are also established.

In Chapter 4, a design for a novel pulsation generator concept (for use with the existing PVRC electric dynamometers) is proposed and the development of a prototype presented. The testing and simulation process for the prototype is detailed; the experimental results are used to validate the simulation and confirm the theory behind the concept. The magnitude, shape and frequency of the fluctuations produced by the concept are also assessed and the concept reviewed against existing technologies.

In Chapter 5, a detailed examination of the torque converter damper hardware is performed and the methods used to simulate the selected damper system are presented. By disassembling the damper system the accuracy of the simulation is ensured; new simulation methodologies for some components found during hardware examination are also proposed.

In Chapter 6, a methodology for simulation parameterisation is developed; the performance of the damper system is also examined, and the experimental data used to parameterise and validate the simulation. Key areas of both excellent and poor damper performance are also identified.

In Chapter 7, the validated simulation is used to investigate the impact of excitation signals on damper behaviour, as well as examine in more detail some observed damper behaviours. The investigation into the impact of the input signal on damper behaviour is divided into three parts; required accuracy of a sinusoidal approximation, quantifying sufficient excitement and optimum excitation for efficient performance mapping. The detailed simulation is used to further investigate the areas of poor damper performance highlighted in Chapter 6, as well as the link between speed and damper stiffness.

Chapter 2 Torque Converter Damper Overview

In this chapter, the torque converter damper technology being studied will be introduced in addition to an examination of the methods that have been used to test and simulate powertrain dampers. Due to the limited amount of literature available on the subject of torque converter dampers, the review has been expanded to investigate any relevant powertrain torsional damper that employs similar technology/designs such as Dual Mass Flywheels (DMFs). This will ensure a comprehensive understanding of the technology is achieved. As part of this review, the technology that has been used to improve the capability of electric dynamometer rigs to produce high frequency fluctuations is also examined. As outlined in the objectives (section 1.2), this project required a novel pulsation generator concept to be developed (see Chapter 4); a review of engine simulation methodologies that could potentially be adapted for use with this concept is also presented.

2.1 Torque converter technology

In the following sections the purposes behind a torque converter and its lock up clutch are discussed, along with the reasons why a torsional damper is included in the system; the range of torque converter damper designs available (from coil spring to pendulum) are also introduced.

2.1.1 Basic purpose and function

Torque converters are used in automatic transmissions (see Figure 2.1) to perform the purpose of the clutch in a manual transmission vehicle. Without this device, the vehicle would be unable to start or stop without preventing the engine from turning over. A torque converter is a form of fluid coupling that transmits torque while allowing the engine to spin almost independently of the transmission.

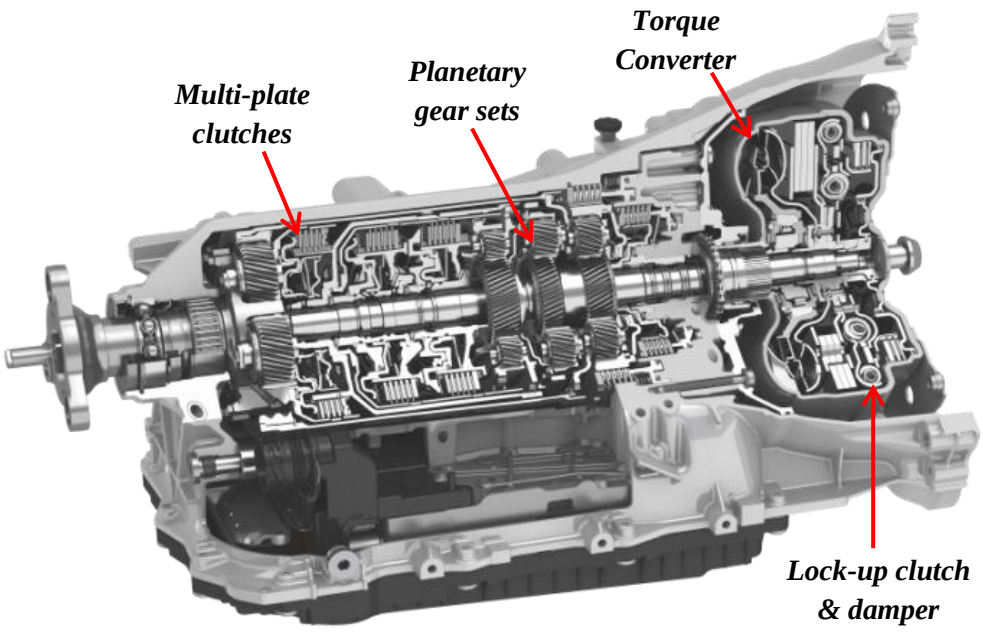

Figure 2.1: Automatic transmission with torque converter [1]

A basic torque converter consists of four components: the pump (also known as an impeller), the turbine, the stator and the transmission fluid. The impeller forms part of the torque converter housing and is attached to the engine via the flywheel, meaning it rotates at the same speed as the engine [2]. The turbine is attached to the planetary gear train (see Figure 2.2) [3]. As the pump spins, the transmission fluid moves to the outside due to centrifugal forces which draws more fluid in at the centre. The fluid leaves the pump and enters the turbine (which is rotating at a lower speed) and is forced to change direction by the curved blades before exiting the centre of the turbine. These changes in angular momentum impose a torque upon the turbine, causing it and therefore the transmission to spin. Thus the pump and the turbine act as opposing centrifugal pumps. The oil flows from the pump to the turbine because the pumping action of the pump is greater; it is directly attached to the engine and therefore usually rotating at a higher speed [3] [4].

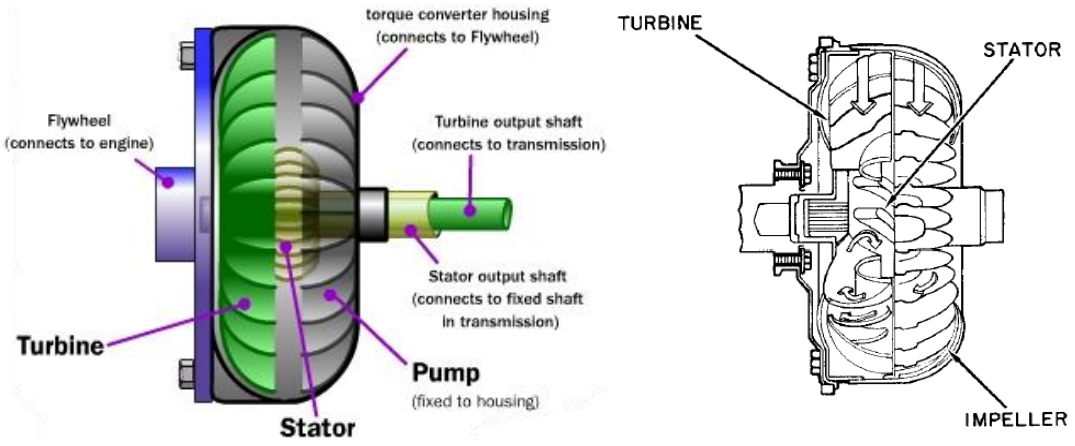

Figure 2.2: Torque converter schematics [2] [3]

The stator redirects the fluid exiting the centre of the turbine before it returns to the pump; this helps to increase the efficiency of the torque converter by preventing the returning fluid hitting the pump in the wrong direction and reducing its angular momentum. The stator is connected to a fixed transmission shaft via a one way clutch, allowing it to spin in only one direction (the opposite direction to the exiting fluid) [2] [4]. If the stator is stationary when it re-directs the oil flow the oil will be rotating in the same direction as the pump; this means that the angular momentum gain required will be lower, resulting in the torque of the turbine being higher than that of the pump – torque gain [4]. If the rotational speed of the turbine is greater than that of the pump the turbine ends up driving the pump, with both sides having equal torques; this is commonly referred to as engine braking or coasting [3].

At around 40mph (64kph) [2] the pump and turbine spin at approximately the same speed, though as mentioned above the pump will usually spin at a slightly higher speed. At this point the fluid exiting the turbine is already moving in the same direction as the pump, though its speed is reduced by the redirection process. When this occurs, the fluid strikes the back of the stator blades resulting in the stator free-wheeling (being over-run) on its one-way clutch. This results in no angular momentum being transferred to the oil, thus the turbine and pump torques are equal [3]. This is the main operating point at which the torque converter clutch (see section 2.1.2) is applied and the torque converter locked to increase efficiency.

2.1.2 Torque converter clutch (TCC)

As discussed in section 2.1.1, at higher vehicle speeds the transmission spins at almost the same rate as the engine; ideally at these speeds the engine and the transmission would move at exactly the same rate to increase efficiency. To achieve this, many torque converters have an additional component assembly – a lock-up clutch. The lock-up clutch is located on the engine (turbine) side of the converter but is connected to the engine and pump via the housing (see Figure 2.3). The oil needed to pressurise (engage) the wet clutch is diverted to it via small cavities in the transmission input shaft [5]. One advantage of the torque converter is that it multiplies torque during pull-away. A converter equipped with a lock-up clutch also has the advantage of having the increased efficiency of a clutch at higher speeds.

When engaged, the lock-up clutch effectively bypasses the hydrodynamic circuit [6]; this eliminates any rotational speed differences and therefore increases torque transfer efficiency. The process by which the lock-up clutch achieves this can be referred to as locking or forcing the two halves (turbine and pump) of the torque converter together; the latter is actually a slight misnomer as it implies that the clutch physically moves one or both of the halves. A more accurate description is that when the lock up clutch is engaged, power is transferred directly from the engine to the lock-up clutch via the torque converter housing; this power is then transferred to the transmission input through the torque converter clutch damper (see Figure 2.3).

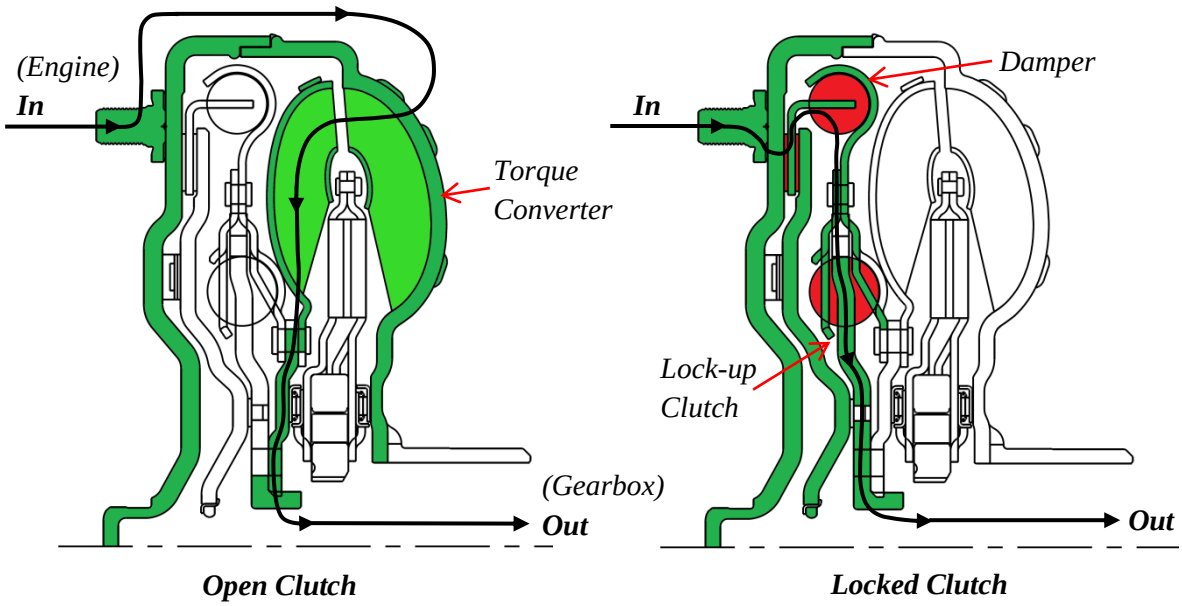

Figure 2.3: Power flow through Open and Locked torque converter (adapted from [7])

Lock-up clutches have three distinct operating modes: open, fully locked and controlled slip [8] [9] (see Figure 2.4). In order to fully lock the torque converter clutch (TCC), a high enough pressure has to be applied to the clutch plate to ensure there is no slip. As the pressure is applied to the clutch the engine speed changes to match the speed of the torque converter turbine, until all the engine torque can be carried and transferred with minimal losses to the transmission by the TCC [6].

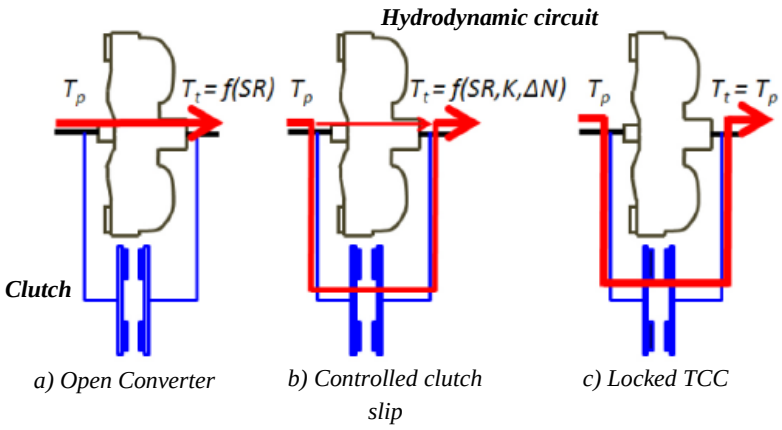

Figure 2.4: Torque flow through a torque converter in the three TCC operating modes [6]

By transmitting a small amount of the engine torque through the hydrodynamic circuit, via controlled clutch slip, additional driveline damping can occur. This additional damping can help reduce torsional vibrations when the powertrain or driveline is operating near a resonance that the converter clutch damper may not adequately attenuate. By using clutch slip to further reduce the torsional vibrations to acceptable levels the lock-up clutch can be engaged more frequently (referred to as a more aggressive TCC schedule), therefore helping to increase the efficiency of the torque converter even further [6]. As mentioned, controlled TCC slip is usually introduced when damper hardware modifications cannot produce adequate isolation. While it can improve driveline torsional isolation, it can sometimes have a negative effect on driveline behaviour; a friction induced vibration called judder can be produced, along with shudder (a vehicle vibration) [10] [11]. As shudder emanates throughout a vehicle, it can cause comfort issues [12]; automatic transmission fluid improvements and friction surface changes have previously been used to combat judder (and shudder) [13] [14].

During controlled slip mode torque transfer takes place through both the clutch and the hydrodynamic circuit. Due to its increased vibration attenuation ability (which allows the damper to be locked more often) this mode is utilised at low slip ratios in order to find an agreeable trade-off between the driveability of an open converter and the fuel efficiency of a locked system [9]. TCC slip control can be quite complicated and difficult to calibrate due to the non-linearity of the behaviour of the hydrodynamic circuit [15].

While TCCs can help increase power transfer efficiency they can usually only be used at higher engine speeds (dependent on engine excitation and vehicle sensitivity) to prevent the previously mentioned driveability issues such as driveline or body boom and gear rattle (see Figure 2.5) [5]. Body boom occurs when the vehicle structure exhibits a low frequency response to the torsional vibrations transmitted from the engine or driveline, often producing an audible sound [16]. Gear rattle occurs when the free play between the teeth of idle gears allows the gears to be excited by the torsional vibrations and knock against each other [17].

While slip does help damp disturbances between the transmission and the engine the use of TCC slip is limited; the clutch surface can introduce friction related instabilities (such as shudder [18] and stick-slip [19] vibration) due to the relationship between the coefficient of friction of the clutch plate material and slip speed [20].

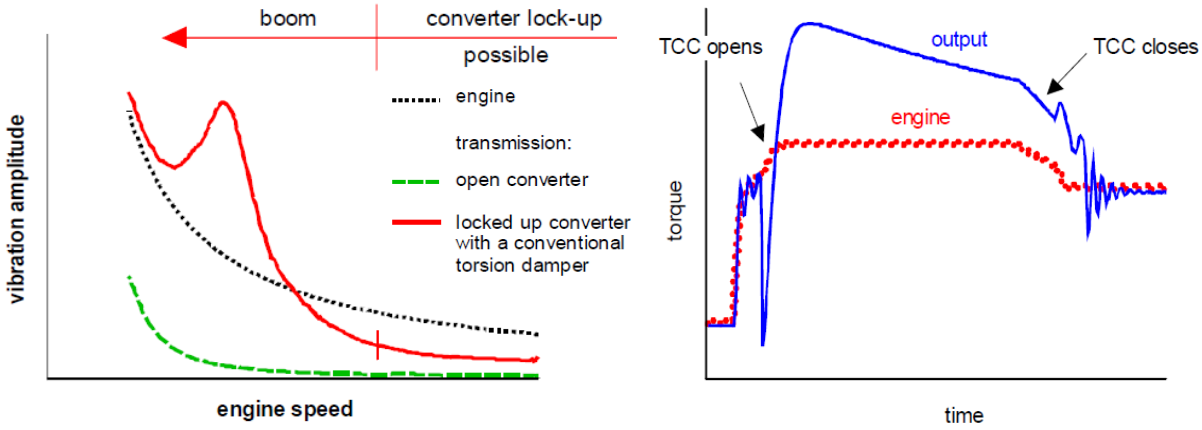

Figure 2.5: Driveability issues caused by clutch slip - Left: Torsional Vibrations in the engine and transmission, Right: Tip-in/back-out cycle with a conventional spring damper [5]

Tip-in and back-out problems occur when engaging and disengaging the TCC; if the driver requests vehicle acceleration via the foot pedal while the clutch is engaged then surge vibrations, (which can sometimes be felt by the driver as a jerking motion of the vehicle [21]) can occur in the drivetrain [5] (see Figure 2.5). The motion of the lock-up clutch is not linear, and its engagement time is dependent on the speed ratio between the engine and the turbine, as well as the rotational speed of the pump [22]. At higher rotational speeds and increased speed ratios the engagement time increases, leading to the conclusion that driveability issues (such as tip-in and back-out) will be more likely to present themselves when engaging the TCC at higher speeds.

Therefore ideally the lock-up clutch system should be engaged lower down in the engine speed range to increase power transfer efficiency and therefore decrease CO_2 production. However, it must be engaged without transmitting unacceptable levels of torsional vibration to the transmission and drivetrain. Thus the lock up clutch system is usually equipped with an isolator system – a torque converter clutch damper. This damper minimises excitation of the drivetrain primarily by attenuating the engine firing frequency torque pulses [6].

2.1.3 Torque converter clutch (TCC) dampers

The drive towards increased powertrain efficiency has resulted in the proportion of operating time that the torque converter spends locked increasing. However, while the torque converter is in this locked state – and during its transition between open and closed – the attenuation of engine torsional vibrations by the hydrodynamic circuit is significantly reduced, resulting in increased noise and vibration issues. Thus the torque converter clutch is fitted with a torsional damper (see Figure 2.6).

The primary purpose of the torque converter damper is to isolate the rest of the powertrain (e.g. the transmission and driveline) from the torsional vibrations produced by the engine. Recent developments in engine technology have been focused around downsizing through engine boosting – essentially reducing fuel consumption while at the same time increasing torque output. This downsizing and efficiency trend has resulted in an increase in the magnitude of the torsional vibrations being transmitted to the drivetrain, due to higher torque and speed fluctuations.

These torsional vibrations affect vehicle performance in numerous undesirable ways; firstly, the worsened acoustics [23] combined with gear rattle and body boom [24] affects driver comfort, reducing the desirability – perceived quality – of a vehicle. These NVH problem-inducing driveline torsional modes are typically found in four cylinder in-line engines applications, where aggressive shift patterns are used along with a frequent torque converter clutch engagement schedule [6]. Secondly, vibrations can lead to issues with the fatigue strength of driveline components (leading to decreased transmission service life) due to the added stress the vibrations place on the transmission [23] [24]. Thirdly, these driveline resonances can affect the performance of other areas of the vehicle, including the engine, propshafts and suspension. In the engine the resonances can impair spark timing due to the oscillating load they place on the system [20]. In rear wheel drive vehicles (depending on the design of the differential mounting system) the torque fluctuations may result in a pitching or rolling motion in the differential (thus exciting the rear suspension) [6] [25].

It is due to these driveability concerns [15] that in low gears and at low engine speeds the torque converter clutch is often not engaged. However, if torsional vibrations are reduced significantly the clutch system would be able to transition to locked at earlier points in the engine speed range, thus helping to reduce fuel consumption.

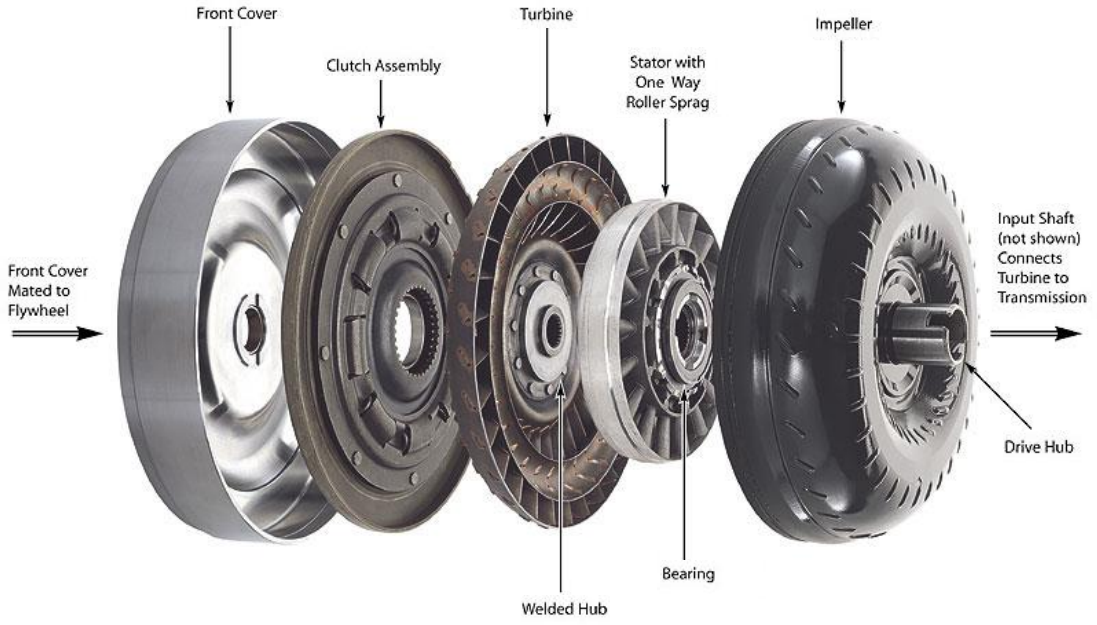

Figure 2.6: Torque converter with lock up clutch and damper [26]

Conventional dampers are located before the turbine, between it and the torque converter housing (see Figure 2.6). There are two main types of torque converter clutch dampers; coil spring and dynamic mass absorbers. Spring based damper designs can utilise straight or arc springs or a combination of the two, while dynamic absorbers use an inertia (such as a pendulum) instead. Some dampers are located behind the turbine, between the turbine and the transmission input shaft. In these turbine dampers the damper springs and transmission input shaft are connected in series; the turbine acts as a mass on the engine side. In these designs the turbine and damper system can be two separate components that are then connected (e.g. using rivets), however more recent designs and concepts have detailed integrating the lock-up clutch into the turbine component (see Figure 2.7). This helps reduce the size of the rotating masses that have to be accelerated, increasing the efficiency of the system [27]. These dampers can also be two-stage; one set of springs connects the clutch to the turbine, while an additional set connects the turbine and the transmission input shaft.

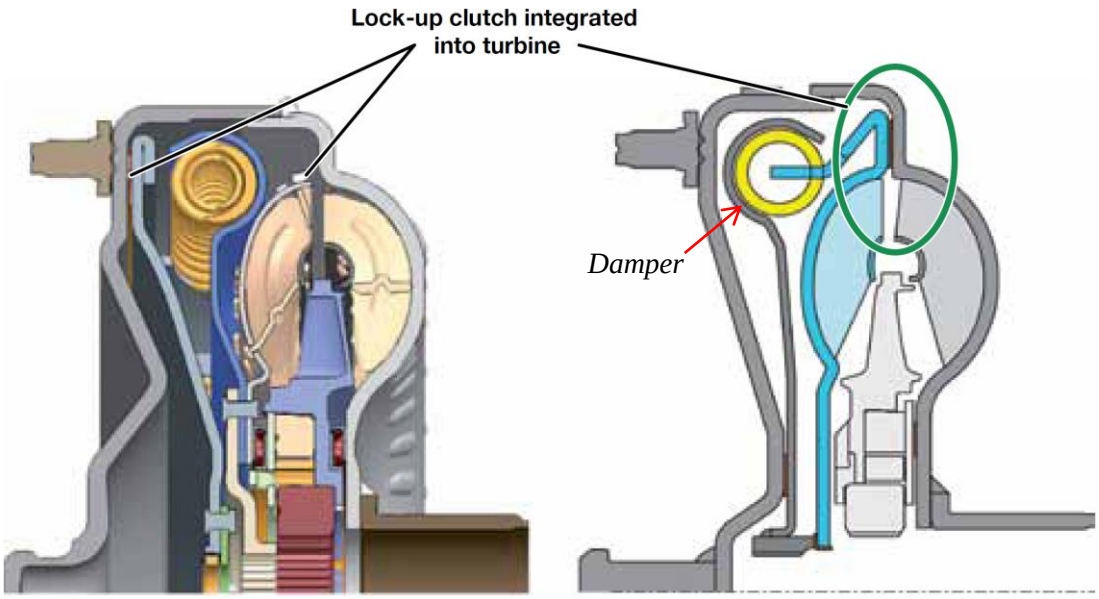

Figure 2.7: Damper concepts with alternative integrated lock-up clutch and turbine designs where the damper is attached to (L) or forms part of (R) the turbine [27]

Turbine dampers can be used to minimise the effects of boom and rattle, where the solution of conventional dampers with lower spring rates is not suitable; the most appropriate solution is determined by which characteristic mode (engine order) is dominant. If boom is a function of the second characteristic mode then damper modifications will have an effect as relative torsion damper movement is fairly high [5]. Turbine (serial torsion) dampers essentially perform the equivalent of a reduced stiffness transmission input shaft (which decreases boom resonance) [5]. It should be noted that in a two stage turbine damper design (when the turbine mass is located between the spring sets) the power still flows through the second stage of the damper, even when the torque converter clutch is open (disengaged).

Coil spring dampers

Conventional torque converter clutch dampers use coil springs to isolate vibration; the energy of the combustion forces is absorbed by the springs and then returned during the compression cycle of the engine (smoothing vibration) [7]. There are four main types of coil spring dampers; long-travel dampers (LTD) that use helical (coil) springs in special eyebrow pockets [28] (see Figure 2.8), those that use curved arc springs in a curved housing that may or may not match the curve of the spring (introducing pre-load to the spring coils), designs that utilise straight linear springs in curved pockets (see Figure 2.8 and Figure 2.11) and those that employ a combination of any of the above – also known as series or two-stage dampers [29] (see Figure 2.11).

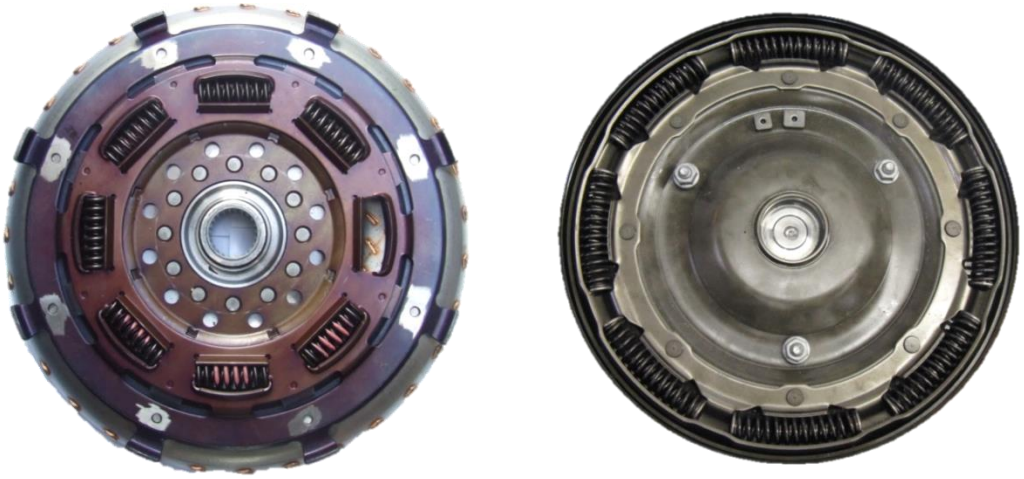

Figure 2.8: Left - Coil spring LTD TCC damper, Right – Linear spring (curved pocket) TCC Damper [30]

The amount of vibration that a coil spring can isolate is dependent on its energy capacity, which is determined by the size of the spring. The greater the number of arc springs used in a single stage the lower the damper travel, but the higher the torque capacity of the damper [29]; the size and number of the springs is limited by the space available to the torque converter in the transmission housing [31]. To improve isolation in coil spring damper designs the clutch damper mode frequency is often lowered and the compliance increased; this is achieved by increasing spring travel and lowering spring rates [6].

Another method by which the coil springs help dampen torsional vibration is through the controlled use of hysteresis (coulomb friction). In coil spring dampers this hysteresis is produced by the relative motion of the damper components, e.g. the springs and their housing/retainer cages. Hysteresis is mainly dependent on the displacement of the springs relative to their housing and the absolute speed of the damper (centrifugal effects). A controlled source of hysteresis can also be provided by inserting washers with a certain friction coefficient characteristic between parts of the damper that are in relative motion [6].

A typical LTD damper spring can be seen in Figure 2.9; the springs used in these dampers are typically of a straight helical open coil design which is usually intended to be loaded in compression only. In order to prevent the spring from buckling and becoming unstable (deflecting in the wrong plane) when used in dampers the springs must be mounted in guide pockets (such as eyebrow pockets) and pre-loaded. The design of the pocket is quite important as it affects the efficiency of the TCC damper; firstly, the friction between the spring and the retaining wall (see section 2.4) is a key source of vibration dampening, and secondly, a pocket must be correctly designed to facilitate the transition between nested springs [28]. Dampers that use straight springs that are placed in curved pockets differ slightly from traditional LTD designs as the springs are radially preloaded as well as along their length. This spring damper design could potentially produce an interesting but complicated hysteresis characteristic, as the springs start by pressing against their inner housing before transitioning to only having contact with the outer housing as damper speed increases.

Figure 2.9: Typical LTD helical coil spring in damper eyebrow pocket [28]

Some types of coil spring damper can use nested springs; this is when a smaller diameter spring is mounted inside the main spring (Figure 2.10). Nested coil springs increase the magnitude of the torque that can be transmitted by the spring set due to the increased stiffness the paired springs offer [32], thus are more likely to be used when spring length is limited, such as towards the centre of the damper unit. The inner spring can be the same length or shorter than its larger partner; some dampers use a combination of the two in one spring set. When the inner spring is the same length as the outer the stiffness of the pair remains constant throughout compression (excluding any changes in stiffness due to friction between the two), with the pair behaving as parallel springs. Additional hysteresis is caused by the coils of the two springs rubbing against each other as they compress. The spring coils can be wound in the opposite direction in the inner springs, in addition to the number of coils being different, in order to fine-tune this hysteresis characteristic and allow the springs to compress smoothly. When shorter inner springs are utilised the main outer spring begins to compress by itself, then once it reaches a certain point the inner spring also starts to compress, altering the overall spring rate of the damper (similar to two stage series dampers – see Figure 2.12); this can be used to fine-tune the damping characteristics and is especially useful when space is limited.

Figure 2.10: Nested springs in a two stage damper

Series dampers (also referred to as two-stage dampers) utilise two damper stages connected in series; the damper assemblies are connected by the use of an intermediate flange (see Figure 2.11 and Figure 2.27). This intermediate flange acts as the output inertia for the primary damper assembly (typically an arc spring assembly around the edge of the damper) and the input inertia component for the secondary assembly (arc or linear springs) [33]. In turbine dampers this intermediate inertia is connected to the turbine portion of the torque converter, with power always transferred from the turbine through the secondary springs set even when the clutch is open (damper unlocked).

Figure 2.11: Arc spring series (two-stage) damper

A typical stiffness characteristic for a two-stage damper can be seen in Figure 2.12. The first damper rate (K_1) is a combination of the spring rate of both the primary (outer) and secondary (inner) spring assemblies; once the outer springs cannot be compressed any further there is a knee point after which the damper assembly has a new stiffness. This new stiffness (K_2) is the rate of the inner springs only [29]. If the secondary set uses nested springs where the inner springs are shorter there will be an additional knee point when these springs start to be compressed, thus increasing the stiffness of the set.

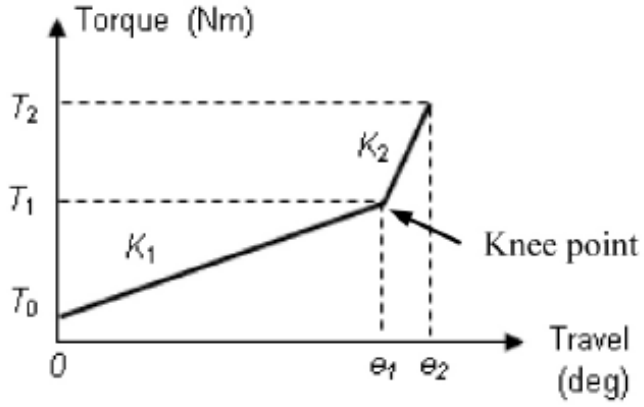

Figure 2.12: Typical series damper stiffness characteristic [29] (T_0 indicates spring preload)

While it is possible that the knee point is caused by the springs bottoming-out – full compression being achieved – as suggested by Li and Sandhu [29], this type of design would likely suffer from durability issues due to the repeated clashing of the spring coils. An alternative cause of the knee point is the presence of a physical hardstop that limits the relative movement of the primary and secondary plates (see section 5.1). Due to the lack of literature available it is unknown how many torque converter damper designs feature these physical hardstops; as no previous studies appear to have examined their use (they do not appear to be a feature of DMFs) the methods used to simulate them cannot be assessed. A knee point which utilises a hardstop is likely to have a much sharper, more sudden stiffness change; if the knee point is caused by the springs becoming coil bound the knee point stiffness change will be more gradual [29].

Dynamic absorbers: Centrifugal Pendulum damper

A simple dynamic absorber consists of a small mass or inertia connected via a spring to a larger mass. The vibration of the larger mass can be cancelled out by tuning the smaller mass to the natural frequency of the larger mass (see Figure 2.13) [7].

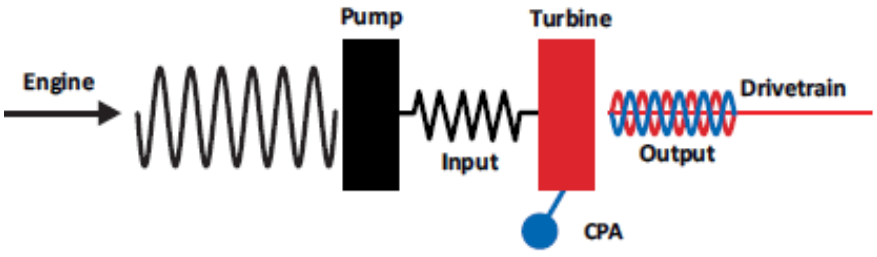

Figure 2.13: Dynamic Centrifugal Pendulum Absorber (CPA) system schematic [7] [31]

However a simple dynamic absorber can only be tuned to cancel one natural frequency, and depending on degrees of freedom and the number of gears available transmissions can have several natural frequencies [31]. A solution to this is to replace the spring-mass system with a pendulum; the natural frequency of a pendulum depends on the length of the pendulum and the centrifugal force applied to it, thus the absorber will have a variable natural frequency that is dependent on engine speed (see Figure 2.14) [34]. This frequency can be tuned to the dominant vibrational order (i.e. firing) of the engine [7], reducing the torsional vibrations transmitted to the transmission.

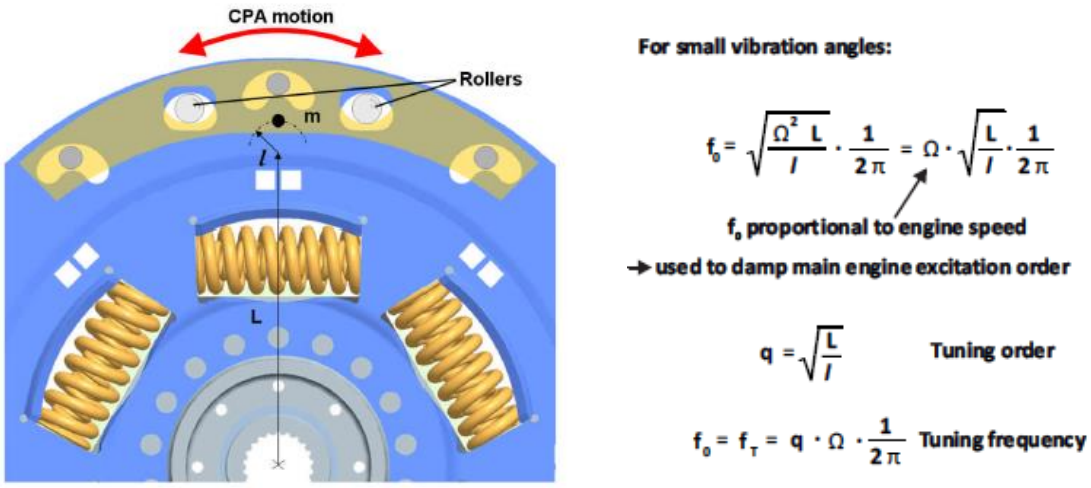

Figure 2.14: A centrifugal pendulum absorber [31] and the accompanying theory [7]

There is a minimal amount of published work reviewing the inclusion of centrifugal pendulum absorbers in torque converter dampers; it appears that centrifugal absorbers were originally developed for inclusion in Dual Mass Flywheels (DMFs). The success of a LuK concept (a 7% increase in fuel saving over a standard DMF [27]) led to a version of a pendulum absorber being incorporated into torque converter dampers (see Figure 2.15).

In the examples available, this pendulum design is used in combination with a coil spring damper rather than by itself, as this allows the mass of the pendulum to be smaller (saving space). The further the centre of gravity of the pendulum is from the centre point, the more effective it is when the mass remains the same [27]. In torque converter damper applications using a two stage spring damper the pendulum is coupled to the intermediate flange between the two spring sets [34].

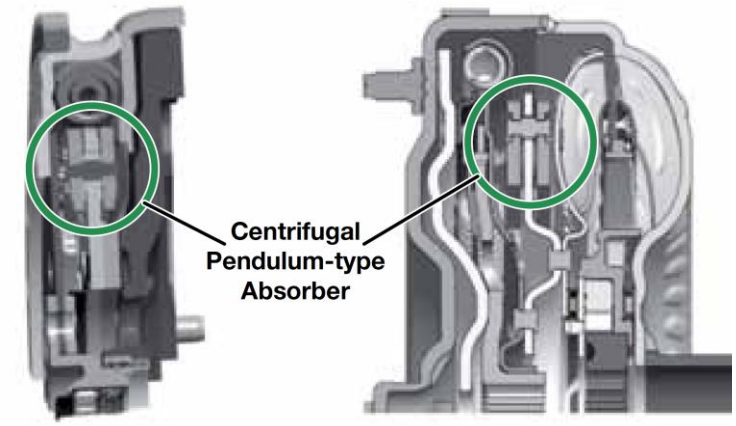

Figure 2.15: Pendulum absorber integrated into coil spring damper in a DMF (Left) and a Torque Converter (Right) [27]

A form of turbine damper design known as turbine tilger (tilger being the German word for absorber) is a combination of coil and dynamic absorber [31]. In this design (see Figure 2.16), rather than the turbine being connected directly to the transmission input shaft, it is attached to the intermediate flange using a small set of straight coil springs. This allows its inertia to be used as a dynamic absorber when the torque converter is locked and the turbine inactive; the turbine oscillates against the intermediate flange in a manner similar to the pendulum mass damper, damping engine frequency oscillations. This design is a type of simple dynamic absorber meaning it is only able to damp a single frequency; however if the ratios between the inertias in the system are tuned correctly friction effects can be used to spread its attenuation ability over a wider range of frequencies [7] [31].

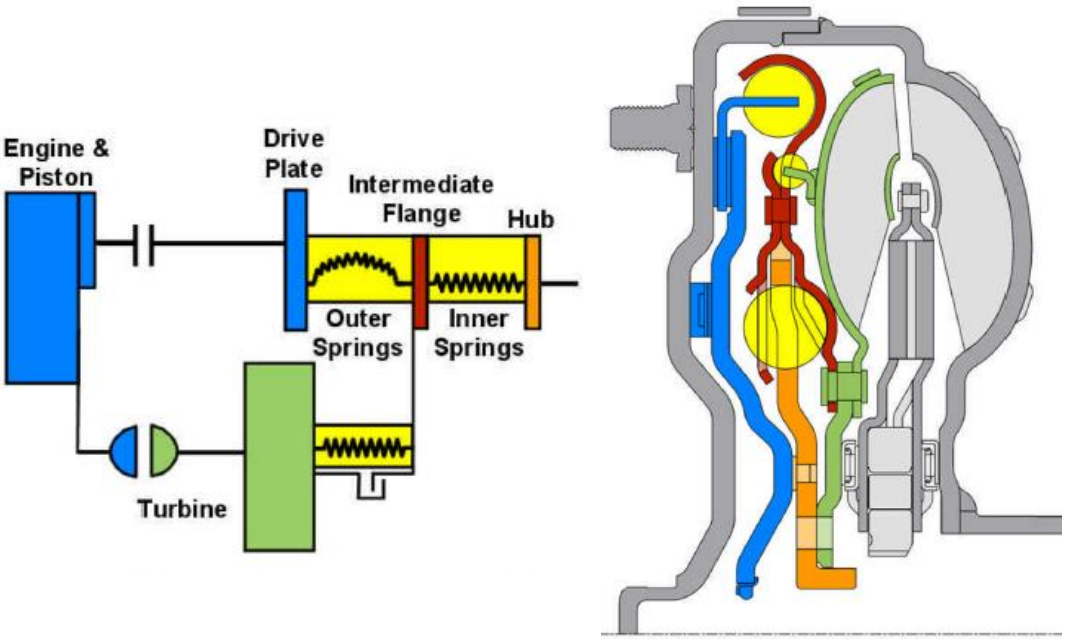

Figure 2.16: Schematic and cross section of a LuK turbine tilger damper design [31]

Experimentation by LuK USA has shown this turbine tilger damper design to be significantly more effective at reducing drivetrain oscillations then an equivalent coil spring turbine damper, especially in the lower engine speed range (1000-2000 rpm) [31].

2.2 Driveline damper testing

This section investigates what methods have previously been used to assess the performance of powertrain dampers when subjected to fluctuating input signal – either from a real engine or a simulated torsional vibration signal. Due to the lack of literature available on the testing of torque converter dampers this review has been expanded to include the testing of other types of dampers (e.g. clutch dampers and dual mass flywheels) and general driveline NVH investigations. The literature appears to agree that while multiple frequencies are excited by the engine pulses, the most significant vibrations (that are required to be reduced by a powertrain damper) occur at the engine's firing frequency [1]. However no studies have taken into account the effect the other (less dominant) vibration frequencies may have on the movement and behaviour of damper components, or that the dominant frequency order may change over the engine speed range. Thus part of this project will need to assess what type of signal (single or multi-frequency) is sufficient to excite the damper in a manner that allows accurate assessment of its performance and sufficient data for simulation validation.

2.2.1 Electric dynamometers

Electrical dynamometers – both AC and DC – have frequently been used to test DMFs, torque converters and transmission systems [35-39]. A typical AC input dynamometer has a power output in the range of 250-300kW with AC absorption (output) dynamometers having a slightly higher capacity of 300-350kW [35]. DC dynamometers range from 100 to 200kW on input and 200 to 300kW on absorption [40]. Power rating is important as along with torque capacity it will limit what torque and speed range the damper can be tested in, as well as the type of testing the driveline can be subjected to; durability or NVH studies tend to require output dynamometers with a much higher torque capacity than those used for efficiency tests [38] (see Figure 2.17). To increase NVH test accuracy some test rig installations use dynamometers with adjustable inertias (removable inertia rings); this allows the input and output inertias to be tuned to match those found in a variety of real vehicles (e.g. different engine or wheel sizes) [41].

Figure 2.17: McLaren Durability & NVH test rig – inside the acoustic chamber (Left) & the external motors (Right) [38]

The number of absorption (transmission output) dynamometers varies across the reviewed literature. Studies that involve minimal sections of drivetrain, i.e. are primarily testing the transmission behaviour, tend to utilise a singular output dynamometer. 2WD [35] and 4WD [36] full drivetrain studies usually use 2 and 4 output dynamometers respectively, in order to more accurately represent the driven wheels. The configuration of the 4WD Ford Motor Company spin-torsional NVH test facility can be seen in Figure 2.18; this particular rig design allows for the input (loading) dynamometer to be replaced with a combustion engine if required. These full powertrain rigs (with 2 or 4 absorption dynamometers) have successfully been used to produce torsional excitations in a powertrain system similar to that found in-vehicle, allowing NVH issues such as gear rattle and torque fluctuation (tip in/out – see section 2.1) to be studied [36].

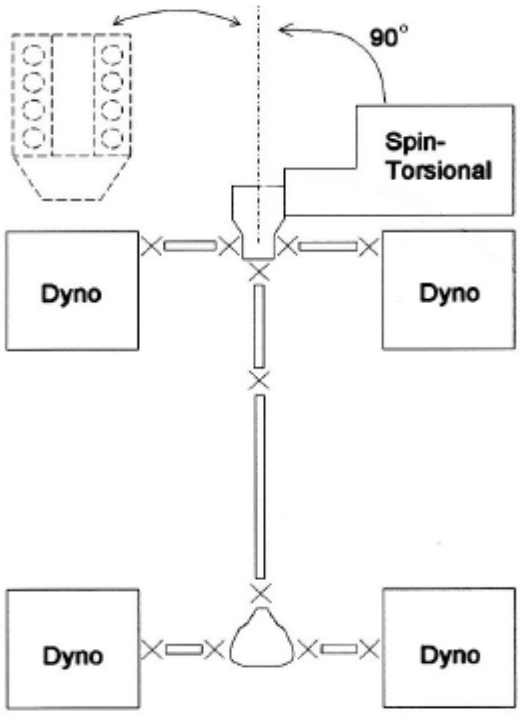

Figure 2.18: The Ford Motor Company spin-torsional NVH test facility [36]

In order to simplify the analysis of experimental results, reduce complexity in validating CAE models and due to limitations on input dynamometer response frequencies, these rigs often use sinusoidal inputs of the same frequency as the desired engine torsional order instead of attempting to replicate a real engine torque/speed signal. However such inputs do not duplicate the complete torsional vibration behaviour of a fired engine across the frequency range, and as a consequence of this the testing results may not correlate as closely as desired with in-vehicle measurements.

Simulating engines using electrical dynamometers has numerous advantages compared to full powertrain (fired engine) testing; not only are engines expensive to maintain (e.g. fuel, oil and other consumables – especially when a prototype engine is being used) but they also produce harmful emissions. Using electrical dynamometers to perform drivetrain testing allows drivetrain components to be designed and tested parallel to engine development, rather than having to wait for the engine development process to be completed. Thus their use in development can improve the time between concept and market for vehicles, potentially saving the industry substantial amounts of money.

2.2.2 Engine and in-vehicle testing

One study conducted by Otanez et al [42] used an entire car (in this case a GM All-Wheel-Drive SUV) that was run on a four wheel drive chassis dynamometer. Torsional velocity measurements were taken from the driveline by using a combination of magnetic pickup (at front and rear propeller shafts) and laser vibrometers [42]. While this approach to studying NVH is obviously the easiest way to accurately excite the damper, it is time consuming [38] and is only really suitable for post-development or competitor vehicle performance assessment. When investigating some NVH phenomena (such as judder) even a chassis dynamometer is unable to replicate exact road conditions; it has been found that when a vehicle is tested in this manner judder frequencies can actually be increased [43].

Some facilities [44] [45] utilise combustion engines on their rigs; not only does this help eliminate the problem of trying to excite the damper in a way similar to that in-vehicle but it also allows dampers to be tested directly with their intended partner combustion engine. In these instances electric hub dynamometers are used to simulate a range of vehicle speeds and loads [44]; an example of a full powertrain and driveline test rig facility can be seen in Figure 2.19. This particular configuration is used for the testing and development of racecars [46]; the principle is the same when testing passenger vehicle drivetrains except testing is usually done without the chassis or bodywork. This type of rig is highly flexible and can be tested with a full range of 2WD or 4WD powertrains but can require a substantially larger test cell area and additional equipment (such as emissions extraction systems); fuel is obviously also required to run tests, further increasing costs.

Figure 2.19: Full powertrain and driveline modular test facility [46]

2.2.3 Testing damper systems separate from driveline

In order to accurately characterise and understand the behaviour of torsional vibration damping systems, it is important to be able to separate the isolation behaviour of the damper from any torsional damping that may come from other areas of the powertrain (e.g. the transmission or driveline). Some studies [23, 39-40] have aimed to separate torsional dampers (including TC dampers and DMFs) from other areas of the powertrain during testing; this approach allows instrumentation to be installed closer to the damper being tested.

The schematics for the test stands designed for studies completed at the Technische Universität München (TUM) [23] and the Southwest Research institute (SWI) [40] can be seen in Figure 2.20 & Figure 2.21. The SWI rig uses a simple input-output electric motor configuration with DC dynamometers used to drive and absorb forces in the rig [40]. The TUM test facility utilises a combustion engine to drive the rig, eliminating the need to replicate engine torsionals and ensuring sufficient excitation, while an 80kW DC dynamometer is used to simulate a range of loading scenarios and operating modes [23].

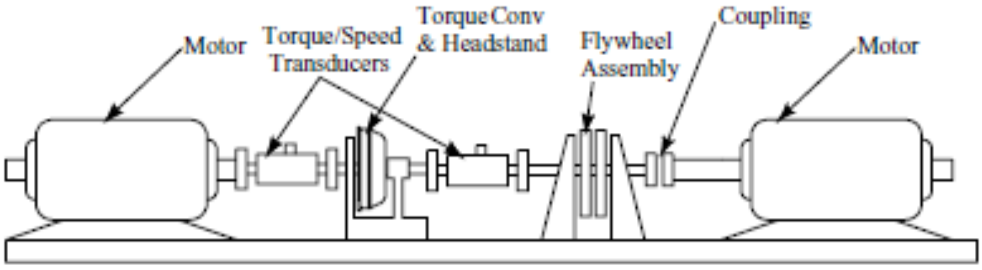

Figure 2.20: Southwest Research Institution torsional vibration dampener test facility [40]

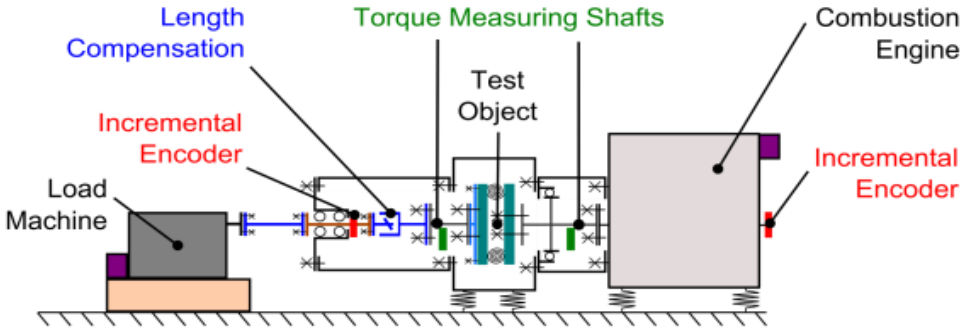

Figure 2.21: Technische Universität München torsional vibration dampener test facility [23]

While the TUM test facility can subject the torsional damper to typical transient conditions using a combustion engine, the SWI rig does not have this capability; if any torsional vibrations were required the electric input dynamometer would be relied on to produce them. The TUM test facility uses an electric dynamometer with a fixed inertia (that may or may not mimic that of a vehicle) to represent vehicle drivetrain loading. The SWI rig uses an adjustable flywheel assembly between the torque converter and the output dynamometer to produce a vehicle equivalent inertial load [40].

In the SWI study – where the torque converter is tested separately from the transmission – a stand is used to support the input shaft and torque converter housing (including the pump) via the flexplate. The turbine output shaft that usually drives the transmission is supported by the stand using a rolling element bearing. The ATF (automatic transmission fluid) is fed into the torque converter using a hydraulic pump located on a charge cart. This charging system allows the temperature of the ATF to be controlled and can charge the torque converter up to ~80psi (5.5 bar) [40].

As the aim of the SWI study was to characterise the transient performance of the hydrodynamic circuit in the torque converter, rather than the clutch damper. It is therefore unknown whether or not this method of oil feed and control would be suitable for use when testing damper designs; in order to engage the lock-up clutch, a separate high-pressure oil feed that reached behind the damper clutch plate would be required. Due to the complexities involved in locking up the torque converter (required to fully activate the damper system) using either a transmission CAN signal or manual oil feed, few studies have investigated the testing of the torque converter and damping system separately from the transmission. When designing rig tests any benefits to separating a damper system from its surroundings – such as increased confidence in what component areas the data represents – should be weighed up against the additional complexities and probably extra cost incurred by doing so.

2.2.4 Instrumentation

The majority of rig based transmission behaviour studies have taken measurements from between the engine or input dynamometer and the torque converter as well as at the output of the transmission; however the methods used to collect the data vary. The three main instrumentation set ups used in the reviewed literature are flexplate measurements, laser vibrometers (shaft measurements) and non-contact rotary transformer torque sensors (more commonly referred to as torque transducers).

Flexplate measurements can be taken by either using a modified instrumented flexplate [47], magnetic pick up [6] [48] or optical sensors [47]. A range of optical sensors can be used; one method uses black and white tape (to generate signal pulses) fixed to the test component in conjunction with a light source to reflect light off the tape and into the photo sensor light receiver [37]. However optical sensors have been shown to suffer from durability and reliability issues when used in-vehicle so RF (Radio Frequency) telemetry in combination with strain gauges installed on the flexplate are more commonly used [47].

In order to power the rotating electronics (strain gauges) an induction power technique is often used, negating the need to install any power sources on the rotating components [47]. Instrumenting the flexplate has the advantage of allowing the same instrumentation to be used in a range of different tests, either in-vehicle or rig tests with different torque converter configurations. Flexplate measurements can be used when there is limited space before the test object, for example when an engine is used to power/excite the system.

Laser Doppler Vibrometers (LDV) are often utilised when the torsional velocities are required to be measured from shafts [48] (such as the propshaft on the output of the transmission) due to their non-intrusive nature; they require minimal to no modifications to the test object [49]. They operate by targeting a laser at patterns mounted around the shafts, or at a particular spot on the test object. The laser beam is focused at the surface of the object, then as the object rotates and vibrates it results in a frequency modulation of the light that is scattered back to the sensor (making use of the Doppler effect); this light can then be compared to the reference beam which has a known frequency [50] (see Figure 2.22). LDVs are suitable for use in controlled testing environments but situations (such as vehicle testing) where there is significant background vibrations can easily affect the quality of the measured data [49] .

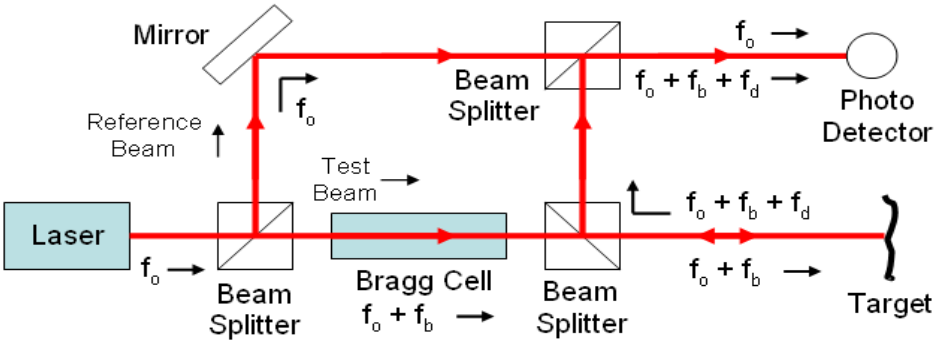

Figure 2.22: LDV schematic [51]

Torque can be measured using non-contact transducers that take measurements from strain gauges; these strain gauges are either fixed to a shaft or on a pre-made flange that is used as a connection flange between rig elements [40]. These types of non-contact rotary transducers are frequently utilised in test rig environments due to their ability to be used in a variety of different configurations; for example, a single flange transducer could be used on a transmission test rig, in an engine test cell or on a completely unrelated test rig.

Specially designed sensors can also be used to take measurements as close as possible to the test object, e.g. damping plate. One such study accomplished this by installing small posts on a clutch damper friction plate (see Figure 2.23) and by using a non-magnetic reluctance type pick up sensor on the transmission shaft guide tube; this sensor produces a pulse when a post passes it [52]. This system can measure the deformation of the clutch plate damper springs by detecting the difference in angular displacement between the hub and the friction plate. However, its sampling rate (and thus measurement error) can be affected by the rotational speed of the test object [53] [54]; its ability to detect high frequency torsional vibrations is also untested.

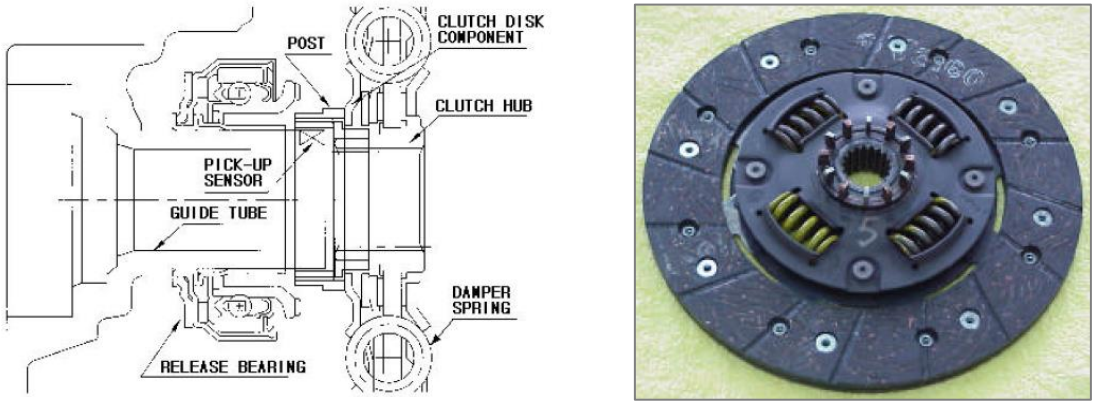

Figure 2.23: Post-based custom clutch disk torque sensor schematic and installation [52]

An alternative sensor design – that was used to measure angular displacement on a DMF – was developed from a torque disc sensor designed to replace the flexplate between an engine and the transmission [53] [54]. The primary design used strain gauges to detect the angular displacement of the DMF; for the secondary design (to allow it to be installed on a DMF) a new coil type sensor was developed – a circumferential variable differential transformer (CVDT).

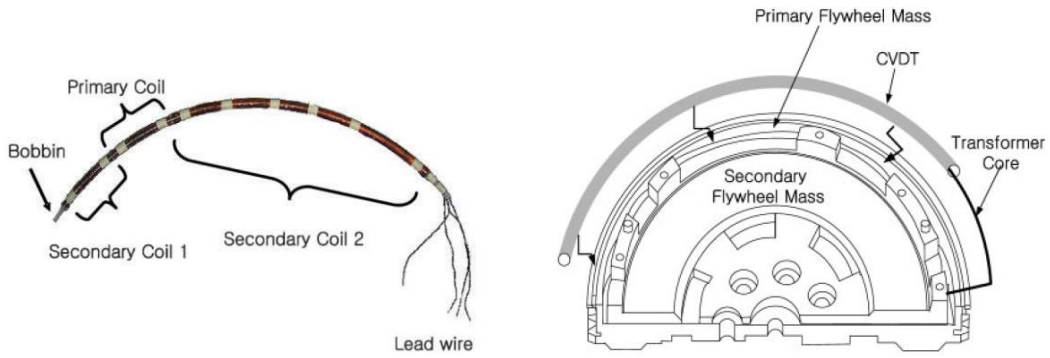

Figure 2.24: CVDT coil sensor (Left) and its installation on a DMF (Right) [53]

The CVDT (see Figure 2.24) is mounted to the primary mass of the flywheel while the transformer core is attached to the secondary mass. In both designs the whole system (including the Bluetooth transmitter) is powered using a magnetic flux based electrical method [53] [54]. It is likely that this system would not be suitable for use in a torque converter damper due to the oil it would be submerged in and the even more limited space available.

2.3 High frequency fluctuations: potential hardware solutions

In order to excite a damper with high frequency fluctuations, modifications were required to be made to the Hardware-In-The-Loop (HIL) transmission testing facility at the University of Bath Powertrain Vehicle Research Centre (PVRC) – see Chapter 4. This section reviews the technology (electrical and mechanical) that has been used to improve representative performance in dynamometer rigs that are similar to the PVRC facility. When upgrading an electrical motor rig for high frequency fluctuation testing there are two main solutions: either upgrade (replace) the rig dynamometers themselves or install an additional signal generator.

2.3.1 Electrical

While the bandwidth of electrical dynamometers can be improved to enable them to produce the correct frequency of torsional vibrations they also need to be equipped with a controller that is able to mimic the shape of the engine fluctuations – engine torsionals are not perfect sinusoidal signals. These controllers are often referred to as virtual engines [36]. Ideally, in order to simulate the dynamic performance of a fired engine, an input electric dynamometer should have a small response time (enabling higher frequency signals to be mimicked) and a low moment of inertia [55].

A study to compare the performance of a virtual engine dynamometer with a fired engine was performed by Newberger et al for Horiba Instruments [56]. This advanced test rig design used a high bandwidth (500 Hz) dynamometer in conjunction with a model based programmable control system that allowed the user to alter the characteristics (i.e. number of cylinders, fuel) of the virtual engine [56]. A similar study by Li et al also developed a model-based engine controller; the engine simulation is fairly simple, with the torque signal being split into mean, combustion and inertia torque components (frictional torque was neglected) [55]. These rigs require a complicated control system, with the outputs of the Powertrain Control Module (PCM) being simulated and interactions between the dynamometer control and data acquisition systems needing to be managed.

Both virtual engine dynamometers have the potential to simulate a range of different engines due to their programming capability, however, they both have so far only been iteratively adjusted to match, and tested against, a single engine design each; a 5.4L V8 petrol engine [36] and a 4.8L four cylinder [55]. The transient torque capability of the Horiba dynamometer was 10,000 rpm/s while the transient capability of the torque pulsations produced in each cylinder was 50,000 rpm/s [56]. The results of the Horiba virtual engine dynamometer testing compared favourably with the results from a fired engine, with tests performed in the range of 500-2250rpm and with torque output fluctuations ranging from -60Nm to 1300Nm. However, this study mainly focused on matching the mean speed and torque of a fired engine over repeats of a Key Life Test (KLT), rather than comparing its ability to produce torsional vibrations of the same frequency of an engine; thus its suitability for use in NVH or damper characterisation applications has not yet been assessed.

While electric dynamometers can provide quite a fast torque response, the main issue associated with using them for pulsation generation (engine mimicking) is their high inertia. A high inertia prevents the dynamometer from altering speed at a rate that accurately simulates fired engine speed fluctuations, especially in the low engine speed range required to characterise damper systems. In order to produce a representative torque response, the electric dynamometers need to be accompanied by a control system that can mimic the engine output; while this could potentially be done using a combination of test data, lookup tables and a sine wave generator [41] the most common solution is a form of engine simulation. However, this means that the output of the electric dynamometer will only be as good as the engine models are accurate. If an engine model is too simple it will not produce a representative response (ignoring any failings of the dynamometer system to respond to the virtual engine commands) while too complex a simulation will take too long to run, delaying the response of the control system and thus the dynamometer even further.

2.3.2 Mechanical

An alternative solution proposed and implemented by the Powertrain Control Research Lab (PCRL) at the University of Wisconsin-Madison is to use a hydrostatic hydraulic system controlled by high speed servo valves [57]. This hydraulic system generates torque fluctuations by using a pump (motor) with a constant inlet pressure and a servovalve on its outlet. In this application the servovalve is used to restrict flow rather than reverse it (see Figure 2.25 for the concept schematic) [57].

This concept provides a faster speed response then an electric dynamometer at higher engine speeds; however, this hydrostatic dynamometer does not quite generate a torque profile that matches a fired engine due to the frequency of the torque pulsations it is capable of producing. The bandwidth of the servovalves is a limiting factor in this; this study utilised a 120Hz valve, the fastest available [57]. While this hydraulic system has been shown to be an effective solution at higher engine speeds at lower engine speeds it struggles to produce the rapid torque fluctuations required.

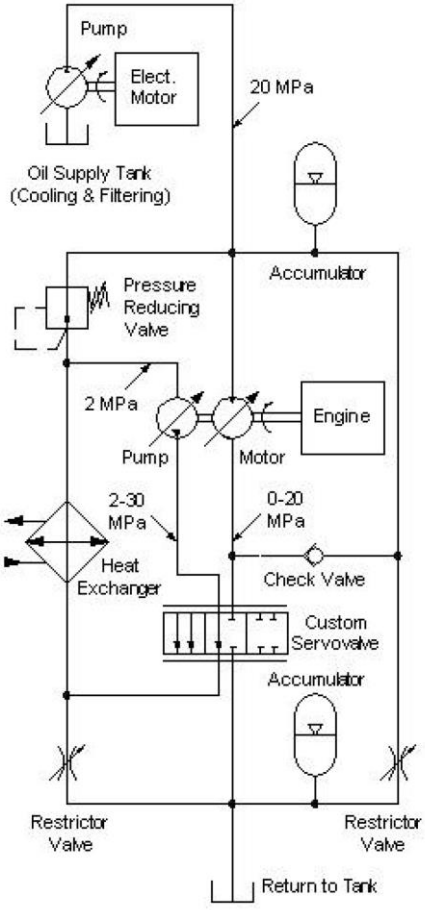

Figure 2.25: A hydrostatic transient dynamometer used to test one cylinder engine prototypes [77]

The general aim with lock-up clutch dampers is to be able to engage them at lower speeds, thus an understanding of damper behaviour at these speeds is key; hence a substantial proportion of damper characterisation tests will take place at less than 2000rpm. Because of this, and the substantial amount of space that is required by a hydraulic solution (space is at a premium in this transmission cell) this method is not a suitable solution. A simpler alternative is the use of an offset universal joint driveshaft (cardan shaft) in conjunction with an electric motor (see Figure 2.26); this method has previously been used to investigate the NVH response of a vehicle body [58] and a clutch system [59]. These studies used a single universal joint to mimic the 1st engine order [58] and two universal joints (with one rotated by 90°) to produce 2nd order vibrations [59]. However, while the magnitude of the speed fluctuations is controllable (by changing the angle offset of the driveshaft), it cannot be easily adjusted at each test point to match the changing magnitude of the torsional fluctuations along the engine speed range.

In neither study is this method shown to be capable of matching the engine torsional fluctuations, either in magnitude or through the simultaneous excitation of multiple frequencies (i.e. frequencies other than the dominant firing frequency). This method is obviously capable of producing torsional vibrations, but whether or not it is capable of producing the frequencies and magnitudes required to sufficiently excite the damper is unknown. This, combined with the lack of flexibility and difficulties controlling the response or output of the system means it is considered unsuitable for this investigation.

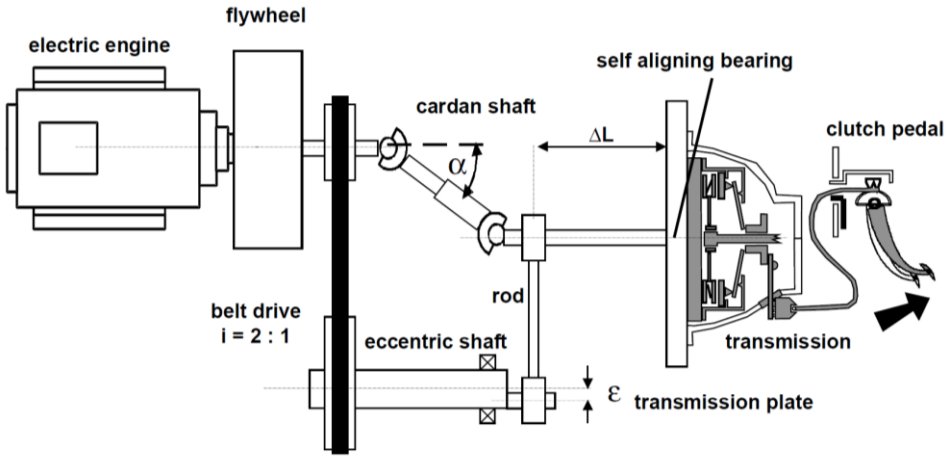

Figure 2.26: Excitation of a clutch using a cardan shaft [59]

2.4 Damper simulation

In order to fully investigate the methods that could potentially be used for the modelling of torque converter dampers, this section examines the simulation and modelling of a wide range of powertrain spring dampers, including Dual Mass flywheels (DMFs). While there are varying types and uses of spring dampers (e.g. multi-stage, clutch) the typical methods used in modelling linear and arc springs are common across the majority of coil spring damper configurations.

2.4.1 Spring representation

There are two main methods that are used when modelling spring damper systems; a simplified method that uses a static spring rate with a constant value for hysteresis [60] and a more complicated method in which the system is discretised into sections of massless springs and lumped masses [61]. The basic spring model is extremely over simplified and does not fully track the movement or behaviour of the spring, thus is not able to provide an accurate representation of the behaviour of either linear or arc springs. The simplified model – with a constant value for hysteresis – also does not take into account the changing friction profile that occurs over the spring's range of motion and slip speeds; it would most likely only be valid or useful when the only spring type used is linear, with those springs mounted in straight pockets.

An example two stage (arc and linear spring) damper design schematic can be seen in Figure 2.27. The linear and arc springs contact the walls of their housing – the inner and outer races. The damping effect that comes from these springs is produced by friction between the springs and the housing (see section 2.3.3). This friction is dependent on engine speed and torque (see section 2.4.2), and therefore the stiffness and hysteresis of the spring is variable (dynamic) and must be taken into account [29] [62] [63]. Thus modelling a spring by breaking it down into discrete sections of spring-mass systems will provide a more accurate model of the dynamic behaviour, especially for arc springs. As linear springs are less sensitive to torque and engine speed changes the simplified static rate method is sometimes seen as adequate [29]. However, unless computing power is at a premium, the trade-off between simulation accuracy and time is not substantial enough to warrant not using the discretized model for the linear springs as well.

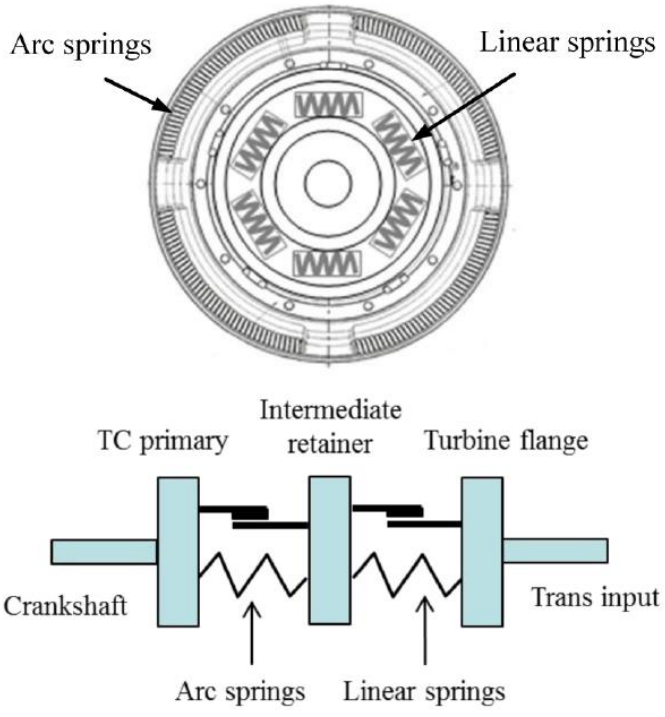

Figure 2.27: Schematic of a series (two stage) torque converter damper with linear and arc springs [29]

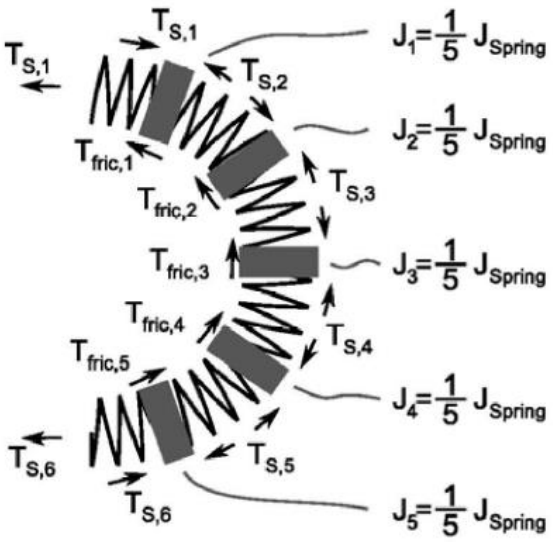

Figure 2.28: Discretised arc spring model [61]

While some studies have modelled each individual coil of the arc spring [63] [64], it is recommended that the long arc springs used in powertrain dampers are discretised into a minimum of six sections [29]; the spring is broken down into six elastic segments between 5 lumped masses [61] [62] (Figure 2.28). The optimum number of segments varies with the length of the spring; the longer the spring, the more segments will be needed to maintain the same level of accuracy. While a higher number of discrete masses will increase the accuracy of the simulation they will also require a higher level of computing time and power; thus there has to be a compromise between simulation accuracy and time taken. The use of the simulation should also be taken into account; a high number of discretised segments may be acceptable in a model of just the damper system, however if that model is then included in larger rig or drivetrain simulation the computing resources available may be reduced.

An example of how a discretised arc spring model can be implemented (e.g. in MATLAB Simulink®) can be seen in Figure 2.29. This particular simulation was developed for a Dual Mass Flywheel (DMF) model; the spring has been discretised into six segments, with each segment having a mass and a massless spring.

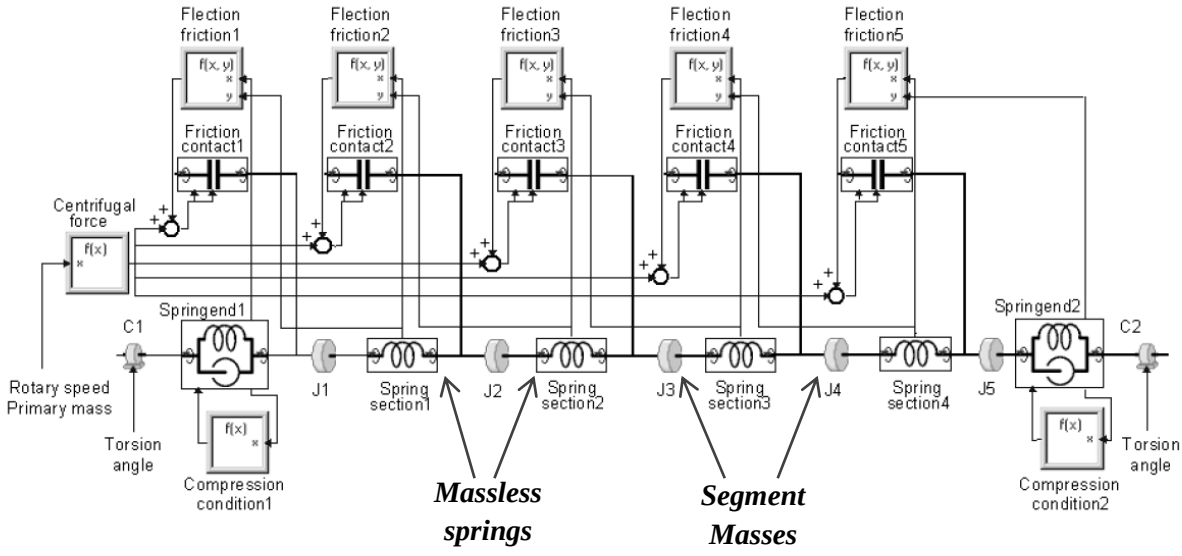

Figure 2.29: Example arc spring simulation model (constructed in MATLAB Simulink®) [62]

2.4.2 Arc spring behaviour

As discussed in section 2.1.3, when designing torsional dampers it is desired that the spring rate of the damper be as low as possible in order to increase compliance and therefore lower damper mode frequency into the desired range. However low stiffness linear springs have a lower torque capacity (as they are shorter) and are generally weaker. Arc springs provide an acceptable compromise as they can have a lower rate while still maintaining capacity; due to their shape they can extend around the outer edge of the damper plate so can be longer – see Figure 2.11 [63].

Different varieties of spring designs and combinations can be seen in Figure 2.30; these combinations adjust the friction and capacity characteristics of the springs by introducing 2-stage nested spring configurations (see section 2.1.4) or by changing the design of the coils. Series springs offer a two-stage characteristic however the knee point (see Figure 2.12) may be unreliable and variable; they also have less friction than an arc spring of the same overall length, decreasing the damping provided and minimising their usefulness. Nested (parallel) springs offer a higher torque capacity; by using a shorter inner spring a two stage characteristic (allowing fine-tuning of damper behaviour at higher speeds) can be gained. Special damping springs are available that have better impact behaviour (impact occurs when the spring becomes coil bound and cannot be compressed any further); however these are not widely used due to higher manufacturing costs and because they cannot be nested [63].

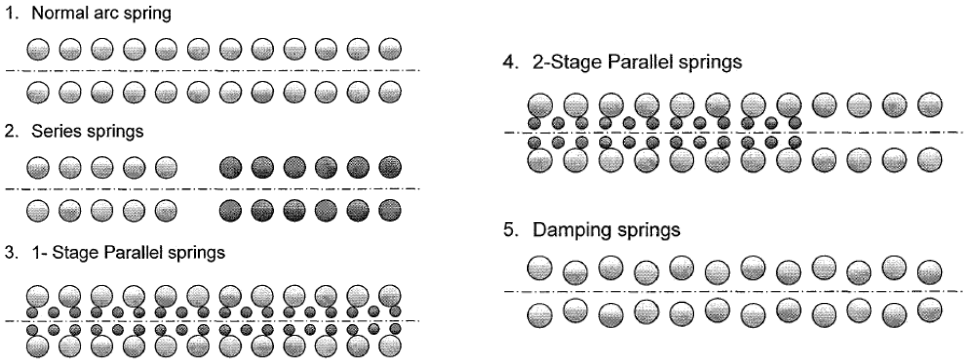

Figure 2.30: Arc spring set-ups [63]

Arc springs are designed to transmit power in both tangential and radial directions; the friction between the spring coils and their housing is another way the springs can transfer power. As the rotational (engine) speed increases, the centrifugal force (F_Z) exerted on the arc spring coils also increases, forcing the coils against the outer race of their channel (see Figure 2.32). The curve of the springs also results in a (normal) redirection force ($F_{i*,}$ also known as wedge effect [30]) being created when a torque is applied [65] (see Figure 2.31). These radial forces increase the friction between the coils and the plate [62]; the higher frictional force (F_{Ri}) affects the stiffness of the springs and contributes to damping of oscillations (by dissipating energy) [64]. This friction also increases the resistance of the springs to impacts at high engine torques, decreasing the risk of damage to the coils [63].

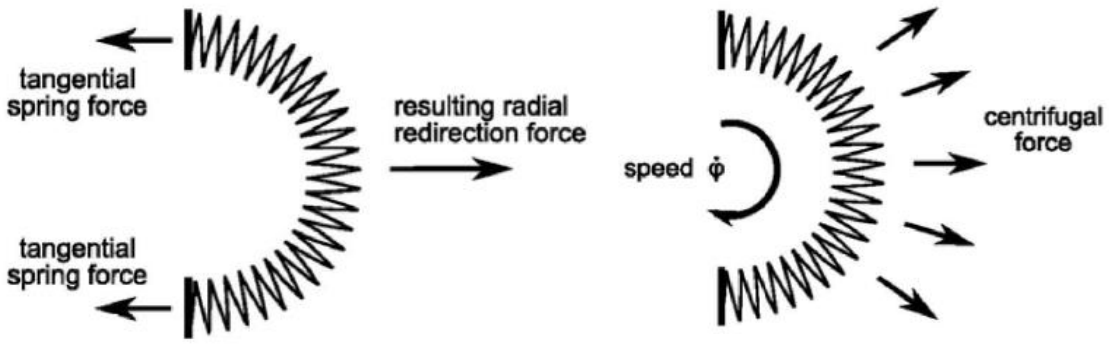

Figure 2.31: Radial forces caused by spring redirection forces and centrifugal effects [62]

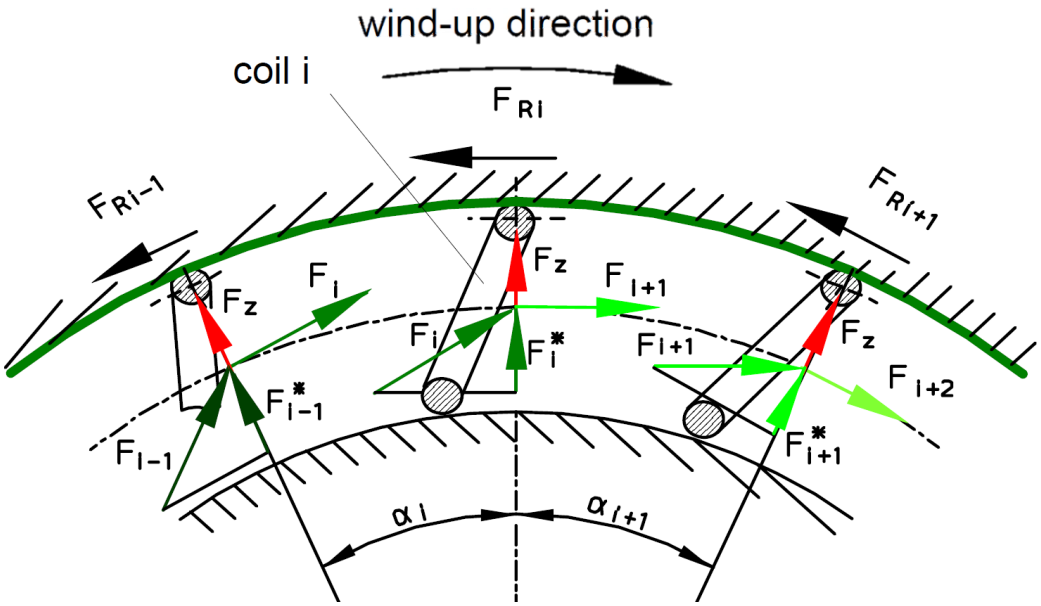

Figure 2.32: Radial forces on the individual coils of a (DMF) arc spring when load (F_i) is applied [65]

It is important to note that linear springs in curved pockets behave in a similar manner with regards to housing friction; however, the linear springs will have a much greater contact with the inner race at low rotational speeds. As the speed increases the spring moves away from the inner race and increases its contact area with the outer wall; depending on the design of the spring housing there will be a mid-point at a certain speed range (centrifugal force magnitude) where the spring may have minimal contact with either wall. This potential behaviour highlights the importance of using an advanced modelling method with variable hysteresis (friction coefficient).

In order to create a model certain spring design parameters are required; these can be taken from product literature, measured from the test object, or calculated from other design parameters. These parameters fall into two main categories: geometrical (the layout, initial position and motion range of the springs) and physical (stiffness, friction coefficient) [29]. The typical parameters used can be seen in Table 2.1; these parameters are used to calculate the redirection and centrifugal forces applied to the spring elements. These redirection components, along with the frictional forces between the spring and its housing, can be used to predict the movement and instantaneous position of the individual spring elements when a torque is applied.

Table 2.1: Typical parameters used in spring modelling [29] [61]

Parameter	*Units*
Plate Inertia: *Primary/Intermediate/Output*	Kgm^2
Effective spring radius	mm
Friction radius	mm
Starting angle	degrees or radians
Angle of arc spring	degrees or radians
Relaxed arc spring angle	degrees or radians
Clearance angle	degrees or radians
Spring inertia	Kgm^2
Mass of each spring element	Kg
Number of spring elements	
Number of active coils	
Spring stiffness of each element	Nm/degree
Coefficient of friction (μ) *(calculated, not constant)*	

As can be seen from Table 2.2, there are two key radii that are required for the calculations; the friction radius and the effective radius. The effective radius of an arc spring refers to the radius of the centre of the spring and is used where the mass or inertia of a spring is involved (e.g. redirection calculations), while the friction radius is the radius at which the arc spring contacts with the outer wall of the spring channel (Figure 2.33) [29]. Some studies assume these two radii are the same [61] which may lead to either the redirection forces being exaggerated or the magnitude of the frictional forces being underestimated.

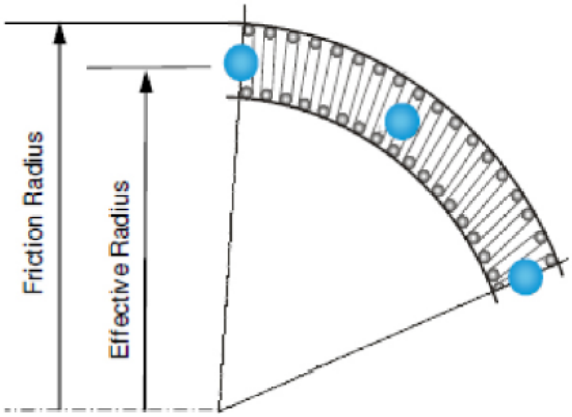

Figure 2.33: Characteristics required for modelling: arc spring effective and friction radii [29]

The spring angle information required for these models (see Figure 2.34) is used in the equations of motion for the arc springs. These parameters are used to determine damper preload, the stacking point of the springs and clearance levels (if any). The preload on the damper springs can be calculated by examining how far the springs are compressed when mounted in their pockets (if they are compressed at all), while the stacking point that occurs when the springs are unable to be compressed further provides the maximum angle of spring travel. Sometimes there is a deliberate small amount of clearance between the springs and the end stops; this feature can be used to reduce torsional vibrations at vehicle idle conditions, as during the clearance angle of travel there is no deformation and the damper rate is zero [29].

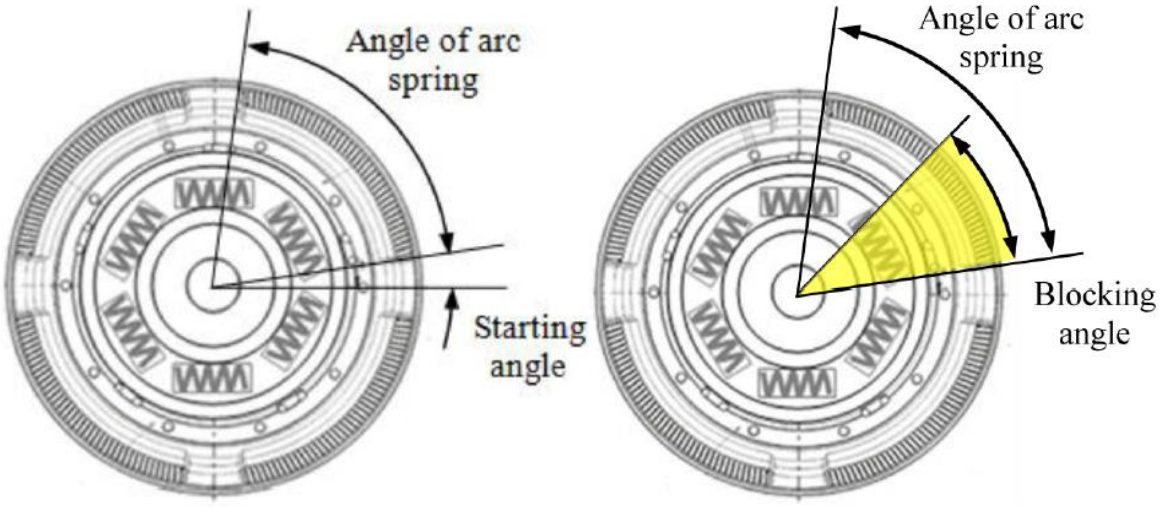

Figure 2.34: Arc spring angles required for simulation [29]

A discretized model is required for arc springs primarily because arc springs do not compress homogeneously as their stiffness is partly dependent on engine speed [61]. This occurs because the centrifugal forces affect the frictional forces between the spring coils and their housing. This coil friction means that the force at each contact point between the coils and the housing may be different, resulting in a varying amount of compression in each coil or segment [64] [65]. The range of forces that act on the coils of the arc spring can be seen in Figure 2.35.

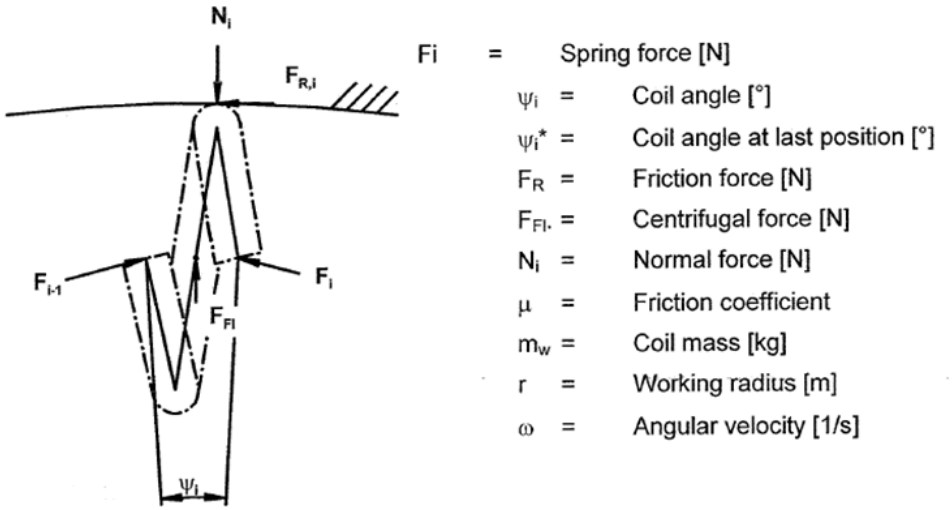

Figure 2.35: Forces acting on arc spring coil [63]

A discretized model also allows the aforementioned stacking effect – where parts of the spring become coil bound and cannot be compressed any further – to be taken into account. In a paper by Li and Sandhu [29] the term *stack-up effect* is instead used to refer to a process by which at higher engine speeds centrifugal forces become so high the torque applied to the spring cannot overcome them. This results in sections of the spring becoming immobile, shortening the effective length of the spring and increasing its stiffness. This effect is used to explain the increase in dynamic stiffness of the arc spring that is seen when engine speed is increased.

The de-activation of spring coils causing an increase in spring rate at higher engine speeds (4000rpm) is also noted by Albers [65]. However, this study suggests that there is a substantial increase in dynamic spring stiffness only when the vibration angle (spring movement) is low. The general theory is that the higher centrifugal force in turn increases the frictional force, slowing the arc spring coils, reducing their movement range and thus increasing the apparent stiffness of the spring. This potential non-homogeneous compression of the springs highlights the need for a discretised, validated arc spring damper model; there is also scope for expanding existing knowledge on the occurrence and cause of speed-dependent spring behaviour.

2.4.3 Friction modelling

A key part of producing a representative spring damper model is developing an accurate dynamic friction model; more basic spring simulations have used simple static friction models created from velocity and friction force maps. However by examining literature reviews on the subject [66] [67] it can be concluded that an accurate friction model can only be obtained when dynamic effects are also incorporated. This is a challenging area and dynamic models are typically either discontinuous or only piecewise continuous. The disadvantage of these types of models is reduced accuracy when used in situations with continuously changing friction and when friction effects are important or exaggerated – such as in spring dampers.

Simpler friction models are typically solely static based; however it is generally agreed [67] that in order for a friction model to be truly representative it should also include dynamic effects. Several dynamic models have been proposed (e.g. the Dahl [68] and LuGre [69] models) and developed or modified over the years (including the Leuven model [70]). However, as mentioned above, all of these models struggle to accurately represent changing frictional force direction at small slip speeds, often due to the time derivative of the velocity (which the friction force calculation is dependent on) being discontinuous at zero. Some attempts have been made to develop continuous approximations of the LuGre models [71] [72] however the stability and accuracy of these approximations can be difficult to prove.

Table 2.2: Friction model components

Friction component	*Description*
Static Friction (Stiction)	*The friction between surfaces that are not moving relative to each other - the frictional force that must be overcome before an object can move*
Coulomb friction	*A source of energy dissipation - friction is produced by relative motion of two surfaces.*
Viscous (fluid) friction	*Friction between moving layers of fluid*
Asymmetries	*Direction-dependent friction behaviour*
Stribeck effect (Lubricated friction)	*When a fluid separates surfaces reducing contact and stiction*

There are 5 main components that can be included in a friction model [73] – these (along with their definitions) can be seen in Table 2.2. The way in which these different effects can combine in a dynamic, speed dependent friction model can be seen in Figure 2.36. These friction profiles demonstrate why the use of a dynamic model is so important in a situation such as this; as the arc springs vibrate in their housing (frequently changing direction) the relative direction of the friction profile will also be constantly changing. As can be seen from Figure 2.36, when the slip speed (the speed between the two friction components, e.g. spring and housing) is zero, the friction coefficient must also be zero – if there is no relative movement there cannot be any friction. This effect, along with increased friction coefficient at low slip speeds (stribeck effect), is not taken into account in static models.

A newer, continuously differentiable model that can take into account system nonlinearities, such as the effects of directionally dependent friction effects, has been developed by the University of Florida [73]. This model (referred to here as the Makkar model) appears to be able to quite accurately approximate experimental data that exhibits static, viscous and stribeck friction effects [74].

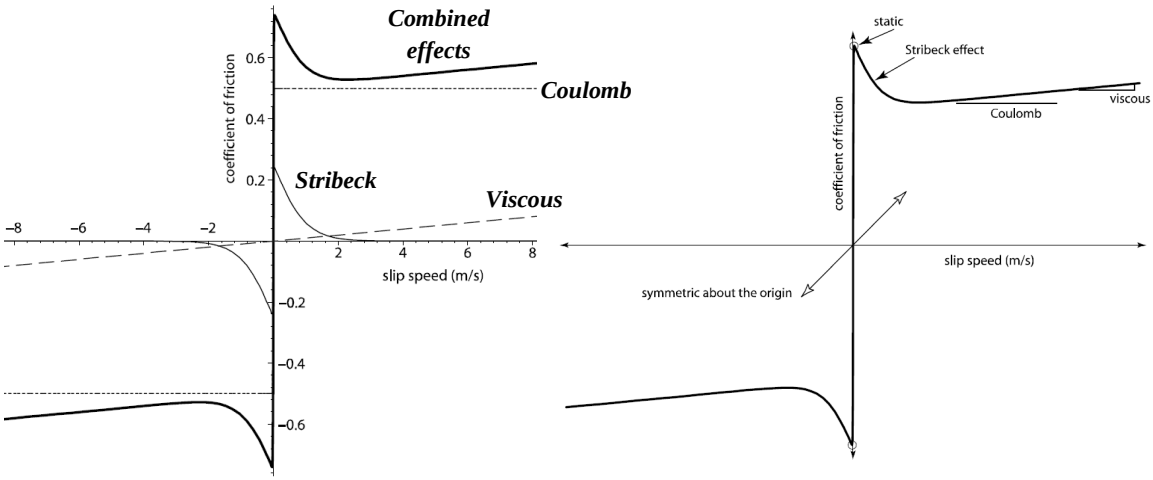

Figure 2.36: Overall dynamic friction model and its individual components [73]

2.5 Review of existing engine simulation techniques

As part of the development of a novel pulsation generator (see Chapter 4), a simulation was required to be developed. This section presents a brief review of the types of engine simulations that were considered for adaptation.

One of the disadvantages of linear and quasi-linear models is that they rely heavily on experimental data [75-77] (such as in-cylinder pressure measurements). This reduces the usefulness and ease of application of the models as they can only be used when experimental data is available (i.e. when an engine has already been developed). Another disadvantage is that their accuracy at high engine speeds is sometimes reduced [78]; the transient response of the engine isn't accurately represented due to model limitations [79]. Linear and quasi-linear models do have the advantage of requiring less simulation (computational) time [77]; however, their inflexibility and reliance on empirical data [77] renders them unsuitable for this application.

An accurate transient simulation requires detailed multi-cylinder and friction modelling; while the assumption that friction torque is constant during an engine cycle may be suitable for quasi-linear models, simulations based on crankshaft angular position require a more complex model [77]. Previous studies investigating the prediction of engine torque and speed have produced non-linear transient simulations that have improved the accuracy of the outputted torque profile; however these models are either time domain based [80] [81] or do not include inertia variations of the crankshaft assembly [82] [83].

An alternative solution is the use of commercially available simulation software, such as Ricardo WAVE. Commercial software has the advantage of being well established, with a wide range of advanced SI and combustion models [84]; using WAVE, an engine simulation can even be run in a motored state (similar to the pulsation generator). Commercially available solutions have one key disadvantage however; their inflexibility for use for a purpose other than that originally intended. Whichever solution that is chosen for pulsation generator simulation must be able to incorporate the inertias of the electric dynamometers to ensure all potential behaviours are captured. Ideally the pulsation generator simulation should be able to be combined with the torque converter damper model in a full rig simulation. While a commercial engine simulation software solution is likely to allow vehicle inertias to be included downstream of the engine, there is unlikely to be a mechanism for including an upstream inertia that is also providing drive to the crankshaft. Thus the ideal solution for this application is likely to be crank-angle based, allowing cylinder pressures and friction profiles to be calculated from engine geometry. The ability to simulate a flexible crankshaft or to be able to adjust cylinder properties individually is also desired.

A potential solution is a model proposed by Zweiri et al [85]; this method is an analytical non-linear dynamic model for single-cylinder diesel engines that operates in the crank angle domain (as opposed to the time domain) and includes crankshaft assembly inertial variations. This model does not require empirical inputs, and utilises an instantaneous friction model that includes multiple sources of friction torque (e.g. piston assembly, bearings) [86]. The transient behaviour of this model was validated with experimental results from a direct injection single-cylinder diesel. The measured and simulated data have good correlation; sources of error were identified as the single-zone combustion model (not required for pulsation generator simulation) and estimated engine model parameters.

2.6 Summary

A review of torque converter damper technology and the methods used to test and simulate the dampers has been performed. This review was expanded to include testing and simulation methodologies for Dual Mass Flywheels (DMFs) and other driveline components due to the lack of available literature on torque converter damper procedures.

The key outcomes from this chapter have been summarised below:

- A torque converter is a form of fluid coupling that is used instead of a clutch in automatic transmissions. A lock-up clutch is used to increase the efficiency by effectively bypassing the hydrodynamic circuit. Controlled clutch slip can be used to provide driveline damping but it can have a negative effect on driveline NVH behaviour. Thus modern torque converters are frequently fitted with a torsional clutch damper.

- Driveline component testing methodologies can be roughly separated into two categories; those that use electrical dynamometers and those that use fired engines. Electrical dynamometers typically need to be combined with virtual engine controllers or mechanical solutions (e.g. hydrostatic hydraulic systems) in order to mimic the size or frequency of fired engine fluctuations. Electrical dynamometer controllers are often based on either experimental data or engine simulations; this limits their flexibility, while their accuracy is limited by that of the engine simulation. Mechanical solutions can struggle to produce high frequency fluctuations at low speeds (hydraulic systems) or lack easy adjustability (offset cardan shafts). The literature is lacking a cheap, adjustable mechanical solution that is capable of exciting the damper over a range of speeds, frequencies and mean torques. As part of this project, a novel pulsation generator is developed that aims to fill this gap.

- Torque converter dampers can be roughly divided into two categories; those that use coil springs and others that utilise dynamic mass absorbers. Coil spring dampers can use both straight springs and curved arc springs. The literature has demonstrated that a discretised spring model is far more adept at capturing complex behaviour than a static spring rate method. Ideally, this discretisation methodology should be combined with a continuous dynamic friction model. Some dampers utilise nested springs, where a spring forms the housing for a smaller, inner, spring. There is no available literature on the simulation of nested springs in a discretised model; this thesis aims to expand existing knowledge by presenting a methodology for implementing discretised nested arc springs.

- A multi-stage damper will, at some point in the torque range, have a stiffness change when a spring set becomes inactive; the location of this change is referred to as the knee point. A damper knee point may be triggered either by the springs being fully compressed or by the use of physical hardstops. It is unknown how often hardstops are used; none of the available TC damper or DMF studies have simulated them. As part of this study, an original contribution to knowledge is made by investigating the simulation of spring-limiting hardstops.

- The literature agrees that while multiple frequencies are excited by a fired engine, the vibrational frequency order that has the greatest impact is the most dominant one – typically the firing frequency. However, no studies appear to have taken into account the effect the non-dominant orders may have on damper component behaviour. By investigating what type of signal is sufficient to excite a TC damper, this thesis helps develop existing understanding of optimum damper excitation methodologies.

- Arc springs are designed to transmit power in both tangential and radial directions. Centrifugal force (influenced by the speed of the system) contributes to the radial forces that push the spring into its housing; these radial forces will impact the friction between the spring and the housing, affecting the movement of the spring coils. While this theory is described in literature, there is scope for further investigation (using a damper simulation) into the occurrence and cause of speed-dependent damper behaviour (especially when subjected to higher frequency excitation).

.

Chapter 3 Testing Facilities and Methodology

Previously the Hardware-In-The-Loop (HIL) transmission testing facility at the University of Bath Powertrain Vehicle Research Centre (PVRC) has primarily been used to test CVTs (continually variable transmissions) for orbital traction and powertrain evaluation. This chapter details the technical specifications of the installed dynamometer system, as well as the upgrades that were required in order to perform the necessary tests for torque converter damper characterisation.

3.1 Test Hardware

3.1.1 Transient Dynamometers

The experimental rig used for this study utilises a twin ABB Ltd regenerative drive system to drive two electric dynamometers (input and output) in conjunction with a Sierra CP CADET v12 control system (see Figure 3.1). As discussed in section 2.2, powertrain test facilities that use fired engines to drive the system will provide a more representative way of exciting the driveline. However a twin electric motor rig is far more flexible and easily controllable; for example, an engine-driven rig would be unable to perform simple hysteresis curve tests. The dynamometers are both rated to 4000rpm with the input rated to 109kW, 500Nm and the output rated to 200kW, 1000Nm; these power ratings are fairly typical for transmission testing dynamometers (see section 2.2.1). The 15Hz bandwidth of these motors is inadequate for high-frequency torsional vibration production [87], so a novel pulsation generator unit concept (driven by the input dynamometer) has been developed (see Chapter 4).

Figure 3.1: PVRC rig before torque converter testing upgrades

3.1.2 Transmission and mounting

The transmission used in this project is an 8 speed automatic which uses four planetary gear sets and five shift elements (two brakes and three clutches) [88]. An advantage of this gearbox is its flexibility; multiple torque converter damper designs (single arc spring, turbine dampers or multi-stage) can be used with the same transmission. This means the performance and behaviour of different types of damper can be easily and accurately compared.

In order to ensure that all the rig components (e.g. dynamometers, transmission) can be accurately aligned the rig rails were upgraded from folded metal (see Figure 3.1) to machined bar (see Figure 3.2); misalignment may result in unwanted, uncontrolled torsional vibrations and unnecessary wear on components. These new slotted rails match the design and dimensions of those used on the workbenches and engine test cells; this allows components to be easily prepared outside of the test cell and helps ensure the cell is suitable for future work.

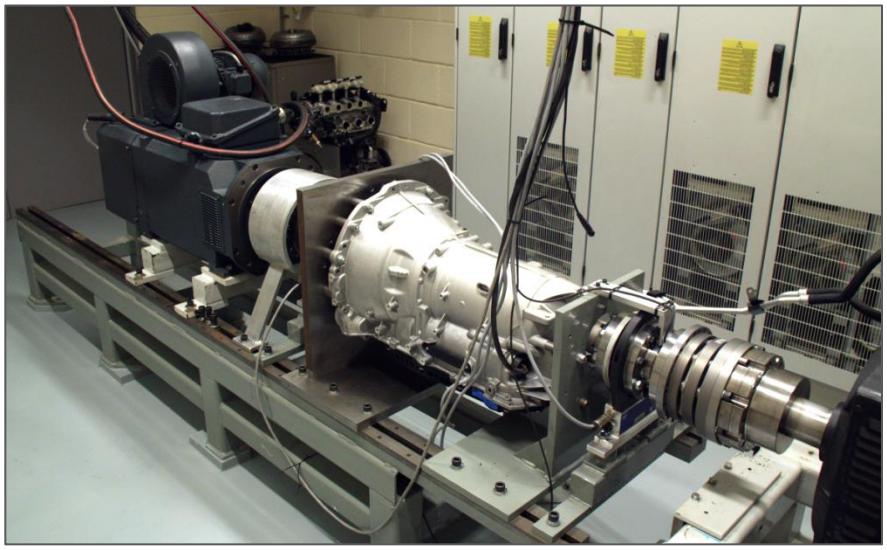

Figure 3.2: Upgraded transmission test facility – hysteresis loop testing mode

The custom connection flanges between the rig components were designed using Siemens NX 7.5 CAD software and manufactured from EN24T steel. The transmission and the pulsation generator were mounted on supporting brackets (steel gauge plate) to minimise any unintended damping of torsional vibrations; i.e. from a source other than the torque converter damper. The design of the flanges allows torque converters to be easily changed and the rig to be easily reconfigured, e.g. from transmission only (hysteresis loop) testing (Figure 3.3) to a pulsation generator torsional vibration arrangement (see Figure 3.4).

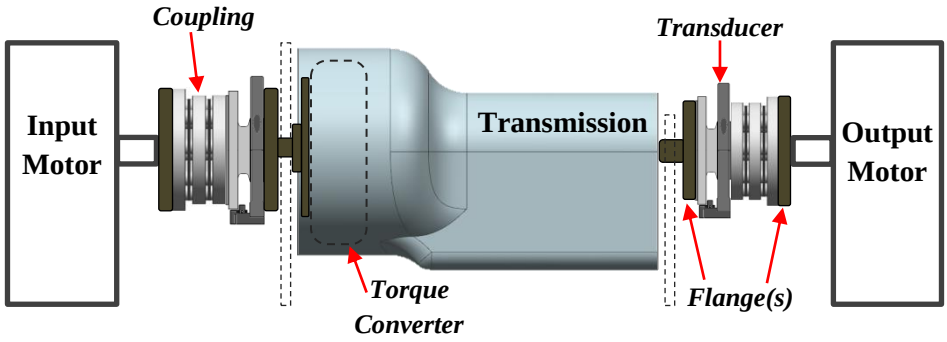

Figure 3.3: Rig schematic for Hysteresis loop testing

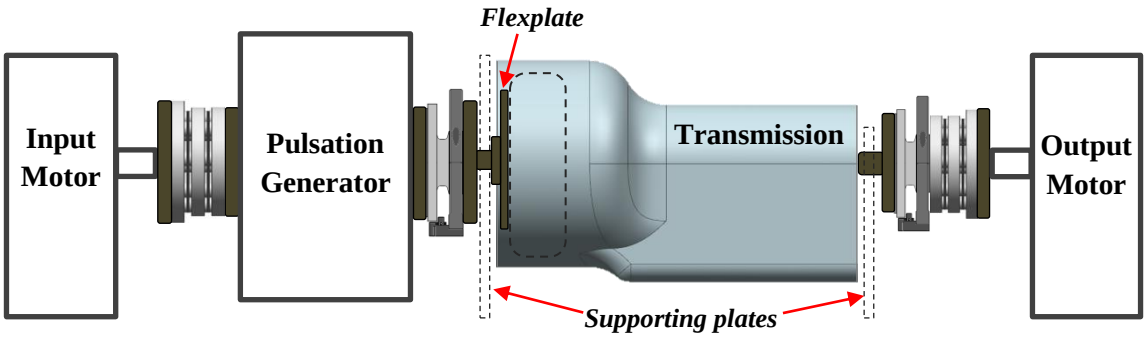

Figure 3.4: Rig schematic for Torsional Vibration testing

To compensate for any axial misalignment and to protect the dynamometers two torsionally stiff ROBA couplings were used; one directly after the input motor and one directly before the output motor (see Figure 3.4). To minimise misalignment a laser level was used to position the transmission, pulsation generator and input dynamometer (see Figure 3.5). The torque is transmitted from the connection flanges to the transmission (torque converter) via a specially designed shaft that is attached to the flexplate; this shaft is supported by the transmission mounting plate using a double row angular contact bearing.

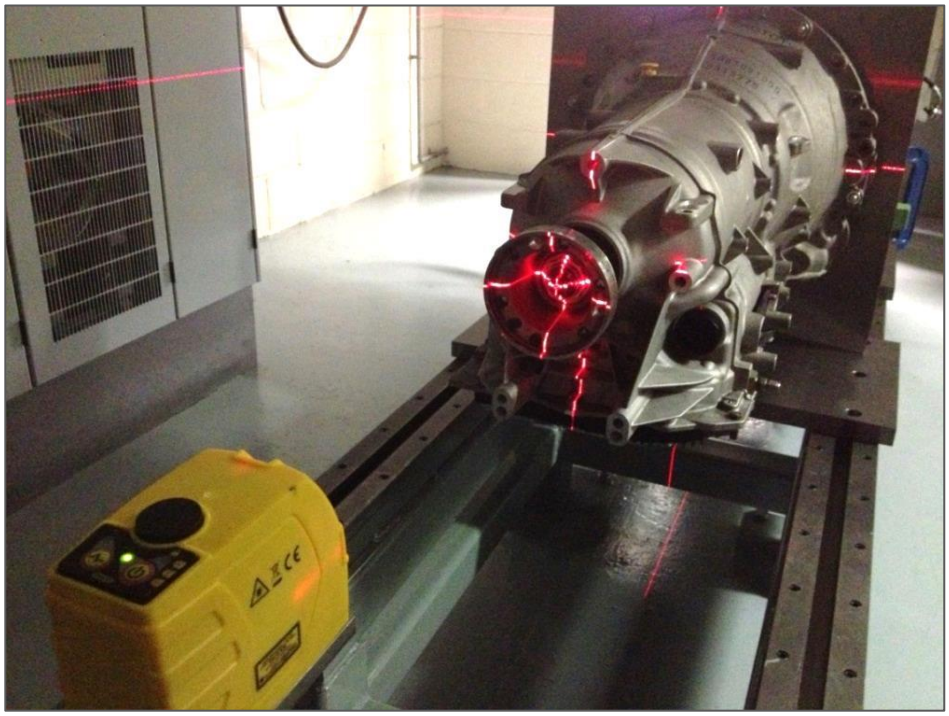

Figure 3.5: Laser alignment of the transmission

3.1.3 Instrumentation

As discussed in section 2.2.4, there are three main methods used to collect torque or speed measurement data from driveline tests; flexplate measurements, Laser Doppler Vibrometers, optical sensors and non-contact rotary sensors (or flanges).

Measurements of torque and speed (angle) were required to be taken simultaneously in at least two locations on the driveline in order to assess the torsional vibration attenuation performance of the damper. The cost of a pair of LDVs exceeded the budget available, especially when the additional cost of a pair of torque transducers was taken into account (LDVs are only capable of measuring torsional velocities). While an instrumented flexplate could be installed (a flexplate is already used to transmit drive to the gearbox system – see Figure 3.4) it would only be capable of taking measurements from before the damper; an additional, different unit would be required in order to take measurements on the transmission output. An instrumented flexplate would allow measurements to be taken very close to the damper input; however, it was preferred that the instrumentation on both the input and output of the damper be identical to ensure as high a level of accuracy as possible. The accuracy and reliability of optical sensors did not meet the desired specification due to their sensitivity to dust (particulates) and oil; thus the decision was made to opt for non-contact rotary sensors.

The instrumentation selected was a pair of T40B 2kNm torque transducers produced by HBM (see Figure 3.6); they were also fitted with an (optional) speed measurement system. Their flange-type design allows them to be easily installed at multiple locations along the rig between the custom connection flanges and Mayr ROBA branded couplings (see Figure 3.4). The T40B transducer uses strain gauges, fixed to the outer diameter of a specially designed flange, to measure deformation (strain gauges change their resistance proportionally with the strain placed on them). Due to the behaviour of the strain gauges used in this form of measuring bridge, this type of non-contact sensor has excellent linearity and hysteresis characteristics; it allows both positive and negative torque to be measured even when the flange is stationary [89]. To ensure adequate torque capacity, the 2kNm version of the T40B transducer was chosen; this transducer has low rotor (flange) weight and low mass moment of inertia, reducing any potential impact on torsional vibrations. It had a bandwidth (measurement frequency range) of 3kHz, and is rated for use at up to 15,000rpm; this far exceeds the 4,000rpm the dynamometers are limited to.

The magnetic rotational speed measurement component is located on the second ring of the flange (see Figure 3.6); this system has a resolution of 1024 pulses/revolution with a digital A/B/Z (reference signal) output. This type of speed encoder consists of a magnetic strip mounted around the flange ring, with a sensor (readhead) that reacts to changes in magnetic fields as the system rotates [89]. For data acquisition a DEWEtron Dewe-43A 8 channel unit (see Figure 3.6) was used; this box is easy to install and compatible with a wide range of instrumentation systems. It is equipped with 8 universal analog inputs and 8 advanced 32-bit counter inputs which support event counting, encoder input, period, pulsewidth, duty cycle and frequency measurement [90]. This unit was used in conjunction with the DEWESoft data analysis and acquisition software (v7), which allows for fast, real-time data analysis including analysis of torsional vibrations and order tracking.

Figure 3.6: HBM T40B torque transducer and speed measurement system (Left) [91], DEWEtron Dewe-43A data acquisition box (Right) [90]

3.2 Transmission communications architecture

Before testing of the transmission can begin, communications between the rig control system (CP Cadet v14) and the transmission ECU (Electronic Control Unit) must be established. The two units communicate using a CAN (Controller Area Network) bus message based protocol, as ECUs would do in a vehicle; each frame (message) consists of an identifier (ID – this must be unique) and up to eight bytes of information. In order for communication to be established and control of the gearbox systems (e.g. gear changes) to be obtained, the transmission must receive certain key CAN messages at particular rates. What messages are required is determined by the calibration that is flashed (programmed) on the gearbox ECU; this flashing process can be performed using ETAS hardware and the accompanying ETAS INCA software.

When establishing CAN communications, a database file that identifies the properties of each of the frames (e.g. length of message, expected numerical range) must be produced. A configuration file is used in conjunction with the database file to set the speeds (e.g. 40Hz) the CAN messages are sent at, as well as their values (e.g. fixed or from a particular CP channel). In order to prevent the communications system failing and timing out it is important to ensure that the transmission ECU receives all of the CAN messages it is expecting and that they are sent at the correct rates.

Some CAN messages are required to send fixed value signals; certain key frames (such as temperature) require an accompanying quality factor message to also be sent. This quality factor tells the (transmission) ECU whether or not the accompanying signal can be trusted (i.e. is accurate). If the quality factor transmits a value that identifies a message as faulty, the transmission will enter a reduced performance mode often referred to as *limp home*. The primary objective of this mode is to ensure the driver and vehicle can still function, while preventing further damage; in an automatic gearbox this mode typically prevents the driver from selecting gears and limits

performance. If the transmission enters this mode on a test rig it will severely impact its behaviour and the results; thus it is important to send the correct values for these error detection messages.

On a test rig (when the transmission is being tested without a vehicle), the rig control system must also be programmed to send some simulated (not fixed value) signals on the CAN bus that the transmission would typically receive in-vehicle; for example engine or vehicle speed. Speed and torque measurements from the input dynamometer can be used instead of engine signals; the value of other signals that would normally be transmitted by instrumentation or vehicle hardware can either be calculated (e.g. vehicle speed) or simulated (gear changes) using programme coding (Visual Basic). In order to establish communications between a gearbox and rig control system it is essential that key required CAN messages are identified (without which the transmission will not function correctly) and that messages from the transmission ECU can be interpreted correctly (e.g. gear selected, fault codes). It is also recommended to have a method for clearing the error code memory of the transmission ECU – for this project an additional computer unit that is produced by the manufacturer of the gearbox was used to clear fault codes, though it is possible to programme and send these signals using the rig control system.

3.3 Experimental Methodology

For all damper tests the transmission was run in Sport mode, allowing gears to be selected manually by the user. As the focus of this study is the simulation of the torque converter damper, rather than the behaviour of other components, 6^{th} gear was chosen due to its 1:1 drive ratio. Torque was controlled using the input dynamometer while the output dynamometer was used to control speed; the 1:1 ratio from running in 6^{th} gear means the input and output speeds would be very similar. The transmission is a complicated system which includes clutches, gear sets, and bearings; many of these components have the potential to contribute to NVH issues or affect torsional vibrations. Unfortunately, there is currently no reliable methodology available for taking the required measurements from between the torque converter and the transmission; the effect that transmission component may have on the torsional vibrations outputted from the torque converter damper cannot be experimentally quantified. Transmission NVH issues can be caused by, among other things, clutches being engaged or disengaged [92]; gear noise can also be produced by the meshing of gears in the planetary gear sets that allow gears to be changed in automatic transmission [93]. Thus using only one gear for all the tests, as well as using a gear with a 1:1 ratio, helps minimise the effect the transmission may have on the torsional vibrations that pass through it.

The standard vehicle CAN was modified to ensure that the torque converter clutch would remain locked-up for as large a proportion of the speed range as possible; the lowest speed that could be achieved with full lock-up was ~830rpm. In order to minimise any potential clutch slip (which could affect the results) the CAN was set to over-lock the clutch – the maximum possible oil pressure was applied to the clutch at all times. These modifications allowed the locked-up torque converter (and therefore damper) to be tested at lower engine speeds, where normally it would either be unlocked or using clutch slip to mitigate torsional vibrations. This larger test range results in more data available for validation and therefore a higher confidence level in the final simulation and resulting conclusions on damper behaviour. Clutch slip is typically used at lower speeds to compensate for the poor performance of the damper (see section 2.1.2); by removing this mitigating factor and more closely examining damper behaviour in these regions the causes of poor damper performance can be more clearly understood.

Before performing any tests it is important to stabilise the system, especially the temperature of the gearbox fluid. To do so, the transmission was run at ~1500rpm in 3^{rd} gear with a ~150Nm mean torque input; a few test runs showed this combination to be one of the more efficient ways of heating the gearbox. The transmission was held at this test point until its oil temperature stabilised at approximately 80-90ºC; this process helps ensure a consistent and repeatable performance during testing.

The cooling system for these experimental tests used the standard in-vehicle radiator with airflow provided by the test cell extractor systems. A later project investigating the efficiency of a similar 8-speed gearbox utilised a Lauda Integral T10000W process thermostat (with integrated cooling system) to control the transmission temperature to a desired set point. These tests demonstrated that the 9kW heater and 13kW (at 20ºC) chiller system were capable of holding the transmission temperature stable anywhere in the range of 10-90ºC (during testing). These transmission efficiency tests (using normal in-vehicle CAN programming) demonstrated that in 6th gear a temperature change of 20ºC (70 to 90ºC) resulted in a mean change in transmission efficiency of only 0.5% across the desired torque and speed range. Thus it can be reasonably assumed that as long as the transmission was run at approximately the same temperature for each test run, the effect of oil temperature on the behaviour of the damper (through changes in oil viscosity) would be minimal and can be ignored.

3.3.1 Hysteresis curve testing

In order to produce a hysteresis curve a torque ramp must be applied to the damper; this was done using the built in test controller in the CP system. The torque demand was set to the starting torque (e.g. 0Nm) and the system allowed to stabilise there; the torque ramp was then applied, the system allowed to stabilise at peak (positive or negative) for 2s before the returning ramp was applied (see Figure 3.7). Data was collected from just before the beginning of the ramp until just after to ensure adequate data capture. Angle windup was calculated by comparing the absolute angle of the flanges before and after the transmission; the difference between them is the windup.

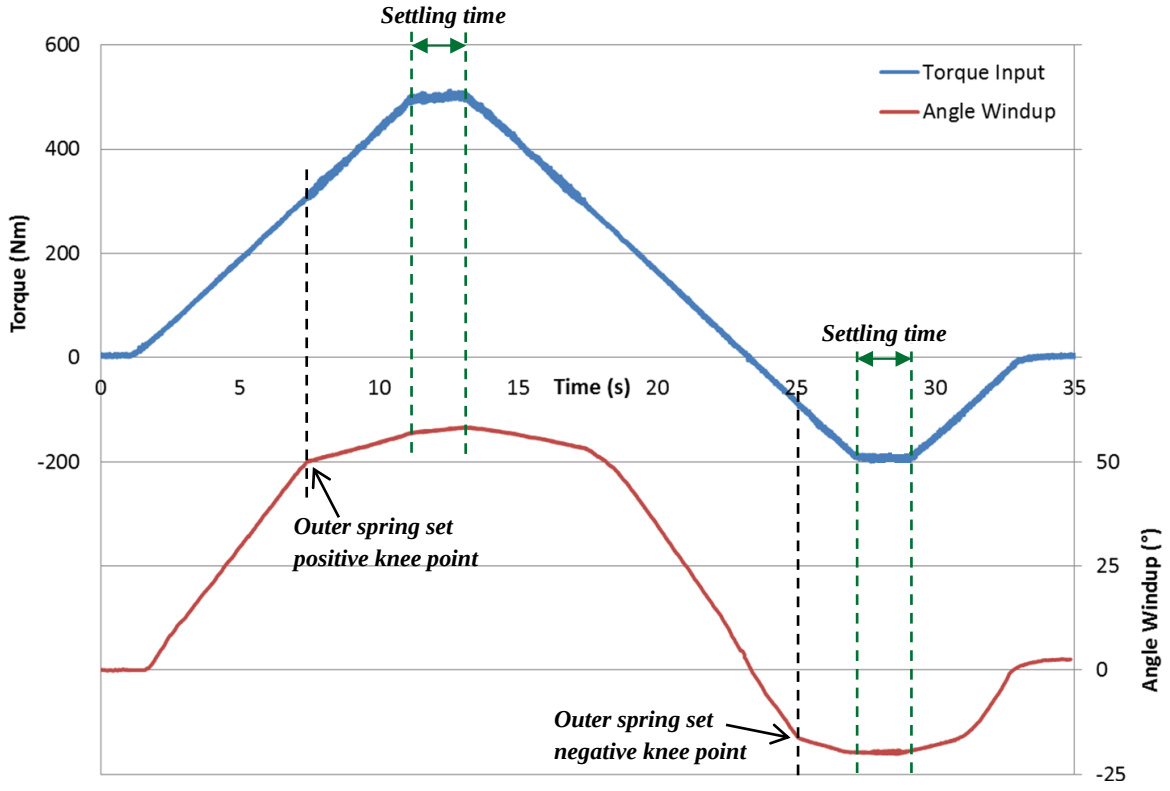

Figure 3.7: An example full torque ramp used to examine the hysteresis curve behaviour of the damper

As can be seen from Table 3.1, two general forms of torque ramps were performed; neutral ramps starting at 0Nm and those starting at a set positive or negative torque. The ramps that begin at 0Nm can be used to produce either a positive or negative only ramp or full ramps that cover both regions. In order to reach torques below ~20Nm (including negative torques) a false torque level signal was sent to the gearbox ECU; by telling the ECU the torque is higher than it actually is (e.g. 100Nm) the transmission can be tested at low and negative torque levels without the selected gear changing or the clutch becoming unlocked.

The torque ramps in Table 3.1 were selected in order to ensure the damper was tested in a variety of situations; it was unknown how damper behaviour might change with regards to speed or as the transition between positive and negative torque occurred. For the majority of the torque ramps four speed points (250rpm apart) were considered sufficient; however, to ensure any speed-dependent behaviour was fully captured, one torque ramp set was performed with speed increases of just 100rpm between each test. As it was also unknown if and how damper behaviour may be affected by the test torque start point (e.g. 0Nm or 100Nm) some positive and negative only loops were performed at 1500rpm; two of these loops crossed the damper knee points while the other two tested below or above only. Testing the damper with some torque loops that do not approach the 0Nm crossover – the zone where some unwanted slip may occur – allows whether or not crossing the neutral position has an effect on damper behaviour at higher torque levels to be determined. While an excess of data is not a disadvantage, in hindsight fewer tests could have been performed; for simulation purposes two test types are recommended, one that forms a loop that stays below the damper knee points and another that extends above them (both should go into the positive and negative torque regions). While tests that begin at non-zero levels can be used to check consistency (e.g. overlay loops onto full ramp results) in this situation they cannot really be used with the simulation as the construction of the model requires each test run to begin at 0Nm torque input.

Table 3.1: Hysteresis loop (torque ramp) test matrix – performed tests highlighted in green, with power range given

					Power Range (kW)								
	Start point	**+ ve Peak**	**- ve Peak**	**End Point**	*Speed (rpm)*								
					1000	**1100**	**1200**	**1250**	**1300**	**1400**	**1500**	**1750**	**2000**
Torque (Nm)	0	100	-100	0	0-10			0-13			0-16	0-18	0-21
	0	450	-180	0	0-47	0-52	0-57	0-59	0-61	0-66	0-71	0-82	0-94
	0	500	-200	0	0-52			0-65			0-79	0-92	0-105
	100	300	-	100	10-31			13-39			16-47	18-55	21-63
	-50	-	-150	-50							8-24		
	250	350	-	250							39-55		
	350	450	-	350							55-71		

In order to determine the best ramp application rate to produce the most reliable and repeatable results – as the aim here is not to excite the damper with high frequency fluctuations but to assess its windup angle and hysteresis at different torque levels – a range of ramp rates were applied and the angle windup across the transmission at the peak ramp torque compared (see Figure 3.8). A ramp with a very low rate of 20Nm/s (5s to apply a torque change of 100Nm) was used as a baseline for comparison; as can be seen from Figure 3.8, higher ramp application rates increase the error (the difference from the baseline) in the resultant angle windup at the ramp peak torque (120Nm). To ensure accuracy and repeatability, but to minimise test time, a ramp rate of 50Nm/s (2s for a torque change of 100Nm) was selected.

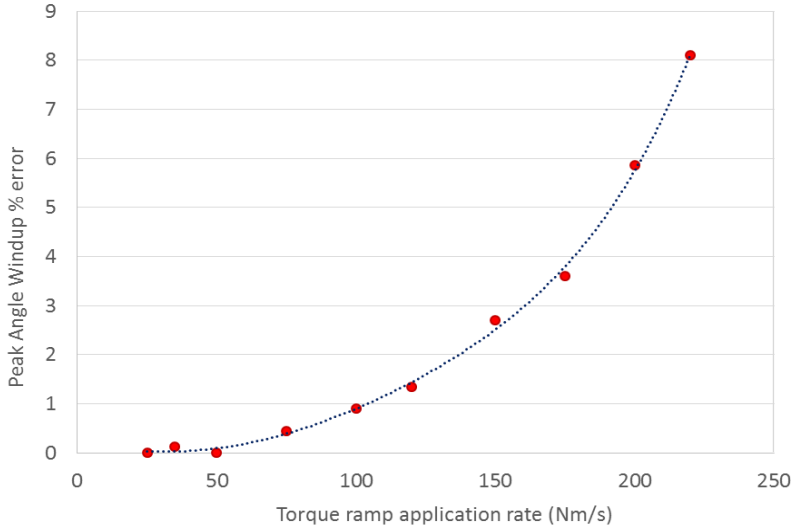

Figure 3.8: Hysteresis loop torque ramp application rate and effect on angle windup value at peak torque

The error is introduced not by damper behaviour changing (these torque ramp rates are far below that of engine excitation) but by the PID control of the dynamometer; the system was programmed to avoid the motor response overshooting the demand. By avoiding overshoot the system is more stable but does give a less responsive controller; essentially the error between the demand and the system response increases at higher ramp rates. As can be seen from Figure 3.9, when the demand approaches its peak value the actual ramp application rate of the dynamometer slows; at higher ramp rates this error between demand and response starts at a much lower torque value than at slower ramp rates. This extended period of higher torque demand-response error appears to cause the compression of the springs to creep, altering the peak torque angle windup value.

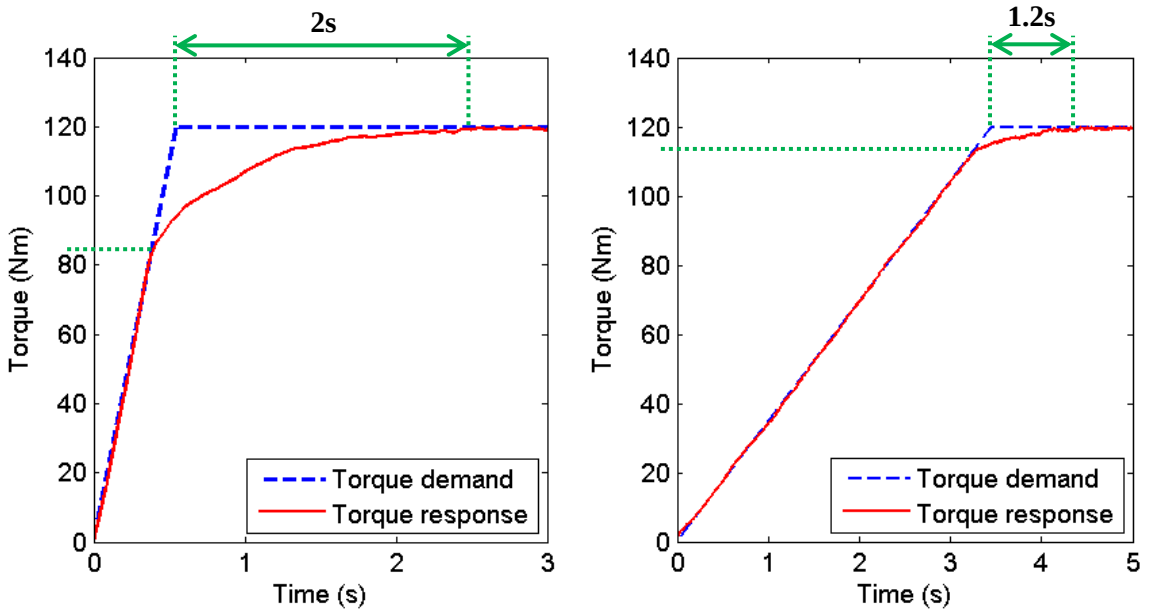

Figure 3.9: Comparing torque demand and dynamometer response – at 220Nm/s (L) and 35Nm/s (R) ramp rates, 1500rpm

For each hysteresis loop (torque ramp) the tests were repeated 4 times; in order to assess repeatability the angle windup values at a range of key points (0Nm crossing, knee point locations, ramp peak torque) were compared for each test. The results from this data quality analysis at each test speed can be seen in Figure 3.10; the mean angle windup error (the difference between each repeated run in a test) was found to be less than 0.5 degrees across the speed range, with the maximum error being 1.2 degrees (at 65 degrees angle windup – a 1.8% error). From this it can be concluded that the windup tests at the chosen ramp rate of 50Nm/s are very repeatable and the confidence level in the accuracy of the results across the speed range is high.

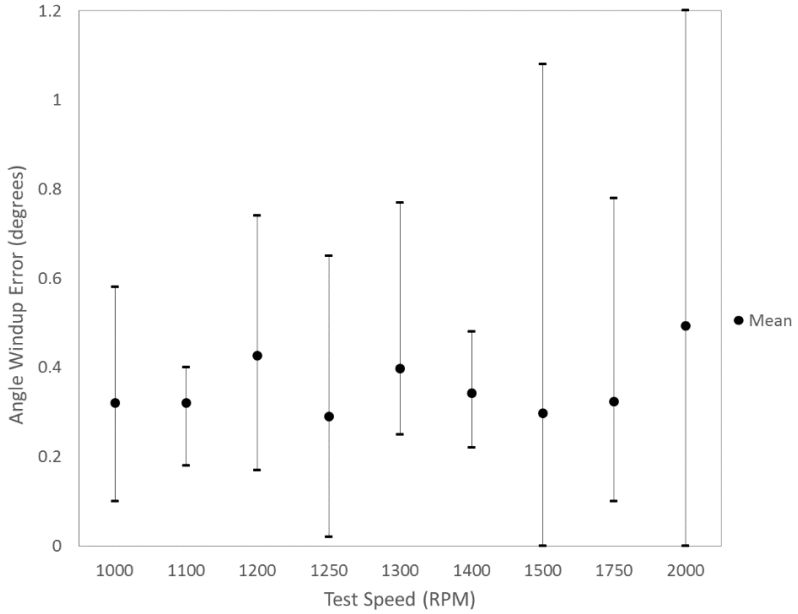

Figure 3.10: Repeatability of hysteresis loop tests: comparing angle windup error at multiple key points on each loop

3.3.2 Pulsation Generator (torsional vibration) testing

As the bandwidth of the electric dynamometers (15Hz) is inadequate for high-frequency torsional vibration production, a novel pulsation generator unit concept has been developed. This unit can be easily installed on the rig between the input motor and the transmission (see Figure 3.4); the input dynamometer is used to control the mean torque level of the fluctuation signal, while the compression of pressurised air (1.5 and 2.5 bar) produces large torque fluctuations. The full development, implementation and analysis of this concept is presented in Chapter 4.

When the pulsation generator was installed on the test rig, the dynamometers were controlled in the same manner as the hysteresis loop tests; the output dynamometer was controlled to a set speed point while the input dynamometer maintained the desired mean torque. In order to ensure adequate resolution (without the need for interpolation) when producing Fast Fourier Transform (FFT) colourmaps the tests were performed every 10rpm. A lower resolution of 20rpm (see Figure 3.11) could potentially have been used (in combination with data interpolation) with minimal effect on overall trends. However, when testing around the location of any knee points, it is recommended that a higher resolution be maintained to ensure that the location of the knee points (the torque level at which they occur) can be accurately detected (see section 6.2.1).

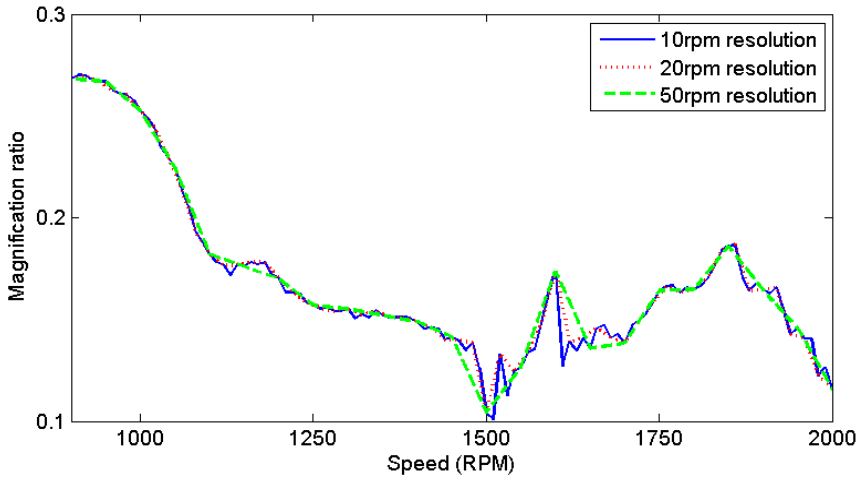

Figure 3.11: Comparing the effect of different test resolutions on magnification ratio (ratio between damper output and input torque) for a 2nd frequency order cut

Two categories of test were performed: engine torque trace and mapping. During torque trace testing the mean torque at each speed test point was set to that of an engine typically used with the damper being tested; the tests mimicked the torque curve of the engine when run using WOT (wide open throttle). The lowest speed tested was 1200rpm, due to availability of torque curve data; the performance of the rig limited the upper speed test point to 2800rpm. For the pulsation generator mapping tests the speed range examined was lower, down to 900RPM; this was limited by the ability of the system to maintain 6th gear and an over-locked damper. Mean torques over the range of 50-500Nm at increments of 50Nm were tested; this allows damper performance to be assessed over a much wider range of mean torques (and therefore mean windup angles) than that seen using the engine torque curve (240-415Nm).

The datasets produced using this mapping testing regime are very useful for damper characterisation, as the performance of the simulation (compared to the test data) in a variety of situations (e.g. both spring sets active or one set inactive) can be examined over the full key speed range (900-2000rpm). The more data available for validation over a wider range of situations, the more confidence will be gained in the representative performance of the simulation. An extended testing regime also allows damper behaviour in areas of poor performance to be examined, which should help increase understanding of why these areas occur. The data produced from torque trace testing – more normal operating conditions – is the primary metric with which damper simulation performance will be evaluated; the smaller increments in mean torque (largest 11Nm, on average 1Nm) are also more suitable for evaluating behaviour around the damper knee points.

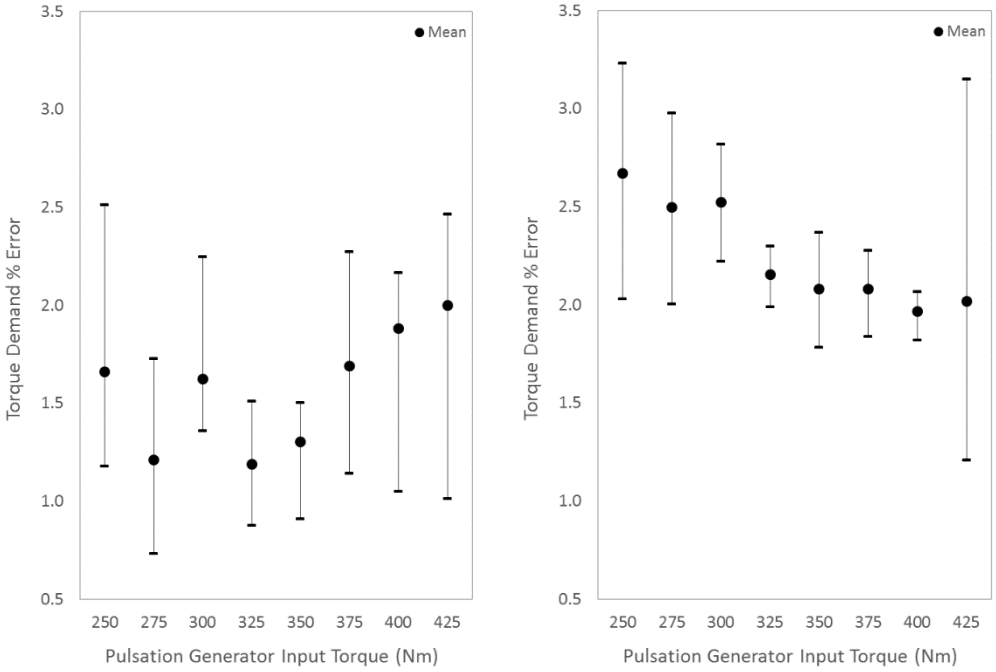

Figure 3.12: Percentage error between actual and demanded torque at torque converter damper input during 1.5 bar (Left) and 2.5 bar (Right) torque trace testing

Due to the design of the pulsation generator some torque and speed fluctuations are sent upstream (to the input dynamometer) as well as downstream (to the transmission). This means that the average torque demanded from the input dynamometer and the torque outputted from the pulsation generator can differ slightly. However, the mean percentage torque error (calculated by comparing the error to the demanded torque) is below 2% when the compressed air pressure is set to 1.5 bar and less than 2.8% when set to 2.5 bar. The maximum error is sometimes slightly higher when the air pressure is increased (see Figure 3.12) or at lower mean torque levels (<250Nm – see Figure 3.13) but it is still within acceptable levels. Low levels of torque error at the input of the damper are essential to ensure that conclusions drawn from comparing test points with the same mean torque levels (e.g. at different speeds) are valid assessments of damper behaviour at that level of spring compression.

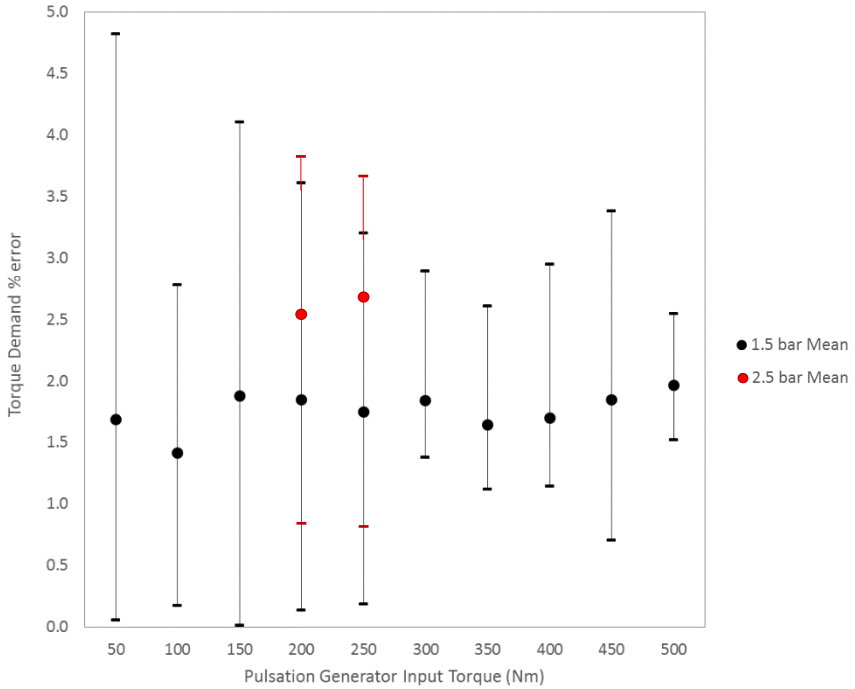

Figure 3.13: Percentage error between actual and demanded torque at damper input during mapping tests[1]

[1] Component failure prevented the completion of mapping tests at 2.5 bar – see section 4.4 for details.

3.4 Data Analysis and processing

Data was logged at a resolution of 1×10^4 points per second for hysteresis loop testing and 2×10^5 points per second during pulsation generator testing. Data logging resolution was lowered for hysteresis loop testing due to the extended time taken for each test (e.g. 20s instead of 2s) and the lack of the requirement to record high-frequency signal fluctuations. A much higher resolution was chosen for the torsional vibration testing to ensure that all the desired signal features were recorded.

As discussed above, each dynamometer (input/output) has a PID controller that controls either torque or speed; here the input dynamometer is used to control the torque that is applied to the rig components, while speed is controlled using the output. When the motors are coupled like this it must be decided which controller performance is more important (torque or speed) otherwise the two controllers will fight each other, possibly resulting in loss of control of the rig and component damage. Even if emphasis is placed on the control of one particular variable (e.g. torque) there will still be an interaction between the two motors; measured torque variations at the input dynamometer will affect the measured speed induced by the output dynamometer. Thus the torque and speed signals inputted into the transmission will not be perfectly smooth demanded levels; there will be some fluctuations (see Figure 3.14). Compared to those produced by the pulsation generator these fluctuations are insignificant; however, for hysteresis loop testing, they result in a filter needing to be applied to the data in order to be able to clearly analyse and present the results. In order to smooth the hysteresis loop data, a 1st order low pass filter with a break frequency of 10Hz was used.

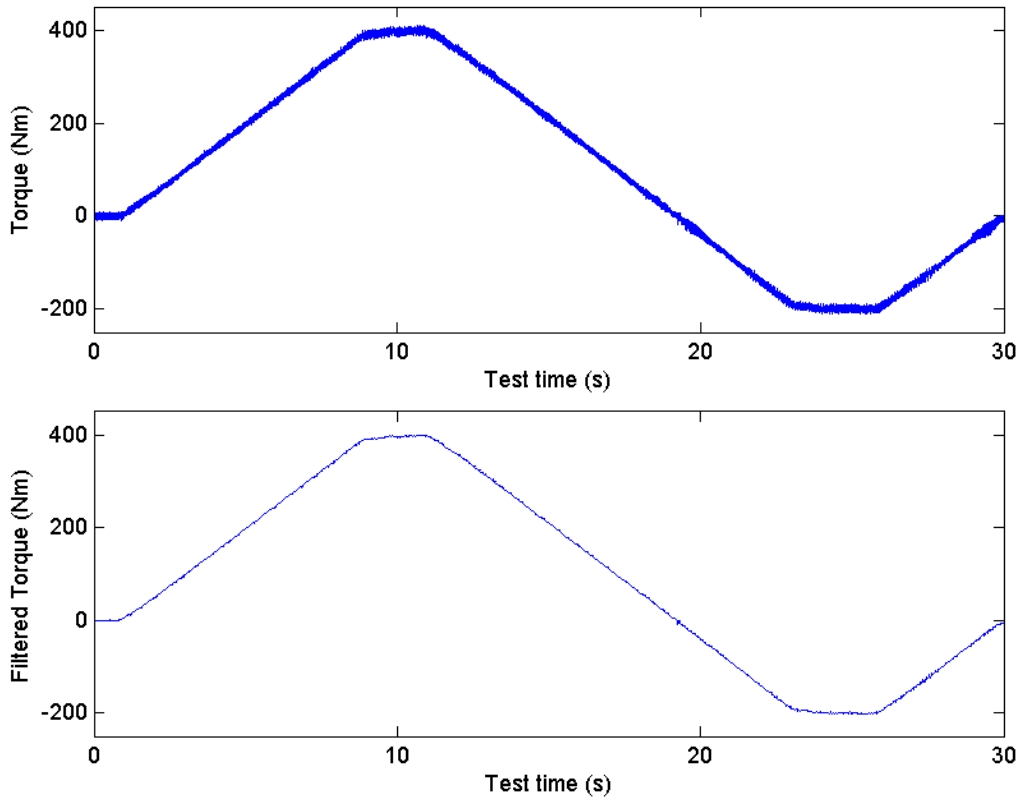

Figure 3.14: Comparing unfiltered (Top) and filtered (Bottom) 1500rpm torque ramp data

When analysing high-frequency torsional vibration data (such as the output from the pulsation generator tests), the results are commonly discussed in terms of orders. An order is the number of times per revolution an event occurs, thus the frequency an order occurs at increases with test speed. In order to find the frequency and amplitude of these peaks (orders) at each speed test point a Fast Fourier Transform (FFT) is used. FFTs allow a fluctuating signal to be separated into its component sine waves.

Fourier's theorem states that any continuous time domain wave function can be expressed as the sum of multiple sine or cosine waves. Each of these waves will have their own amplitude, frequency and phase. To perform the FFT, a sample of data is taken and offset by subtracting its mean value. Offsetting the sample before performing the FFT removes the false peak that can occur at around 0Hz, without affecting the results. The larger the sample, the more accurate the results (the frequencies of the signal are more clearly defined) but the larger the variables (and therefore processing power required). A sample size of 1.25s (2.5×10^5 data points) was found to be optimum; higher sample sizes can be used but do not produce any significant improvement in accuracy. A Hanning window was also applied to reduce any potential spectral leakage. Windowing is a useful tool when performing FFT analysis on measured data; the FFT assumes that there is an integer number of cycles in the test sample. However often this isn't the case, leading to the spreading out of a signal from its frequency bin – also known as spectral leakage [94]. Windowing reduces the amplitude of the discontinuities (differences between beginning and end of the signal due to non-integer periods), thus improving frequency resolution.

Performing a FFT on a torque or speed signal outputted from a fluctuation source (e.g. engine) or a damper allows more to be learnt about the behaviour of the components, through understanding which components are producing or reducing different frequencies. For example, in a four stroke 4-cylinder combustion engine the firing (ignition of the fuel/air mix in one of the cylinders) takes place two times in every 360° revolution of the crankshaft; at 1500 rpm this firing will be taking place 50 times a second (50Hz). This is known as the firing frequency and is typically the dominant (largest amplitude) vibration frequency in an engine signal. By being able to separate a signal into its component sine waves information can be gained by comparing the frequency – how often an event occurs per second – of the event to known event frequencies (e.g. cylinder firing).

3.5 Summary

In this chapter the experimental facilities and transmission setup have been outlined, as well as the basic testing and analysis procedures. Some upgrades to the PVRC transmission test facilities were required, including the development of a novel pulsation generation method; the development of this method can be seen in Chapter 4.

The key outcomes from this chapter have been summarised below:

- The 15Hz bandwidth of the electric dynamometers (paired with a twin ABB regenerative drive system) installed in the PVRC transmission test facility is inadequate for high-frequency torsional vibration production; a novel pulsation generator unit concept was required (Chapter 4).

- The transmission used in this project is an 8 speed automatic; multiple torque converter damper designs can be used with the same transmission.

- The EN24T steel connection flanges have been custom designed to allow the rig to be easily reconfigured between tests. ROBA couplings were used to compensate for any axial misalignment.

- A pair of HBM T40B 2kNm torque transducers (with speed measurement) was selected for use alongside a DEWEtron Dewe-43A 8 channel data acquisition unit.

- Communication between the rig control system (CP Cadet v14) and the transmission ECU was established; an additional computer unit (produced by the manufacturer of the gearbox) was used to clear fault codes and monitor the gearbox status.

- During all damper tests the transmission was run in 6th gear (in Sport mode); the torque converter lock-up clutch was set to over-lock, to allow testing at low speeds, while minimising any potential clutch slip.

- Test runs demonstrated that the most efficient way of stabilising the system (e.g. the temperature) was to run the transmission at ~1500rpm in 3rd gear with a ~150Nm mean torque input; the oil temperature stabilised at 80-90°C.

- Hysteresis curve tests were performed by using the built in CP test controller to apply a torque ramp to the damper; in order to reach torques below ~20Nm (including negative torques) a false torque level signal was sent to the gearbox ECU.

- Ramp tests that investigated the effect of speed, test start point and the 0Nm crossing point were performed; in hindsight fewer tests could have been performed. For simulation purposes two test types are recommended; one that forms a loop that stays below the damper knee points and another that extends above them.

- A clear link between torque ramp application rate and angle windup (hysteresis loop) error has been established; a ramp rate of 50Nm/s was chosen to ensure repeatability while minimising test time.

- When performing torsional vibration testing (for FFT calculations) a test point was taken every 10rpm. A lower resolution could be used with minimal effect on overall trends; however a lower resolution ensures damper behaviour is fully captured (e.g. at knee point locations).

- Data was logged at a resolution of 1×10^4 points per second for hysteresis loop testing and 2×10^5 points per second during pulsation generator testing.

- A low-pass filter was used to smooth the hysteresis loop data. FFTs have been used to separate the torsional vibration testing signals into their component sine waves for vibrational order analysis.

Chapter 4 Development of a Pulsation Generator

The biggest concern when investigating NVH issues is the accuracy of the vibrations the system (e.g. driveline) is subjected to, compared to those in a real-world vehicle scenario; the same applies when investigating how to characterise the behaviour of a torque converter damper. In order to fully understand how the movement of the components affects its ability to dampen torsional vibrations, the experimental data that will be used to validate the damper model must form an accurate representation of how the damper behaves in a vehicle. Essentially, a full overview cannot be obtained by testing a damper at a constant torque or speed or through the use of low frequency torque ramps (hysteresis loop testing). While these methods are acceptable for understanding general trends in drivetrain or damper behaviour, they will not adequately excite the damper. In order to accurately assess damper performance and be able to use the data to validate a simulation, the input to the test object must adequately excite the damper; however, it is currently unknown what this entails. For example, does the excitation signal need to correlate closely to fired engine torque pulsations? Or does adequate excitation mean exciting the damper by a certain fluctuation magnitude over a particular frequency range? The ABB dynamometers installed in the rig at the University of Bath (see section 3.1.1) are able to produce the mean levels of torque (and torque ramps) required in this project but are not capable of producing the high frequency torque fluctuations needed to excite the damper. Thus changes to the rig are required to allow it produce adequate fluctuations. This chapter presents the novel adapted motor concept that was developed and compares other available technology with this novel pulsation generator method.

4.1 Adapted Motored Engine concept

As highlighted in section 2.2 it is not yet understood which engine torsional orders (vibration frequencies) are the most important to produce. Does the signal into the damper need to perfectly match the shape (and therefore full frequency range) of the torque and speed output of a fired engine, or will a signal that just imitates the frequency and magnitude of the most dominant order suffice? While the dominant order is typically the engine firing frequency it can vary across the speed range depending on friction and inertial forces. For characterisation and simulation validation it is unknown if the excitation signal even needs to be representative of a fired engine; can a sufficient level of vibration frequencies and magnitudes be identified that adequately excites the damper? A detailed damper simulation can help answer these questions; however in order to produce a validated model, high-frequency vibration test data is required.

It is clear that due to the lack of knowledge available, caution must be taken when choosing the most appropriate pulsation generator technology. Thus a technology that attempts to replicate the full range of torsional vibration frequencies that are present in the output from a fired engine is required. An electrical system is more likely to be able to provide the desired multi-layer transient response; however, the complexities of integrating a new unit into the existing dynamometer control structure went beyond the scope of this project. The cost of replacing the existing dynamometer units with higher bandwidth models with lower inertias also far exceeds the budget available. While mechanical systems tend to require significantly smaller financial outlay the current technology available has not yet been proven to be capable of producing the complicated frequency input desired; the lack of flexibility and low ease of adjustment is also a factor.

Thus an alternative option is proposed: a novel mechanical solution. This mechanical solution is the adaptation of an easily available engine to run in a motored (no combustion) state, with compressed air fed into the cylinders (resulting in them behaving as air springs). The engine chosen for the prototype of this concept is a diesel 2.2 litre four cylinder, selected due to the availability of both the hardware and the fired engine combustion data; combustion data allows the performance of the pulsation generator to be easily compared with that of the equivalent fired engine. This four-cylinder engine is also typically used in-vehicle with the damper (and gearbox) used for testing; however the adaptation methodology is applicable to a wide range of multi-cylinder engines.

4.1.1 Theory

In a fired engine, the ignition of the fuel/air mix in a cylinder forces the piston downwards; this exerts a torque on the crankshaft, causing it to turn. This motored engine method proposes replacing the fuel/air mix that would normally be in the engine cylinders with compressed air. In this concept, the pistons (via the engine combustion process) are not relied upon to rotate the crankshaft; instead, the input dynamometer turns the crankshaft, driving the pistons. The torque (motion) applied by the electric motor causes the pistons to move, compressing the (already pressurised) air in the cylinders even further. This compression increases cylinder pressure; this pressure then exerts a downwards force on the piston (as it would in a fired engine), therefore exerting a torque on the crankshaft. The crankshaft torque produced by the compression of the air is a fluctuating signal, while the input motor drives the crankshaft with a steady (mean) level of torque. These torque signals (the mean and fluctuating signal) combine to produce a high-frequency torque fluctuation signal that is outputted from the pulsation generator. Both the mean and (theoretically) the magnitude of the output torque signal are controllable; the mean by the level of torque exerted on the crankshaft from the input motor, with the magnitude controlled by the pressure of the compressed air that is fed into the cylinders.

In an engine the combustion air is compressed polytropically (assuming the air is an ideal gas). By using Equation 1, the maximum cylinder pressure (P_{max}, bar) when unfired can be calculated from the ambient pressure (P_a, bar) and the engine compression ratio (CR of 16:1 for this particular naturally aspirated 4 cylinder engine).

$$(P_a \times CR)^{1.4} = P_{max} \tag{1}$$

In modern diesel engines the maximum cylinder pressure during combustion is approximately 130 bar (according to indicator diagrams) at peak torque output; if this is inputted into the polytropic process equation (Equation 1), a value of 32 bar is produced for the ambient pressure multiplied by the compression ratio. Thus an ambient (compressed air) pressure of around 2 bar should produce the same maximum cylinder pressure (and therefore peak torque) of a counterpart fired engine.

Due to this it is proposed that the air pressure in the cylinders of the motored engine be set to between 1-3 bar ambient using a compressed air supply; this will give a range of acceptable maximum cylinder pressures (50-225 bar) that should not exceed the damage threshold of the engine components. By being able to adjust the pressure of the compressed air inputted to the cylinders the magnitude of the torque pulsations in the damper input signal becomes (theoretically) controllable. The schematic for the proposed pulsation generator concept can be seen in Figure 4.1.

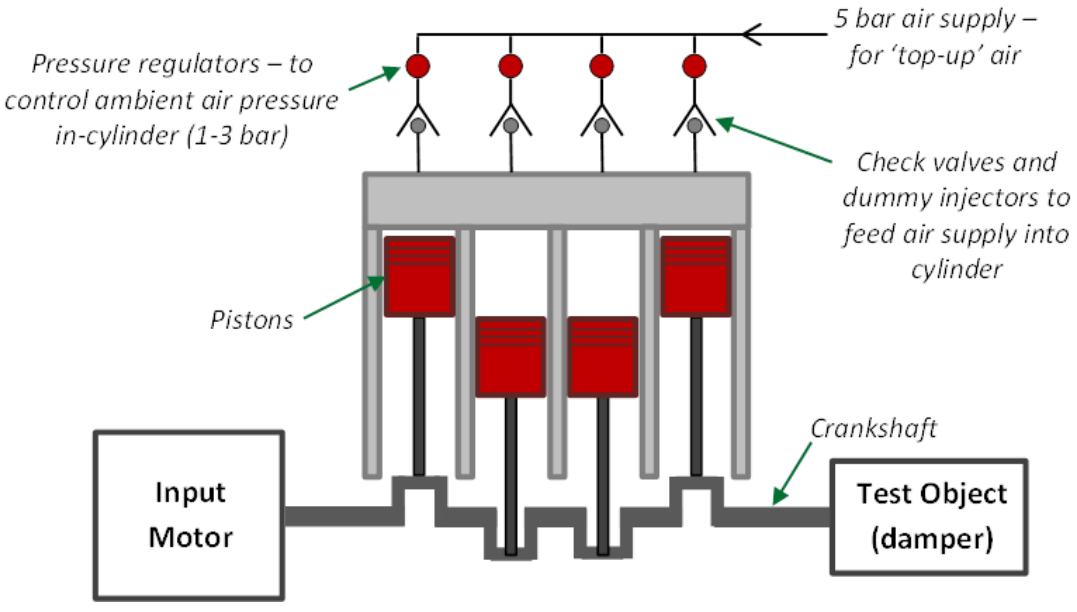

Figure 4.1: Proposed motored engine torque pulse generator

In order for the cylinders to behave like air springs, the inlet and exhaust valves must be deactivated, to prevent the compressed air escaping. This can be done by removing the rockers in the cylinder head (see section 4.1.2). The air is introduced to the cylinder via dummy injectors; to ensure that the cylinder pressure is kept at the required level and to allow *top-up* air flow, a check or reed valve arrangement is required. Top-up air is needed to maintain the cylinder ambient pressure at the desired level, as some losses will occur due to blow-by (air escaping the cylinder past the piston rings). One feature of this concept is the ability to control the pressure of the air being inputted into each cylinder individually, potentially allowing a greater range of torque oscillations to be produced.

Theoretically, these air springs will produce a pulsation similar to the requisite firing torque of a fired engine. However, due to the lack of an exhaust stroke, each cylinder will be firing (compressing pressurised air) every revolution, rather than the once per two revolutions that occurs in a fired engine. This means it is likely that the shape and/or size of torque signal will be affected. Any variance in the frequency of the output torque signal may be a limitation of this system (when compared to a fired engine); the variations from a fired engine are discussed further in section 4.3.2. It should be noted that the aim of the motored engine pulsation generator concept is not to exactly replicate the torque profile of a fired engine; the primary aim is to be able to excite a damper system with high frequency fluctuations.

4.1.2 Implementation

A four cylinder diesel engine that is commonly used in-vehicle with the test object (a torque converter damper) has been selected to be the working prototype of this concept. In order to transform the engine into a torque pulsation generator there are three main modifications that must be completed: the de-activation of the cylinder valves, the addition of a top-up air system and the modification of the oil/cooling circuit. As discussed in section 4.1.1, the cylinder valves can be deactivated by removing the rockers that are located between the valve camshafts and the valves, as well as the cam belts. As can be seen in Figure 4.2 the valves are sprung, so they should remain sealed throughout the pressure cycle without the need for any additional modifications.

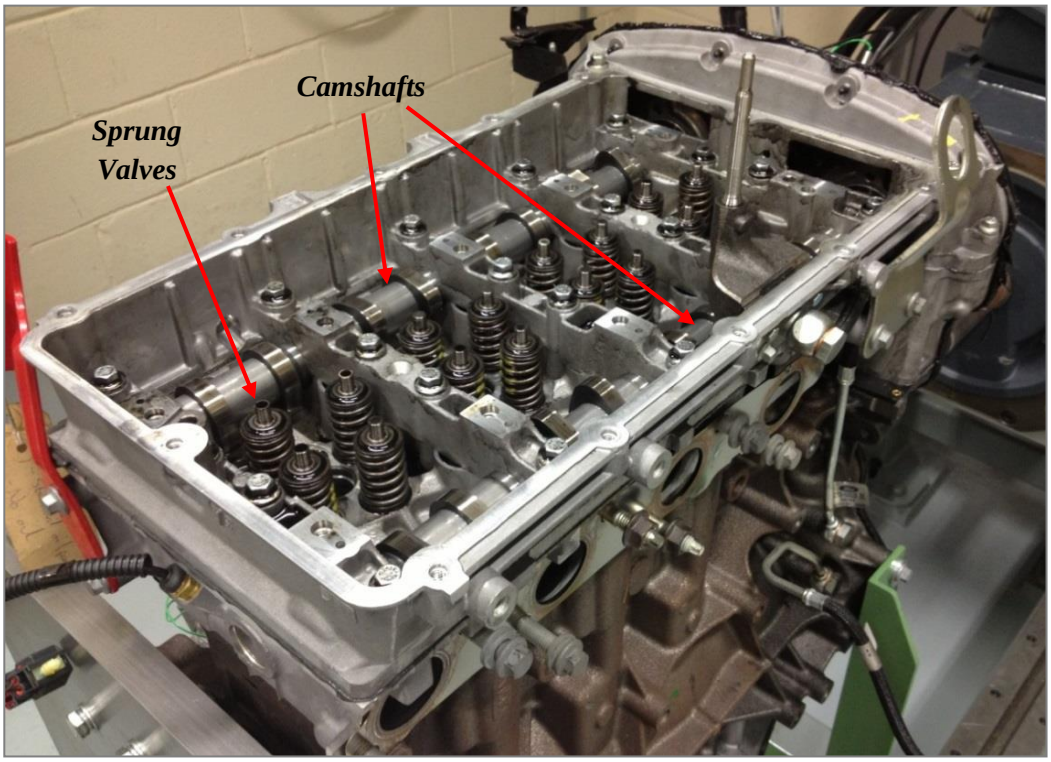

Figure 4.2: Removing the rockers on the pulsation generator to deactivate the valves

The air is introduced to the cylinders via dummy injectors; to minimise cost and ease of conversion the body of the normal engine fuel injectors were used, with the internal components (e.g. nozzle, springs and command piston) removed. This allows the pressurised air to flow freely through them. To ensure that the minimum cylinder pressure (P_a) is maintained at the desired level (1-3 bar) and to allow top-up air flow to enter the cylinder a pressure regulator with an integrated check valve is installed at the top of each dummy injector. The pressure in each cylinder can be controlled individually using these manually adjustable pressure regulators.

Ideally the cylinder air charging system would be controlled remotely from the control desk (outside the test cell). This would allow the ambient cylinder pressure to be adjusted while the rig is running; a control system linked to in-cylinder pressure transducers could also be implemented to ensure the minimum pressure in the cylinder is maintained at the required level. However two of the aims of this concept are to minimise cost and to make the adaptation process as simple as possible; therefore the manually controlled valve system is considered adequate for this proof-of-concept prototype.

No modification of the oil flow path in the cylinder head is required; with the rockers removed the oil drains back into the head, as normal. The completed pulsation generator unit can be seen in Figure 4.3; the unit is cooled using the existing engine water circuit, though the engine water pump has been replaced with an external water feed. The mean torque signal is applied to the crankshaft via a flange attached to the snub nose end, which would normally drive the water pump. This point of the crankshaft is stepped down to a much smaller diameter than the rest of the length, due the lower load profile it would usually be subjected to. This flange-crankshaft connection point was therefore identified as a potential weak point in the system; the torsional forces may well exceed the design limits of this component, causing material failure (see section 4.5). This potential failure could be avoided through the design and use of a custom crankshaft; however this goes against the main aims of this concept (low cost and easily available technology). Thus it was decided that there was an acceptable level of risk associated with this potential component failure; this was after all a prototype design, whose purpose was to test out this concept for a mechanical pulsation generator.

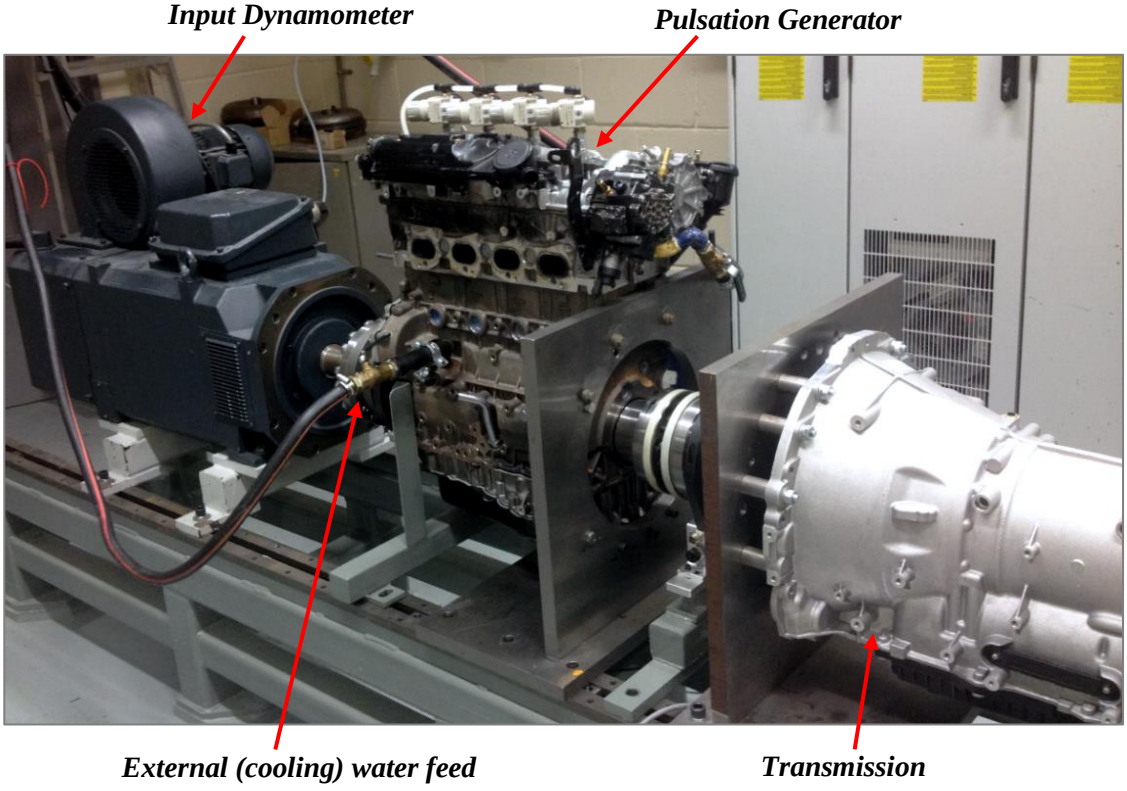

Figure 4.3: Completed pulsation generator mounted on the rig with the transmission

4.2 Development of pulsation generator simulation

The methodology developed by Zweiri et al [85] [86] (see section 2.5) has been chosen as the base from which to develop a model of this four-cylinder pulsation generator unit. The model was constructed in MATLAB Simulink® primarily because it was determined to be the best tool for the accompanying damper simulation (see section 5.6); this methodology was also previously implemented in Simulink by Zweiri et al [85]. A black box model – where only the inputs and outputs of the system are viewable – would not allow the behaviour of different components in the system to be examined. The flexibility of Simulink® also allowed pulsation generator modifications to be more easily modelled than with a typical engine simulation software (e.g. Ricardo Wave). A general schematic of the pulsation generator model can be seen in Figure 4.4. As described in section 4.1.1, in the pulsation generator the torque output is generated by the input electric dynamometer rotating the engine crankshaft (the mean torque input); the resultant movement of the piston assembly compresses the pressurised air in the cylinders producing a pulsating torque signal.

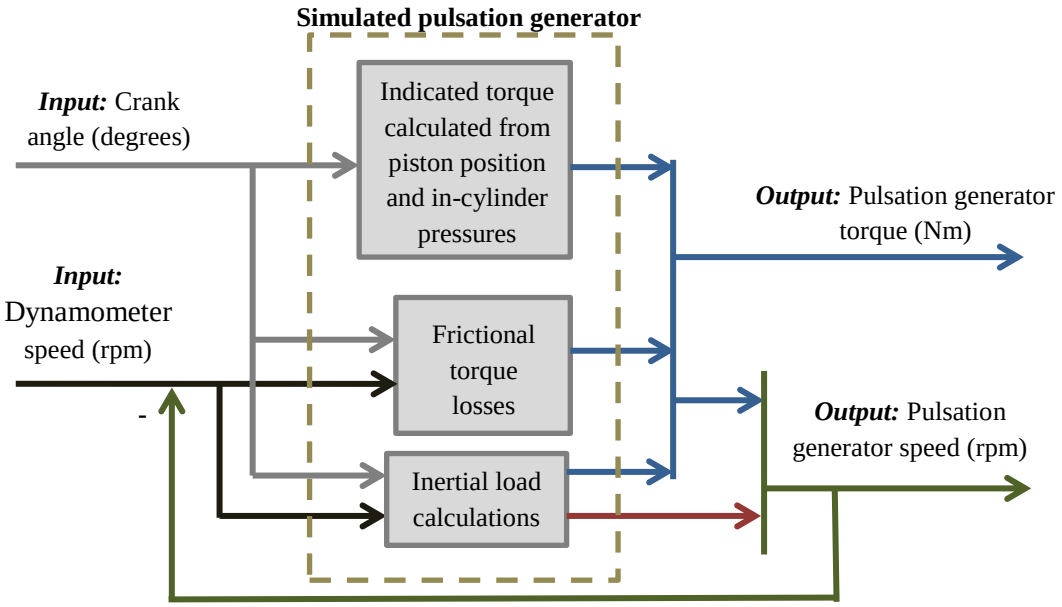

Figure 4.4: Pulsation generator simulation schematic

In the simulation, instantaneous cylinder (air) pressure (P_i) is calculated from piston movement (cylinder volume – V) and the compressed (ambient) air pressure (P_c). It is assumed that the minimum allowable air pressure is maintained with no losses from blow-by; theoretically the top-up air supply achieves this in the real pulsation generator. Engine geometry calculations [85] are then used to calculate indicated torque; this is the pulsation torque that can then be applied to the crankshaft and combined with the mean torque level inputted to the crankshaft by the input dynamometer.

In order to calculate the cylinder volume at a given crank angle, it is assumed that the piston behaves as a crank slider mechanism (see Figure 4.5). The piston height at the current crank angle is calculated from engine geometry and compared to the maximum height of the piston; the cylinder volume is then calculated using the bore (D – diameter) of the cylinder (Equation 2) [95]. The engine selected for adaptation into the pulsation generator has no piston pin offset (the offset between the gudgeon pin axis and the cylinder axis – sometimes included to decrease unwanted noise [96]) so this factor has not been included in the calculations. Maximum cylinder volume (V_M) is calculated using the cylinder volume calculation, but with the current crank angle substituted for the angle at which the cylinder volume is at its maximum (Bottom Dead Centre, BDC). In order to ensure accurate results the Top Dead Centre (TDC) clearance volume (V_c) should be included in the volume calculations. When calculating cylinder pressure (Equation 3), 1.4 is used as the value for heat capacity ratio (γ); the air is assumed to be an ideal gas compressed polytropically.

$$Cylinder\ Volume\ (V) = V_c + \frac{\pi D^2}{4}\left[L + r - (r\cos\theta + \sqrt{L^2 - r^2\sin^2\theta})\right] \quad (2)$$

Where V_c is clearance volume (m^3), D is bore (diameter, m), L is connecting rod length (m), r is crankshaft throw (m), and θ is crank angle (rad).

$$P_i = P_c\left(\frac{V_M\frac{CR}{CR-1}}{V + \frac{V_M}{CR-1}}\right)^{\gamma} \quad (3)$$

Where P_i is indicated air pressure (bar), P_c is compressed air pressure (bar), V_m is maximum cylinder volume (m^3), V is cylinder volume (m^3), CR is compression ratio, and γ is heat capacity ratio.

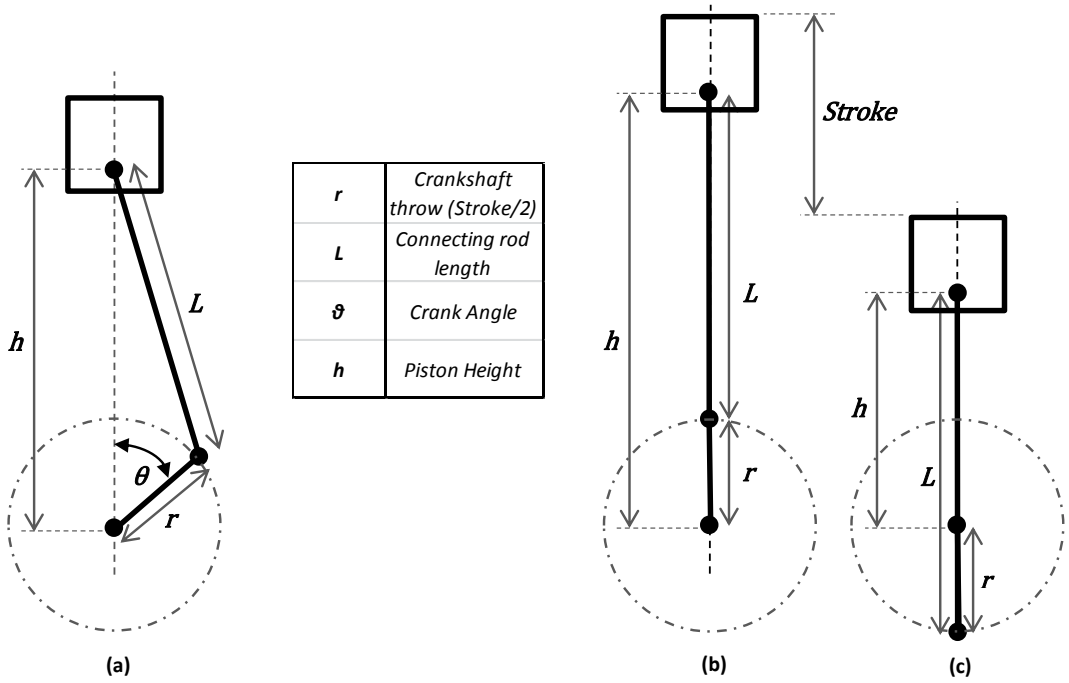

Figure 4.5: Piston crank slider mechanism at (a) Crank Angle θ, (b) Top Dead Centre and (c) Bottom Dead Centre

Torque and inertial load calculations are performed for each cylinder separately; the crankshaft is modelled as a flexible shaft that is divided up into individual cylinder sections. Each section has their own stiffness and inertia parameters (from manufacturer information); the indicated cylinder torques and the torque losses (frictional and inertial) are applied individually at the correct locations along the length of the crankshaft (see Figure 4.6).

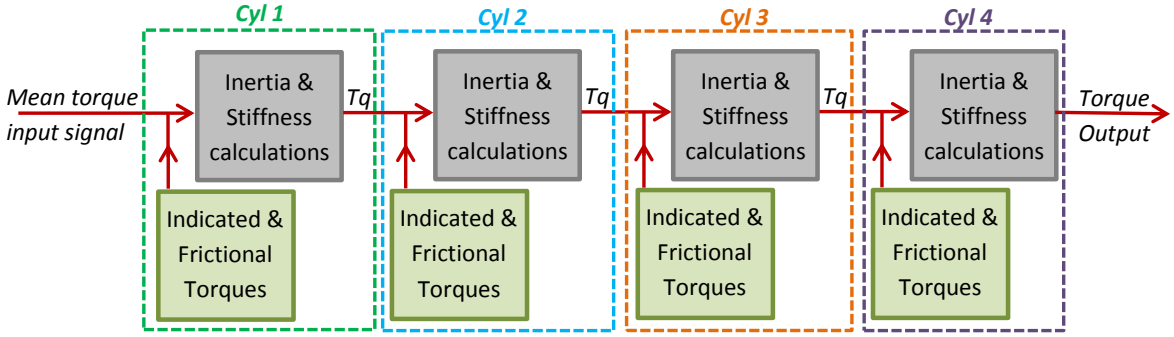

Figure 4.6: Flexible crankshaft schematic

Each cylinder section of the crankshaft was modelled as short, stiff mechanical shafts; manufacturer information provided the values for the stiffness (K) and inertia (J) of each section, with an internal damping factor (B) estimated (see Appendix). Further information on the implementation of the stiffness and inertia calculations used to calculate the torque transferred from each crankshaft section to the next can be found in section 5.7; this method is used to model transmission and rig components in the wider simulation.

An advantage of modelling the crankshaft in sections is that it allows for torsional feedback between components. Without this feedback, the interaction between the cylinders and the inertias either side of the pulsation generator is unlikely to be simulated correctly, potentially resulting in a simulation that does not accurately capture all aspects of real-world behaviour.

As can be seen from Figure 4.4 and 4.8, this model takes into account engine frictional torque losses; these losses (in addition to torque loss from inertia variation) are essentially subtracted from the indicated torque. The fired engine model [85] this pulsation generator simulation is based on includes four main sources of frictional torque losses; bearing friction, piston ring assembly friction, valve train friction and pumping losses [86]. The two main sources of frictional losses in a fired engine have been shown to be the ring assembly and the bearings [86]; these are the only two sources of frictional torque loss taken into account by the adapted pulsation generator model. This is reasonable, as due to the deactivation of the valves there are no valve train friction losses, with no water pump losses as an external feed is used. In the pulsation generator the standard engine oil pump is used for the oil feed; in the simulation any losses due to it are assumed to be negligible. This is an acceptable assumption, as in the fired engine simulation it was found that the frictional losses from all auxiliaries (including the water, oil and fuel pumps) was less than ~4% of the maximum frictional torque [86].

In a typical engine the ring assembly lubrication mode is hydrodynamic (excluding at TDC and BDC where the oil film behaviour changes); a layer of oil separates the rings and cylinder wall. The ring assembly frictional torque losses can be calculated (using a friction coefficient) by making the following assumption: the friction force is equal to the force produced by the interaction of the ring assembly and the cylinder wall [86]. In this model the main journal bearings (used to support the crankshaft) also operate in a hydrodynamic lubrication mode (excluding TDC) and are modelled using the Reynolds approximation to the Navier-Stokes equations [86].

As no combustion takes place in the pulsation generator the temperature of the unit (and therefore the oil) will be substantially lower than in a fired engine; however, due to the frictional losses (e.g. between the piston rings and cylinder wall) and the compression of the air, the temperature will still be higher than ambient. As temperature increases oil viscosity decreases, altering the hydrodynamic lubrication friction coefficient. This simulation assumes that once the pulsation generator has been run-in (heated up – the system allowed to stabilise) the temperature will remain constant; thus it utilises the hydrodynamic friction coefficient applicable at ~85ºC. If deemed necessary, the model could potentially be modified in the future to include oil viscosity as a function of pressure and temperature; this could be done using the non-linear least-squares method utilised by Zweiri et al [86].

While the moment of inertia of the piston and crankshaft components will not change, as the crankshaft rotates the moment of inertia of the assembly as a whole will vary with crank angle (as the position of the masses relative to the crankshaft centreline changes). It is important that the simulation takes into account this inertial variation as it will affect (and potentially contribute to) the fluctuations produced by the pulsation generator. In order to examine the effect inertial loading may have on the fluctuations, the pulsation generator (without the transmission) was run with all cylinders allowed to breathe freely to the atmosphere; the dummy injectors were removed (no pressurised air supplied to the cylinders). The theory is that when allowing the pulsation generator to operate with atmospheric pressure in the cylinders at all crankshaft angles, any fluctuations produced will be due to the varying inertial load of the crankshaft and piston assembly. These tests allowed some simulation calibration to take place; the crankshaft model and torque losses (frictional and inertial) could be calibration separately, without the cylinder air compression model. This helps ensure accuracy, as it eliminates any negative effect the more basic air compression simulation (with no features that account for blow-by loss or any delay in top-up air recharging the cylinder) may have on simulation performance.

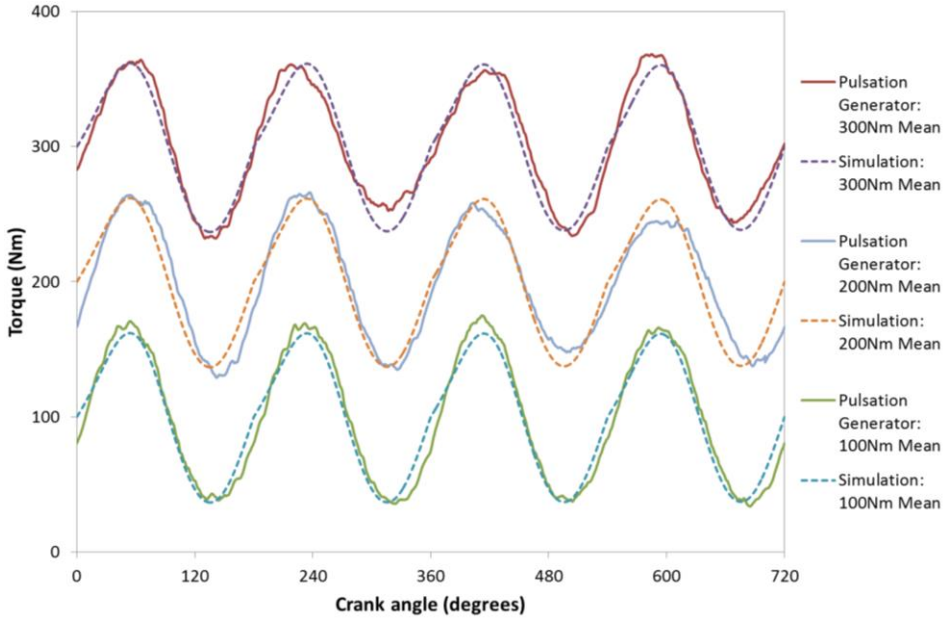

Figure 4.7: Comparison of experimental and simulation inertial load torque fluctuations at 1250rpm

A comparison between the simulation and experimental inertial loading test results can be seen in Figure 4.7. This set of tests was run at multiple mean torque levels (provided by the input dynamometer), including 100, 200 and 300Nm; as no compressed air was used in the system, the fluctuations produced are mostly a result of the varying inertia of the crankshaft-piston assembly (though the interactions between the stiffnesses and inertias of the rig components and dynamometers will likely contribute).

To help further calibrate the model, the cylinder pressure calculation was replaced with measured cylinder pressures from experiments using the unmodified, fired version of the engine. The torque outputted from the simulation could then be compared to the torque measured at the flexplate of the fired engine during testing (Figure 4.8), and any estimated parameters (such as crankshaft damping coefficients) adjusted to improve the simulation's performance. This method of simulation calibration was chosen (rather than using the data measured on the pulsation generator output during transmission testing) due to the complexity of the interactions between the pulsation generator and the inertias of the input motor and the rest of the rig; when used with the pressure cylinder measurements no input motor inertia was required and the vehicle inertia/stiffness could be easily and simply represented.

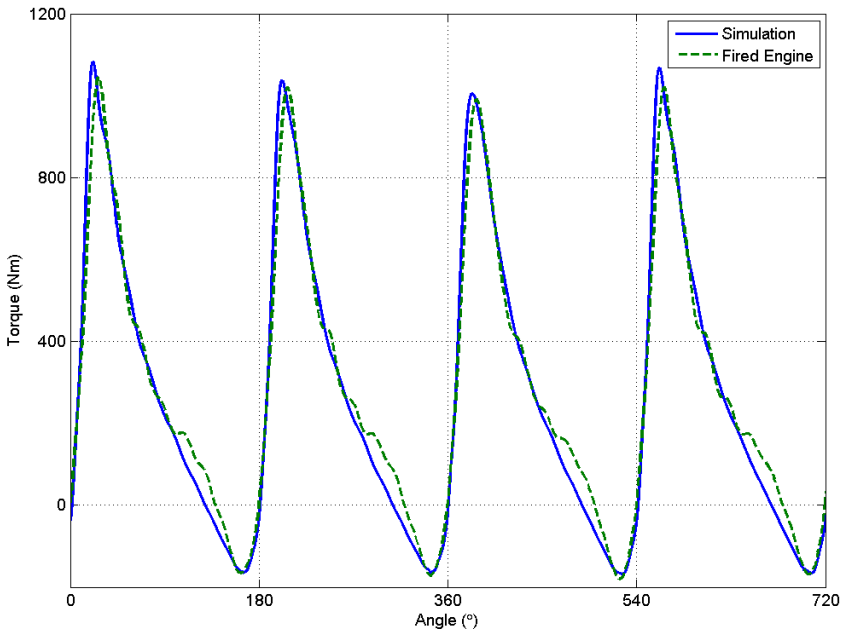

Figure 4.8: Comparison of simulated and experimental torque trace output from the base fired engine (at 1200rpm)

Both graphs (Figure 4.7 & Figure 4.8) demonstrate the potential accuracy of the pulsation generator simulation; by calibrating parts of the simulation with experimental data from both the pulsation generator and a real engine, confidence in the final results can be high. Calibrating the simulation using data that does not involve the extra complexity of the damper transmission system also increases confidence in any results that are obtained when the transmission stiffness and inertia are finally included. If experimental results from more complicated tests were to be used the system may be calibrated in such a way as to not accurately reflect the real world behaviours.

4.3 Proof of concept results

The behaviour of the pulsation generator can be examined using two different groups of testing data; basic proof of concept testing which took place without the transmission (and therefore damper) installed on the rig and the more rigorous testing that took place with the transmission. The first part of this section examines how the pulsation generator functions in real world experimental situations (as opposed to theory or simulation); is the concept capable of producing substantial fluctuations whose magnitude can be adjusted using cylinder compressed air pressures? The second part of this section examines how the torque fluctuations produced by the pulsation generator differ to a fired engine; this primarily focuses on the frequency of the fluctuations and the altered dominance of the component frequency orders. Lastly, the limitations of the method that have become clear from experimental usage are examined, including the concept's adjustability and durability.

4.3.1 Proof of concept

A demonstration of the capabilities of the pulsation generator can be seen in Figure 4.9. The pulsation generator performs its basic functions as expected; the mean torque is controlled using the input dynamometer, with the superimposed torque pulses produced by the pistons compressing the pressurised air in the cylinders. The mean torque level was controlled using the value measured on the output from the pulsation generator; doing so compensates for any torque loss that occurs in the pulsation generator, ensuring the damper is excited with the correct level of mean torque.

One method for assessing the performance of the pulsation generator is through examining fluctuations above and below the mean torque level supplied by the input dynamometer. As can be seen from Figure 4.9, fluctuations above the mean are classed as positive torque fluctuations, with fluctuations below the mean labelled as negative.

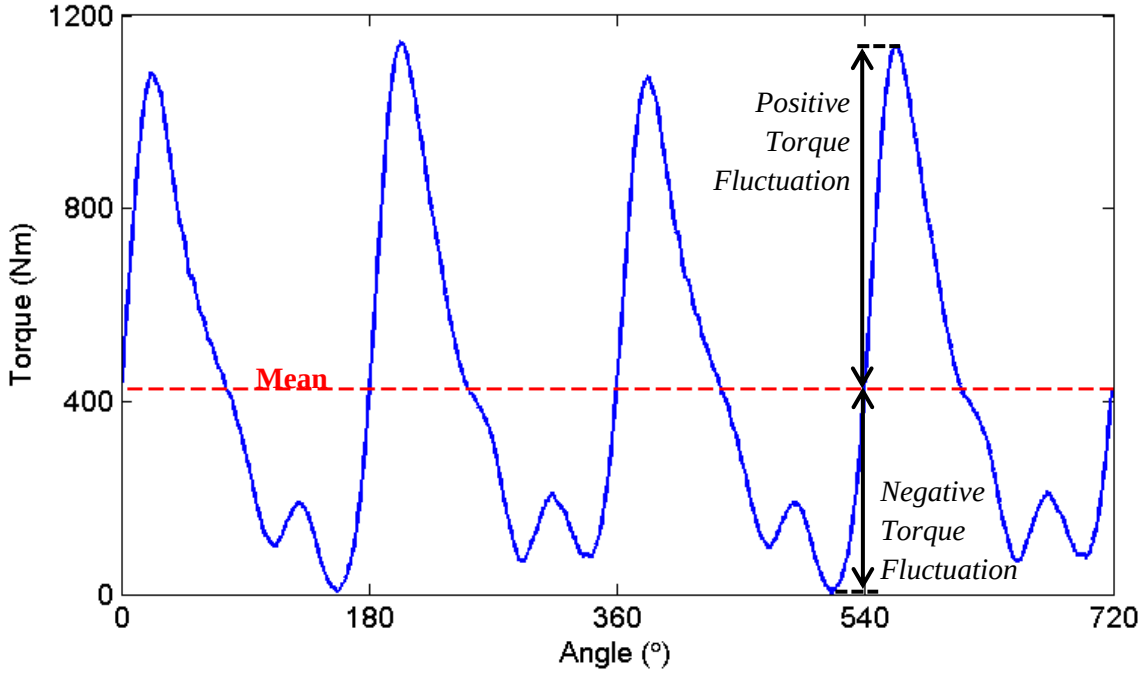

Figure 4.9: Torque fluctuations above (positive) and below (negative) the mean torque produced by the pulsation generator unit (with transmission and 2.5 bar cylinder pressure at 2800rpm).

The positive/negative connotation is irrespective of their actual value; the term *negative torque fluctuations* is used to signify fluctuation levels below the mean rather than fluctuations that extend below 0Nm. Assessing the fluctuations in this way allows the effect of both rig speed (rpm) and cylinder air pressure on fluctuation magnitude to be examined, as well as demonstrating how fluctuation magnitude varies above and below the mean torque.

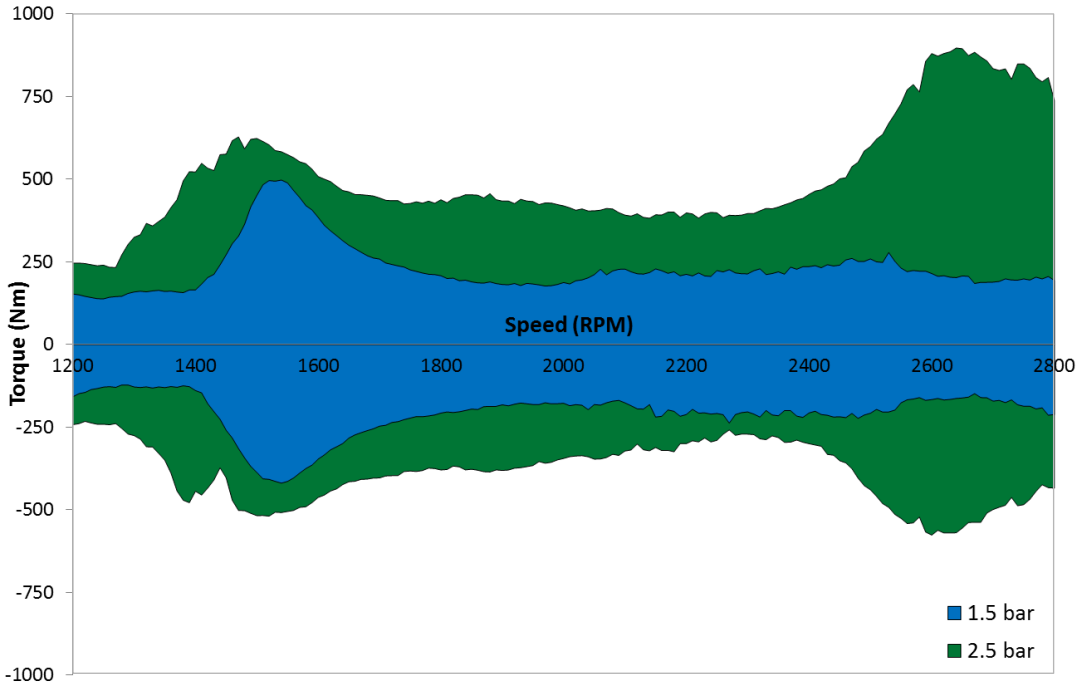

Figure 4.10: Effect of increased cylinder pressure on torque fluctuation magnitude above and below the mean torque for engine torque trace tests (pulsation generator coupled to transmission)

Figure 4.10 demonstrates that the pulsation generator produces torque fluctuations above and below the mean torque level (controlled by the dynamometer). It also confirms the theory that cylinder pressure could be used to control fluctuation magnitude; increasing the pressure of the compressed air supplied to the cylinders increases the magnitude of the fluctuations measured on the output of the pulsation generator unit. However, as can be seen from Figure 4.10, fluctuation magnitude (and the effect pressure has on it) is not necessarily uniform. The magnitudes of both the positive and negative fluctuations appear to be partly dependent on engine (rig) speed, a factor that was not necessarily considered in the early stages of the concept. The increase in fluctuation magnitudes seen in both the 1.5 and 2.5 bar datasets at 1300-1700rpm; as the increases are seen at both pressure levels, it suggests that they may be caused by interactions between different rig components. Thus factors such as crankshaft stiffness and the inertias and stiffnesses of other rig components – such as the transmission and damper – may have a greater impact on pulsation generator output than expected.

There is another area of increased fluctuation magnitude above 2400rpm; however, in this case, the increase is only seen in the 2.5 bar pressure dataset. This suggests that this increase is dependent on the load applied to the piston; as the pressure of the compressed air is increased, the cylinder pressure through the whole piston cycle also increases. This higher load may be affecting the behaviour of other parts of the system at these increased speeds; for example, the compressed air supply system. Higher cylinder pressures will exert greater forces on the one-way check valves used to supply the compressed air to the cylinders; increased engine speeds will also require the valve to respond (allow top-up air flow in) at a higher frequency. These forces may result in unexpected valve behaviour. Some of the torsional vibrations produced by the pulsation generator will be going upstream in the rig, towards the electric dynamometer; the control system will attempt to maintain the mean torque level. In doing so, it is possible that any variations in torque level (caused by the control system adjusting to the vibrational feedback) may interact with the fluctuations produced by the pulsation generator, affecting their magnitude.

The size of the fluctuations across the speed range may also be affected by cylinder pressure variations due to blow-by or by friction regimes (behaviour) changing. The cause of the fluctuation magnitude variations (with speed and cylinder pressure) could be studied further in a future project. Cylinder pressure measurements (potentially combined with a more advanced air supply system, see section 4.4.3) would allow a greater understanding of any causal link between cylinder pressure and pulsation generator output to be developed.

The theory that interactions between different rig components affects pulsation generator output is confirmed by comparing the results from the two sets of pulsation generator experimental testing. The pulsation generator system was tested both with and without the transmission and damper system; initial basic concept testing for the pulsation generator took place before the transmission had been programmed and installed. Testing the pulsation generator unit separately allows a greater understanding of what external factors affect the behaviour of the unit to be gained.

As can be seen from Figure 4.11, the key difference between the two testing sets is the frequency of the torque pulses produced by the unit. The pulsation generator only tests (which were performed by connecting the output of the unit to the output dynamometer using a torsionally stiff propshaft) produced the expected two fluctuations per 360 degrees of rotation (2^{nd} order); however, the addition of the transmission system (with a higher inertia and lower stiffness than the propshaft) resulted in the frequency of the fluctuations increasing to four fluctuations per rotation (4^{th} order dominant) in some of the speed range. The variation in fluctuation frequency across the speed range when the pulsation generator is coupled to the transmission (see Figure 4.12) also suggests that the increased inertia of the transmission system may be a cause of the altered frequency dominance. This may be due to inertia effects having less of an effect at higher speeds; other forces may become more dominant, returning signal frequency to the expected two fluctuations per revolution that is typically seen with a four cylinder fired engine.

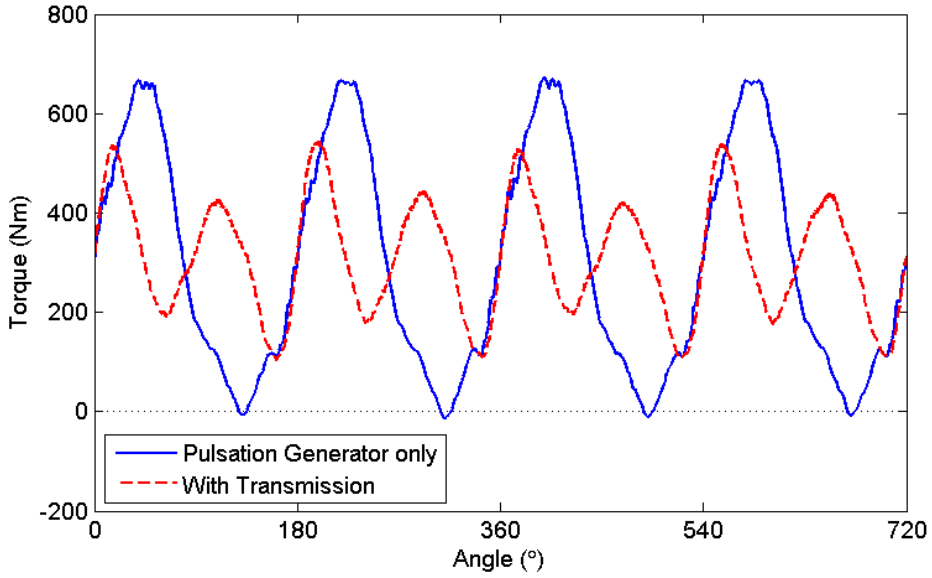

Figure 4.11: Demonstrating how the increased inertia and altered rig stiffness that occurs when the transmission is paired with the pulsation generator affects the torque profile outputted from the pulsation generator unit

4.3.2 Variations from a fired engine

The aim of the motored engine pulsation generator concept is not to exactly replicate the torque profile of a fired engine. The primary aim is to investigate whether a novel method of damper excitation that can be used with an existing electric dynamometer system can be developed for minimal cost; the concept must be capable of adequately exciting a damper (a more detailed investigation of what constitutes adequate can be found in section 7.1.2) in a way that allows simulation characterisation to be performed. However, comparing the pulsation generator output signal to that of a fired engine can help when assessing which method is more suited to different testing scenarios (see section 4.5).

As discussed in section 4.3.1, the primary difference between the fluctuation signals produced by the pulsation generator and a fired engine is the frequency of the fluctuations. A four-cylinder fired engine typically produces four torque pulses per two shaft rotations (720° of crankshaft movement) – see Figure 4.8. As can be seen from Figure 4.12, while the pulsation generator adheres to this pattern in certain situations – e.g. above 2500rpm (with 2.5 bar cylinder pressure) – the number of fluctuations per revolution is actually dependent on rig (engine) speed. This graph set also demonstrates how the dominant order dictates the overall frequency and shape of the torque pulses.

As discussed in section 3.4, a signal can be broken down into its component frequencies using Fast Fourier Transforms (FFTs); the peaks that occur at certain frequencies relate to frequency orders. An order is the number of times something occurs per revolution; a 2nd order frequency will have a peak occur twice in every revolution, a 4th order four times per revolution and so on. The dominance of an order is determined by its magnitude relative to the magnitude of the other orders; the order with the greatest amplitude is considered dominant.

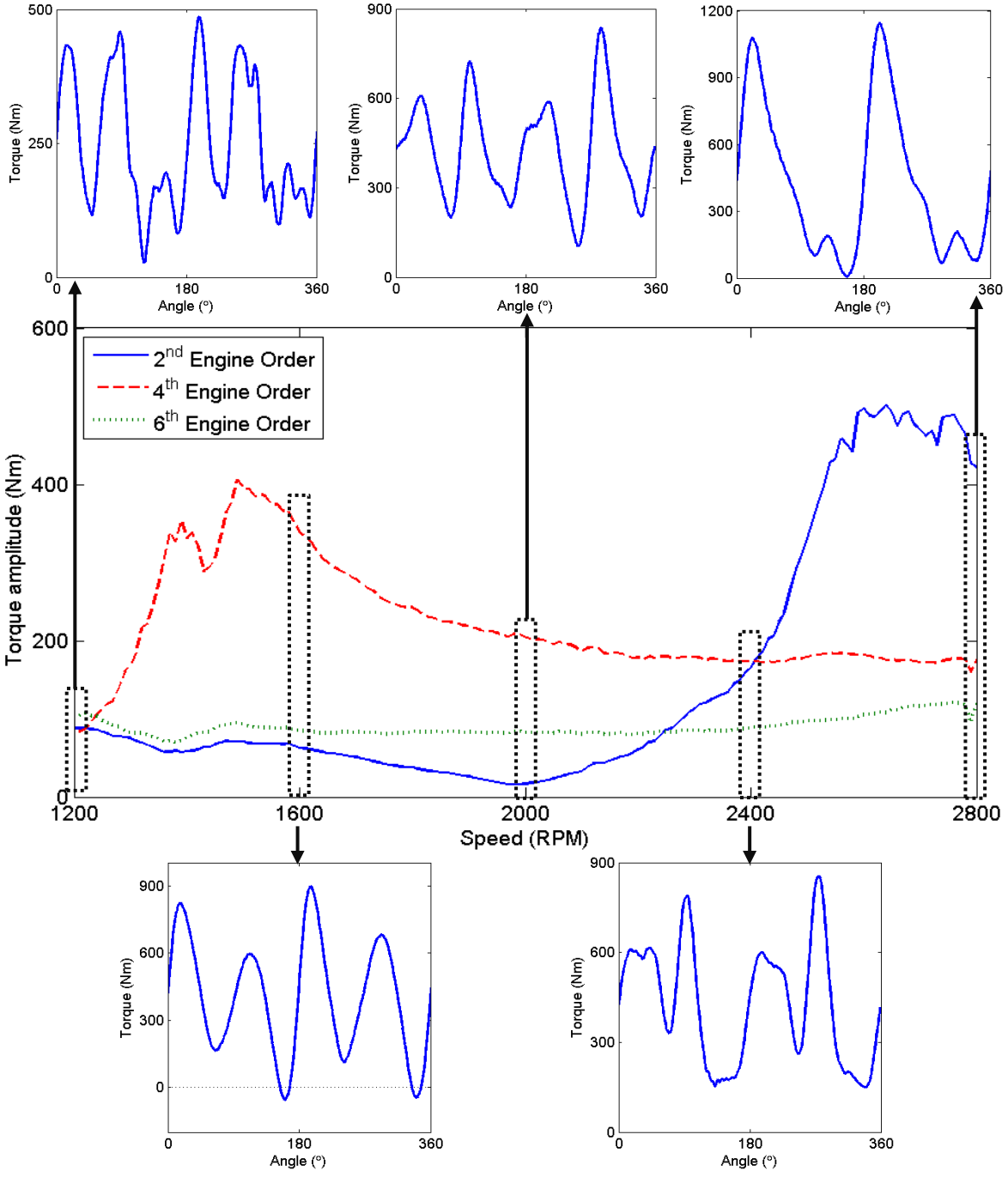

Figure 4.12: Demonstrating how order dominance changes across the speed range (2.5 bar torque converter damper testing) and how this affects the torque profile outputted from the pulsation generator

The frequency of the overall pulsating signal will typically depend on which order is dominant. If the 2nd order is dominant (as it would be in a fired 4-cylinder engine) there are two pulses per 360 degrees; however if the 4th order is dominant the system instead mimics an 8 cylinder engine, with four pulses per rotation. As can be seen from Figure 4.12, in the middle of the speed range the 4th order is dominant, resulting in an overall torque signal that has four peaks per 360 degrees of rotation; as the engine speed increases the 2nd order becomes dominant, resulting in a signal with two clear peaks per revolution.

An alternative method of demonstrating how the constituent frequency orders in the overall torque pulsation signal affect its frequency, magnitude and therefore form can be seen in Figure 4.13. As discussed above, dominance of an order is determined by its magnitude relative to the magnitude of the other frequency orders; the overall frequency of the pulsating signal will be determined by the dominant order, with the other orders affecting the overall shape of the fluctuation profile. When there is no clear dominant frequency – for example at around 1200rpm when using a pulsation generator cylinder pressure of 2.5 bar (see Figure 4.12) – the fluctuating signal is less uniform (though still repeatable). While the magnitude of the frequency orders in the fired engine output will vary depending on speed and torque output, the dominance of the orders does not tend to change with speed, unlike the output of the pulsation generator. Testing the damper at frequency/speed combinations not typically seen using a fired engine is not necessarily a disadvantage, especially when testing for simulation characterisation. The ability to investigate damper behaviour at higher frequencies in the lower end of the speed range may reveal damper behaviour that could otherwise be obscured by speed effects, improving simulation accuracy.

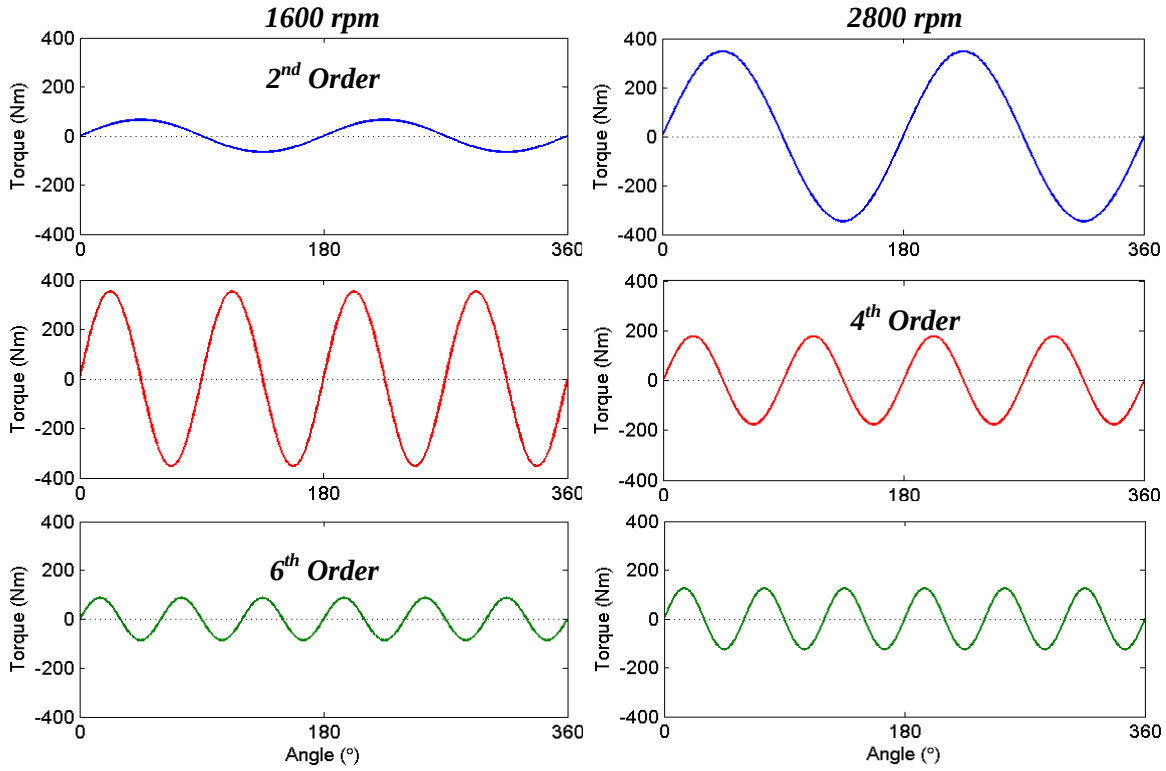

Figure 4.13: Magnitude of the three primary frequency order (2nd, 4th and 6th) components of the pulsation generator output signal at 1600rpm and 2800rpm; the dominant frequency dictates the frequency of the signal as a whole

The simulation confirms that the cause of the increased pulsation frequency is the interaction between the pulsation generator and the other rig components. When the pulsation generator simulation is included in a larger rig model that includes inertia and stiffness representations of key components (such as the electric dynamometers and transmission), the simulation ceases to produce the 2nd order fluctuations seen during initial pulsation generator only testing (see Figure 4.11). Instead, the simulation reproduces the 4th order dominant fluctuations seen in a large section of the combined pulsation generator and transmission testing results (see Figure 4.12).

A demonstration of the simulation's ability to reproduce the signals produced by the motored engine pulsation generator concept can be seen in Figure 4.14. While the magnitude and frequency of the signal is quite closely replicated, the discrepancy between the predicted and actual signal may be due to more complex blow-by behaviour (cylinder pressure loss).

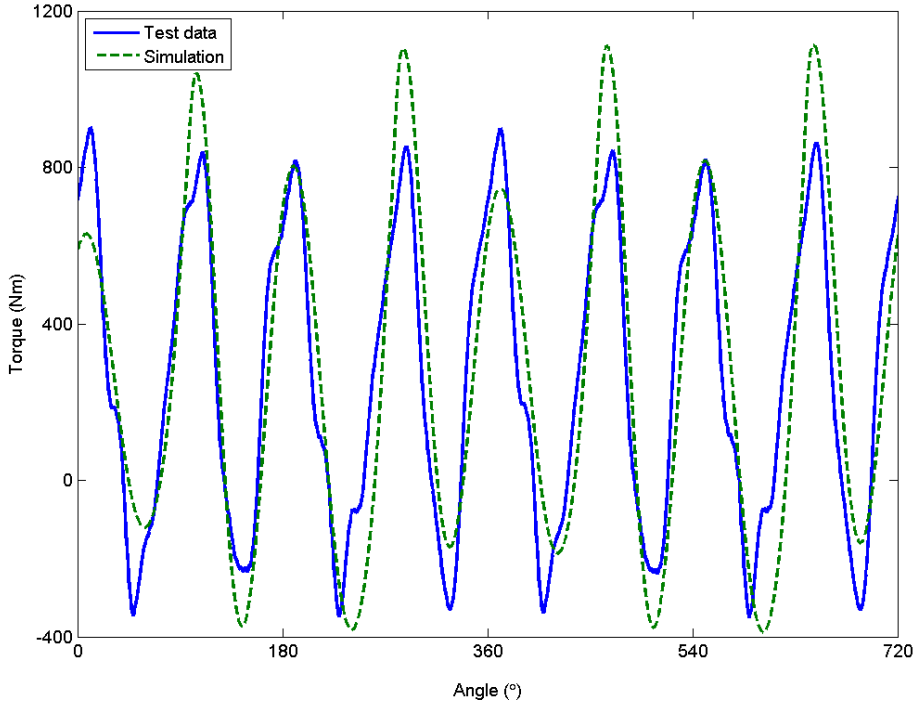

Figure 4.14: Comparing simulation and testing data for the output of the pulsation generator when coupled with the transmission (2.5 bar, 1500rpm)

As the simulation is capable of reproducing the unexpected frequency behaviour of the pulsation generator, it could be used to investigate any potential alterations to crankshaft design that may alter the frequency of the fluctuations. It was decided that further investigation was outside the scope of this project, primarily due to the costs involved; however, it would be investigated if further study into the pulsation generator concept was completed.

4.3.3 Concept limitations

So far it has been demonstrated that the motored engine pulsation generator concept is capable of producing fluctuations of a substantial magnitude over a wide frequency range. However this concept is a prototype design, and therefore has limitations; these potential usage restrictions are detailed here.

The basic principle that the magnitude of torque fluctuations can be adjusted using cylinder pressures has been proven. However, as demonstrated in Figure 4.10, the relationship between magnitude and pressure is not necessarily linear; it is suspected that this non-linearity is due to stiffness and inertia interactions changing with speed. While some peaks in magnitude may be unavoidable (due to system resonances), controllability could be improved with a more advanced cylinder pressure control system; the current system cannot be remotely controlled during testing and has no feedback system built in (e.g. cylinder pressure sensors).

Potential improvements to the pulsation generator cylinder pressure management system include remotely controllable valves, used in combination with in-cylinder pressure sensors. By monitoring the pressure inside the cylinders, an assessment can be made on whether the desired minimum cylinder pressure is being maintained, or if the response time of the top-up air supply valves is too low. While the increased fluctuation frequency is likely to be due to interactions between the inertias and stiffnesses of the rig system (see section 4.3.2), a cylinder pressure profile that is more variable (less uniform) than expected may be contributing to the frequency variations observed.

Frequency cannot be actively controlled, though changes to the design of the system may be able to improve the consistency of the fluctuation frequency. These changes could potentially include a crankshaft with a higher stiffness, or the deactivation of the cylinders. An approximation of cylinder de-activation was briefly investigated during testing; the modified injectors of one cylinder pair were removed, allowing them to breathe freely at atmospheric pressure (the other pair charged with 1.5 bar compressed air). Allowing a cylinder pair to breathe directly to the atmosphere (no/minimal pressure change in the cylinder) did not halve the frequency of the fluctuations. This may be due to the fact that the inertias of the piston assembly for each of the de-activated cylinders are still present, contributing to the pulsating torque signal. As demonstrated in Figure 4.12, the varying inertial loading of the crankshaft-piston assembly can have a substantial effect on the fluctuations produced by the pulsation generator.

The magnitude and frequency of the pulsation generator fluctuations are dependent on the inertia and stiffness of the whole rig system; this means that the pulsations outputted from the generator unit may vary depending on the set up of the system. For example, the pulsations inputted into the damper at a particular test set point may vary when an alternative gearbox or damper design is utilised. However, small variations in pulsation size or shape should not prevent damper behaviour from being compared; the primary method used to assess damper performance is attenuation, which is defined as the ratio between the torque fluctuation magnitudes at transmission input and output. Thus as long as the signals are similar (same frequency, similar magnitudes) comparisons on damper behaviour could be made. Further information and analysis on the effect of pulsation fluctuation frequency and magnitude on damper behaviour can be found in Chapter 7.

4.4 Prototype Limitation: Crankshaft Failure

In the early stages of the concept development process the potential failure modes were identified. The weakest point in the system was determined to be on the input side of the pulsation generator; the snub nose end of the crankshaft. In a fired engine this end of the crankshaft is not required to withstand heavy loading; the diameter of the crankshaft is stepped down significantly, while keyways are used to connect to the gears that transfer drive to the oil and water pumps. In the pulsation generator concept, the water pump is removed; the pump drive gear was replaced with a flange designed to connect the pulsation generator to a ROBA coupling. The flange was secured to the crankshaft using both the keyway system and shrink fit; the flange was heated, causing the metal to expand, then fitted to the crankshaft and allowed to cool. This flange allows drive from the input dynamometer – used to provide mean torque levels – to be transferred to the pulsation generator.

Due to the reduced shaft diameter and the keyways, combined with the improper usage of the end of the crankshaft (it was not intended to be used to provide drive to the rest of the system), the point at which the diameter of the crankshaft is stepped down was identified as a potential failure point (along with the keyways). However it was determined that as this was a prototype – the first attempt at adapting a fired engine to a pulsation generator – the cost involved in eliminating these potential failure points (for example by using a custom crankshaft) was too substantial. Basic material failure calculations (combined with estimated torsional forces) suggested that while failure was a possibility, the crankshaft should last for a sufficient number of testing hours (in order to prove the concept and obtain an appropriate amount of damper excitation results).

Before the crankshaft failed, a substantial volume of testing was completed; initial proof-of-concept results (testing the pulsation generator without the transmission) were obtained, along with three full sets of damper excitation tests (engine torque curve testing at 1.5 and 2.5 bar cylinder pressure as well as 1.5 bar mapping tests). Crankshaft failure occurred while completing the 2.5 bar mapping tests; as can be seen from Figure 4.15, the snub nose end of the crankshaft sheared, effectively disconnecting the pulsation generator from the input motor.

Minimal damage to other components occurred; the journal bearings successfully supported the majority of the crankshaft, though the momentum of the flange and the now unsupported (disconnected) snub nose of the crankshaft did result in damage to the external engine casing (Figure 4.16).

Figure 4.15: Failure of crankshaft snub nose end (pulsation generator input)

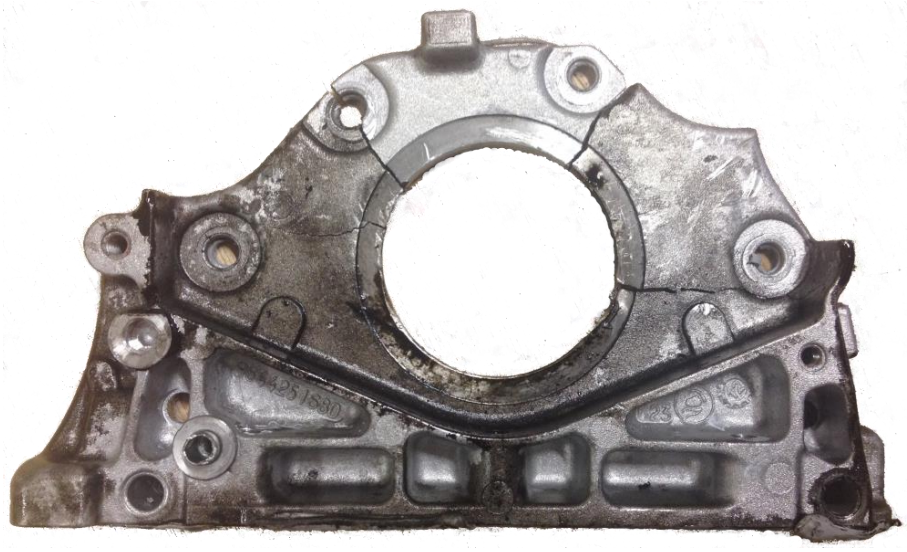

Figure 4.16: Casing damage caused by crankshaft failure

When this component was first identified as a potential failure mode during the concept development process some potential solutions were explored. Two main options were investigated; replacing the entire crankshaft with a custom designed component or strengthening the existing crankshaft to include the coupling connection flange. Replacing the entire crankshaft is the more expensive option; though if further simulation investigations were completed, a modified crankshaft could potentially be used to alter the frequency of the torque pulses produced (resulting in a torque pulse with a greater similarity to the original fired engine signal). However, the cost of such a crankshaft is very prohibitive; one of the main aims of this prototype was to investigate whether or not a pulsation generator could be produced for minimal cost – e.g. from cheap, readily available components. The alternative solution was to modify the weak end of the crankshaft (see Figure 4.17); in this design, the reduced diameter portion of the crankshaft is removed and replaced with a component that has an integral flange (for connection to the input dynamometer via a coupling – see section 3.1.2).

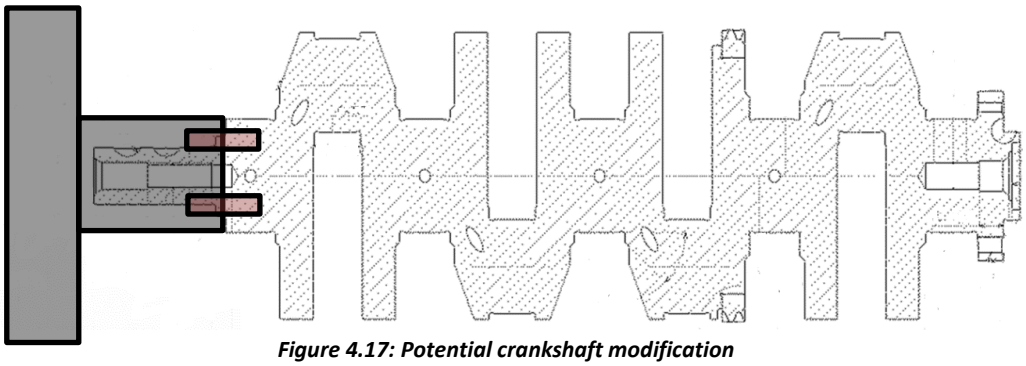

Figure 4.17: Potential crankshaft modification

This flange end component could be secured using a combination of pins and bolts or via a laser sintering process. The casing and bearing housing for this end of the crankshaft would also require modification and replacement (due to the increased diameter); this would be a fairly simple process as the water pump has already been removed (an external cooling water supply is used) and the oil pump could also easily be replaced with an external pump. Basic Finite Element Analysis (FEA) was completed on a bolt-secured concept for both typical (Figure 4.18) and maximum expected operating conditions; a tetrahedral mesh was used for the element nodal FEA calculation, with Von Mises yield criteria. It was found that while the concept should cope with normal operating conditions, the potential maximum torsional force exerted on the component may exceed the shear strength of the steel (EN24). The likely failure mode would be the holes for the pins/bolts deforming; the location of the pins is dictated by the design of the existing crankshaft.

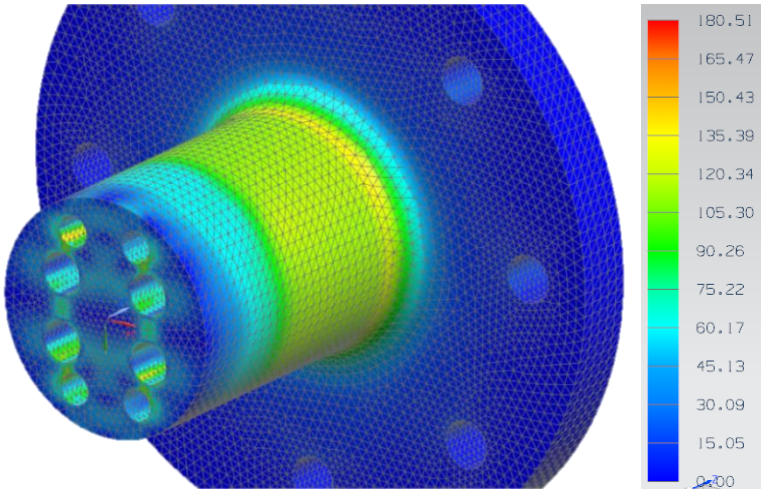

Figure 4.18: FEA analysis of typical expected operating conditions of a crankshaft modification component concept (stress given in N/mm^2 – MPa)

While potential solutions were investigated, when the crankshaft failure finally occurred it was decided that the quantity and quality of the data already obtained was sufficient to complete this simulation and characterisation project; thus the pulsation generator was not repaired. This was only a first pass, proof of concept prototype; the analysis required to re-engineer the crankshaft and fully explore the modifications available goes beyond the scope of this particular project.

4.5 Comparison of pulsation generation technology

As discussed in section 2.3, there are two main methods that are typically used to test driveline components (including torque converter dampers); those that use a fired engine to excite the components and those that utilise electric dynamometers. While fired engines are guaranteed to provide a pulsation signal that excites the system in a real-world manner, they are expensive to run and maintain (especially when using prototype engines that may have reliability issues). Fired engines are also a source of harmful emissions and CO_2; manufacturers are aiming to reduce the environmental impact of their manufacturing processes as well the impact of the final product. By using electrical dynamometers to perform driveline testing, components can be designed and tested parallel to engine development, thus increasing the efficiency of the design process.

While electric dynamometers have reduced running costs, the initial outlay required for electrical dynamometers that have the low inertia and high bandwidth required to perform high-frequency pulsation testing can be very prohibitive. Thus the concept for a motored engine pulsation generator was developed; this concept can be manufactured from existing, end-of-life, engines that may otherwise be scrapped. This section will examine the features of all three testing solutions and evaluate them against the varying requirements of different testing scenarios.

The key testing scenarios that are typically used in either a commercial and academic environment include durability, damper performance and characterisation for simulation. Durability is primarily a commercial test; assembled powertrains are tested as part of the vehicle development process to ensure that the final vehicle meets customer requirements. Damper performance testing is likely to be used on new components to assess their performance; these components may be designed in-house, bought in or taken from competitor vehicles. Characterisation for simulation is more likely to be used in a research context when investigating how to model new features or to expand knowledge of component behaviours.

In Table 4.1, the performance of each pulsation generation methodology against a range of criteria (cost, general performance and flexibility of the pulsation signal produced) has been assessed and rated from 1 to 5; a rating of 5 indicates very good performance (a high rating in a monetary category translates to reduced costs). Each criteria has also been allocated a weighting factor (from 1-5), with a different set of weighting factors for each testing scenario (durability, performance, characterisation); some criteria may be more important for different test categories. For example, initial outlay is less important when assessing the suitability of a pulsation technology for durability testing; this is because the extended testing hours required for durability testing gives better value for initial outlay vs testing time. The weighting factors have also been set so that they take into account the varied requirements for each type of test; due to the extended operating hours required for durability testing, reliability is much more important than the flexibility of the signal (a full durability test set will be performed with the same pulsation signal form).

Table 4.1: Pulsation generation method performance across commercial, general performance and output signal flexibility criteria and the weighting factors of each of these criteria for different testing scenarios

		Rating: 1-5			***Weighting: 1-5***		
Criteria		*Fired Engine*	*Electric Motors*	*Pulsation Generator*	*Durability testing*	*Performance testing*	*Characterisation for Simulation*
Commercial	Initial costs	4	1	5	3	4	5
	Running costs	1	3	5	2	2	1
	Environmental Impact	1	4	5	2	2	1
General	Reliability	4	5	1	5	2	1
	Real-world signal	5	3	2	5	2	1
Signal Flexibility	Control over signal	2	5	3	1	4	3
	Order Magnitude	2	3	3	2	4	3
	Order Frequency/Dominance	1	4	2	1	4	3
	Non-standard	1	4	4	1	4	3
	Multiple frequency signal	4	3	3	4	2	2

While durability testing doesn't require a pulsation signal that can be easily and quickly adjusted, damper performance or characterisation tests do require signal flexibility. Damper performance testing doesn't necessarily require a damper to be tested with a specific type of engine pulsation signal; damper performance will need to be assessed with a range of potential partner engines. In order to do so, performance must be able to be tested over a wider range of pulsation frequencies and magnitudes; it is important to investigate areas of poor damper performance and these areas may fall outside of the normal operating range. Damper performance tests (for example mapping procedures) may not require as much rig time as durability tests (hence a higher weighting given to initial outlay), however they are likely to be more strenuous than tests for simulation characterisation; hence a higher reliability requirement.

The ability of a pulsation generation method to perfectly mimic a real-world fired engine signal is most likely to be important when performing durability tests. The purpose of durability testing is to ensure that components perform as expected when subjected to real-world forces and that they last for an acceptable length of time without unexpected failure. Durability testing is an important part of the design and manufacture process and helps ensure customer satisfaction and product quality.

While exciting a damper with a fired engine fluctuation signal is important when investigating real-world behaviour, damper simulation results have revealed that when assessing the general performance and behaviour of a damper a perfect replica signal is not required (see section 7.1). As long as the three primary orders (the three most dominant frequency orders) in a signal are replicated the damper will behave in a representative manner, with equivalent real-world performance. Detailed analysis of the impact that the form of the pulsating damper input signal can have on damper behaviour can be found in Chapter 7. In summary, as long as a damper can be excited with a range of high frequency signals that satisfy magnitude requirements (see section 7.1.2) the performance of a damper in a wide range of situations can be assessed.

Table 4.2 summarises the performance of the pulsation generation methods in each testing scenario; these ratings have been calculated using the performance ratings and criteria weightings assigned in Table 4.1. As can be seen from Table 4.2, no overall conclusion can be drawn on which methodology for exciting dampers is optimum; the suitability of each method depends on the requirements of the testing scenario. Due to low initial set-up costs (as it can use engines that would otherwise be scrapped) and the ability to create an adjustable signal that covers frequency ranges that a fired engine does not, the motored pulsation engine concept is an optimum solution when performing tests to characterise a damper and validate simulation results. However, while the low running costs and minimal environmental impact of the motored engine are an advantage over a fired engine for long-running durability tests, the pulsation generator's lack of reliability (with the design of the concept as-is – no crankshaft alterations) means that it would be an unsuitable solution for this testing scenario.

Table 4.2: Comparing the performance of different pulsation generation methods for damper excitation in three different testing scenarios

		Durability testing			***Performance testing***			***Characterisation for Simulation***		
Criteria		*Fired Engine*	*Electric Motors*	*Pulsation Generator*	*Fired Engine*	*Electric Motors*	*Pulsation Generator*	*Fired Engine*	*Electric Motors*	*Pulsation Generator*
Commercial	Initial costs	12	3	15	16	4	20	20	5	25
	Running costs	2	6	10	2	6	10	1	3	5
	Environmental Impact	2	8	10	2	8	10	1	4	5
General	Reliability	20	25	5	8	10	2	4	5	1
	Real-world signal	25	15	10	10	6	4	5	3	2
Signal Flexibility	Control over signal	2	5	3	8	20	12	6	15	9
	Order Magnitude	4	6	6	8	12	12	6	9	9
	Order Frequency/Dominance	1	4	2	4	16	8	3	12	6
	Non-standard	1	4	4	4	16	16	3	12	12
	Multiple frequency signal	16	12	12	8	6	6	8	6	6
	Totals	**85**	**88**	**77**	**70**	**104**	**100**	**57**	**74**	**80**

A fired engine is obviously capable of producing perfect fluctuations as would be expected in-vehicle; however, the fluctuations produced by the fired engine are not adjustable – it cannot mimic a different engine. This means that the design process for an engine must be almost complete before testing or assessment of driveline components can take place; this could potentially delay the vehicle design process, especially since prototype engines can have reduced reliability (when compared to production versions). This dependency highlights the need for accurate driveline component – such as a torque converter damper – simulations; accurate simulations will minimise any unexpected failures during the late stages of the vehicle design process (e.g. during durability testing). Thus while a fired engine scores highly for reliability and the ability to excite the damper in a real-world manner (see Table 4.2), the flexibility and reduced environmental impact of high bandwidth electric dynamometers is an advantage when testing for durability.

The substantially lower running costs of the electric dynamometers (due to the cost of petroleum fuel vs electricity) and the significantly reduced environmental impact (approximately 5 times less CO_2 produced) help offset the substantially higher initial cost of the electric dynamometers.

In summary, the importance of reliability and running costs, along with the ability to produce or mimic a real engine signal, means that for durability tests fired engines or high bandwidth electric motors would be the most suitable solutions for pulsation generation. While the electric dynamometers would not have to be capable of mimicking every single component frequency order in the fired engine torque output signal, simulation results (see section 7.1.2) show that the dynamometers must be capable of mimicking at least the two most dominant frequency orders. A dynamometer system capable of simulating the three primary (most dominant) frequency orders would produce the optimum representative performance. The flexibility of electric dynamometers and the range of signals that can be produced by the motored engine pulsation generator concept give them the edge over a fired engine when investigating damper performance in a wide range of situations. However, the signals produced by the electric dynamometers would be much easier to control than those outputted by the pulsation generator concept. The electric dynamometers will have some limitations, depending on the system that is chosen; if the inertia of the system is too high the dynamometers will struggle to produce high frequency pulsations of a significant magnitude.

Simulation results have also shown that when characterising a damper system (producing a validated simulation) a real-world engine signal is not required; as long as the system can be excited to a significant magnitude over a wide range of frequencies (see section 7.1.2) a validated simulation can be produced. Thus despite its reduced adjustability (when compared to an electric motor system) and reliability issues, the motored engine pulsation generator concept developed for this project is a potential solution for excitation for characterisation. The minimal set-up and running costs of the pulsation generator make it an ideal solution for a smaller institution; for example, in an academic research environment.

4.6 Summary

In this chapter a design for a novel pulsation generator concept (for use with the existing PVRC electric dynamometers) has been proposed and the development of a prototype presented. The prototype has been successfully tested, with the results used to validate a simulation and confirm theory. The magnitude, shape and frequency of the fluctuations produced by the concept have been assessed; it should be noted that the purpose of the pulsation generator is not to perfectly mimic a fired engine, but to be able to adequately excite a damper.

The key outcomes from this chapter have been summarised below:

- A novel pulsation generator has been developed from a 4 cylinder motored diesel engine. The cylinders are filled with compressed air (between 1-2.5 bar) through modified (dummy) fuel injectors and the crankshaft driven using the input electric dynamometer. The input dynamometer provides the mean torque level, while the compression of the pressurised air in the cylinders creates the fluctuations.

- The cylinder valves have been deactivated by removing the rockers; the water pump has been replaced with an external water feed, though no modification to the oil pump or flow path was required.

- An analytical non-linear dynamic model for single-cylinder diesel engines was chosen from literature to be adapted and implemented in Simulink®. In the crank-angle based simulation, piston geometry is used to calculate instantaneous cylinder pressure and indicated torque; torque losses from both frictional and inertial sources are included, with the crankshaft simulated as a very stiff flexible shaft.

- Experimental data from both fired engine tests (in-cylinder pressure measurements) and pulsation generator inertial loading experiments (cylinders allowed to breathe to atmosphere) have been successfully used to validate the simulation.

- Experimental data also demonstrates that the basic functions of the pulsation generator perform as expected; the mean torque can be effectively controlled using the input dynamometer, while the pressure of the compressed air in the cylinders alters the magnitude of the fluctuations produced.

- The frequency of the pulsations produced by the pulsation generator varies from the expected (fired engine output); below ~2400rpm the 4^{th} order is dominant rather than the 2^{nd} order. However, the ability to investigate damper behaviour at higher frequencies but lower speeds may reveal damper behaviour that could otherwise be obscured by speed effects.

- The altered frequency output is likely to be due to reactions between the pulsation generator and the stiffness and inertias of other components on the rig; this theory has been confirmed with test and simulation data.

- Crankshaft failure did occur, though the location of the failure (the snub nose – input – end) had been identified earlier in the development process. Two potential solutions have been presented; a modification of the existing crankshaft (may still fail at high cylinder pressures) and a custom designed replacement crankshaft (expensive).

- A comparison of the damper excitation methods – electric dynamometers, fired engine and the new pulsation generator concept – reveals that each is more suited to a different type of test. Fired engines and electric motors are more suitable for durability testing due to their reliability and ability to produce a real-world torque output signal; the flexibility of the electric motors and the low running costs of the pulsation generator suit damper performance tests. Cost is a substantial factor when evaluating methods for characterisation tests; the low initial outlay of the pulsation generator unit makes it an attractive solution.

- It has been shown that the pulsation generator is capable of exciting the TC damper over a range of speeds and frequencies; however a validated damper simulation is required to quantify what adequate excitation entails. Further analysis of the effect of damper input signals on performance and behaviour can be found in Chapter 7.

Chapter 5 Simulation of arc spring torque converter dampers

This chapter details the methods used to create a model of a two stage (arc spring) turbine damper from a torque converter. Before simulation can begin, an assessment of the hardware to be modelled takes place. Without an accurate understanding of damper construction a model will struggle to accurately simulate damper behaviour, as some hardware features may not be represented. The arc springs are modelled by discretising them into segments, with the inertia and spring behaviour modelled in a manner developed from a method previously used to simulate DMFs; a continuously differentiable model is used to simulate friction behaviour.

5.1 Damper construction - Hardware

When modelling any physical system, the more knowledge that can be obtained from the hardware the more accurate the simulation will be. To this end, two torque converters (including their dampers) were disassembled for this project. Both have two separate sets of arc springs (inner and outer) and are classed as turbine dampers (the turbine inertia is attached to the intermediate plate – see section 2.1.3) but the number and design of the springs in both sets differ. In order to disassemble the torque converters, a lathe was used to remove the weld joining the two halves of the housing (see Figure 5.1). This allowed the pump (which forms part of the housing) to be separated from the clutch and the damper system. The rivets that hold the damper system together were then drilled out, allowing all components to be examined separately (see Figure 5.2).

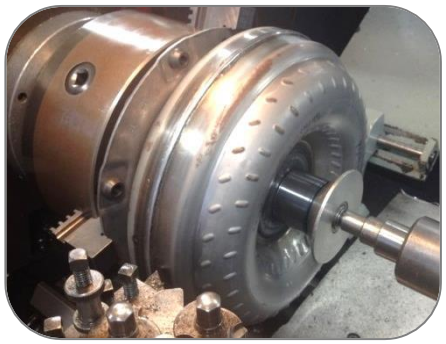

Figure 5.1: Using a lathe to remove the weld sealing the two halves of the torque converter

As discussed in section 2.1, the torque converter hydrodynamic circuit consists of a pump, turbine and stator, while the lock up circuit includes a clutch and a damper; in turbine dampers the turbine also forms part of the damper system. This simulation models the damper system when there is no clutch slip – the system is locked-up and the hydrodynamic circuit bypassed. Thus in this situation the pump is treated as no more than an inertia; it is assumed that any oil flow in the hydrodynamic circuit will have a negligible effect on the behaviour of the pump. It is also assumed that there is no slip in the lock-up clutch, as the test data was obtained while the system was over-locked (see section 3.3); if any slip was present it would be very low (1-3rpm) and not have a significant impact.

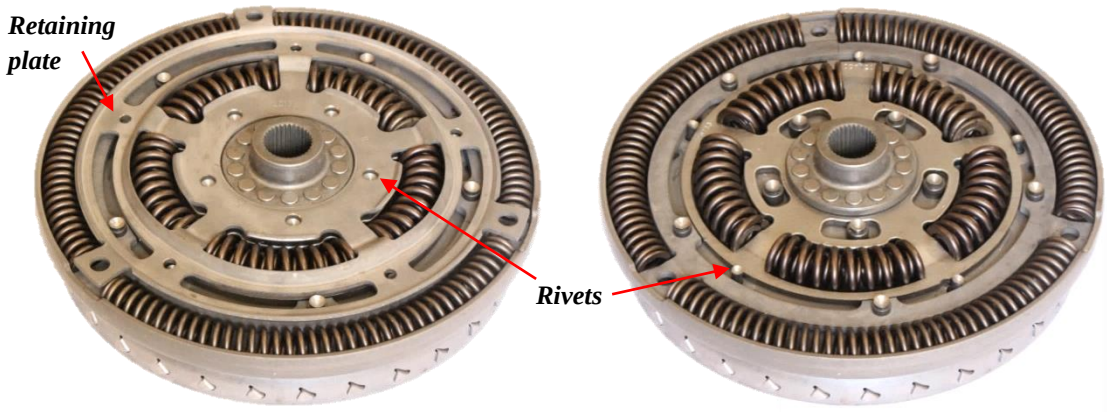

Figure 5.2: The two-stage turbine damper being modelled

The two-stage damper system is essentially made up of 3 inertias: the primary, secondary and tertiary, with the inertias separated by two individual spring sets (outer set between the primary and secondary, inner set between secondary and tertiary). Power is transferred from the lock-up clutch to the damper via a splined connector (the spline meshes with the clutch plates) which is attached to the primary spring set driving ring. Any mass in the torque converter system that is positioned before the primary spring set in the power flow is treated as part of the lumped primary inertia. Thus the lumped primary inertia consists of the torque converter housing, pump, lock up clutch and primary drive ring (see Figure 5.3).

When a force (torque) is applied to the primary drive ring (and therefore primary inertia) it in turn exerts a force on the outer spring set, causing it to compress; power is then transferred from the primary inertia, through the spring set and to the secondary inertia. This secondary inertia consists of a retaining plate (to keep both spring sets positioned correctly in their pockets – see Figure 5.2), the damper housing and the turbine (the housing is attached directly to the reverse of the turbine). Once a force is applied to the secondary inertia (by the outer spring set) it compresses the inner springs, transferring power to the tertiary inertia – an output plate that connects to the input shaft of the transmission using a spline (see Figure 5.3).

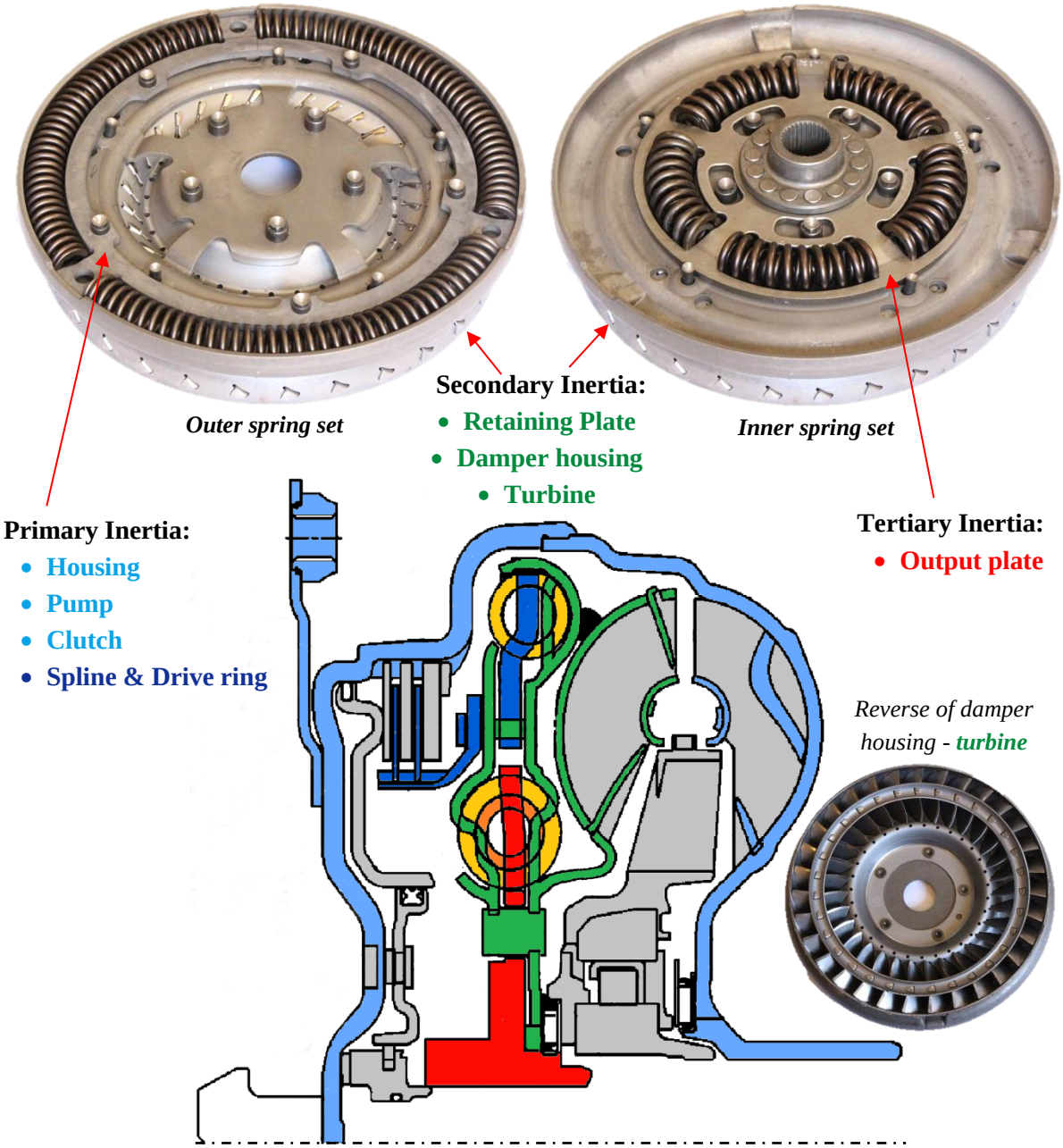

Figure 5.3: Deconstructed damper showing the outer (Top Left) and inner (Top Right) spring sets with a cross-sectional schematic demonstrating the grouping of components to form the three key inertias (adapted from [97])

In order to prevent the springs from becoming compressed too far (potentially damaging them) and to give more control over when the damper stiffness changes (the knee point occurs) these dampers are equipped with hardstops. There are two hardstop assemblies; one for the outer spring set and one for the inner (see Figure 5.4). Both sets consist of 5 nodes, each in their own slot; when a node reaches the end of a slot the spring set cannot be compressed any further and the power is transferred directly between the inertias. This is the knee point at which the damper stiffness changes; as one spring set cannot be compressed any further the stiffness of the spring set that is still able to move becomes the stiffness of the overall damper (rather than the total stiffness of the spring sets in series).

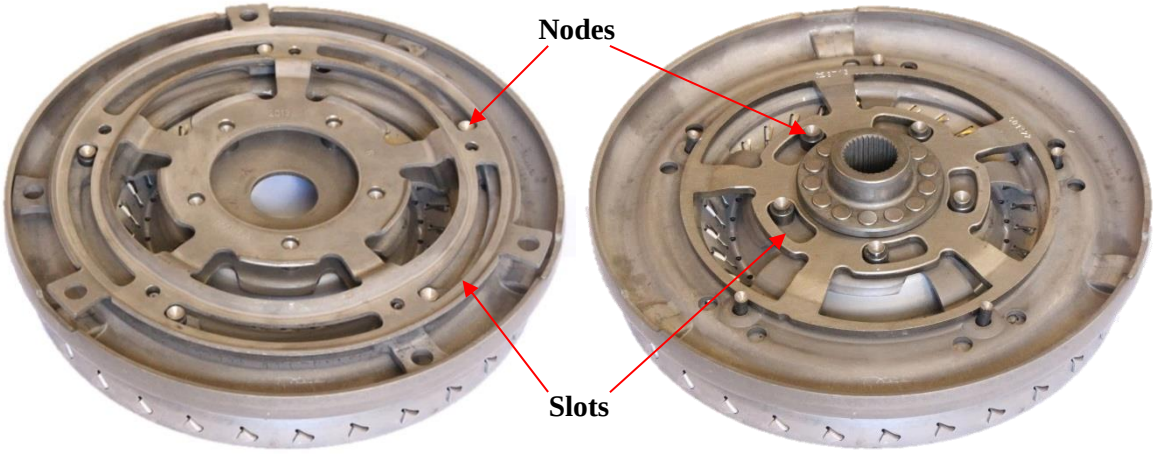

Figure 5.4: Demonstrating the outer (Left) and inner (Right) spring set hardstops; hardware pictured at maximum possible relative movement when a positive torque is applied

Without the deconstruction and studying of the hardware, it may have been (incorrectly) assumed that the knee points occur when the coils of the springs become stacked and the springs cannot physically be compressed any further (as simulated in [29]). However, as discussed in section 2.1.3, the use of physical hardstops will provide more consistent, predictable knee points (as the knee point will always occur at a set angle windup value). They are likely to be positioned to prevent the springs from becoming completely coil bound as this may lead to hardware damage, thus shortening the lifespan of the damper.

As can be seen from Figure 5.5, when the system is in neutral position (there is no compression of the springs) the nodes for both hardstop systems do not sit in the centre of their slots. This means that allowable relative movement between the damper plates varies depending on whether a positive or negative torque is applied. Hysteresis curves show that more angle windup is allowed when the applied torque is positive (Figure 6.27); this information allows which direction the plates must move relative to each other to be determined.

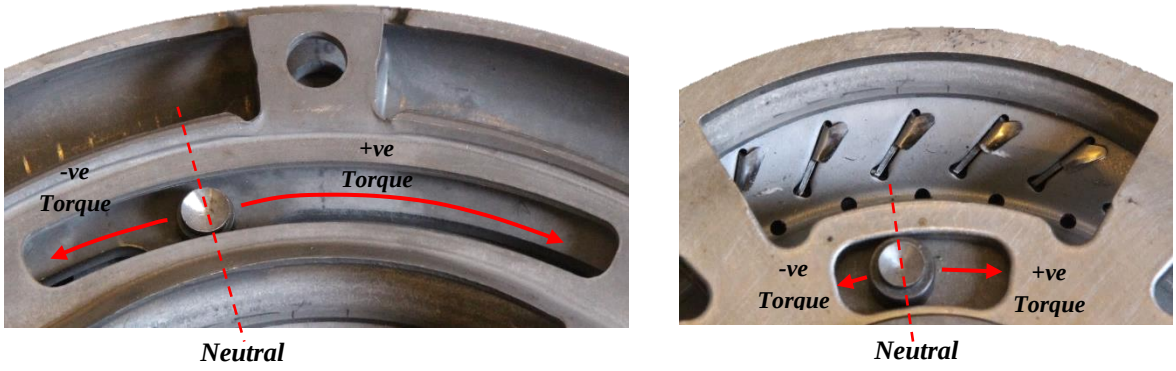

Figure 5.5: Positioning of hardstops in their retaining slots at neutral position – no spring compression (outer spring set – Left, inner spring set – Right)

Examining the hardware also means that the location of the hardstops – the windup angle at which knee points will occur – can be accurately measured for inclusion into the damper simulation, rather than relying on test data. There is a much smaller range of movement allowed in the spring sets when a negative torque is applied. This is likely due to the behaviour and torque profile of a fired engine; the torque profile only briefly enters the negative region, with peak negative torque levels being much lower.

The two deconstructed turbine dampers have essentially the same design (e.g. two spring sets, turbine attached to intermediate inertia) with minor differences in mass; the two systems behave in a similar way. Both dampers utilise only arc springs; however the larger of the two dampers uses 3 long springs in its outer spring set, as opposed to the 5 used by the smaller damper (see Figure 5.6). Literature suggests that the use of fewer, longer springs increases the torque capacity of the damper [7]; the design of the hardware corroborates this, as the longer springs can be compressed twice as far than their shorter counterparts before becoming stacked (though the hardstops mean that in practice the compression arc of the longer springs is only 1.5 times longer). The more a spring can be compressed the more torque it can transfer, though this is also dependent on spring stiffness, which may differ between the dampers. While the number of active coils (and therefore the number of coils in contact with the housing) is the same in the outer sets of both dampers, the reduced wire thickness of the springs in the smaller damper (see Figure 5.6) suggests a desire by the designer to reduce spring stiffness as well as friction levels (by reducing the surface area available for contact with the housing).

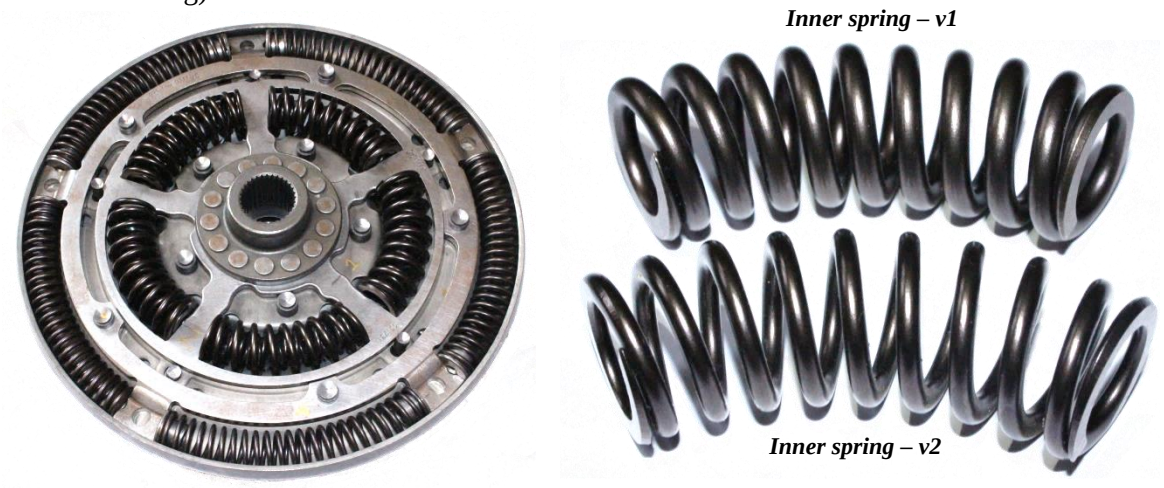

Figure 5.6: Design changes in the smaller damper (a later version of the damper being simulated)

The inner spring set in both dampers is nested; a smaller diameter spring is housed inside the larger (outer) spring. All the springs in the inner set of the larger damper are the same length, meaning both springs in the nested pairs are compressed at the same time. However, in the smaller of the two dampers the nested spring pairs are the same length in only 3 out of the 5 pairs; in the remaining two pairs the internal spring is shorter than its partner. This means that these pairs will have a two-stage stiffness; to begin with only the larger spring is compressed, so only its stiffness will be active. However once the spring has been compressed past a certain point, the internal spring and its stiffness will become active, resulting in the overall stiffness of the pair changing to the sum of both (as they are in parallel). This clearance angle design feature allows the damper to have three different overall stiffnesses rather than the two typically seen in a two-stage damper. This feature may have been introduced in order to increase the torque capacity of the damper (or mitigate any reduced capacity caused by a reduction in spring stiffness). While the damper that was tested and simulated – the larger of the two deconstructed dampers – consists only of arc and one-stage nested springs, reviews of literature and examination of hardware have revealed that additional designs of springs are used in dampers. Once this damper simulation has been validated using test data, new library component representations of these alternative designs could be produced, allowing the model to be adapted to suit a variety of configurations.

5.2 Inertia modelling

When designing a model with components that move relative to each other (especially when all the components are also rotating) one of the first steps is to define a frame of reference; in this situation it is recommended that the inertia positioned before each spring set in the power flow becomes the frame of reference for that set. This means that the frame of reference for the outer spring set is the primary inertia, while the reference for the inner set is the secondary (the spring sets are modelled separate from each other so a different frame of reference is not an issue). Essentially, for the purposes of calculating spring compression (by examining the relative positions of the 'primary' and 'secondary' inertias) it is assumed that the primary inertia for each spring set is stationary.

As can be seen from the hardware (see Figure 5.5), when a positive torque is applied to the system the secondary inertia must move anti-clockwise relative to the primary in order to compress the springs in the correct direction; as both inertias are rotating this means that the secondary inertia must be moving slower than the primary. The same applies to the inner spring system; the tertiary inertia (the secondary inertia of the inner spring system) must move slower than the secondary inertia (the frame of reference for the inner spring set) in order to move anti-clockwise relative to the secondary. The movement that occurs when a positive torque is applied to the system is represented in Figure 5.7[2]; spring contact points during this process (e.g. first spring segment in contact with the secondary inertia, Nth segment in contact with the primary) are also illustrated (σ).

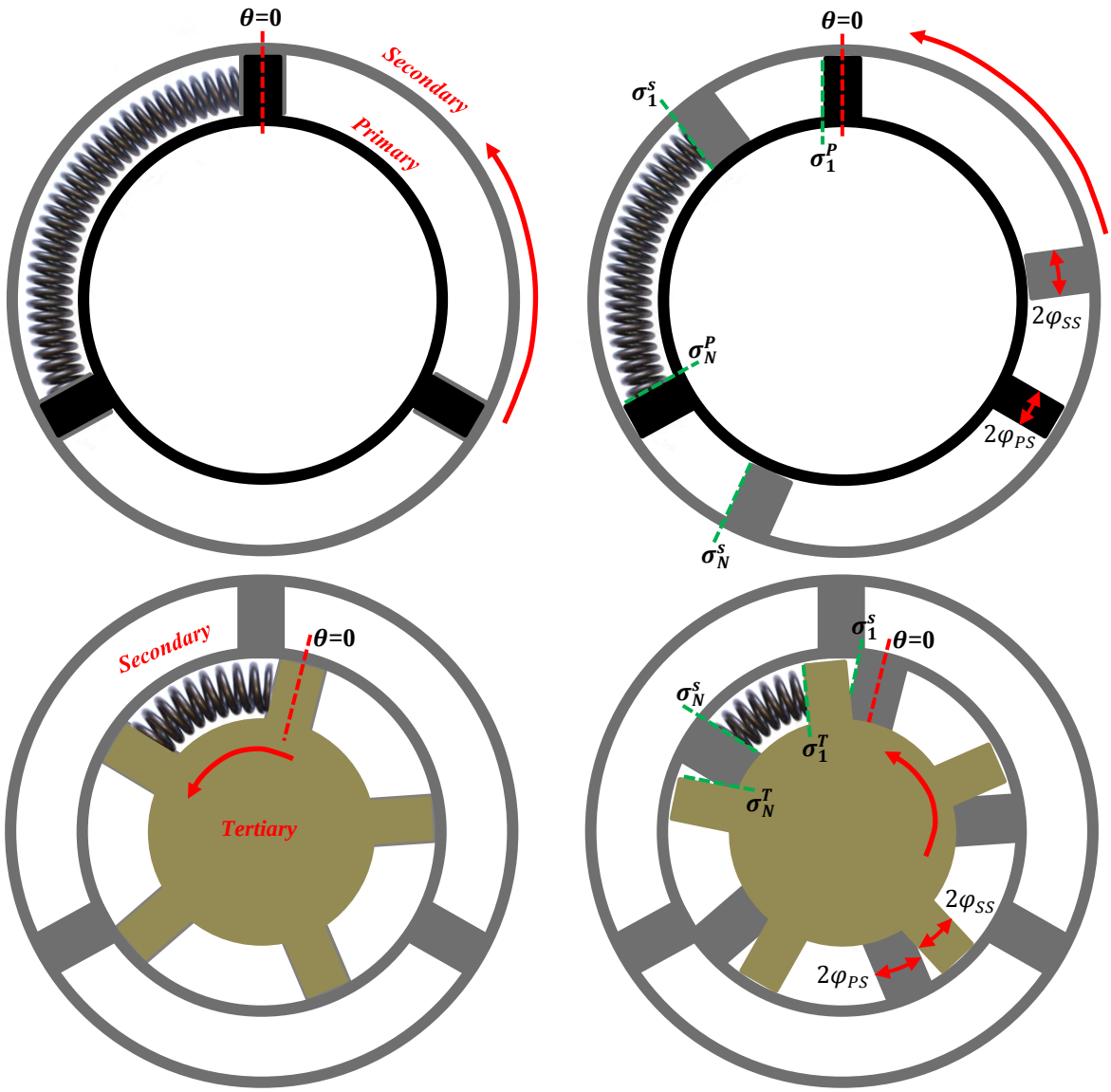

Figure 5.7: Compression of spring sets & movement of inertias relative to each other when a positive torque is applied

[2]Note that the small difference in size between the stoppers of the three inertias are for illustration purposes only; in this particular damper design there is no clearance angle.

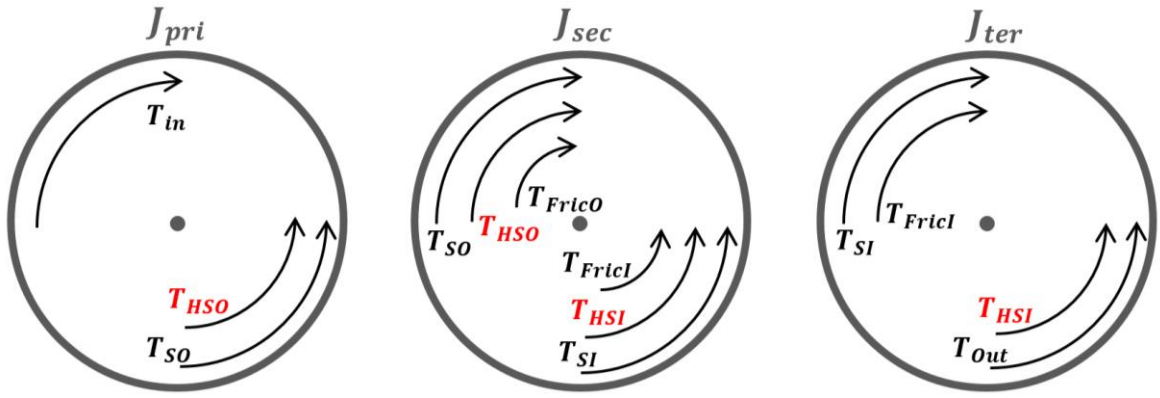

Figure 5.8: Free body diagrams demonstrating the torques acting on the primary (Left), secondary (Centre) and tertiary (Right) inertias; hardstop torque (T_{HS}) only acts on the inertias when they contact the hardstops

The principle of conservation of angular momentum can be applied to each of the three inertias (J_{pri}, J_{sec} and J_{ter}) in order to calculate their individual accelerations ($\ddot{\theta}_{pri}$, $\ddot{\theta}_{\text{sec}}$ & $\ddot{\theta}_{ter}$) [61] – see Equations 4 - 6. The torque applied to the inertia is compared to the resistance torque applied and any frictional torque (T_{Fric}) that is acting on that inertia (Figure 5.8); the resultant torque produces the movement of the inertia. The torque applied to the inertia is either the torque inputted to the damper (T_{in}) or the torque exerted on the inertia by the spring set that precedes it (T_S). The resistance torque is the reaction of either the spring set (T_S) or the physical hardstop (T_{HS}) to having a force exerted on them. In order to ensure the torque from the correct end of the spring is applied to each inertia, triggers (σ_1, σ_N) are used; a subscript of 1 signifies the first segment, while N signifies the last – the Nth – segment. Superscripts of P, S & T are used to indicate which inertia the trigger is indicating contact with. To identify which spring set is contacting the inertia, notation of O (Outer) and I (Inner) is used.

$$J_{pri}\ddot{\theta}_{pri} = T_{in} - nS_O\left(\sigma_N^{PO}T_{SO,1} - \sigma_1^{PO}T_{SO,N}\right) - T_{HSO} \tag{4}$$

$$\begin{aligned} J_{sec}\ddot{\theta}_{sec} = {} & nS_O\left(-\sigma_N^{SO}T_{SO,1} + \sigma_1^{SO}T_{SO,N} + \textstyle\sum_N^1 T_{FricO}\right) + T_{HSO} \\ & - nS_I\left(\sigma_1^{SI}T_{SI,1} - \sigma_N^{SI}T_{SI,N} + \alpha_{sec}\textstyle\sum_N^1 T_{FricI}\right) - T_{HSI} \end{aligned} \tag{5}$$

$$J_{ter}\ddot{\theta}_{ter} = nS_I\left(-\sigma_1^{TI}T_{SI,1} + \sigma_N^{TI}T_{SI,N} + \alpha_{ter}\textstyle\sum_N^1 T_{FricI}\right) - T_{out} - T_{HSI} \tag{6}$$

Alternatively, Equations 4-6 can be represented in the following matrix format:

$$\begin{aligned} \begin{bmatrix} J_{pri}\ddot{\theta}_{pri} \\ J_{sec}\ddot{\theta}_{sec} \\ J_{ter}\ddot{\theta}_{ter} \end{bmatrix} = {} & nS_O\begin{bmatrix} -\sigma_N^{PO} & \sigma_1^{PO} \\ -\sigma_N^{SO} & \sigma_1^{SO} \\ 0 & 0 \end{bmatrix}\begin{bmatrix} T_{SO,1} \\ T_{SO,N} \end{bmatrix} + nS_I\begin{bmatrix} 0 & 0 \\ -\sigma_1^{SI} & \sigma_N^{SI} \\ -\sigma_1^{TI} & \sigma_N^{TI} \end{bmatrix}\begin{bmatrix} T_{SI,1} \\ T_{SI,N} \end{bmatrix} + \begin{bmatrix} 0 & 0 \\ 1 & -\alpha_{sec} \\ 0 & \alpha_{ter} \end{bmatrix}\begin{bmatrix} nS_O\sum_N^1 T_{FricO} \\ nS_I\sum_N^1 T_{FricI} \end{bmatrix} \\ & + \begin{bmatrix} -1 & 0 \\ 1 & -1 \\ 0 & -1 \end{bmatrix}\begin{bmatrix} T_{HSO} \\ T_{HSI} \end{bmatrix} + \begin{bmatrix} 1 & 0 \\ 0 & 0 \\ 0 & 1 \end{bmatrix}\begin{bmatrix} T_{in} \\ T_{out} \end{bmatrix} \end{aligned} \tag{7}$$

Presenting the equations in this format allows the theoretical natural frequency of the damper system (when subjected to a positive torque) to be calculated. If a positive torque is applied to the system (as in Figure 5.7 and Figure 5.10), the values of the triggers σ_N^{PO}, σ_1^{SO}, σ_1^{SI} & σ_N^{TI} are set to 1, while their counterparts (σ_1^{PO}, σ_N^{SO}, σ_N^{SI} & σ_1^{TI}) are set to 0. By assuming that no hardstop contact occurs (T_{HSO} & $T_{HSI} = 0$) and that the inertia-spring system is frictionless, Equation 7 can be simplified:

$$\begin{bmatrix} J_{pri}\ddot{\theta}_{pri} \\ J_{sec}\ddot{\theta}_{sec} \\ J_{ter}\ddot{\theta}_{ter} \end{bmatrix} = nS_O\begin{bmatrix} -1 & 0 \\ 0 & 1 \\ 0 & 0 \end{bmatrix}\begin{bmatrix} T_{SO,1} \\ T_{SO,N} \end{bmatrix} + nS_I\begin{bmatrix} 0 & 0 \\ -1 & 0 \\ 0 & 1 \end{bmatrix}\begin{bmatrix} T_{SI,1} \\ T_{SI,N} \end{bmatrix} + \begin{bmatrix} 1 & 0 \\ 0 & 0 \\ 0 & 1 \end{bmatrix}\begin{bmatrix} T_{in} \\ T_{out} \end{bmatrix} \tag{8}$$

Using Hooke's law, inertia movement and stiffness values (Equations 9 and 10) can be substituted for spring torques:

$$T_{SO,1} = T_{SO,N} = k_O(\theta_{Pri} - \theta_{Sec}) \tag{9}$$

$$T_{SI,1} = T_{SI,N} = k_I(\theta_{Sec} - \theta_{Ter}) \tag{10}$$

Where T_S is spring torque (Nm), k is spring stiffness (Nm/rad) and θ is inertia position (rad)

By substituting these values, and the values for the number of springs in each spring set ($nS_O = 3$, $nS_I = 5$), Equation 8 can be rearranged as an equation of motion of the system:

$$\underbrace{\begin{bmatrix} J_{pri} & 0 & 0 \\ 0 & J_{sec} & 0 \\ 0 & 0 & J_{ter} \end{bmatrix}}_{Mass\ Matrix} \begin{bmatrix} \ddot{\theta}_{pri} \\ \ddot{\theta}_{sec} \\ \ddot{\theta}_{ter} \end{bmatrix} + \underbrace{\begin{bmatrix} 3k_o & -3k_o & 0 \\ -3k_o & 3k_o + 5k_i & -5k_i \\ 0 & -5k_i & 5k_i \end{bmatrix}}_{Stiffness\ Matrix} \begin{bmatrix} \theta_{Pri} \\ \theta_{Sec} \\ \theta_{Ter} \end{bmatrix} = \begin{bmatrix} 1 & 0 \\ 0 & 0 \\ 0 & 1 \end{bmatrix} \begin{bmatrix} T_{in} \\ T_{out} \end{bmatrix} \tag{11}$$

By using the appropriate values for the inertias and stiffnesses of the system, the mass and stiffness matrices (see Equation 11) can then be used to calculate the eigenvalues (and therefore natural frequencies) of the idealised (no friction) mass-spring system. It is the natural frequency that falls into the range of 10-20Hz that is of the most interest. The damper is designed so that the natural frequency associated with the mode that is most likely to be excited during the standard operation of the damper falls outside the standard operating range; a 1st order torsional vibration at 1200rpm will excite the damper at 20Hz. Experimental data appears to confirm that the damper has a natural frequency below 20Hz; more detail on the resonance potentially caused by this natural frequency can be seen in section 7.2.

The accelerations of the secondary inertia for each spring set (J_{sec} for outer set, J_{ter} for inner) relative to their respective primary inertias (J_{pri} for outer set, J_{sec} for inner) can be obtained by subtracting the secondary acceleration from the primary acceleration (Equations 12 & 13). As the inertias on the input to both springs sets move faster than those on the output, this results in the relative acceleration values having the correct direction (signage).

$$\ddot{\theta}_{sec,Rel} = \ddot{\theta}_{pri} - \ddot{\theta}_{sec} \tag{12}$$

$$\ddot{\theta}_{ter,Rel} = \ddot{\theta}_{sec} - \ddot{\theta}_{ter} \tag{13}$$

It is only necessary to model the full movement and forces of one spring from each of the spring sets; an exception is if multiple spring types are used in a set, e.g. a mix of one and two-stage nested springs. Each spring in a set is compressed in exactly the same way as its partners, is of the same design and has the same radial forces applied to it; thus it is reasonable to assume they will behave in the same manner. However, when applying the spring torques to the inertias, the total torque applied by all the springs in the set must be used; this is done by multiplying the sum of the spring torques (including the summed frictional torques from each spring segment T_{FricO} and T_{FricI}) by the number of springs in each set (nS_O and nS_I).

The springs in the outer sets only contact the outer wall of their housing; this means that they exert a frictional torque on only J_{sec} and no frictional forces are exerted on J_{pri}. When static, the only contact between the inner springs and their housing (with the exception of the ends of the springs on the end stops) is between the two end coils and the outer housing (see Figure 5.9). However once the damper is rotating and enough centrifugal force applied to the spring, it is likely that contact with the outer housing is made along its entire length. Unlike the outer springs the housing of the inner springs (in this damper design) is made up of parts of both J_{sec} and J_{ter}; through the manual application of an outward radial force to the spring, contact is obtained between the spring coils and both the secondary and tertiary inertias.

The damper chosen for disassembly had been subjected to light use; this light use has produced wear marks on the tertiary inertia that are also suggestive of contact – see Figure 5.9. This means that the frictional torque produced by the inner spring set must be applied to both inertias; in order to account for this, the terms α_{sec} and α_{ter} are used (see Equations 5-7). These terms allow the amount of frictional torque applied to each inertia to be tuned to reflect the balance of surface area contact; the two terms must always sum to 1, as the total frictional torque produced by the spring set must be preserved.

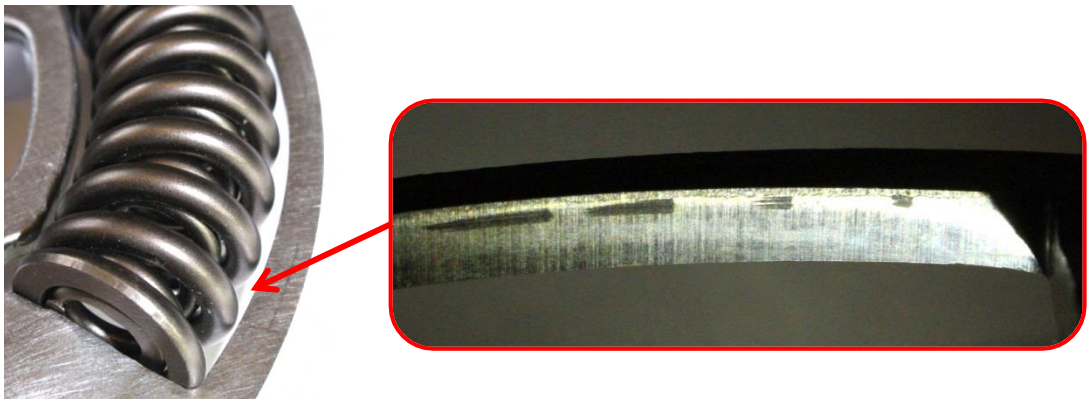

Figure 5.9: Inner spring set tertiary housing contact (Left) and wear marks on tertiary inertia (Right)

As can be seen from Equations 4-6 (and Figure 5.7) the torque exerted by a spring on an inertia is dependent on which end of the spring is in contact with it (the 1st or Nth – end – segment, see Figure 5.11); in order to ensure the correct torque is applied to each inertia, triggers (σ_1, σ_N) are used. This method was proposed by Schaper [61] while studying the simulation of dual mass flywheels; not only does it allow the determination of which end of the spring is in contact with the inertia (dependent on the direction of movement) but the triggers can also be used to detect when a spring end is not making contact, e.g. if there is a clearance angle (the slot is longer than the spring). Each spring set (outer and inner) has its own set of triggers with a designation for either the 1st or Nth (end) segment; notation of P, S and T is used to distinguish which inertia (primary, secondary or tertiary) the switching function is assessing segment contact with.

For example, when a positive torque is applied to the first stage of the damper (as in Figure 5.7) the first segment of the outer spring is in contact with the secondary inertia, and the end segment is in contact with the primary inertia. Thus $\sigma_1^S = 1$ and $\sigma_N^P = 1$; while under compression a spring end segment cannot be in contact with more than one inertia, so in this situation $\sigma_N^S = 0$ and $\sigma_1^P = 0$. The value of the triggers is determined by looking at the position of the spring ends relative to their frame of reference – their distance from the zero point (see Figure 5.10). If the spring end is more than a half width of the stopper (φ_S) away from the neutral point it cannot be in contact with the primary inertia.

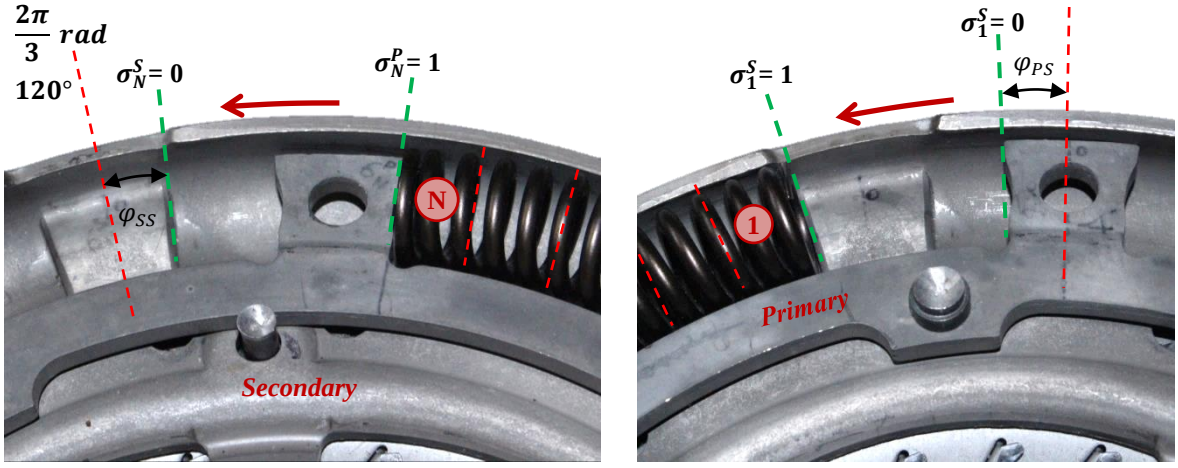

Figure 5.10: Spring end contact with primary and secondary stoppers when positive torque applied

5.3 Spring simulation

As discussed in Chapter 2, two main techniques are typically used for modelling springs. The first is a simple static spring rate method that models the entire springs as one object and does not take into account the speed dependent aspect of frictional forces. The second is a discretisation method, where a spring is broken down into either individual coils or sections of massless springs and masses, allowing the spring to have a dynamic stiffness. In order to accurately model the behaviour of the springs, without an excessive amount of computing power being required the discretisation into segments method has been deemed the most suitable solution.

5.3.1 Arc springs

An illustration of how the arc springs are discretised into segments and the torques that act on them can be seen in Figure 5.11. The direction of the resultant spring and frictional torque is dependent on the direction of the torque applied to the spring; in this diagram a positive torque has been applied. Initially the number of segments (N) chosen (to divide the outer and inner springs into) were 16 and 8 respectively; it was felt that this would give an acceptable compromise between simulation time and accuracy while developing and parameterising the simulation. Investigations completed once validation of the simulation had taken place (see 6.2.2) confirmed the links between segment numbers and simulation time and accuracy; the chosen numbers of segments were also revealed to fall in the optimum range.

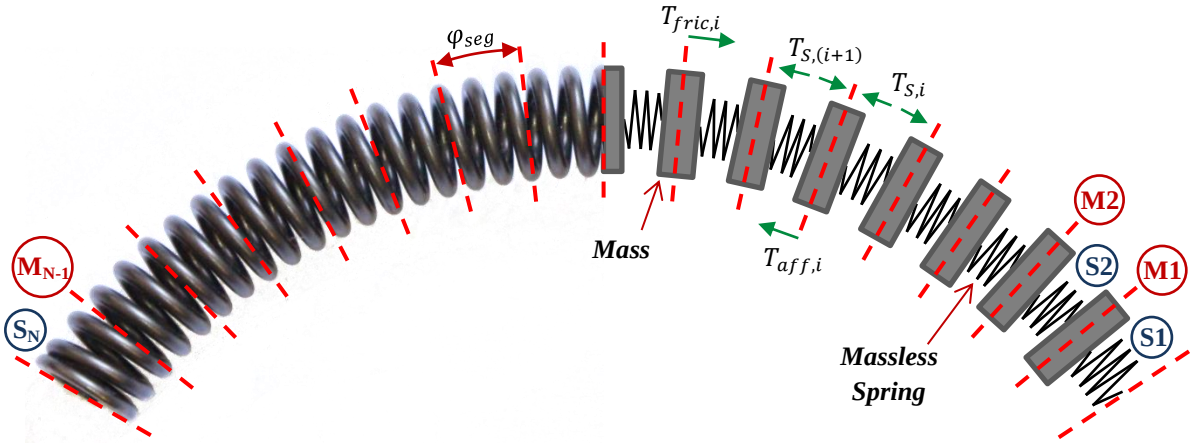

Figure 5.11: Discretising an arc spring into N segments (positive torque applied to system)

The acceleration of each of the segment masses can be calculated in the same way as that of the inertias; by the application of the principle of conservation of angular momentum (Equation 14) [61]. Each mass or spring segment is denoted by i, where $i = 1{:}N-1$ for the masses and $i = 1{:}N$ for the springs. The resultant spring torque (T_{res}) of a mass is the difference between the torque applied to it by the adjacent massless springs (input and reaction force). The frictional torque (T_{fric}) is produced by the contact between that segment and the housing; it is then applied to the mass (which has an inertia J_{Sm}), opposing the motion of the spring. In order to examine the movement of the spring masses relative to their frame of reference (the inertia before the spring set), the acceleration of the primary ($\ddot{\theta}_{pri}$) must be subtracted from the acceleration produced by the application of the torques to each mass; the remainder is the relative acceleration of the spring mass ($\ddot{\theta}_{Sm}$). Inertias are given in kgm^2, torques in Nm and angular acceleration in rad/s^2.

$$J_{Sm,i}\left(\ddot{\theta}_{Sm,i} + \ddot{\theta}_{pri}\right) = \underbrace{T_{S,i} - T_{S,(i+1)}}_{T_{res,i}} - T_{fric,i} \tag{14}$$

The acceleration applied to the spring masses causes them to move; the movement of each individual mass (relative to their initial position) is tracked, allowing the compression of each massless spring between the masses to be determined (see Figure 5.12). If the compression of the spring segment and its spring constant is known, then Hooke's law ($F=kX$) can be used to determine the torque transferred by the spring segment.

The implementation of Hooke's law can be seen in Equation 15; here, T_S is the spring torque and $k_{i,}$ is the stiffness of the spring segment. This distance between two adjacent masses (denoted by i, where $i = 1{:}\,N-1$) is calculated from their current positions (θ_S); this distance is the current length of the spring segment between them. By comparing the current length to the original, uncompressed length of the spring segment (φ_{seg}), the compression of the spring segment is determined. Angular position is given in radians, with stiffness in Nm/rad.

$$T_{S,i} = k_{i,}(\varphi_{seg,i} + \theta_{S,i+1} - \theta_{S,i}) \tag{15}$$

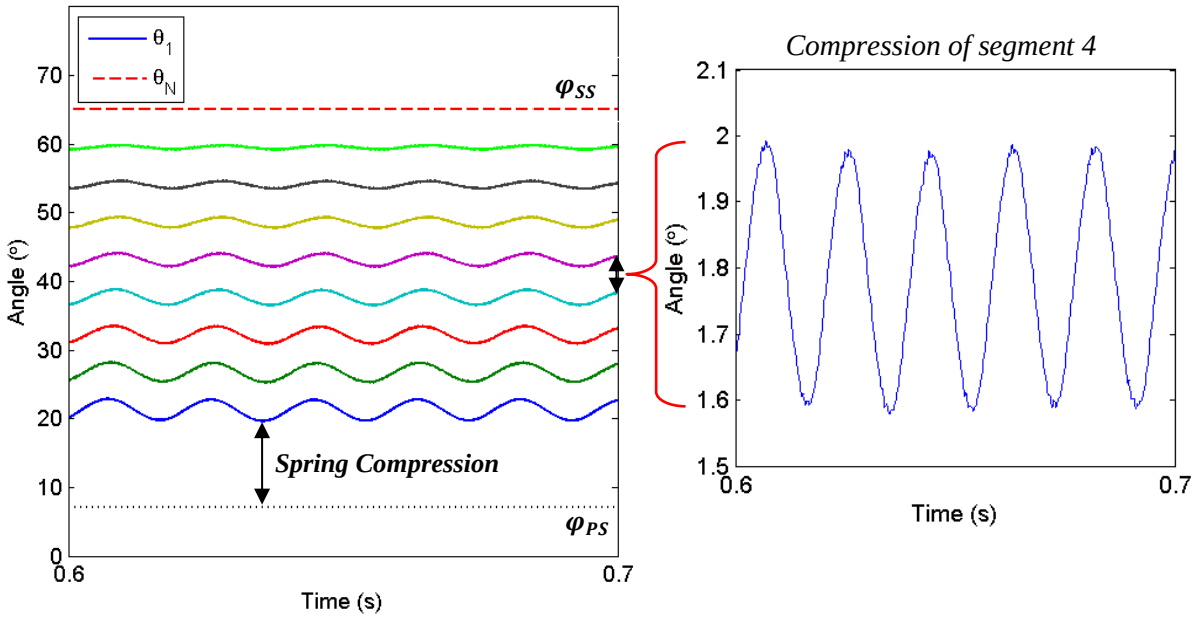

Figure 5.12: Compression & movement of (inner) spring segments when subjected to a fluctuating torque signal

The movement of the inertia positioned after the spring set (secondary inertia) relative to the preceding (primary) inertia (θ_{Rel} – see Equations 12 & 13) determines the movement and compression of the spring segments. The positions of the ends of the spring ($\theta_{S,1}$, $\theta_{S,N}$ – where N is the number of segments) are determined by comparing the positions of the primary and secondary end stops (Equations 16 & 17) [61].

When calculating the position of the first spring end, the position of the primary end stop is given by the half width of the primary stopper (φ_{PS}). The position of the secondary end stop is calculated from the relative movement of the secondary (θ_{Rel}) and the half width of the secondary stopper (φ_{SS}). When calculating the position of the last (N^{th}) spring segment, the positions of the end stops are calculated in the same manner, except the length of the arc between the centre of the primary stoppers must also be included. This arc length is calculated by dividing the total number of radians in a circle by the number of springs (nS).

The position of the end of the spring if completely relaxed (the position of the end mass θ_{Sm} combined with the relaxed segment length φ_{seg}) is also compared to the end stop locations. This component is required when there is a clearance angle (spring arc is smaller than the housing slot), as the end of the spring when relaxed may not necessarily be touching the end stops of one of the inertias. All angular positions, segment lengths and stopper half widths are given in radians.

$$\theta_{S,1} = max\{\varphi_{PS},\ \theta_{Rel} + \varphi_{SS},\ \theta_{Sm,1} - \varphi_{seg}\} \tag{16}$$

$$\theta_{S,N} = min\left\{\frac{2\pi}{nS} - \varphi_{PS}, \theta_{Rel} - \varphi_{SS} + \frac{2\pi}{nS}, \theta_{Sm,N-1} + \varphi_{seg}\right\} \tag{17}$$

$$\theta_{S,2:N-1} = \theta_{Sm,i} \tag{18}$$

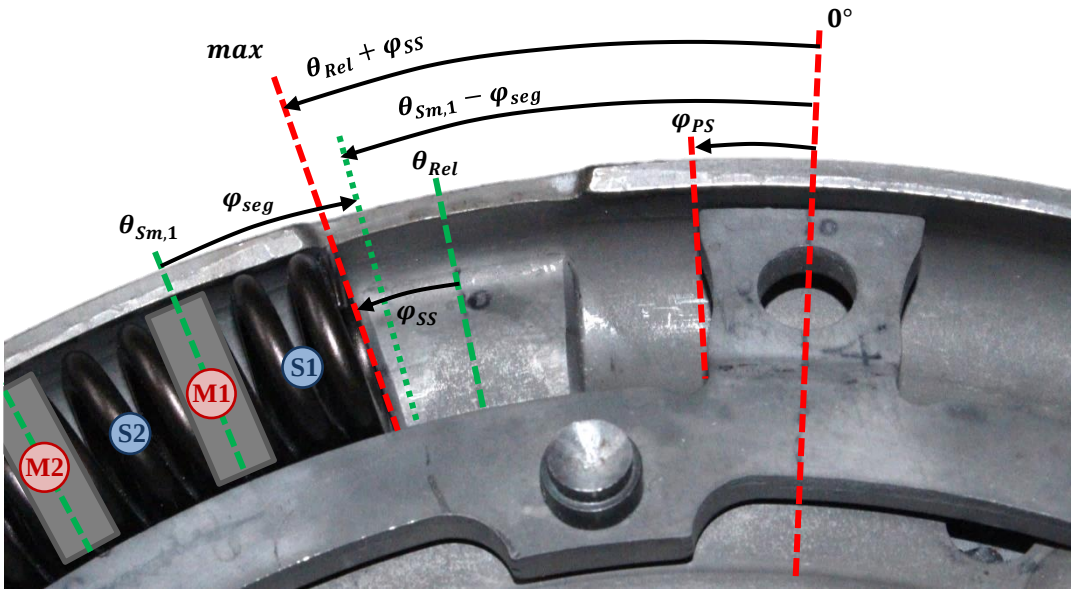

Figure 5.13: Determining the position of the end of the arc spring

A demonstration of these equations can be seen in Figure 5.13, when a positive torque is applied to the outer spring system, J_{sec} moves anti-clockwise relative to J_{pri}, compressing the spring. In the simulation as the angular displacement (from the zero point) of the secondary end stop is now larger than that of the primary end stop, the first spring segment is therefore being compressed and its location must change.

As the damper system rotates, the coils of the arc springs are forced into the outer race of their housing (see section 2.4.2) due to centrifugal force (F_c). A (tangential) force applied to the ends of the arc spring also produces a redirection force (F_{red}) – see Figure 5.14. Sometimes the springs are subjected to a radial pre-load force (F_p); for example, when the slot they are housed in is either shorter than their relaxed length or when it does not have the same curvature. F_p) has an individual value for each discretised mass; this allows it to be fine-tuned for situations where the preload is not evenly distributed across all the coils (i.e. when preload is caused by housing curvature). The sum of these forces gives the total radial force (F_R, Newtons) exerted on the spring segments.

$$F_{R,i} = F_{c,i} + F_{red,i} + F_{p,i} \tag{19}$$

The methods displayed in Equations 19-24 for calculating the radial forces were originally used in a DMF model [61]; modifications have been made to adapt them to the torque converter damper, but the general principles of an arc spring in a curved housing remain the same.

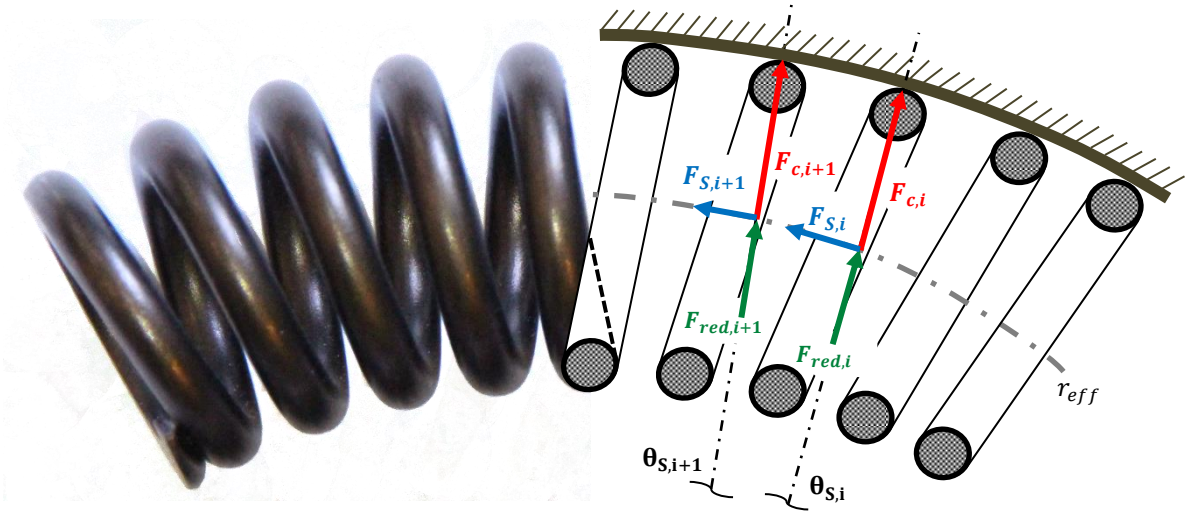

Figure 5.14: Radial forces on spring coils; spring load (F_S) is transmitted from coil to coil, creating a normal reaction force F_{Red} which combines with centrifugal force F_c (and preload force F_p if present) to give the total radial force F_R

The centrifugal force (F_c) is calculated using Newton's second law of motion ($F = ma$), where the mass of each spring segment is given by m_i and the acceleration is calculated by multiplying the square of angular speed ($\dot{\theta}_{pri}$) by the radius at which the mass is rotating. As the centrifugal force depends on the distance the mass is from the centre of rotation, the effective radius (r_{eff} – see Figure 5.14) of the spring is used.

$$\boldsymbol{F_{c,i}} = m_i r_{eff} \dot{\theta}_{pri}^{\,2} \tag{20}$$

The deflection forces (F_{defl}) on the spring elements (denoted by i, where $i = 1{:}\,N-1$) are calculated using Equation 21, where T_s is spring torque (Nm), r_{eff} is the effective radius (m), n_W is the number of coils per segment and the angular position (rad) of the spring segments is represented by θ_S.

$$F_{defl,i} = \underbrace{\frac{T_{S,i}}{r_{eff}} \cdot 2n_{W,i}}_{\boldsymbol{F_{S,i}}} sin\left(\frac{\theta_{S,i+1}-\theta_{S,i}}{2n_{W,i}}\right) \tag{21}$$

These deflection forces (F_{defl}) are applied to the adjacent masses using Equation 22, where F_{red} is the redirection force (N) that is used to calculate the total radial force in Equation 19. Equations 23 and 24 represent the special cases of the end (first and last) masses; here, the deflection forces from the end spring are applied fully to the end masses.

$$\boldsymbol{F_{red,i}} = \frac{1}{2}F_{defl,i} + \frac{1}{2}F_{defl,(i+1)} \tag{22}$$

$$F_{red,1} = F_{defl,1} + \frac{1}{2}F_{defl,2} \tag{23}$$

$$F_{red,(N-1)} = \frac{1}{2}F_{defl,(N-1)} + F_{defl,N} \tag{24}$$

5.3.2 Nested arc springs

The simulation of a nested spring pair is very similar to that of the basic arc spring; the friction, movement, torque and radial forces are calculated in the same manner as a standard arc spring for both the outer and inner springs in the pair. Each spring in the pair has its own mass (m) and stiffness (k); as they are essentially parallel springs the sum of their stiffnesses equals the total stiffness of the second stage of the damper. The torque loading is shared across both springs, with each transmitting an amount linked to its respective stiffness and compression; the sum of the two torques gives the total spring torque, which is then applied to the damper inertias. As the end positions of the springs are determined by the movement of the plates (inertias) they will be the same for both springs in the pair; however the movement of the individual segments may be different due to the differing accelerations.

The reason for modelling the nested set as a pair of parallel springs, rather than as a single stiffer arc spring, is the friction between – and radial forces on – the inner and outer spring. The radial forces and friction from the inner spring are applied to its housing as per normal, except the housing in this case is the inner surface of the outer spring of the nested pair (see Figure 5.15). As the spring set is compressed, the re-direction forces on the inner nested spring may push it against the outer spring; it is unknown what effect this may have on the radial forces of the outer spring. In the final simulation the radial forces were calculated separately, with no extra force being exerted on the outer spring. The concept that the inner spring may force the outer spring further into its housing was tested during simulation development, by assuming that the radial forces on the outer spring are the sum of those calculated for both the inner and outer spring. However the inclusion of this feature appeared to have little to no impact on the behaviour of the damper; therefore as the concept could not be verified or independently measured during testing it was not included as a separate feature. Any effect will likely be accounted for during calibration of spring friction terms.

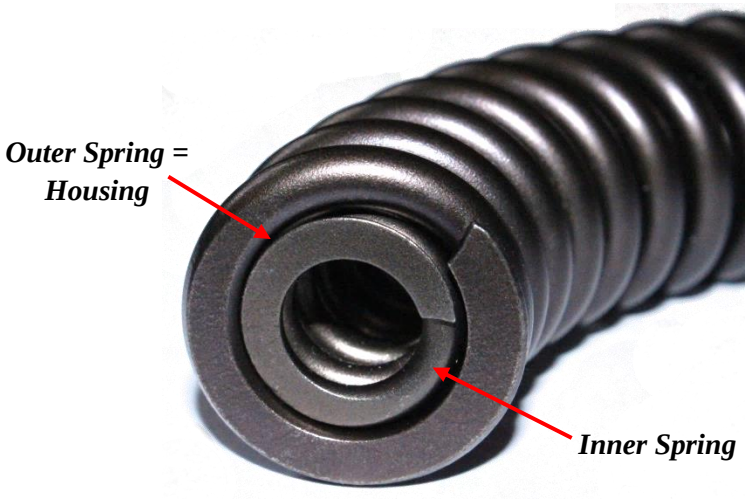

Figure 5.15: Nested springs in the inner spring set

The accelerations of the segment masses of the two springs are calculated separately using conservation of angular momentum (Equations 25 & 26); the only frictional force (T_{fric}) on the inner spring comes from its interaction with its housing (the outer spring). However, as the outer spring is subjected to frictional forces on both its inner and outer surface, both frictional torques ($T_{fric,Out}$ and $T_{fric,Inn}$) are applied. In order for the inner frictional force to be applied correctly in the simulation, the inner and outer springs must be discretised into the same number of segments. The subscript *Out* denotes the outer spring of the nested pair, and the subscript *Inn* denotes the outer spring. Here, the inertia positioned before the spring set is the secondary inertia, denoted by the subscript *sec*.

$$J_{Sm,Out}\left(\ddot{\theta}_{Sm,Out,i} - \ddot{\theta}_{sec}\right) = \underbrace{T_{S,i} - T_{S,(i+1)}}_{\boldsymbol{T_{res}}} - T_{fric,Out,i} - T_{fric,Inn,i} \tag{25}$$

$$J_{Sm,Inn}\left(\ddot{\theta}_{Sm,Inn,i} - \ddot{\theta}_{sec}\right) = T_{S,i} - T_{S,(i+1)} - T_{fric,Inn,i} \tag{26}$$

Where J_{Sm} is the inertia of the spring mass (kgm^2), $\ddot{\theta}_{Sm}$ is the relative acceleration of the spring mass (rad/s^2), T_s is the torque applied to the mass by the adjacent massless springs (Nm) and T_{fric} is the frictional torque (Nm).

5.4 Friction modelling

The friction model utilised in this study was developed by Makkar [73] and is a continuously differentiable model, as opposed to the discontinuous or piecewise continuous models that are often used (see section 2.4.3). The greatest advantage of the Makkar friction model is that it does not assume that friction is constant; Equation 27 allows the friction model (the coefficient of friction – μ) to change with speed (see Figure 5.16). For this equation, the linear speed ($\dot{x}_{Sm}$ - m/s) must be used instead of the angular speed ($\dot{\theta}_{Sm}$ - rad/s); the angular speed can be easily converted by multiplying it by the radius at which friction contact occurs (r_{fri} - m). For the smaller of the inner springs, the speed used in this friction calculation should be the speed of the smaller spring relative to larger spring. This is because the larger spring forms the housing for the smaller spring and friction occurs when two surfaces move relative to each other.

The first bracket set represents the Stribeck friction component, the second Coulombic (the dominant term) and the final term Viscous (see section 2.4.3).

$$\mu = f\left(\dot{x}_{Sm,i} r_{fri}\right) = \underbrace{\gamma_1(tanh(\gamma_2\dot{x}_{Sm,i}) - tanh(\gamma_3\dot{x}_{Sm,i}))}_{\textbf{Stribeck}} + \overbrace{\gamma_4\, tanh(\gamma_5\dot{x}_{Sm,i})}^{\textbf{Coulombic}} + \underbrace{\gamma_6\dot{x}_{Sm,i}}_{\textbf{Viscous}} \tag{27}$$

The $\gamma_1$and γ_4 terms represent the static coefficient of friction – in this case, the coefficient of friction between two lubricated steel surfaces (0.2). The $\gamma_2$term controls the rate at which the friction coefficient increases from zero (at very low slip speeds). The $\gamma_3$and γ_5 terms control when the stribeck term ceases to be dominant and the coulombic region begins. All of these terms can be adjusted, i.e. using experimental validation; for the purposes of this simulation the example terms provided by Makkar [74] were used ($\gamma_2 = \gamma_5 = 100, \gamma_3 = 10, \gamma_6 = 0.01$).

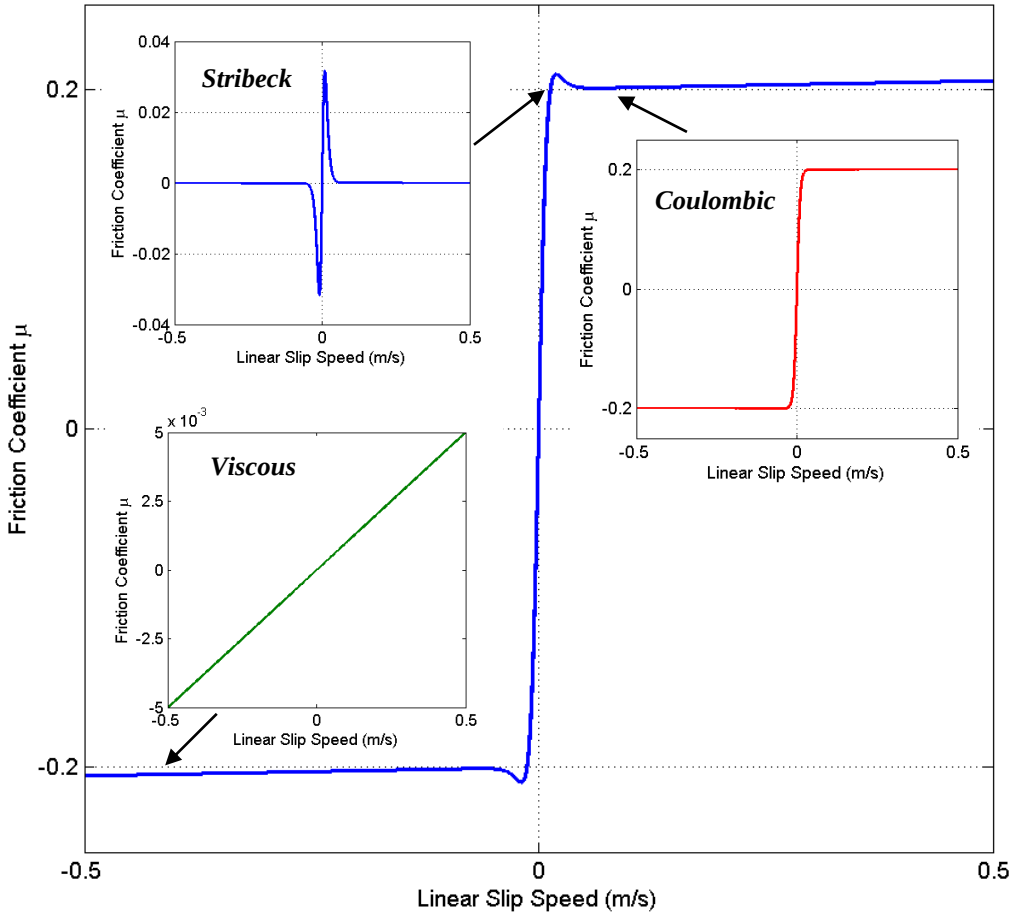

Figure 5.16: Overall friction coefficient profile and profiles of components (Stribeck, Coulombic and Viscous)

In order to calculate the frictional force on the spring segments (the force that opposes the motion of the spring) the radial (normal) force ($F_R - N$) is multiplied by the dynamic friction coefficient (μ). To convert this force into a frictional torque (T_{fric} – Nm) it must then be multiplied by the radius (m) at which it acts – r_{fri} (Equation 28). A tuning factor (α_{fric}) is also included; each of the three spring types (outer and both nested inner springs) are assigned their own factor. These factors are used to fine-tune the frictional behaviour of the individual springs and allow additional design variables to be taken into account– primarily the level of spring to housing contact. The amount of contact a spring has with its housing – and therefore the amount of frictional torque exerted on its coils – is dependent on a number of factors from housing shape to spring wire shape. The use of a single tuning factor (that can be approximated from hardware and adjusted using test data) is the simplest method for ensuring these important design features are included (spring behaviour is dependent on friction).

$$T_{fric,i} = \alpha_{fric}(\mu \times F_{R,i} \times r_{fri}) \tag{28}$$

5.5 Additional components

5.5.1 Stacking of spring coils

It is important to include spring segment movement limitations in the model; each spring segment should not be allowed to compress further than is physically possible in a real spring. Not doing so would potentially allow multiple coils to occupy the same physical space, which due to its lack of realism would undoubtedly affect simulation results. In order to implement this limitation, the position of each segment (θ_S – rad) is compared to the position of the one adjacent to it; this distance is then compared to the minimum allowable distance between them (φ_{stack} – rad, calculated from the thickness and number of coils in the spring). Thus the segment is not allowed to move further than physically possible (Equation 29).

$$\theta_S = \begin{cases} max(\theta_{S,i-1} + \varphi_{stack}, \theta_{S,i}) & i = 2{:}N \\ \theta_{S,x} & i = 1, N+1 \end{cases} \tag{29}$$

5.5.2 Hardstops

As discussed in section 5.1, both spring sets have physical hardstops that limit the relative movement (angle windup) between the inertias. These hardstops provide more consistent knee points (improving performance repeatability) and help prevent the springs from becoming completely coil bound (which may lead to hardware damage). For ease of explanation, the outer hardstops are described here; the same methods are used to simulate the inner spring set hardstops, except J_{sec} becomes the 'primary' inertia and J_{ter} becomes the 'secondary' inertia – the primary inertia is located before the spring set, the secondary after it.

Two potential methods for simulating hardstops were examined. The hardstops could be implemented either by directly transferring the torque from the input to the secondary inertia (instead of the primary inertia) once hardstop contact is made, or by simulating the hardstop as a block with a very high stiffness that essentially takes over from the springs. Both methods were attempted; however the secondary method (a stiff block) proved to be unnecessarily complex to simulate, as well as introducing extra unknown variables (block stiffness and damping). It also appeared to have poorer performance when the mean torque of the pulsating input signal was very close to the hardstop location (simulation stability was reduced).

The hardstop triggers (σ_{HS}) are activated by comparing the angular positions of the inertias before and after the spring set (e.g. θ_{pri} and θ_{sec}); if their relative movement (the distance between them) reaches the allowable limits (φ_{HS_P} and φ_{HS_N} – see Figure 5.17) the trigger value (σ_{HS}) is set to 1. Once the relative movement drops below the limit, the hardstop is no longer in contact and ceases to transmit torque (values is set to 0); a demonstration of this, using a pulsating input signal with a mean torque close to the allowable limits, can be seen in Figure 5.18.

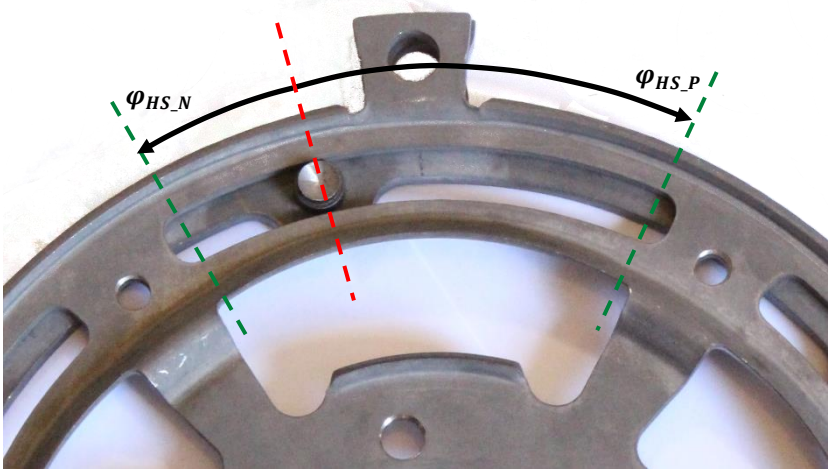

Figure 5.17: Outer spring set hardstop limits

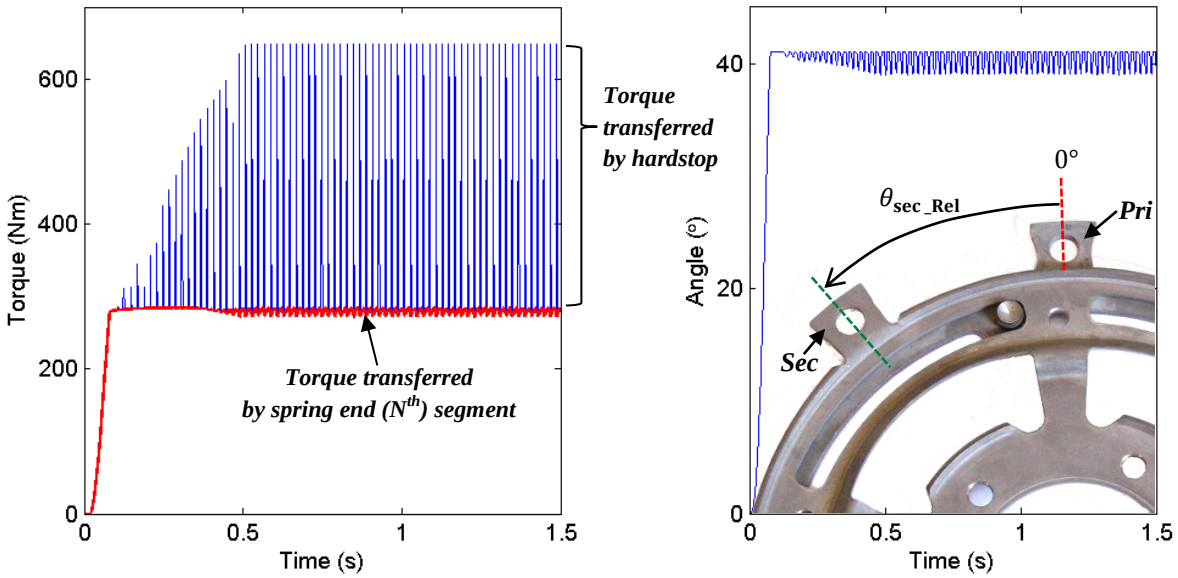

Figure 5.18: Behaviour of outer spring set when subjected to a fluctuating torque signal at a mean torque close to the spring set knee point. Torque transfer (not including frictional torque) to secondary inertia (Left) and relative movement of inertias (Right)

Once the triggers (σ_{HS}) are activated, the torque applied to that spring set cannot increase any further; the excess torque starts to be transferred directly to the secondary inertia (T_{HS} – Nm), Equation 30. The torque transferred by the hardstop is calculated by comparing the inertia (T_{in} – Nm) and the resistance torque. The resistance torque is calculated by multiplying the number of springs in the set (nS) by the torque (T_S – Nm) applied by the end of the spring that is in contact with the inertia (determined using the contact triggers, σ).

$$T_{HS} = \sigma_{HS}\left(T_{in} - nS_{outer}\left(\sigma_1^P T_{So,1} - \sigma_N^P T_{So,N}\right)\right) \tag{30}$$

The torque applied to the damper at this point is shared between the spring set and the hardstop, as if they are parallel springs. Torque is still transmitted by the springs, but once the hardstop is engaged any torque above the level the compressed spring can transmit (determined by Hooke's law, $F = kx$) is instead transmitted via the hardstops. The hardstop applies torque directly to the secondary inertia; it also provides a resistance torque to the preceding inertia (Newton's third law). By resolving the torques acting on the secondary inertia (including the frictional torques T_{fric}, see Equation 5) this resistance torque (T_{HS_Res}) can be calculated (Equation 31). If the resistance torque is not calculated (e.g. T_{HS} applied to primary inertia instead of T_{HS_Res}) the inertia plates will not move at the same speed when the hardstops are activated; the overall angular positions of the inertias will not be correctly simulated (i.e. their relative angular displacement will increase further than physically possible).

$$T_{HS\_Res} = \left\{nS_{inner}\left(\sigma_1^{Si}T_{Si,1} + \sigma_N^{Si}T_{Si,N} - \left|\alpha_{sec}\sum_N^1 T_{innfric}\right|\right) - nS_{outer}\left(\sigma_1^{So}T_{So,1} + \sigma_N^{So}T_{So,N} - \left|\sum_N^1 T_{outfric}\right|\right)\right\} \tag{31}$$

When the hardstops are active, the inertias either side of the spring set (e.g. J_{pri} & J_{sec}) are in direct contact and have begun moving at the same speed; thus their angle of separation (windup angle) becomes constant. As the inertias are in direct contact, it is proposed that they essentially become one mass; the inertia resisting the torque inputted to the damper increases from just the primary inertia to the sum of the primary and secondary (Equation 32). The same applies to the secondary inertia; the resistance torque exerted on it by the inner spring set (the torque going in the opposite direction to the movement of the inertia) is pushing against the sum of both the primary and secondary inertias (Equation 33). Hardstop application can be controlled using the trigger (σ_{HS}).

$$J_{pri} = \begin{cases} J_{pri\_x} & \sigma_{HS} = 0 \\ J_{pri\_x} + J_{sec\_x} & \sigma_{HS} = 1 \end{cases} \quad (32)$$

$$J_{sec} = \begin{cases} J_{sec\_x} & \sigma_{HS} = 0 \\ J_{pri\_x} + J_{sec\_x} & \sigma_{HS} = 1 \end{cases} \quad (33)$$

5.6 Model structure

MATLAB Simulink® was chosen as the simulation environment, partly due to its flexibility and partly due to the availability of software. Models in Simulink® are created using block diagrams, with a wide range of both fixed and variable-step solvers available; in this instance a discrete fixed-step solver was used. Both variable and fixed-step solvers were trialled; no improvement in simulation time was observed when using a variable step solver (some solvers actually increased simulation time, possibly due to the frequent state changes in the spring segments) so a fixed-step solver (with a timestep of $1x10^{-06}$) was chosen. This timestep equates to a 0.009° angular movement if an object is rotating at 1500rpm; this timestep should therefore provide excellent resolution (see section 6.2.2 and Figure 6.10 for more detailed information on timestep selection). A discrete (rather than continuous) solver was considered the most appropriate due to the construction of the simulation. The damper simulation is made up of subsystems, with three main types; Inertia, Spring and Connector (see Figure 5.19). These subsystem blocks can be saved and stored as library blocks, which can then be used to create new damper configurations; additional library blocks (such as two-stage nested springs or linear springs) could also be produced.

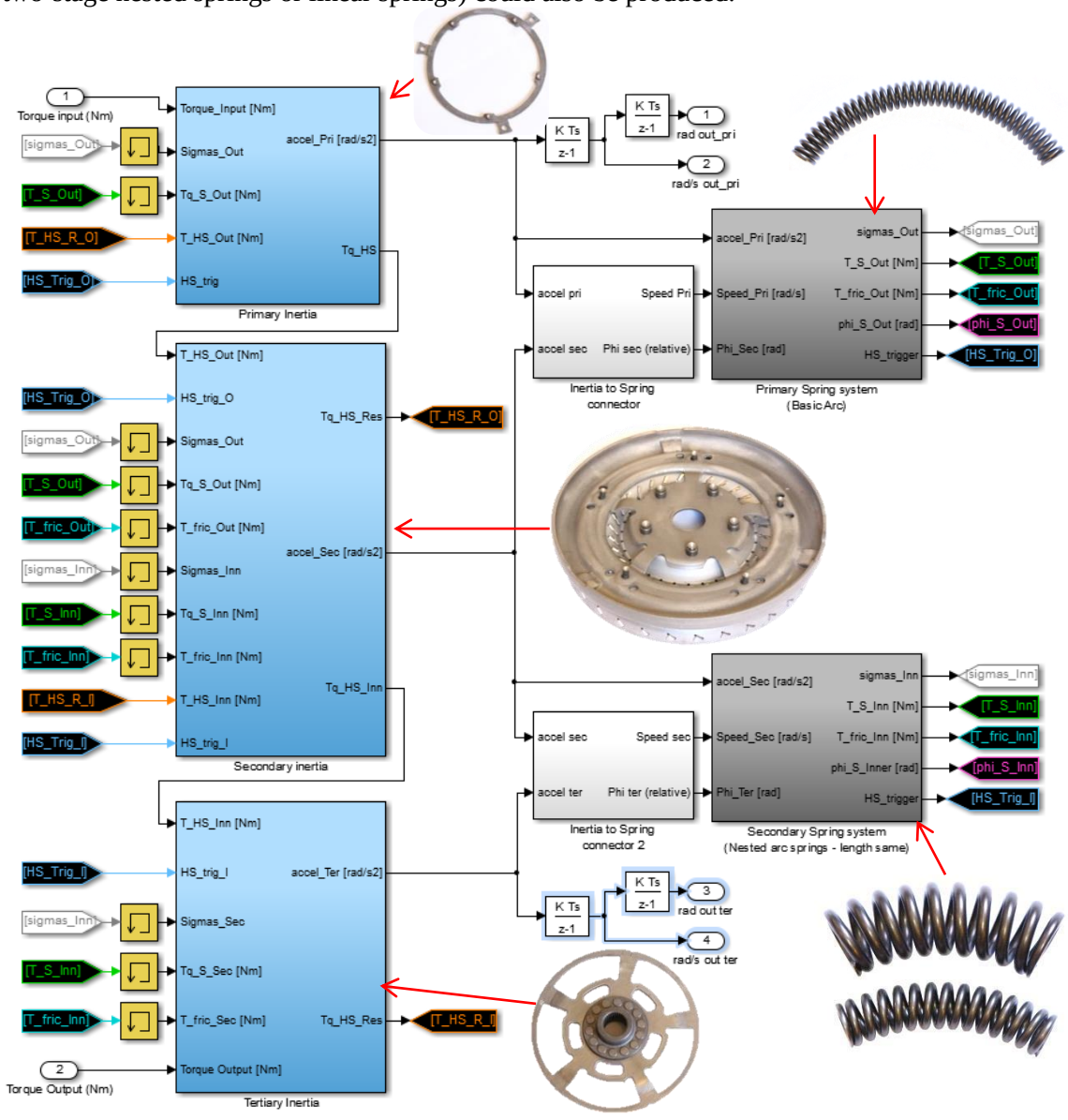

Figure 5.19: Damper model structure in Simulink®

Parameters can either be adjusted by modifying a script file, or through the use of subsystem masks. Masks are a more user-friendly option; when a user double clicks a subsystem block (e.g. Basic Arc Spring) a dialog box with all the adjustable parameters for that block (as well as recommended values) appears.

5.7 Rig (test facility) and vehicle component modelling

The rig components (including the gearbox) were modelled by assigning each component (or flange group) a stiffness (K – Nm/rad), an inertia (J – kgm^2) and an internal damping factor (B) [98]; essentially, the components were modelled as short, very stiff, mechanical shafts (see Equations 34 & 35). In these equations, T is torque (Nm), $\dot{\theta}$ is angular speed (rad/s) and $\ddot{\theta}$ is angular acceleration (rad/s^2).

$$T = K\int(\dot{\theta}_{In} - \dot{\theta}_{Out})dt + B_k(\dot{\theta}_{In} - \dot{\theta}_{Out}) \tag{34}$$

$$\ddot{\theta} = \frac{(T_{In} - T_{Out} - B_J\dot{\theta})}{J} \tag{35}$$

For components that were bought in (e.g. couplings, transducers) manufacturer data sheets provided the required information (see Appendix). For the custom-made flanges, the CAD models were assigned the appropriate material and then used to calculate the inertia; an approximation of the stiffness was calculated using the shear modulus of the material (G - GPa), the polar moment of inertia (J – kgm^2) and the length of the component (m) – see Equation 36.

$$K = \frac{G \times J}{length\ of\ 'shaft'} \tag{36}$$

The implementation of the equations for the inertia and stiffness calculations (above) into the Simulink® model can be seen in Figure 5.20; the methods used allow for torsional feedback between components, an important feature when examining system vibration behaviour. By constructing each component as an individual subsystem, the positioning of the components in the power flow can be easily adjusted and new components included (e.g. if an additional instrumentation flange is installed).

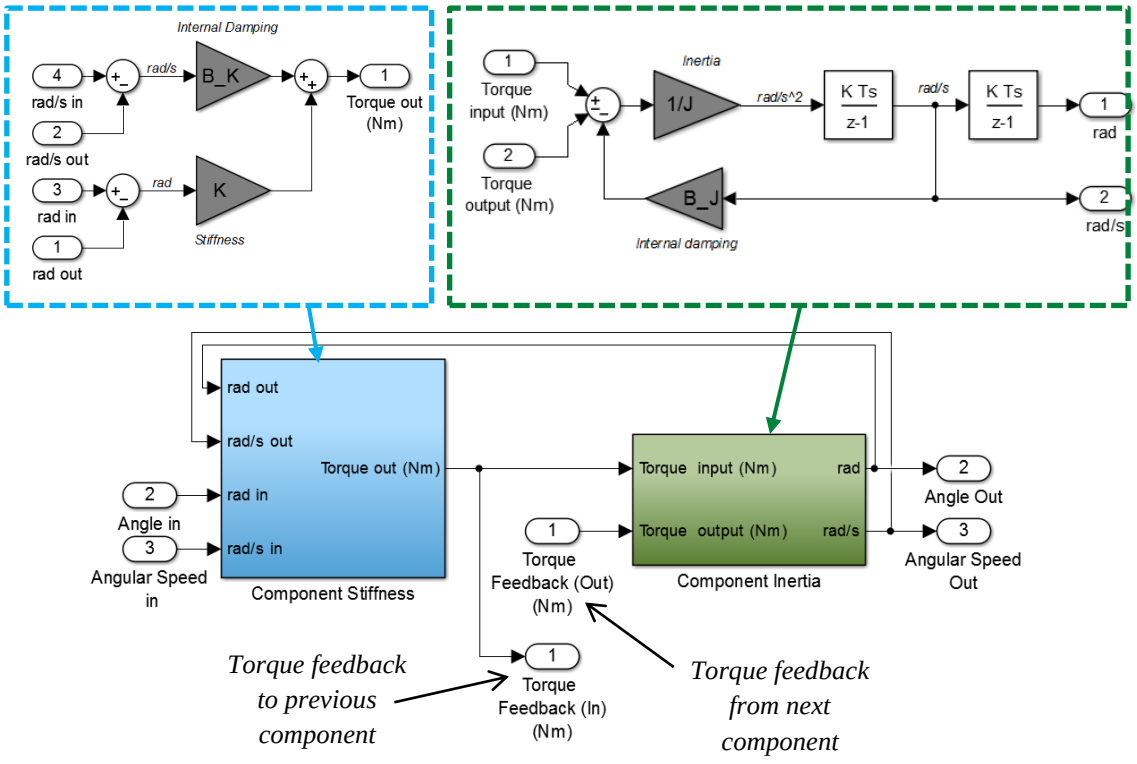

Figure 5.20: Implementation of rig/vehicle component stiffness (Top Left) and inertia (Top Right) equations and component subsystem (Bottom) in Simulink®

5.8 Summary

In this chapter, a detailed examination of the hardware has taken place and the methods used to simulate the selected damper system have been presented. Disassembling the torque converter damper system and examining the hardware ensures the accuracy of the simulation.

The key outcomes from this chapter have been summarised below:

- This model simulates a two-stage arc spring turbine damper; three inertias (primary, secondary and tertiary) are separated by two spring sets. The outer spring set of the simulated damper has 3 individual arc springs, while the inner spring set has 5 nested pairs. The movement of both spring sets is limited by physical hardstops; the hardstops are positioned so that more movement is allowed when a positive torque is applied. Disassembling the hardware allows the location of the hardstops to be measured rather than relying on the test data.

- The principle of conservation of angular momentum is applied to each of the three inertias in order to calculate their individual accelerations. By comparing the torque applied to the input of each inertia and its resistance torque (the reaction torque of the spring set or the hardstops) the movement of the inertia is calculated.

- If all the springs in a set are identical it is only necessary to model the full movement and forces of one spring from the set; however, care must be taken to ensure the spring torques for all the springs are applied to the inertias (by multiplying the spring torques by the number of springs in each set).

- The springs in the outer sets only contact (exert a frictional torque on) the outer wall of their housing – the secondary inertia. When static, the bulk of the larger spring in the inner spring set does not contact the housing; however, wear patterns on the tertiary inertia (combined with the ease of deformation of the spring) suggest that once the damper is rotating the centrifugal force causes the inner spring set to contact both the secondary and tertiary inertias.

- The arc springs are discretised into mass and (massless) spring segments; the acceleration of each of the segment masses is calculated in the same way as the inertias – the principle of conservation of angular momentum.

- The movement of the inertia positioned after the spring set (secondary) relative to the preceding (primary) inertia determines the movement of the end spring segment.

- As the damper rotates, centrifugal and tangential forces exerted on the springs force them into the outer race of their housing; the overall radial force (along with the relative movement of the spring segments and their housing) is used to calculate the frictional force exerted on the segments and the housing.

- When simulating the nested spring pairs the friction, movement, torque and radial forces are calculated in the same manner as a standard arc spring (for both springs in the pair). The torque loading is shared across both springs, with each transmitting an amount linked to its respective stiffness. The nested springs are simulated as a pair of parallel springs, rather than as a single stiffer arc spring; this is because of the friction between the springs. The housing for the smaller spring in the pair is formed by the inner race of the larger spring; thus friction occurs between them. The concept that radial forces from the inner spring may force the outer spring further into its housing was tested during simulation development; however, the inclusion of this feature appeared to have little to no impact on damper behaviour and it was therefore removed.

- The Makkar continuously differentiable friction model has been used as it is both dynamic (does not assume that friction is constant) and robust enough to cope with the segments changing direction (the direction of the linear slip speed changing). Each spring (outer and both nested inner springs) has its own tuning factor; these factors are used to fine-tune the frictional behaviour of the individual springs (design variables such as wire shape will affect the level of spring to housing contact).

- Spring segment movement limitations have been included in the simulation; each spring segment is not allowed to compress further than is physically possible in a real spring. This has been implemented by comparing the position of each segment to the position of the one adjacent to it; this distance is then compared to the minimum allowable distance between them.

- Two potential methods for simulating hardstops were examined. The hardstops could be implemented either by directly transferring the torque from the input to the output inertia once hardstop contact is made, or by simulating the hardstop as a block with a very high stiffness. The latter method proved to be unnecessarily complex to simulate and had poorer performance when the mean torque was close to the hardstop location.

- MATLAB Simulink® was chosen as the simulation environment, partly due to its flexibility and partly due to the availability of software. The block-based simulation method Simulink® employs allows subsystems and library components to be easily constructed; parameters can either be adjusted by modifying a script file, or through the use of subsystem masks.

- The rig components were also simulated by assuming they function as short, very stiff, mechanical shafts; each component was assigned a stiffness, an inertia and a damping factor. This method allows for torsional feedback between components, an important feature when examining system vibration behaviour.

Chapter 6 Damper performance and simulation validation

This chapter details the method used to *parameterise* the simulation – the adjustment of estimated or unknown parameters to improve the match between the damper simulation output and the equivalent test data. Simulation (as opposed to hardware) variables are also examined with the final results of the parametrised damper simulation presented, including a demonstration of the behaviour of specific key components.

6.1 Parameterisation

Parameter values for the simulation can be split into three categories: observed, calculated and estimated. Observed values can be measured from the hardware (see Figure 6.1) and then used to calculate other required parameters, such as the minimum length of a spring or segment (when a segment is coil bound and can be compressed no further). Estimated parameters are either calculated values that are not accurate enough to become fixed variables (e.g. primary/secondary/tertiary inertias) or those that can be approximated from hardware measurements or test data; these estimated parameters are the ones that require tuning through comparing simulation performance to that of the test rig.

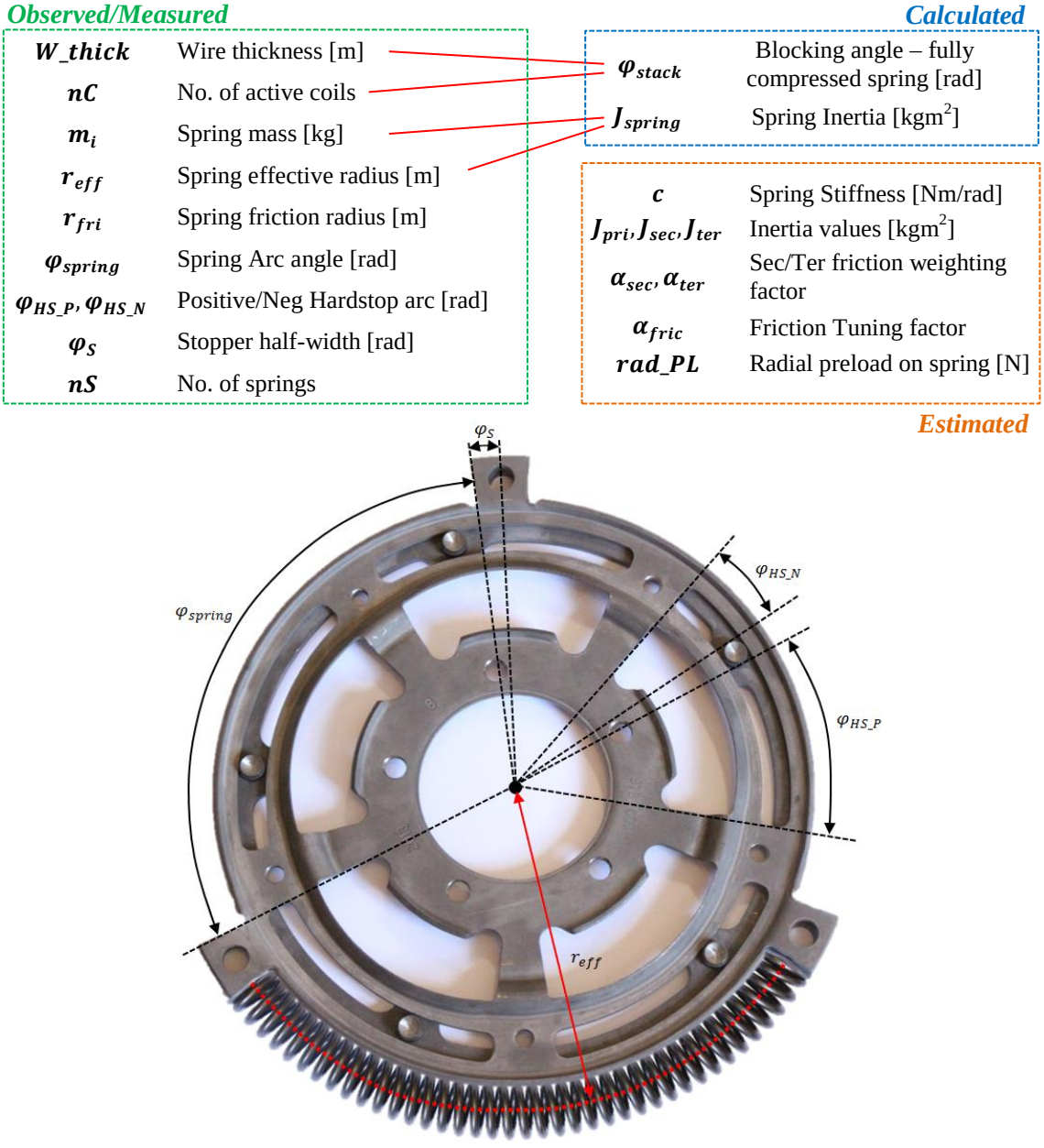

Figure 6.1: Taking parameter measurements from hardware

Estimated values require fine-tuning through iterative simulation; however initial estimates can be obtained by examining the hardware or test data. Each spring type (outer and both inners) has a friction tuning factor that can be used to take into account actual surface area contact (rather than incorrectly assuming the entire spring surface touches the housing) and wire shape (frictional surface area of coil).

Figure 6.2: Assessing outer spring contact with its housing (secondary inertia)

In order to assess what percentage of the (outer) spring surface area is in contact with the secondary inertia – and therefore determine a reasonable approximation for the outer spring set friction tuning factor – a red wax-based substance[3] was used to mark a section of the housing track on the secondary inertia (see Figure 6.2). The spring was then inserted into the housing and manually moved in the track. This allows the contact points between the spring and the housing to be visualised; the exact location of the contact points may change slightly due to centrifugal forces but size will remain approximately the same. The amount of wax based dye transferred to the spring surface was measured and found to be equal to approximately 30% of the outer surface area of the spring coils; hence a value of 0.3 was used for the outer spring set friction tuning factor ($\boldsymbol{\alpha_{fric,Out}}$). Knowing the location of the contact points between the spring and the housing also allows a more accurate spring friction radius ($\boldsymbol{r_{fri}}$) to be estimated.

The same method was used to estimate the friction tuning factor for the larger spring of the nested pair ($\boldsymbol{\alpha_{fric,InnOut}}$ = 0.15). However, the housing for the smaller nested spring is not a solid, constant surface (the housing is the larger spring in the pair); so in order to calculate the tuning factor for the friction of the smaller spring ($\boldsymbol{\alpha_{fric,InnIn}}$), the potential surface area available for contact on the outer surface of the smaller spring was compared with that of the inside of the larger spring, with the ratio between them (0.55) providing the estimated value.

Figure 6.3: Inner spring set contact with secondary and tertiary inertias (when static and no outward force applied)

[3] Also known as lipstick - more specifically, Maxfactor Scarlet Ghost.

The frictional weighting factors – how the friction from the inner set of springs is shared between the secondary and tertiary inertias – can also be estimated by observing the hardware (see Figure 6.3). However this parameter is slightly harder to estimate due to potential centrifugal effects on the spring; at rest, only the very end coils of the spring contact the secondary and tertiary inertia, but the springs can be manually deflected outwards (by hand) and into full contact with both inertias with minimal force. As the amount of surface area contact between the larger inner spring and the housing is approximately the same on both the secondary and tertiary inertia, the frictional weighting factor is set to 0.5 for both, thus evenly sharing the friction force.

The inertia of the primary, secondary and tertiary masses can be estimated by weighing their lumped components and applying the rotational inertia equation for a hollow cylinder (Equation 37). Using this equation rather than the solid cylinder version is preferable as (through adjustment of the two radii measurements) it allows the uneven distribution of mass across the disc to be taken into account (see Figure 6.4). Due to the complex shapes of the mass components, these estimations for inertia should not be assumed to be the final fixed values; however, they can be very useful for producing initial values and approximate ranges for model parameterisation, with iterative adjustment and simulation/test data comparisons being used to fine-tune the values.

$$Inertia = \frac{1}{2}M({R_2}^2 + {R_1}^2) \qquad (37)$$

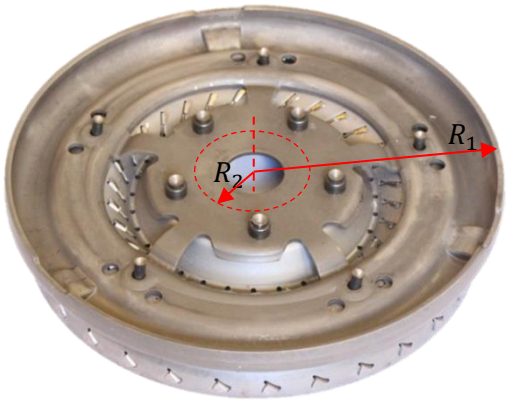

Figure 6.4: Estimating secondary inertia

An alternative method of determining the inertia of some of the hardware components would have been to use the trifilar measurement method. This procedure uses a trifilar suspension system (often with a plate to support the test object) to measure the oscillation period of an object when it is displaced. The oscillation period, combined with the mass of the object, can then be used to determine moment of inertia. As the primary objects to be measured are circular, with their mass symmetrically distributed, the accurate alignment of the centre of mass of the object to the centre of the supporting plate would be fairly simple (though it has been shown that this is one of the more insignificant potential sources of error [99]). Due to the substantially varying masses of the inertias multiple different support plates would be required; it is recommended that the ratio of plate to object mass be less than 0.25 [99]. Suspension wires could be connected directly to the test objects but evenly positioning the wires could be difficult and require modifications to the objects – e.g. holes drilled in casings. A plate that passes the 0.25 ratio rule for the tertiary inertia is unlikely to be able to support the mass of the primary inertia. While using the trifilar method may provide a more accurate estimation of the inertia values, the extra equipment and testing time required, combined with the minimal impact small (<20%) changes in inertia values have on simulation output (see section 7.1.2), allows the conclusion to be made that inertia estimation using hollow cylinder equations was adequate.

Approximations for the stiffness of the springs can be obtained from hysteresis loop testing; the hysteresis loops must extend above the knee point where the outer spring set becomes inactive. A value for the inner spring set stiffness can then be obtained and used to calculate the stiffness of the outer spring set from measurements taken below the knee point (the spring sets are in series). However when doing so, the effect that frictional forces have on these loops should be taken into account; the friction between the spring and its housing (or between the nested springs) may alter the stiffness of the springs. This means that the stiffness values obtained from hysteresis loops are likely to differ from the actual stiffness of the springs.

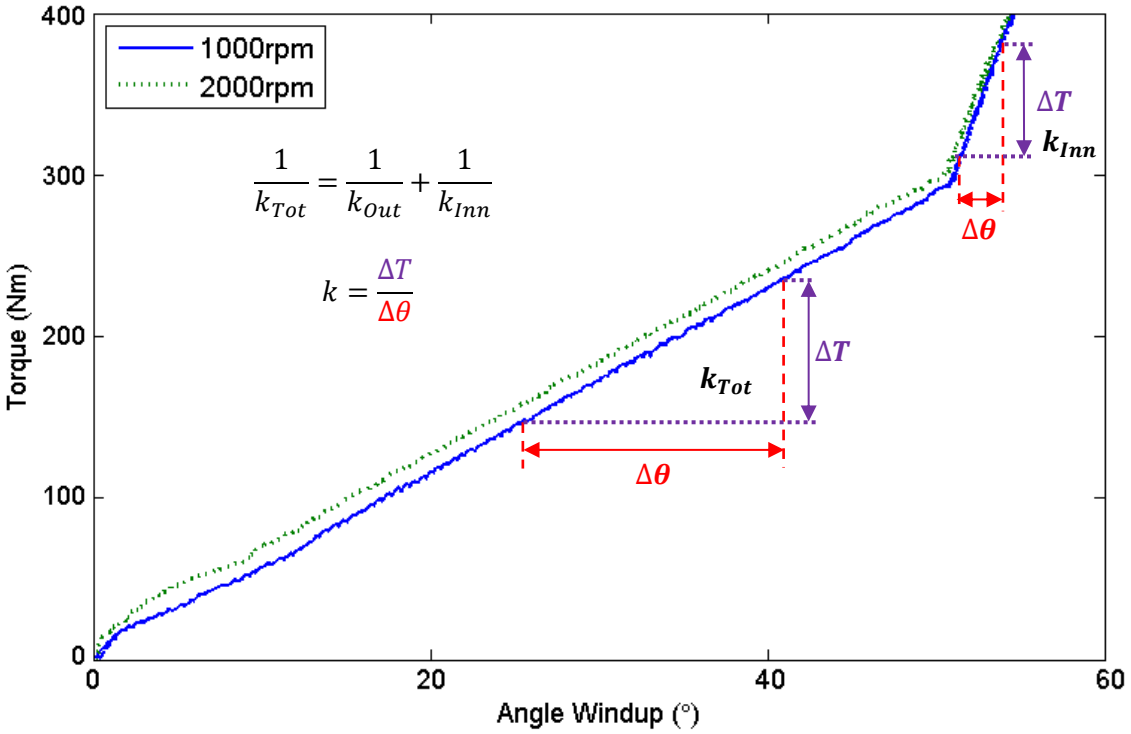

Figure 6.5: Estimating spring stiffness from torque ramp testing results

This effect can be seen in Figure 6.5, by comparing the stiffness values obtained from the same hysteresis loops taken at different rotational speeds (e.g. 1000 and 2000rpm). Increasing the speed by 1000 rpm alters the angle windup value at which the positive knee point occurs by ~1-2°. Thus to minimise error, spring stiffness values were approximated by averaging measurements from a 20-strong set of 1000rpm hysteresis loops, with stiffness values taken from above 100Nm. The effect of speed of damper dynamic stiffness and spring behaviour is investigated further in section 7.3.

The differing speed-dependent behaviour of the two spring sets (the stiffness of the inner spring set decreases as speed increases) is likely due to the nested springs (see section 5.3.2). The nested springs act as a pair of parallel springs; their combined stiffness is equal to the stiffness after the knee point. However, each spring is modelled separately in the simulation (rather than assuming they are one, stiffer spring) and thus an estimation for each of their separate stiffnesses is required; this is impossible to determine from hysteresis loop testing data. Static spring tests where the spring is gradually loaded with increasing force (using weights) could be used to test the springs individually; this would also remove any speed-dependent error. While this method is often used to test the stiffness of linear springs in extension, constraining and loading the arc springs in a way that would ensure they behaved (compressed) in a manner representative of the real damper can be difficult. Thus for the initial estimation it was assumed that the nested springs have the same stiffness; the total stiffness for that spring set was split evenly between them.

6.2 Validation using test data

6.2.1 Iterative Parameter Tuning

In order to improve the accuracy of the estimated parameter values, iterative simulation testing was used. The simulation was run using torque test data taken from before the gearbox as the input signal, with the output from the simulated gearbox then compared to the test data. The simulation measurements used for comparison were taken from the same locations as they were on the test rig; directly before the torque converter and directly after the gearbox (see Figure 3.4).

The torque input signal for each test point (e.g. 1200rpm, 200Nm mean torque) was formed by taking a 2 second sample of the corresponding test data (see Figure 6.6). This sampled data was then combined with a 0.3s ramp from 0Nm to the mean torque level and a 0.3s *ramping sin* section (a sin wave with a frequency matching that of the dominant order and with an amplitude gradually increasing to match the sampled signal). The ramp is required as the simulation must start from 0Nm torque input; the springs must not be loaded when the simulation initiates. A longer ramp time can be used but is unnecessary; there is no accuracy improvement to the final results thus the extra simulation time required is not justified. However too short a ramp time can result in the output torque signal overshooting the demand at the ramp peak; this results in the model taking longer to stabilise. This in turn reduces the amount of data available to take a FFT sample from, for comparison to the test data. As FFT sample size is directly related to accuracy (see section 3.4) the minimum ramp length that could be used without reducing the amount of data available for comparison was selected. The ramping sin is used to introduce the fluctuations to the signal; this is again primarily used to maximise the amount of usable comparison data, as the model needs to stabilise once the input signal starts to fluctuate. By using the ramping sin section the model stabilises before the sampled test data part of the signal begins.

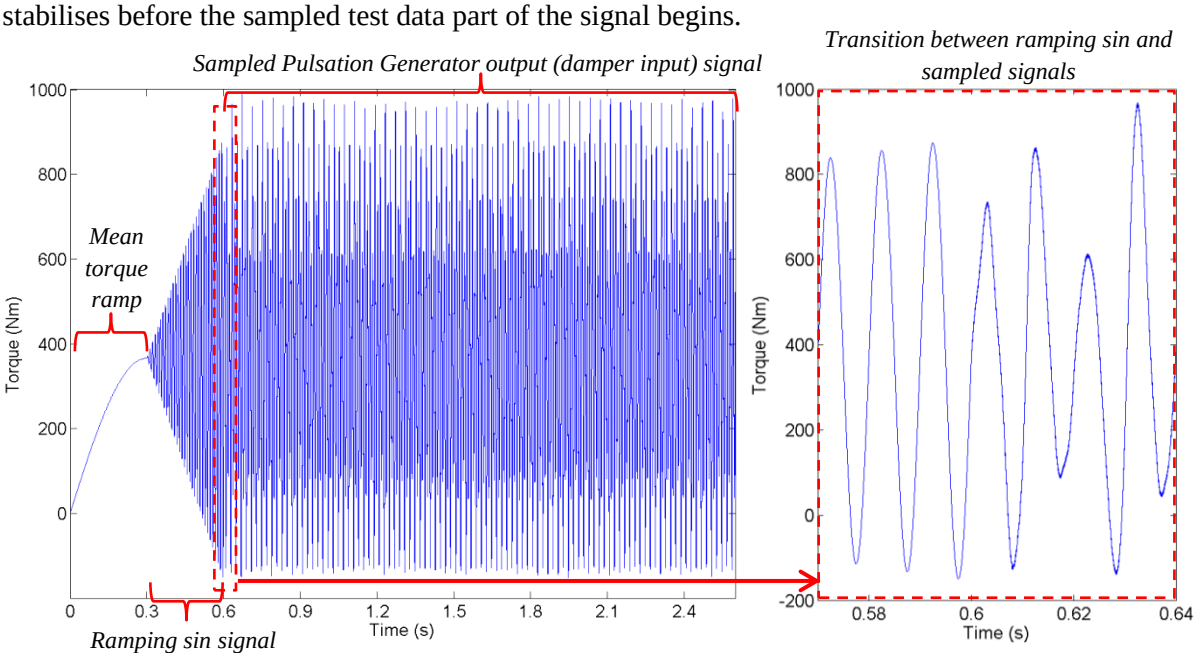

Figure 6.6: Construction of simulation torque input signal using measured damper input test data

Ideally, each time a parameter is adjusted the entire simulation set (covering the whole speed range) would be run again, to allow an accurate assessment of the impact of the change across the entire speed or mean torque range. However this is impractical, as to run an entire torque curve set of 160 tests (1200-2800rpm, test every 10rpm) would take at least 1.5hrs. Thus certain key speeds were identified and only a selection of these tests run whenever a change was made. The exact test set used varied depending on which parameter is being adjusted (and therefore what mean torque level was key), but typically a minimum of 4 different speed test points were used (e.g. 1200, 1500, 1800, 2100rpm). Key test points were selected by looking at the input magnitude of the primary (2^{nd}, 4^{th} and 6^{th}) damper orders and the magnification ratio of the other orders; ideally the vibrational input to the damper should be as large as possible, as test data shows that a torque input of below 20Nm can have a significant impact on attenuation performance (see Figure 6.24). Single test points (speeds) can be examined individually, but this is not recommended unless making minor changes; the effect parameters have is not always uniform across the frequency (or torque fluctuation magnitude) range (see section 7.1.2). A set of parameter changes may improve simulation performance at one test point, but have an adverse reaction at another. Thus to avoid lengthening the time taken to complete the total parameterisation process, it is recommended that this more comprehensive multi-test point approach is used, even though it increases the time taken to run each parameter set point test.

Initially, parameterisation was focused on tests with a mean torque above the outer spring set knee point; doing so removes some uncertainty, as only the inner springs would be active, reducing the number of adjustable variables that may have an impact on the results. Simulation input signals created from the mapping test data sets are primarily used for testing simulation performance below the knee point; these data sets cover a lower mean torque range. Due to the large steps (50Nm) in mean torque between mapping data test points, these data sets cannot be used to accurately locate the outer spring set knee point; torque curve data sets are utilised instead. Basic spring stiffness and movement calculations (also hysteresis loops) can provide the approximate torque level at which the knee point occurs. This can then be cross-referenced with the torque curve; by examining the attenuation behaviour of the damper over a small speed window, changes in the magnification ratio can show a more precise location (see Figure 6.7). Magnification ratio is a measure of a damper's ability to attenuate a fluctuating signal; it is the ratio of the torque order magnitude on damper (gearbox) output to damper input (see section 6.3.1). As can be seen from Figure 6.7, between 1360 and 1380rpm there is a sudden change in the attenuation ability of the damper, suggesting a change in damper behaviour; i.e. contact has been made with the outer spring set hardstop.

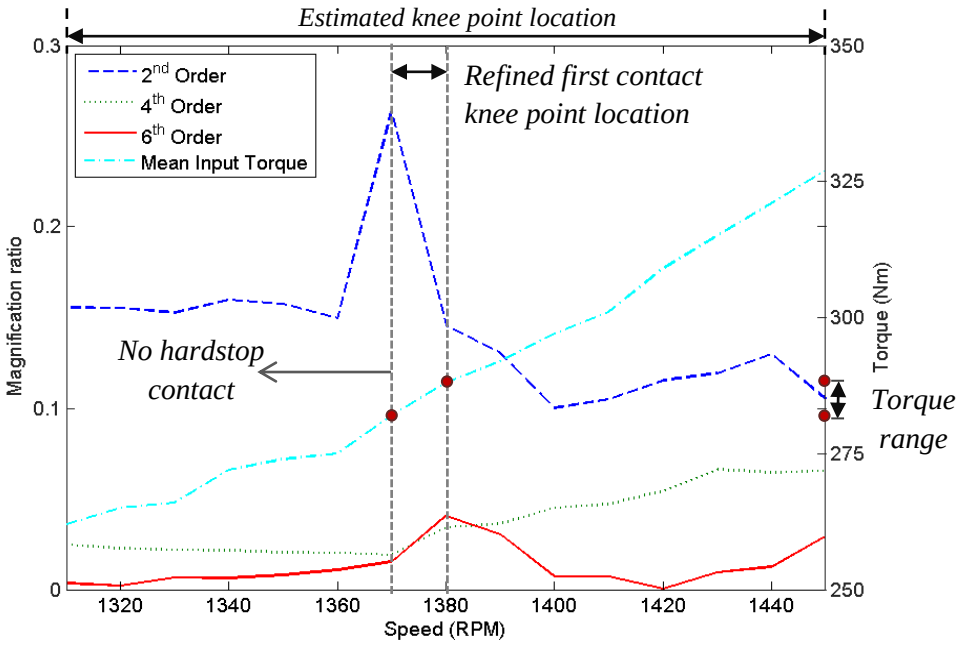

Figure 6.7: Using 2.5 bar torque curve testing results to refine the estimated location of outer spring set knee point

Once a more accurate estimate for hardstop location (mean torque level at which contact is made) is found, spring stiffness (primarily outer spring) can then be altered and the relative position between the primary and secondary inertias examined (to detect if hardstop contact has occurred). This process can then be repeated until (in the simulation) contact is made with the hardstop at the correct (same as test data) input torque level (see Figure 6.9). As there is a larger amount of frictional contact between the outer spring and its housing (the secondary inertia) than found with the inner springs, the knee point of the outer springs can be quite significantly affected by frictional forces (e.g. outer friction tuning factor α_{fric_out}). Therefore, this process will need to be repeated periodically throughout the parameterisation process (see Figure 6.9); other parameters may affect the location of the knee point, requiring the spring stiffness to be adjusted to compensate.

A similar process cannot be performed for the inner spring set as test data at the required mean torque level is not available. This is partly due to test facility restrictions (maximum dynamometer torque of 500Nm) and partly because it is suspected that subjecting the damper to large torque fluctuations outside of its normal operating range (above the inner spring set knee point) would cause significant damage to the damper hardware, rendering it unusable for any future testing. However while the estimation of stiffness for the outer spring set from hysteresis loop test data may not be hugely accurate, the differing frictional contact behaviour of the nested inner springs appears to have a smaller impact on the measured stiffness of the inner springs.

A summary of the parameterisation process can be seen in Figure 6.9, with the key processes of knee point location verification and parameter alteration mapped out. The test point (maximum mean torque) at which the outer spring hardstop is not contacted is denoted by X_1; the test point at which initial contact is made with the hardstop (the lowest mean torque that contact occurs at) is denoted by X_2 (see Figure 6.9, top right). Each time the parameter set is (permanently) modified, a new base simulation must be run to give a comparison point for altered simulations. The effect (including no effect) parameter modifications have on the simulation results (e.g. 2nd order increased by 2Nm) should be recorded to ensure the most effective (best improved accuracy) parameters are chosen to be altered. The maximum allowable error between the simulated damper output results and those from the testing data was set at 10%; this equates to an average torque error of less than 5Nm. This value ensures that the performance of the simulation reaches an acceptable level before being considered completed, without unnecessarily (for minimal accuracy gain) lengthening the amount of time taken to complete the parameterisation process.

When assessing damper performance, the key engine orders that are examined are 2nd, 4th and 6th; therefore these are the primary orders that need to have good simulation performance. While the performance of other orders should not be significantly different (a significant error in any order indicates a problem with the parameters), the focus of the iteration process is the reduction in error of prediction of these key orders. A typical FFT graph can be used to compare the simulation output to the test data baseline; however, as can be seen from Figure 6.8, when plotting multiple simulation results on the same graph (in order to examine the impact of a parameter change, here a decrease of the primary inertia) it can be difficult to assess any changes in order magnitude. Thus a piece of code known as Peakfinder was written and used; this code extracts the first eight orders and their frequencies from the FFT results. Extracting the peak points allows the order magnitude data to be saved for trend analysis and a far more accessible plot to be produced (see Figure 6.8).

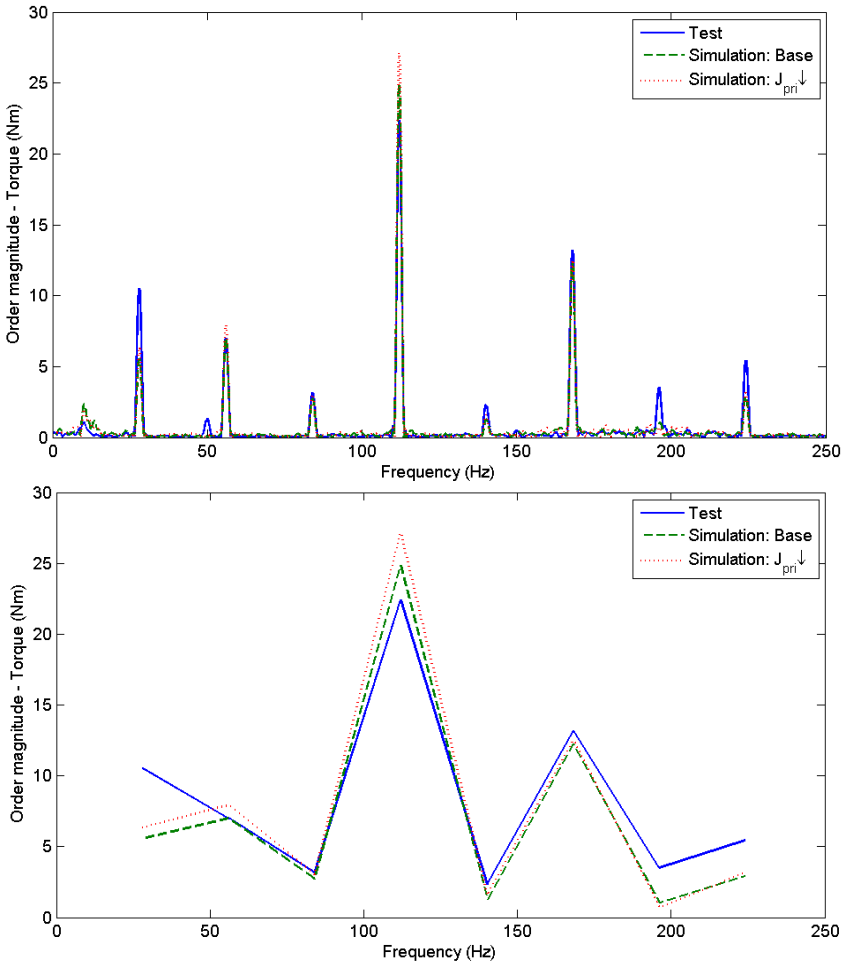

Figure 6.8: Comparing the performance of simulation parameter sets to test data using a traditional FFT graph (Top) and a Peakfinder graph (Bottom)

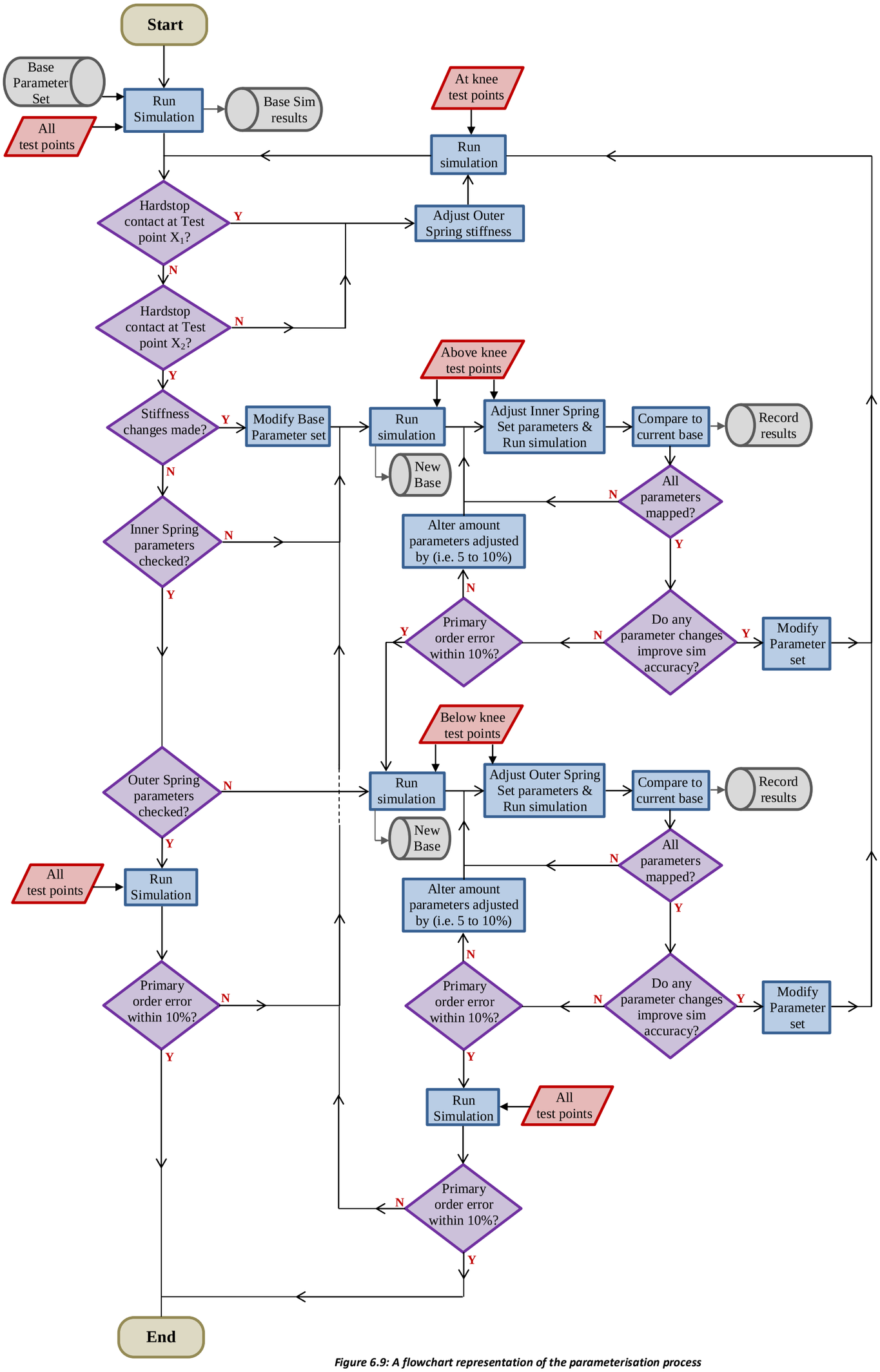

Figure 6.9: A flowchart representation of the parameterisation process

6.2.2 Effect of simulation properties

In addition to damper (hardware) parameters, there are also simulation properties that can impact the accuracy of the results; the simulation timestep and the number of segments used to model the springs. As discussed in section 5.6, with all these features there is a trade-off between simulation accuracy and time taken to complete (computing power required); they may also have an effect on model stability, especially if the state of the damper is changing (e.g. at/near knee point locations).

In order to compare the performance of the model over a range of these simulation parameters, a test point (input signal) that had excellent simulation performance was selected as the base signal. The test point was chosen by examining the torque error in the three primary orders (2^{nd}, 4^{th} and 6^{th}) over a range of speeds and selecting the speed test point with minimal error across all three. The only other restriction was that the test point must have a mean torque below (clear of) the outer spring set knee point, as both spring sets need to be active; the chosen test point was 1520rpm, with a mean torque of 200Nm. This test point has excellent primary – 2^{nd}, 4^{th} and 6^{th} – order performance, with errors (comparing simulation to test data) in torque output of just 0.8, 1 and 0.6Nm respectively.

Due to the small magnitude of the output torque at this data point (all three are less than 10Nm), when presented as an error percentage (error against test data) this torque discrepancy can seem misleadingly significant (18.9%). While this error percentage metric is not suitable for assessing the performance of the simulation overall (see section 6.3.1), applying it in this situation allows the effects that simulation properties have on the output to be clearly displayed. Thus error magnitudes in the following comparisons are purely for demonstrating trends in the data, rather than absolute values.

With simulation timestep there is a very clear relationship between timestep magnitude and time taken to complete the simulation run; the chosen timestep can also have a significant impact on the performance of the model. As can be seen from Figure 6.10, below $1.6x10^{-06}$ seconds further decreases in simulation timestep have minimal impact on simulation accuracy; the performance plateaus. However, as timestep decreases, the time taken to complete an iteration of the model increases; timesteps below $1x10^{-06}$s produce significant increases in simulation time. Thus the ideal timestep is in the range 1-$1.6x10^{-06}$ seconds; $1x10^{-06}$ s was chosen for ease of simulation (all simulation time lengths are divisible by this timestep) and to ensure a safety margin for more unstable (changing state) test points.

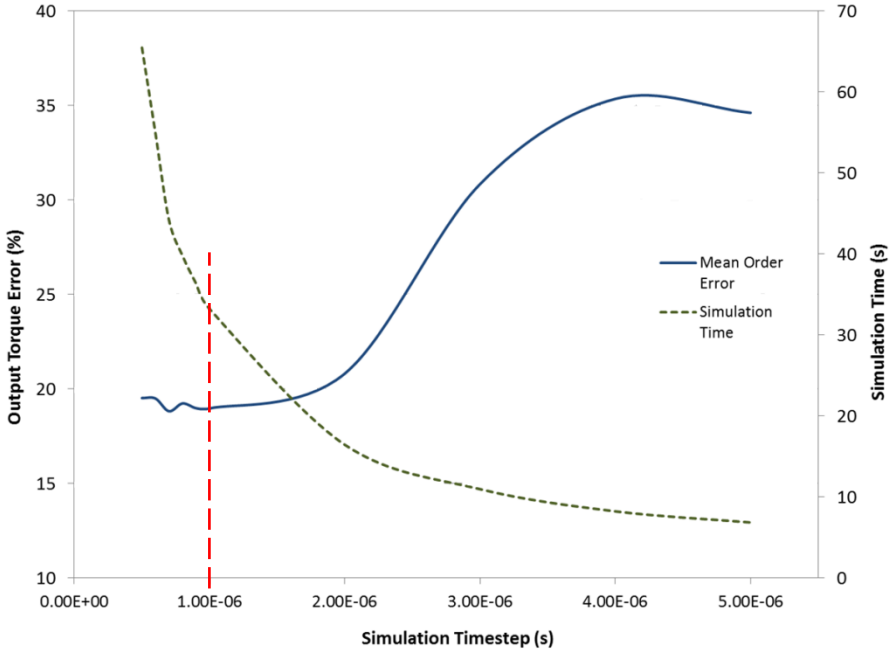

Figure 6.10: Impact of simulation timestep on accuracy and simulation run time

When selecting the optimum number of segments for spring discretisation, the general rule is the greater the number of segments, the more computing power is required and therefore the longer the simulation will take. However, as can be seen from Figure 6.11, there is a point where the rate of improvement to accuracy reduces (at around 20 segments for the outer springs); when the number of segments used to model the inner springs is increased above nine, the accuracy actually starts to decrease. This may be due to the number of spring coils per segment; above 9 segments there is less than 1 coil per segment for the inner spring. The minimum number of segments required for all springs is 4, due to the methodology used to calculate resultant redirection force in the simulation. For the inner springs, 8 segments is clearly the optimum number; 9 segments give a very minimal increase in accuracy for the extra computing power. It was decided that discretising the outer spring into 18 segments offered the best balance between computing power and simulation time.

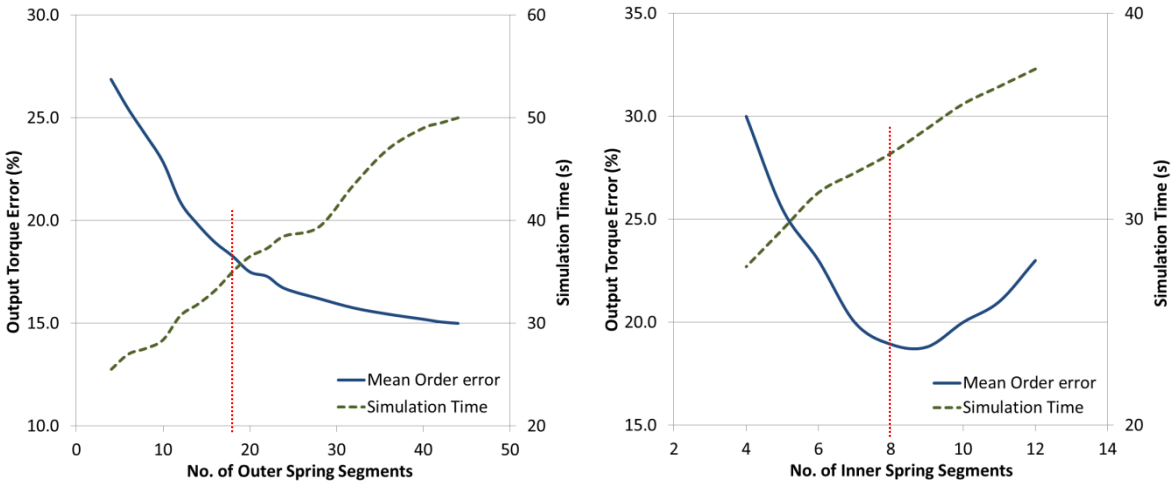

Figure 6.11: Impact of number of spring segments (Left – Outer, Right – Inner) on simulation accuracy and run time

6.3 Final Iteration results

6.3.1 High frequency vibration excitation

Once an acceptable parameter set was found (the aim was to have less than 10% error across the primary orders), simulations of all (complete) test data sets were performed; this included the 1.5 bar mapping sets and the two (1.5 and 2.5 bar) torque curve sets. This allows the accuracy of the simulation and parameter set to be verified across a wide speed range, 900-2800rpm (test points at 10rpm intervals). There are a range of methods available for displaying torsional vibration data; a selection of the different methods that can be used to evaluate simulation performance relative to the test data can be seen in Figures 6.12 to 6.21.

The first type of graph that is sometimes drawn from FFT data in NVH research is a colourmap (see Figure 6.12); these graphs are very useful for demonstrating how the frequency of orders change with speed, as well as highlighting resonance points. An order is the number of times something occurs per revolution; in situations where different components are moving at very different speeds (e.g. in-vehicle when a gear without a 1:1 ratio is selected) the orders must have a frame of reference – e.g. engine order, propshaft order. Here, the orders are essentially engine orders (EO) – the speed of the rig is used to simulate engine speeds. Knowing the frequencies of an order helps to ascertain its cause; the frequency of an order (how often it occurs per second) can be compared to known event frequencies (e.g. cylinder firing). These FFT colourmaps were produced by running a large series of tests (2s of data collected at each test point), increasing speed by 10rpm each time; by using such a high resolution (see section 3.3.2) the need for interpolation was eliminated. The main advantage of this graphing method is that it displays vibration behaviour that occurs outside of the orders – such as resonance points (see Figure 6.13). When a frequency order crosses a resonance frequency band, damper behaviour can be dramatically affected; thus colourmaps can help explain why damper performance may be worse in certain situations.

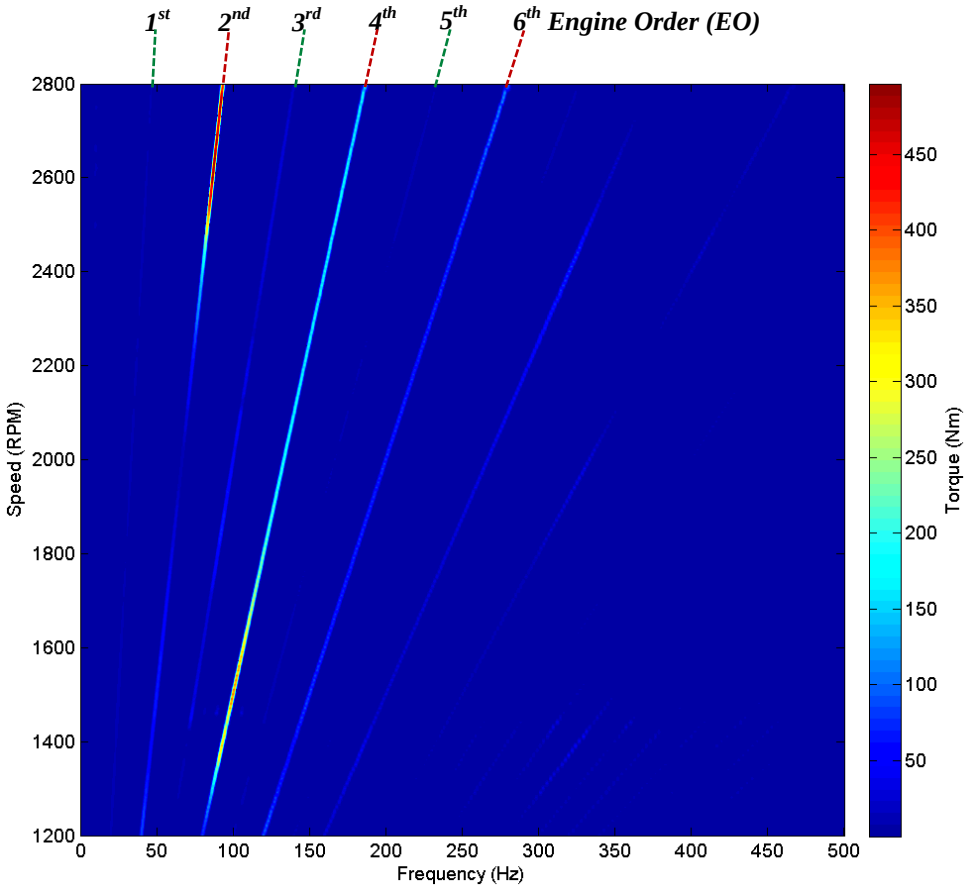

Figure 6.12: 2.5 bar torque curve damper input torque torsionals – test data

As can be seen from Figure 6.13, the simulation appears to have excellent performance; the order frequencies match the test data and the magnitudes of the torque torsionals outputted from the damper also correlate. The narrow band resonance that occurs at very low frequencies (<25Hz) is also reproduced. In the test data, at around 1400-1500rpm, it would appear that there is some excitation of half-orders; the location of this excitation band correlates with the location of the outer spring set knee point in the torque curve. This behaviour is also seen in the simulation data, albeit shifted slightly up the speed range. This suggests that while the behaviour of the damper hardstops is being accurately replicated, the simulation may be reacting in a slightly different manner to the actual hardware. While these graphs are very useful for displaying damper performance over a range of speeds and frequencies, as well as general trends, it is difficult to accurately compare the performance of the simulation against the test data. In order to assess behaviour across the entire speed range the orders must be extracted, allowing the simulation and experimental data curves to be directly compared.

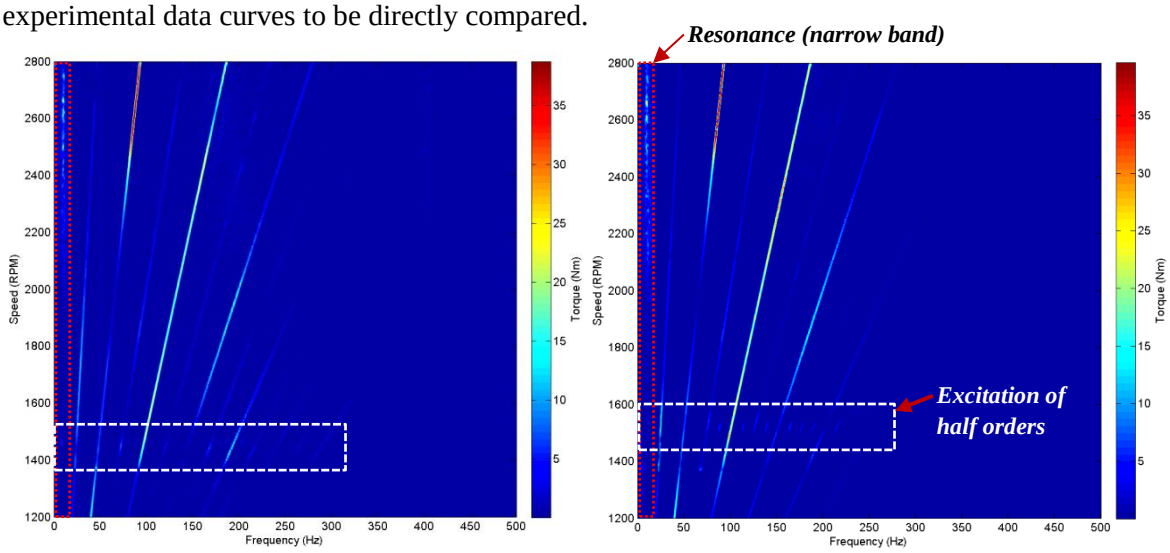

Figure 6.13: Damper output torque torsionals – test data (Left) and simulated damper response (Right)

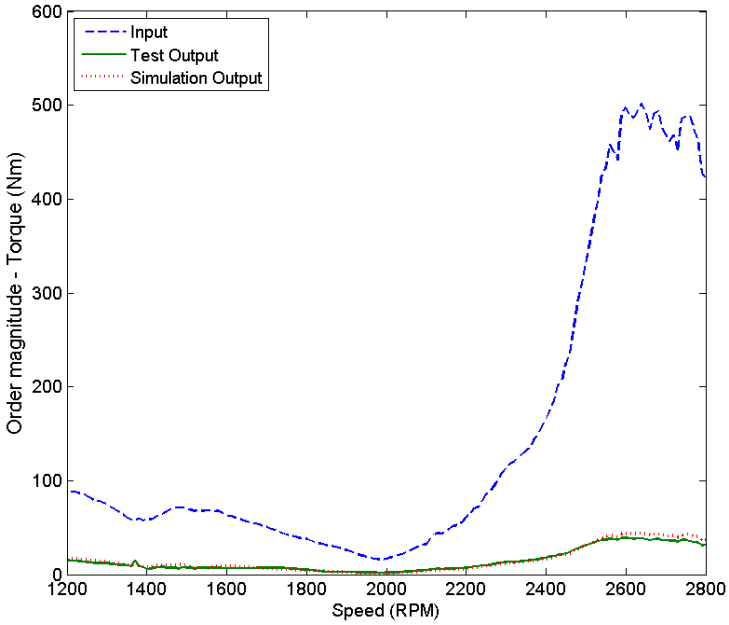

Figure 6.14: 2nd order cuts – comparing input magnitudes to test and simulation output values (2.5 bar torque curve)

This second group of figures (Figures 6.14 & 6.15) shows the magnitude of the primary orders; the orders have been cut out from the FFT map. These orders were extracted by using a MATLAB script to find the location and magnitude of each peak in the FFT data sets (each speed test point has a FFT performed on it). These graphs allow for the easy comparison of simulation performance to the test data, as well as an assessment of the performance of the damper (attenuation ability). The inclusion of the damper input magnitude line for each order provides context to the results; for example, a 5Nm difference between simulated and experimental damper torque output may seem substantial until the magnitude of the attenuation (500Nm to less than 50Nm) is taken into account.

The primary orders are here defined as the 2nd, 4th and 6th engine orders; as discussed in section 4.3, in the signals produced by both a fired engine and the pulsation generator these orders are typically dominant (they have the greatest magnitude). In a fired engine, the dominant frequency is dependent on the number of cylinders (and therefore the number of firing pulses) in the engine; a 4 cylinder engine primarily excites the 2nd order, while a V8 produces higher 4th order torsionals. These orders are where the magnitudes of the torsionals will generally be greater, on both input and output; they are the ones that will impact damper behaviour (and therefore performance) the most. Therefore, the focus should be on ensuring the simulation is performing satisfactorily in these primary orders. As can be seen from Figures 6.14 & 6.15, the simulation performs well, with good correlation and general trends captured; however, in these figures, the error between the simulation and experimental data has not yet been quantified.

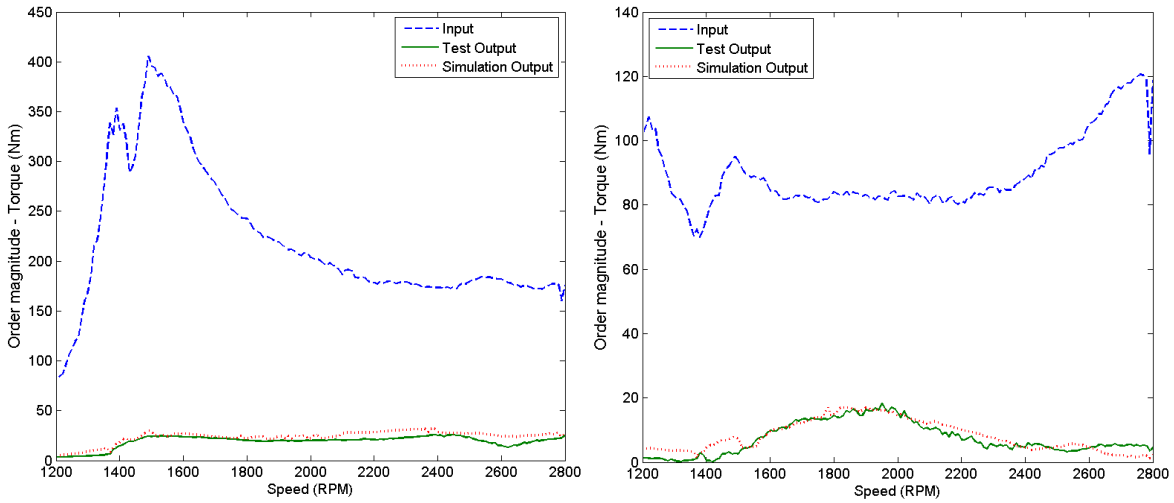

Figure 6.15: Comparing 4th (Left) and 6th (Right) input and output order magnitudes – test and simulated results

When examining the error between two data sets (e.g. performance of simulation vs test data for individual orders) the error can be represented as a percentage; doing so adds further context to the results (similar to the inclusion of the input torque line in Figure 6.14 & 6.15). However, care must be taken when choosing the baseline values the error will be compared to in order to produce this percentage value. As discussed in section 6.2.2, in this situation if the error (the difference between the simulated and experimental output) is compared to the measured (test data) torque output, false highs may be produced. For example, a 2Nm error on a signal where the damper output value is just 10Nm would produce an elevated error of 20%; however, when the fact that this signal has just been attenuated by 400Nm is taken into account, the error seems less significant than the percentage would suggest. Thus when assessing the error between simulation and test data damper outputs, the error is compared to the torque inputted to the damper; this allows the error to be assessed with context, without affecting the results.

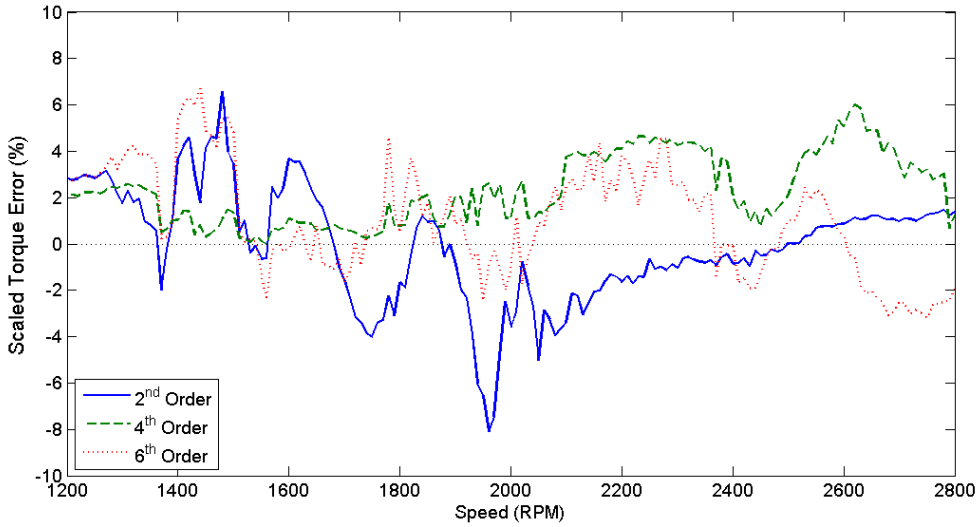

Figure 6.16: Simulation performance of primary orders over a large speed range (2.5 bar torque curve)

Examining the error between the simulated output and the test data allows the performance across the orders (here, the primary orders – Figure 6.16) to be evaluated, rather than having to display the results separately. The results presented here are from one test data set – the 2.5 bar torque curve test run, where a test point was taken every 10rpm in the speed range 1200-2800rpm. While a graph assessing primary order percentage error could be produced for each data set, an alternative is to assess the maximum, minimum and mean torque error across multiple datasets (see Figure 6.17 & 6.18); for example, the 1.5 bar mapping test set (900-2000rpm with mean torques from 50-500Nm). This method could also be used to compare simulation performance above and below the outer spring set knee point, with data sets sorted into two categories depending on the mean torque.

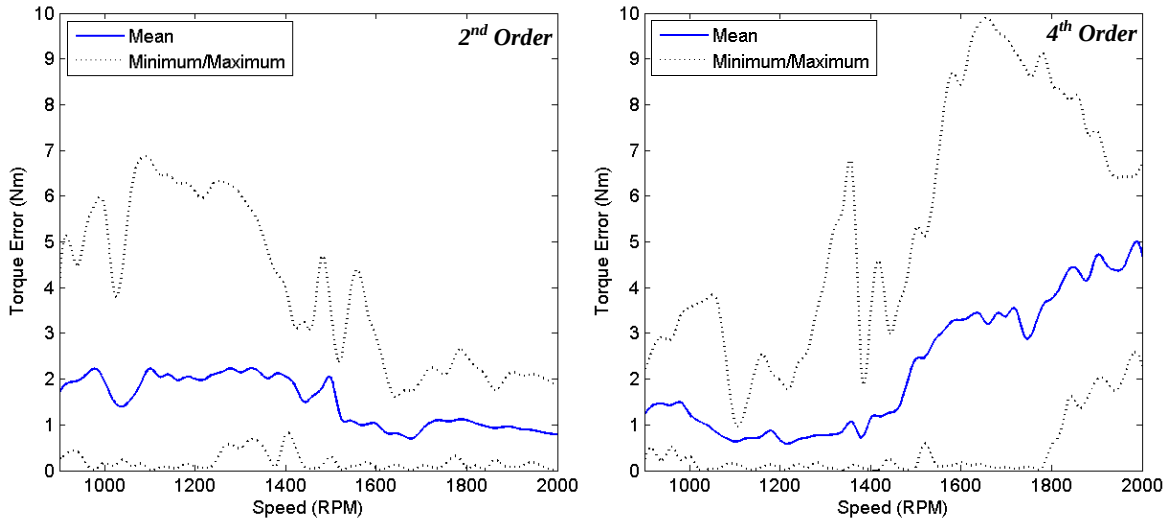

Figure 6.17: Maximum, minimum and mean torque error between damper output in simulation and test data

In order to accurately assess the mean, maximum and minimum torque error between the simulation frequency orders and the test data, the absolute torque error values have been used; this has been done to avoid artificially decreasing the mean value by including both negative and positive results in the calculation. Data from above 2000rpm has not been included due to the small sample size; below 2000rpm 12 data sets per speed test point were available, compared to just 2 per test point above 2000rpm. On average, the error between the test data damper output torque magnitude and the simulation is less than 5Nm, with the maximum error not exceeding 10Nm.

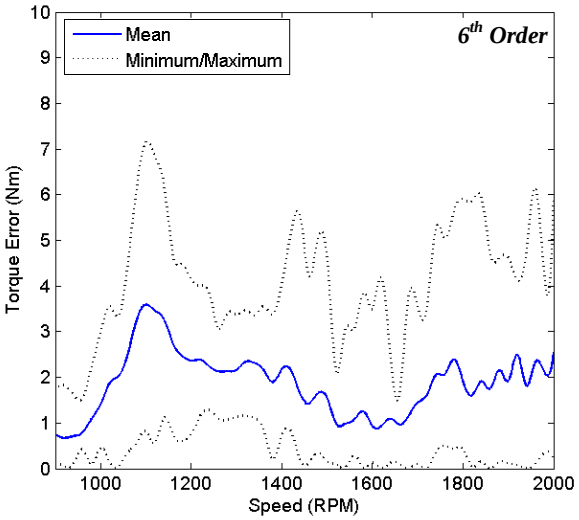

Figure 6.18: Torque error range for 6th torsional order

Using a range of metrics to assess simulation performance increases the likelihood that any discrepancies will be revealed, before the model is used to draw conclusions about damper behaviour. As can be seen from Figures 6.16 through to 6.18, this simulation has strong correlation with the experimental data across the entire frequency range, especially the primary orders. Torque error is less than 10% across the tested speed range (900 to 2800rpm), with mean torque differences between simulated and tested order magnitudes of less than 5Nm.

The following graph (Figure 6.19) demonstrates why it is more effective to assess damper performance using FFTs, rather than by directly comparing simulation and real transmission output signals. This method would be very time consuming (an individual graph required for each test point); it is also very difficult to produce a single number that represents the performance of the simulation at each test point. Using this as a metric may result in time being wasted on improving performance in unimportant areas; for example, very high frequency orders or orders that are unlikely to excite the natural frequencies of downstream components. However, comparing damper output torque profiles can be used to provide an added layer of confidence in simulation behaviour, by ensuring the simulated damper is behaving in a similar manner to a real-world damper. This method is more commonly used to assess performance of engine simulations (see section 4.3).

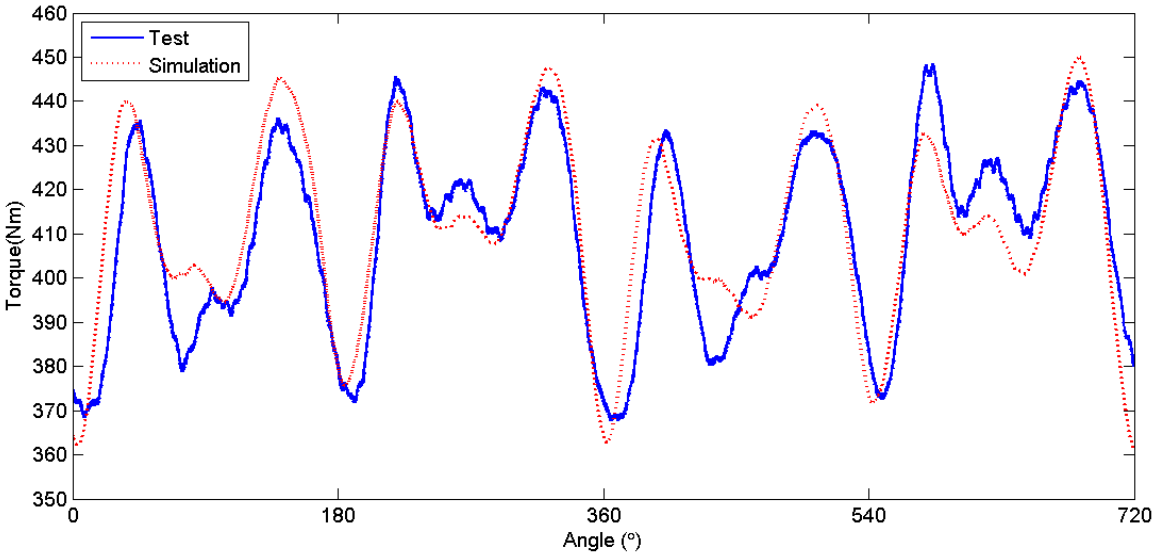

Figure 6.19: Comparing the simulated torque profile at transmission output with that recorded during testing for a selected test point.

All of these methods of analysing damper outputs (from both simulation and test data) have a variety of advantages and disadvantages. However, none allow for a clear depiction of how damper behaviour – and its most important feature, its ability to attenuate torque signals – changes depending on the mean torque level of the torque input. A magnification factor map (see Figure 6.20 and 6.21) allows the variation in magnification ratio with speed and mean torque level (and therefore the position and activation of the different spring sets) to be displayed.

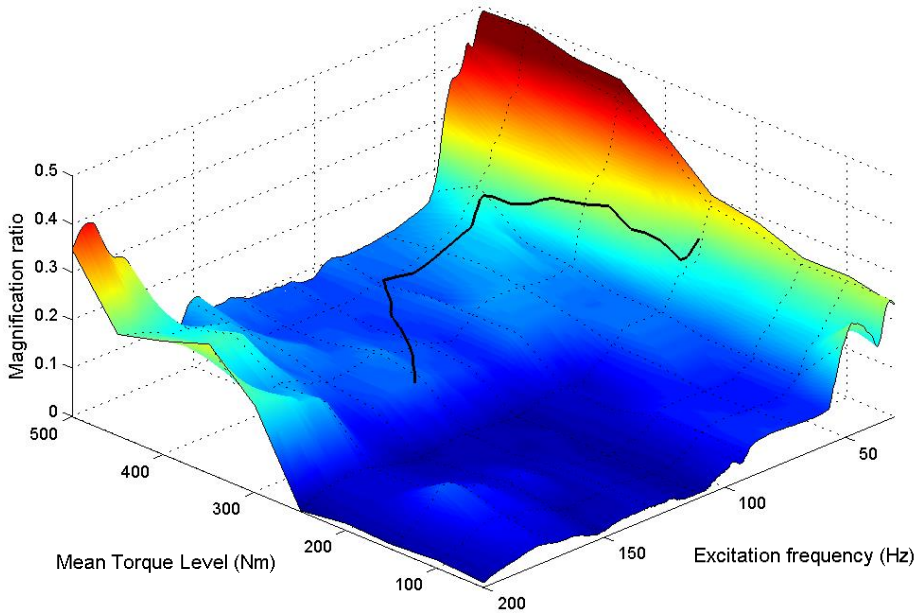

Figure 6.20: Experimental damper attenuation performance across the frequency and mean torque ranges

These maps were produced from both the experimental and simulation test results in the same manner. Firstly, all of the results (from both the torque curve and mapping tests) were collated; if any test points were repeated (had the same mean torque and excitation frequency) an average magnification ratio value was calculated from them and assigned to that test point. In order to produce a smooth surface plot, the data was then interpolated, primarily along the torque range; between 30 and 200Hz there is on average less than 0.1Hz between unique test points, but in some places the mean torque level can jump by 50Nm. The excitation frequency range was limited to 30-200Hz due to the availability of data; in the tested speed range (900-2800rpm) only the 5^{th} and higher orders produce frequency levels greater than 200Hz. A typical torque curve from a 4-cylinder engine commonly used with this damper design has been overlaid on the map in Figure 6.20; this helps demonstrate the normal operating regime for the damper.

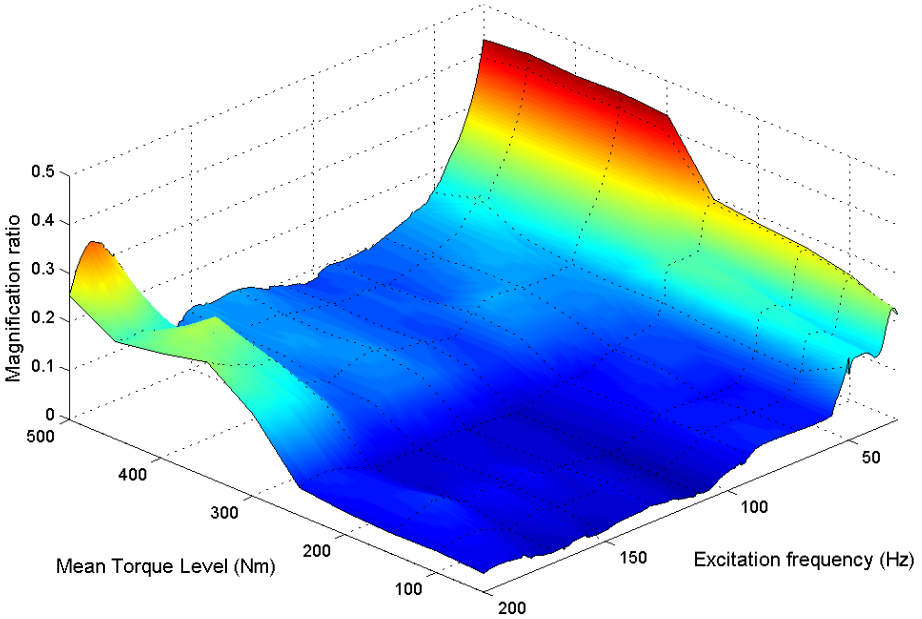

Figure 6.21: Simulated damper attenuation performance across frequency and mean torque range

Magnification ratio is a measure of a damper's ability to attenuate a fluctuating signal; it is the ratio of the order magnitude on damper output to damper input (though here gearbox output is used due to locations of the test rig transducers). Magnification ratio has previously been used to investigate the effective speed range of a DMF arc spring damper [65]. A magnification ratio greater than 1 signifies that the damper is actually increasing the magnitude of the torsional vibration (e.g. at very low frequencies or low order magnitudes). At lower mean torques (below ~250Nm), and higher excitation frequencies (>80Hz), there is a trough in the map, signifying an area of excellent damper attenuation performance; in this region (below ~300Nm) both spring sets are active.

There is a marked improvement in attenuation ability of the damper when both spring sets are active across the whole frequency range, with the greatest reduction in magnification ratio being seen at low frequencies (one of the key areas of damper performance – see section 2.1). A similar graph format has been previously used to demonstrate the isolation effect achieved with a Dual Mass flywheel over a range of engine speeds and flywheel vibration angles [65]; here, those properties have been replaced with mean torque and vibration frequency. There are three different potential meanings for *vibration angle*; it is either the angle at which the spring set is compressed at and then vibrates around (as can be seen from hysteresis loops, this is directly linked to mean torque), the amount the springs vibrate (difference between their maximum and minimum displacements) or the phase lag between the input and output of the damper or spring (see Figure 6.22).

Measuring phase lag (between the damper input and gearbox output signals) from test data requires confidence that the two signals were initially perfectly synced (zeroed). Measuring the angle range over which the spring vibrates (the maximum and minimum values of angle windup) is easier, though it is prone to error, as even brief fluctuations in the mean torque will affect the results. Both signals also only give results for the damper as a whole, as opposed to the individual spring sets. While the mean angle of vibration (damper windup angle) can only be potentially measured on a test rig if measurements start from 0Nm (requiring CAN modifications, see section 3.2), the mean torque of the input signal can be easily measured and/or requested; as the hysteresis loops demonstrate (see Figures 6.25 to 6.28) torque input is directly related to spring compression. Thus it was determined that the mean torque of the input signal would be the most suitable metric to replace vibration angle; it can be easily measured from both test and simulation data, and would demonstrate the varying behaviour of the damper depending on the activation of both spring sets.

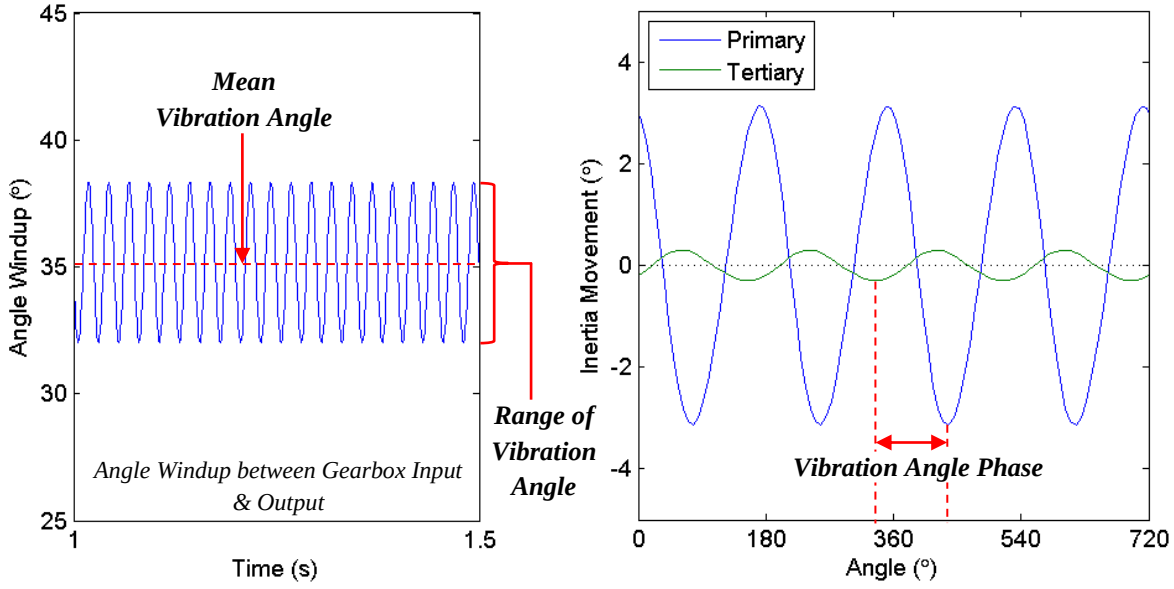

Figure 6.22: Alternative definitions of damper vibration angle

Engine speed could still be used, though it would not allow for the production of a complete map, as different maps would be required for individual frequency orders; the attenuation of the 2nd engine order may be different to that of the 4th order at the same speed point, due to their differing vibration frequencies. Thus before the maps were constructed, a decision was made to examine the test data and investigate if there is a link between damper attenuation performance – its magnification ratio – and the frequency of the vibrations; if a link exists, frequency could be used to map and assess damper performance. As can be seen in Figure 6.23, it was found that attenuation is dependent on both mean torque level (primarily either both spring sets being active or only the inner set moving) and frequency of vibration. While there is a clear trend, there is some variation; this is partly due to differences in mean torque, though engine speed may be contributing. There is a clear enough relationship to allow magnification ratio maps to be produced, but further investigation into the effect of speed is required.

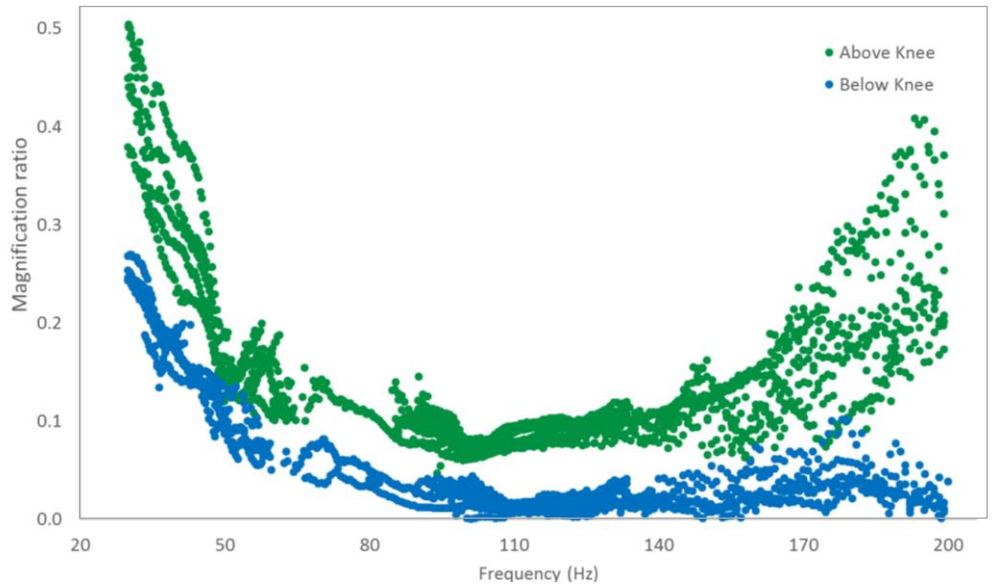

Figure 6.23: Assessing if damper attenuation performance can be linked to fluctuation frequency (independent of engine speed) below and above the outer spring set knee point

While collating the experimental data, as can be seen from Figure 6.24, it was found that the magnitude of the torque fluctuations inputted to the damper can have an effect on attenuation. When a torque signal has a magnitude lower than ~20Nm the magnification ratio can substantially increase, including to above 1 – this means that at very low torque inputs the damper actually increases that particular fluctuating torque signal. However, it should be taken into account that a 5.4Nm signal with a magnification ratio of 2 is still only 10.8Nm – fairly insignificant when compared to the magnitude of the primary orders on damper input (the maximum recorded order magnitude outputted from the pulsation generator is around 1000Nm).

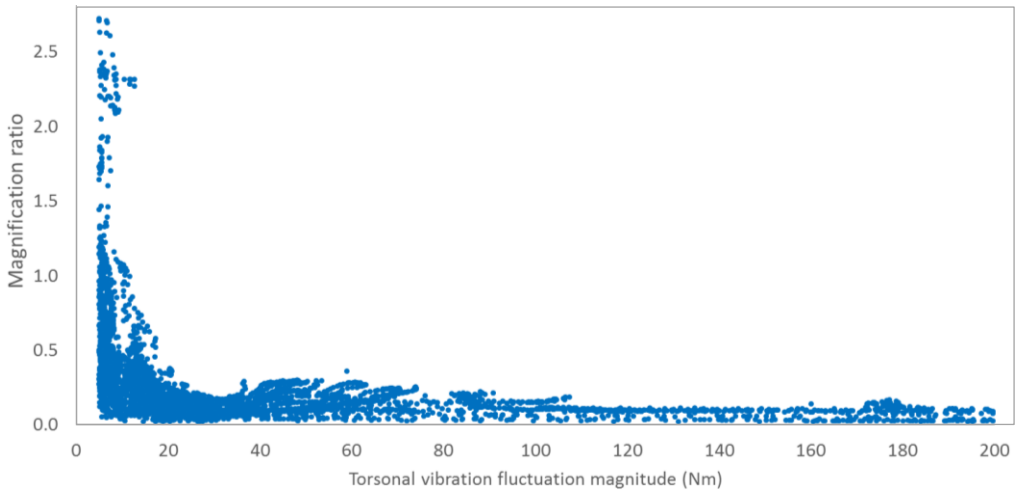

Figure 6.24: Damper attenuation performance at the lower end of the vibration fluctuation magnitude range

This noise (test points where torque input was less than 20Nm) was filtered from the data for the purposes of examining a link between frequency and attenuation performance (Figure 6.23). It was found that the majority of this noise occurred below 20Hz; by filtering the noise, data can be more easily displayed with minimal impact on trends.

The potential link between frequency and attenuation (independent of speed) is investigated further in section 7.1; in section 7.1.3, the simulation is used to more closely examine what effect speed has on attenuation at set frequencies. In section 7.1.3, the optimum test point set for mapping is also investigated, as well as the effectiveness of the maps – their ability to predict damper performance. The effect of fluctuation magnitude on damper behaviour is also further examined in section 7.1.2.

6.3.2 Torque Ramps - Hysteresis loop testing

Various forms of hysteresis loops are commonly used to investigate damper behaviour [61] [65]; they can provide information about the stiffness of springs (see Figure 6.5), as well as a representation of the friction in the system. To obtain the required data, the test object is subjected to a loading-unloading cycle (see section 3.3.1); because of losses in the system (e.g. friction between the springs and housing) the unloading curve does not follow the exact same path as the loading curve, creating a loop (see Figure 6.25). The area inside this hysteresis loop denotes the energy dissipated by the damper during a motion cycle.

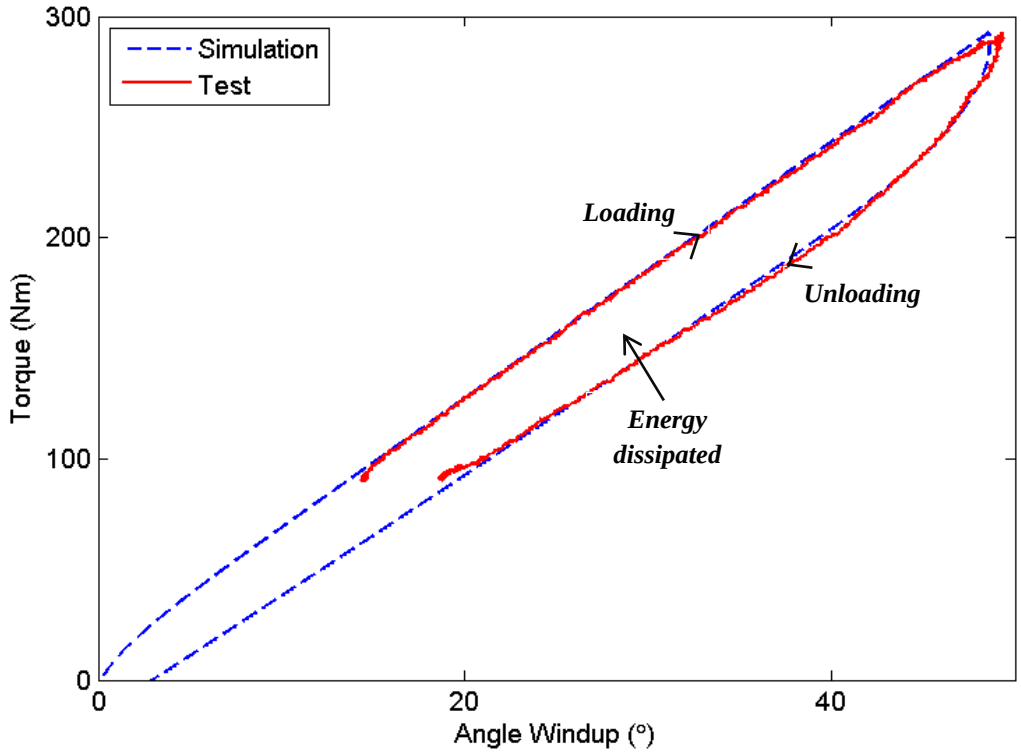

Figure 6.25: Hysteresis loop created using a torque ramp at 1500rpm

In multi-stage spring dampers, hysteresis loops can be used to estimate the location of the hardstops, as well as the torque level at which they occur; however, both the speed at which the hysteresis loops are performed (e.g. 1000 or 2000rpm) and the ramp rate of the loop can impact these variables (see section 3.3.1). While performance was found to be consistent during repeats of a specific torque ramp test, the shape of the resulting hysteresis loops may not be consistent between different types of test. This effect can be clearly seen when comparing three types of 1500rpm hysteresis loop tests (Figure 6.26); while the loading curve is consistent, the positioning of the unloading curve – and therefore the location of the negative outer spring set knee point – is dependent on the peak torque of the ramp (and if the ramp is held at this peak torque).

One of the key aspects of these hysteresis loops that should be noted is the unbalanced effect pausing the torque ramp at peak positive and negative values has on the angle windup of the system. As can be seen from Figure 6.26, at the peak positive torque the two second stabilising pause causes slip to occur; the angle windup of the system increases without the further application of torque. This results in the end point of the ramp not meeting with the start point and makes the energy dissipated in the positive half of the loop appear larger. When this pause effect was noted during initial test data analysis it was assumed that it may be a result of clutch slip; while the system was over-locked (see section 3.3.1) the reaction of the TCU to this type of testing was not fully known.

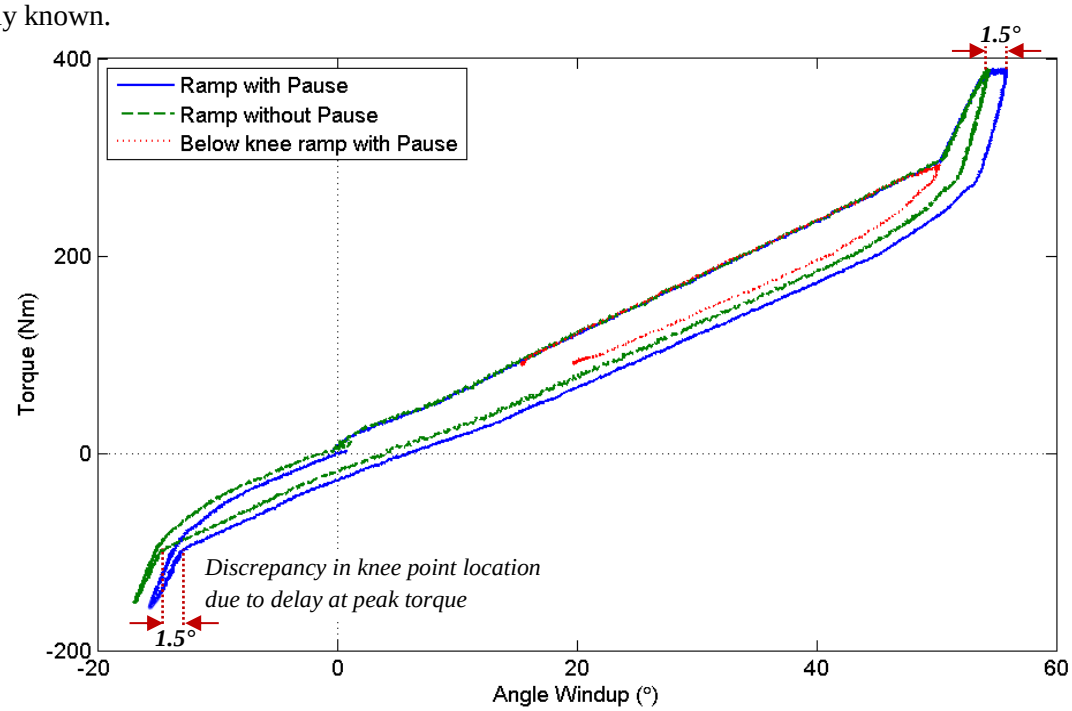

Figure 6.26: Comparing multiple types of hysteresis loop test (1500rpm)

This behaviour is not seen when the torque ramps do not exceed the knee point torque of the outer spring set (the effect is only seen when outer spring set is no longer active) or when a ramp with no peak pauses is used (see Figure 6.25), and appears to have minimal impact at the smaller negative peak torque. Producing a ramp with no pause at peak torque proved difficult; if the built in test controller was used (but with the stabilising pauses removed from the test) some slip was still observed at peak positive torque (if >300Nm). This was likely due to the torque demand-response error (see section 3.3.1). The only way a true loop could be performed was to manually input the test commands, with the downward ramp command being sent to the system before it had completed the upward ramp (i.e. instructed to peak at 500Nm, ramp direction manually changed at ~400Nm). While this method does produce a hysteresis loop that is not affected by demand-response error or torque pauses, it is not as repeatable as the pause method.

The performance of this damper simulation with respect to hysteresis loop testing can be seen in Figure 6.25, Figure 6.27 and Figure 6.28; correlation during the initial application of the torque ramp is strong, though the area enclosed by the loop (energy dissipated) is slightly smaller in the simulation at certain points. In the following hysteresis loops, experimental data from torque ramps without peak pauses is used to assess simulation performance. This is because the damper simulation is unable to reproduce the slip seen in the experimental data when a ramp is held at a peak torque above the knee point. The inability of the simulation to replicate this slip suggests that it is caused by a feature not included in the model; for example, the lock-up clutch. The inclusion of this feature (to attempt to confirm the cause of the peak torque slip) was considered; however it was felt that the simulation of the clutch was unnecessary and outside the scope of this project. The only time this situation (the damper system held at a steady state mean torque level above the knee point) occurs is during hysteresis loop testing; the focus of this project is high-frequency excitation.

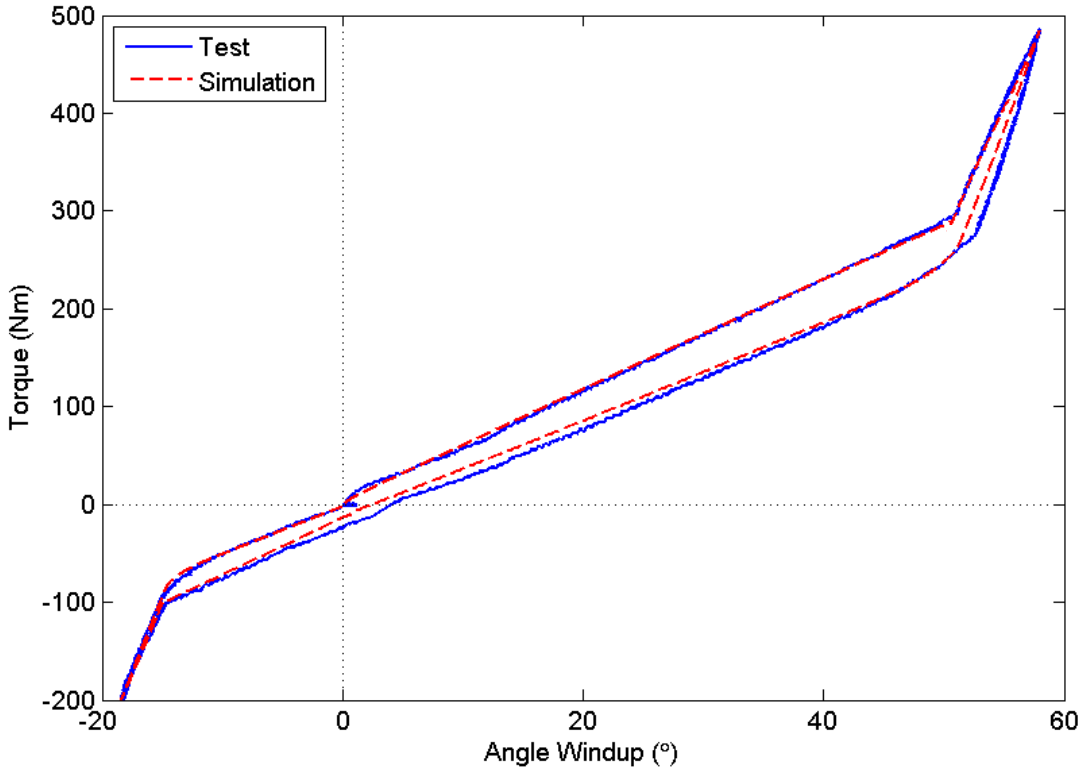

Figure 6.27: 1000rpm hysteresis loop – comparing test results to simulation

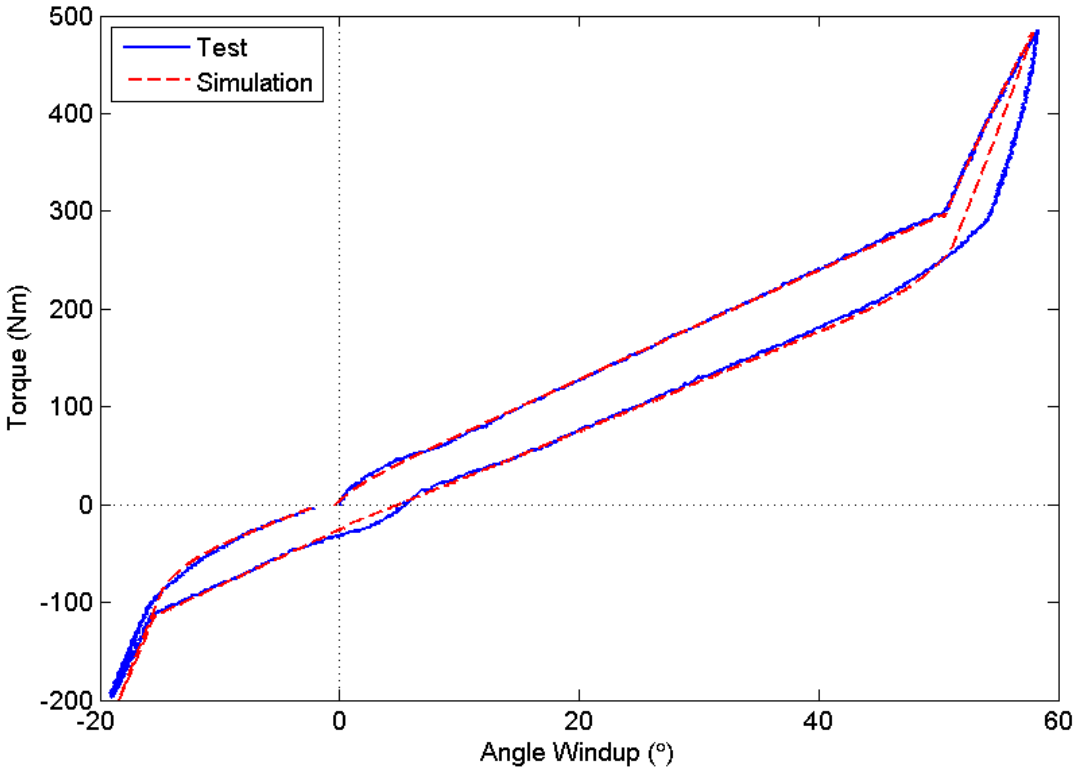

Figure 6.28: 2000rpm hysteresis loop – comparing test results to simulation

This study has shown that hysteresis loops are not an accurate predictor of real-world damper performance, as the range in which they excite the damper is limited; while hysteresis loops can help ensure a model is approximating general trends, they do not test the damper in its normal operating condition. This could potentially lead to incorrect conclusions being drawn about damper behaviour.

6.4 Summary

In this chapter, a methodology for simulation parameterisation has been developed and presented; the resultant validated simulation has excellent correlation with test data. Key areas of both excellent and poor damper performance have been identified and links between damper behaviour and performance (torque output) confirmed.

The key outcomes from this chapter have been summarised below:

- Simulation parameters can be split into three categories: observed, calculated and estimated. Estimated parameters require tuning through comparing simulation and experimental damper performance.

- A wax-based substance can be used to estimate surface contact between springs and their housing (provide a value for friction tuning factors). The tuning factor for the smaller spring in the nested pair is calculated by comparing the available contact surface area on the outside of the smaller spring to the inside of the larger spring.

- Estimations for inertia values of the mass assemblies were calculated using the rotational inertia for a hollow cylinder equation; an alternative would be the trifilar estimation method, but this would require extra equipment and more testing time.

- Spring stiffness approximations can be obtained from hysteresis loop testing; however, frictional effects mean that the stiffness values obtained from hysteresis loops are likely to differ from the actual stiffness of the springs. Static spring tests would remove any speed-dependent error, but constraining and loading the arc springs in a representative manner would be difficult. For the parallel nested springs, stiffness was equally distributed.

- A simulation torque excitation (damper input) signal was formed by taking a 2 second sample of experimental data and combining it with both a 0.3s ramp (from 0Nm to test point mean torque) and a 0.3s ramping sine signal. The purpose of both ramping signals is to stabilise the simulation before the sampled experimental excitation data is introduced.

- As re-testing the entire simulation set would take an impractical amount of time, each time a parameter change was made a set of key test points were selected in order to assess simulation performance change. Single test points (speeds) can be examined individually; however, this is not recommended as parameter changes may improve simulation performance at one test point but have an adverse reaction at another. While the recommended comprehensive approach may increase the time taken to run each parameter set point test, it will make the overall parameterisation process more efficient.

- When investigating knee point location, test points with small steps in mean torque are required (e.g. torque curve rather than mapping data sets). The location of the knee points can be signified by a sudden change in the attenuation ability of the damper.

- The parameterisation methodology created and used has been presented in a flow chart. Parameterisation initially focuses on above the knee test points where only the inner spring set is active; this reduces the number of variables, removing some uncertainty. Once inner spring behaviour has reached a satisfactory performance level (primary order error within 10%), below the knee test points (when the outer spring set is also active) are used; knee point behaviour is periodically examined to ensure hardstop location remains accurate.

- An alternative method for analysing damper simulation performance has been introduced; the peaks of the first eight frequency orders are extracted from the FFT data, allowing for clearer graphical representation and the ability to use peak data in trend analysis.

- A clear causal relationship between simulation timestep and accuracy (as well as simulation run time) was found; however, below $1.6x10^{-06}$ seconds further decreases in simulation timestep have minimal impact on simulation accuracy. A timestep of $1x10^{-06}$ s was chosen for ease of simulation and to ensure a safety margin for more unstable (changing state) test points.

- The link between the number of discretised segments and simulation accuracy (and run time) has also been confirmed, though once the number of segments exceeded the number of coils in the inner springs the simulation error started to increase again. It was determined that 8 segments was optimal for the inner springs and 18 outer segments offered the best balance between computing power and simulation time.

- Traditional FFT colourmaps are very useful for displaying damper performance over a range of speeds and frequencies, as well as resonance bands; however, they do not allow for a clear comparison of simulation to experimental damper performance.

- The primary orders can be extracted from the FFT data and the simulation and experimental damper output data directly compared; this method demonstrates simulation performance, with the input torque magnitude line providing context to the results.

- By comparing simulation vs experimental percentage error the performance of the simulation across the speed range for the primary orders (2^{nd}, 4^{th} and 6^{th}) can be assessed. For the 2.5 bar torque curve experimental data set the simulation performs excellently, with on average less than 5% error. Overall torque error is less than 10% across the tested speed range (900 to 2800rpm), with mean torque differences between simulated and tested order magnitudes of less than 5Nm.

- An engine simulation performance method can also be used (comparing output signal shape/pattern); while this method is inefficient, it does help demonstrate that the shape of the signal outputted from the damper simulation correlates well with the experimental data.

- A magnification factor map allows the variation in magnification ratio with speed and mean torque level (and therefore the position and activation of the different spring sets) to be displayed. At lower mean torques (below ~250Nm), and higher excitation frequencies (>80Hz) – when both spring sets are active – there is a trough in the map, signifying an area of excellent damper attenuation performance. Damper performance is worst at low excitation frequencies (below 50Hz) and in the high frequency, high mean torque region.

- It was found that attenuation is dependent on both mean torque level (primarily either both spring sets being active or only the inner set moving) and frequency of vibration, independent of the order of a signal. It was also found that when a torque signal has a magnitude lower than ~20Nm the magnification ratio can substantially increase (>1).

- Hysteresis loops: while performance was found to be consistent during repeats of a specific torque ramp test, the shape of the resulting hysteresis loops may not be consistent between different types of test. When there is a pause at peak torque above the positive knee point a form of slip can occur; this slip is not reproduced in the simulation, leading to the conclusion that the TC clutch is the source (as it is not included in this model).

- Hysteresis loops are not an accurate predictor of real-world damper performance, as the range in which they excite the damper is limited; while they can help ensure a model is approximating general trends, they do not test the damper in its normal operating condition.

Chapter 7 Analysing Damper Behaviour

It has been established that the proposed method for simulating and parameterising a two-stage turbine damper design produces an accurate model that is representative of real-world damper behaviour. This chapter aims to use the validated simulation to answer questions on damper behaviour, performance and characterisation requirements.

The first area of investigation is how the torsional vibration signal inputted into the damper affects its behaviour. As discussed in section 2.2, other studies have focused on the attenuation of the firing frequency (the main dominant order), without considering if the magnitude of the other frequency orders affects the behaviour and therefore performance of the damper. The ability of a sinusoidal signal to replicate a complex real-world signal is examined, as well as what form of excitation signal (or range of signals) is most suitable for simulation characterisation and performance mapping.

Areas of poor damper performance have already been identified in section 6.3.1; for example, regions of low frequency and low torque fluctuation magnitude. The second part of this chapter aims to further investigate these regions (beyond the scope of the experimental data) and establish potential causes. The final part of this chapter examines the link between engine speed and apparent damper stiffness changes. The situations in which speed-dependent behaviour occurs are investigated, with the aim of the section to establish potential causes.

7.1 Effect of input signal on damper behaviour

One of the main issues this project faced when attempting to characterise a damper through experimental testing was the question of what defines *sufficient excitement*. It has already been established (see section 6.3) that high frequency torsional vibrations are needed to fully assess damper behaviour; however, the property requirements of this vibrational input signal are unknown. Essentially, does a damper have to be excited in a manner as close to real-world as possible (e.g. with a fired engine) or will a more basic sinusoidal approximation be sufficient?

The investigation into the impact of an input signal is threefold. Firstly, if a sinusoidal replica signal is required (e.g. testing damper performance with a specific engine design) how accurate does this signal have to be? Here, accuracy is defined as the number of orders from the original experimental signal that must be included in the sinusoidal approximation to produce representative damper behaviour. The second part of this investigation aims to quantify sufficient excitement by establishing what form of input signal is optimum for simulation. An ideal signal – one that increases the efficiency and effectiveness of the parameterisation process – may be completely different to a typical real-world engine torsional signal.

The third part investigates what type of signal, and what signal range, is needed to accurately and efficiently map damper performance. Testing and simulation has already shown that there is a strong correlation between frequency and attenuation ability; this allows performance maps to be produced for the majority of the damper operating range. These performance maps may potentially be an efficient method of approximating damper behaviour for a wide range of engine designs. This investigation should establish methodologies for the three main aspects of testing dampers; testing for performance, testing for simulation and testing for characterisation (mapping).

7.1.1 Replicating real-world signals

One of the potential issues when trying to replicate a fired engine signal – that has not been assessed in previous literature – is the impact that additional orders have on the behaviour of the damper. The investigation into this issue has been approached in two ways; the first by examining if a complex vibration signal (e.g. inputted by the pulsation generator or an engine) can be represented by a sinusoidal signal and still produce the same damper behaviour.

If a real-world signal can be effectively replicated, the next stage is to investigate how many and which orders must be included in the sinusoidal approximation. The second approach is to understand how additional orders may affect a signal; does the inclusion of other orders alter the ability of the damper to attenuate the dominant (primary) orders, and if so, what effect does the magnitude of the additional orders have.

When assessing the ability of a sinusoidal signal to replicate a fluctuating signal, torque profiles from both the pulsation generator and a fired diesel engine (the same type of four cylinder engine used to make the pulsation generator) were used. The ability of a sinusoidal signal to replicate fired engine signals can be used to assess the performance of a range of signal generators (see section 4.5), while the more complex pulsation generator signals allow an examination of the limitations of this method to take place. Knowing how to effectively replicate engine signals is not only useful for testing damper units; it also helps quantify how accurate engine models need to be to excite a damper model in a representative manner. Deciding if a model is sufficiently accurate is a fairly arbitrary process; however, if a particular level of accuracy can be recommended (i.e. the model replicates the 2nd, 4th and 6th orders) this may potentially help to save time in the design process.

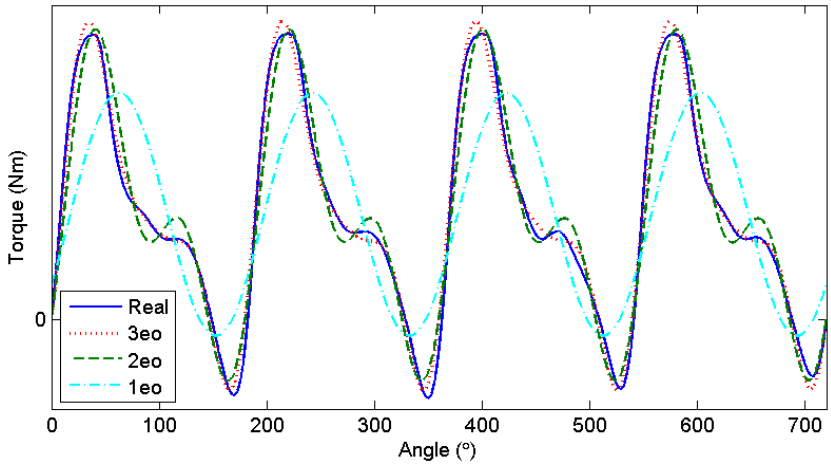

Figure 7.1: Reproducing a fired diesel engine torque profile with varying complexity sinusoidal signals – from a signal with only 1 frequency order (eo – engine order) to one that includes 3 orders

The first set of approximation tests were performed using real fired engine signals as the baseline. FFTs were used to break the torque profile down into its component frequencies and magnitudes; individual sine waves with these frequencies and magnitudes were then layered to produce a sinusoidal approximation of the engine signal. A demonstration of this can be seen in Figure 7.1; this graph compares the original engine torque profile to approximations using the 3 most dominant orders in the signal (typically 2nd, 4th and 6th). It also demonstrates how the shape of the signal changes as orders are removed, down to an approximation of the major order only.

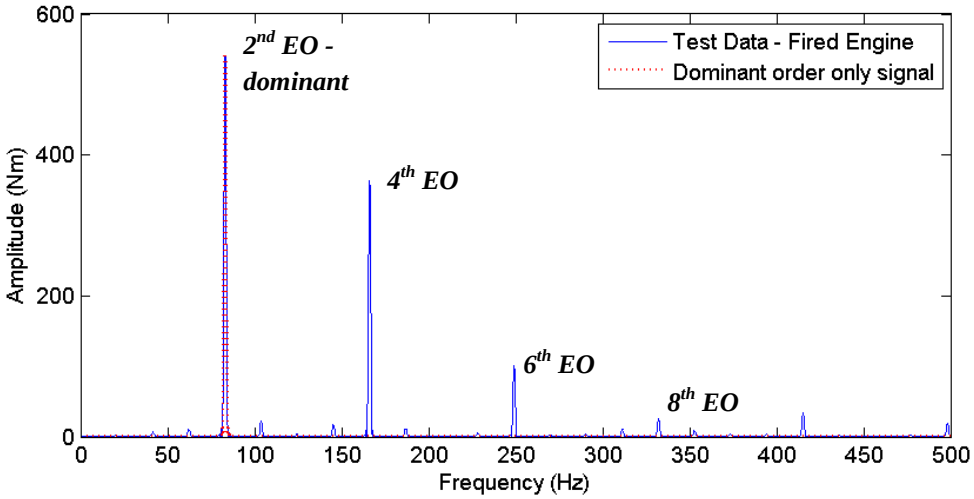

Figure 7.2: Breaking down a fired diesel engine torque signal (2000rpm) into its component frequency orders

Initially the simulation was performed using a signal based on the experimental data; this provided a baseline to compare the performance of later simulations against. In the first test (see Figure 7.2 and Figure 7.3) a sinusoidal signal with the same magnitude and frequency of the dominant order in the test data signal (e.g. 2nd order) is used to excite the damper simulation. The magnification ratio – the amount the damper reduces the input vibration signal – is then compared to the baseline, with the percentage error demonstrating how realistically the damper was excited. For each subsequent test an additional order was included in the sinusoidal signal, with the orders introduced in magnitude dominance order; essentially, as the test number increases, the complexity of the sinusoidal signal used to excite the damper also increases. The tests were performed at three different points along the speed range to ensure the accuracy of any conclusions drawn; these speed points were primarily chosen due to the availability of data.

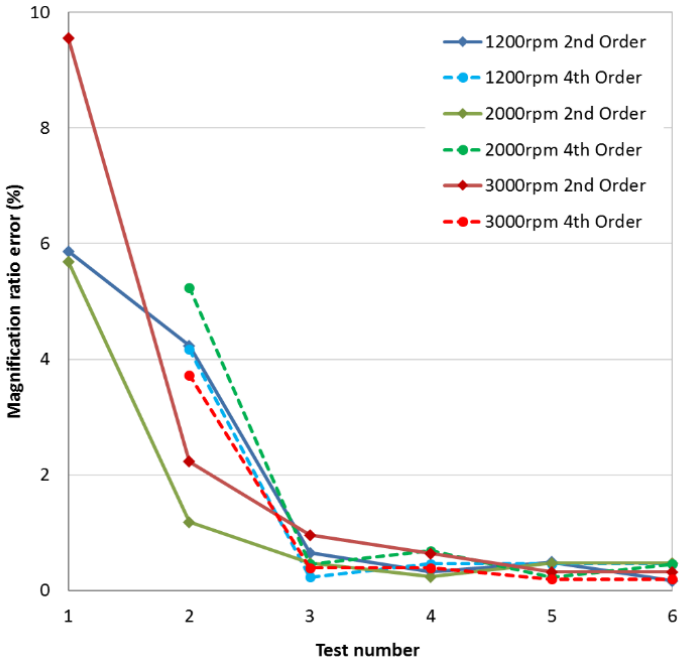

Test	Sine Signal
1	Dominant Order Only
2	Dominant Order + 1
3	Dominant Order + 2
4	Dominant Order + 3
5	Dominant Order + 5
6	Dominant Order + 7

Figure 7.3: Using varying complexity sinusoidal signals to replicate a fired engine torque signal

In all three fired engine signals replicated in Figure 7.3, the 2nd order is dominant, with the 4th and then the 6th orders the next dominant; with this particular fired engine the 4th order does not become dominant until >3500rpm. These three orders are quite clearly dominant, with magnitudes in the range of 100 to 550Nm; the maximum magnitude of the next most dominant engine order (e.g. 8th) is less than 50Nm, with the majority of additional orders typically being less than 25Nm. As can be seen from Figure 7.3, the ability of a sinusoidal signal to replicate the complex torsional vibration signal produced by a fired engine – and therefore produce a representative response in the damper – is quite clearly dependent on the number of frequency orders included in the signal.

Using a very basic signal where only the dominant frequency is replicated can result in magnification ratio error of up to 10%; magnification ratio is a common, useful metric for assessing damper performance (see section 6.3.1). Introducing the next largest frequency order (here the 4th engine order) reduces the error; however, if a third order is included in the sinusoidal replica signal the change in magnification ratio from the baseline test drops to less than 1%. Including further orders (e.g. 8th) does not appear to significantly alter the performance of the damper; this may be due to the low magnitudes of these frequency orders.

The fired engine signals have the same dominance order (2nd, 4th then 6th) at all three tested speeds, so signals based on pulsation generator test data – where the order dominance varies across the speed range (1200-3000rpm) and magnitudes can be lower – were used to confirm results. The construction of these signals in terms of frequency orders can be seen in Figure 7.4.

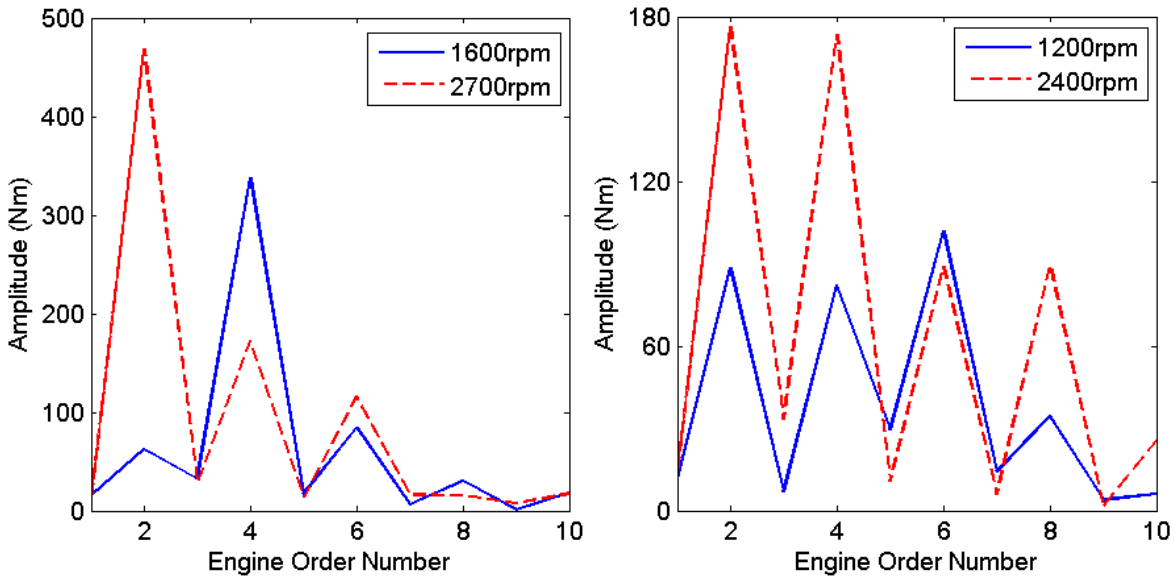

Figure 7.4: Variations in order dominance in Pulsation Generator signals – used to further validate theory on sinusoidal signal replication

These pulsation generator test data signals allow regimes that are not typically found in fired engines to be examined; for example, when order magnitudes are low, or dominance is unclear or altered. Four types of pulsation generator signals are displayed in Figure 7.5. For each speed point, the excitation signal was broken down into its component frequencies; the increasing test numbers signify the re-introduction of a frequency into the signal. The first test uses just the dominant frequency (e.g. 2nd at 2700rpm); when there is no clear dominant order, a test has been run for each major frequency (i.e. 2nd, 4th and 6th – 1200rpm). For each subsequent test, the next dominant frequency is included in the excitation signal, hence why some order lines only begin at later tests.

While the 2700rpm (2.5 bar) torque profile format is similar to the fired engine (same order of dominance and approximately same magnitudes), at 1200rpm there is minimal difference in the magnitudes of the top three orders (2nd, 4th & 6th); their magnitudes are also much smaller than typically seen in a fired engine (~100Nm). However, both of these test sets display the same behaviour as the fired engine signal approximations (Figure 7.3). When only the dominant order is included, the error in the simulated magnification ratio (when compared to the baseline test – the real signal) is substantial, especially when attempting to approximate the more complex pulsation generator signals. When the next dominant order is included in the signal, the error drops; the error reduces even further when all three most dominant frequencies are included. The inclusion of further frequencies (e.g. 8th order) does again not appear to increase the accuracy of the simulation behaviour.

The other two types of signal displayed have either an altered order of dominance (1600rpm – 4th, then 6th and 2nd) or no clear dominant order (2400rpm – both the 2nd and 4th orders have equal magnitudes of ~200Nm). As can be seen from Figure 7.5, while the smallest error in all 3 major orders is seen once the dominant three are all included with the sinusoidal signal, simulating only the dominant order has a much smaller impact. Introducing lower frequency orders does not appear to impact the behaviour as much as introducing higher frequency orders does. The general trend across all tests is that minimal error is produced when the 3 most dominant frequencies are included in a replica sinusoidal signal. These figures also demonstrate that a sinusoidal signal is capable of replicating a complicated torque profile; a 2% error in magnification ratio is equivalent to approximately a 0.5Nm damper torque output error.

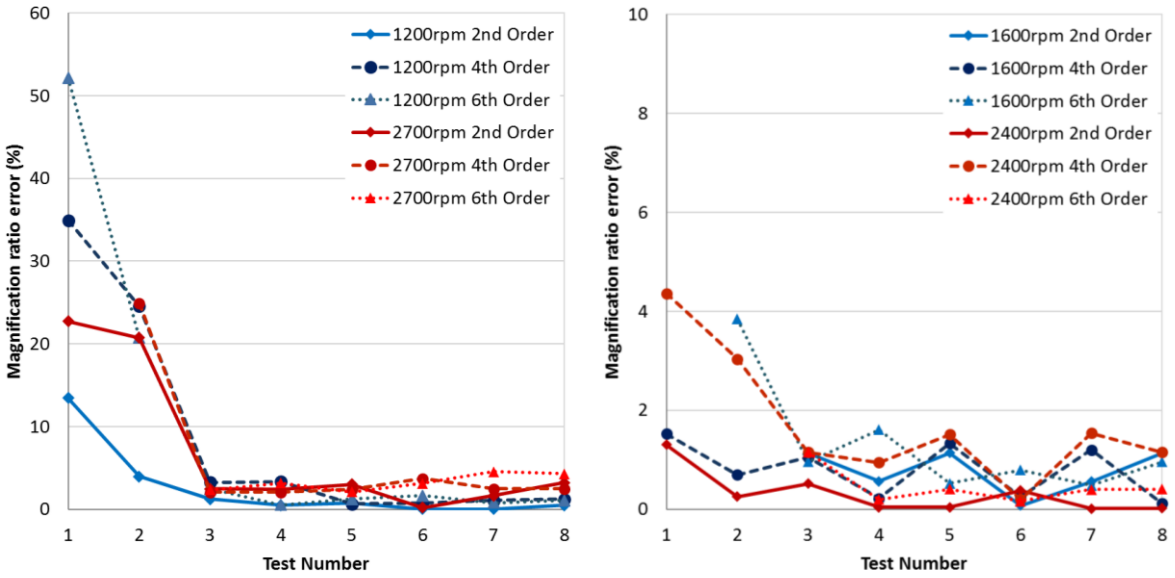

Figure 7.5: Using sinusoidal signals to replicate pulsation generator torque profiles

To quantify the impact additional frequency orders have on the behaviour of the damper (its ability to attenuate the dominant orders), a range of simulation tests were performed. These tests covered a variety of situations, including when the orders are of the same magnitude or when one order is clearly dominant; the impact the magnitudes of the additional orders have on the reaction of the damper was also studied.

Tests were performed at mean torques both above and below the outer spring set knee point. An order (2^{nd}, 4^{th} or 6^{th}) was selected to be dominant with a fixed magnitude (200-500Nm); other orders were then included with varying magnitudes (25-500Nm, maximum dependent on magnitude of dominant order). In order to be able to compare the results independently of the magnitude of the dominant and additional orders (e.g. comparing 500Nm dominant magnitude, 250Nm additional with a 300Nm dominant, 150Nm additional signal), the magnitude of the additional orders as a percentage of dominant frequency magnitude was calculated – see Figure 7.6.

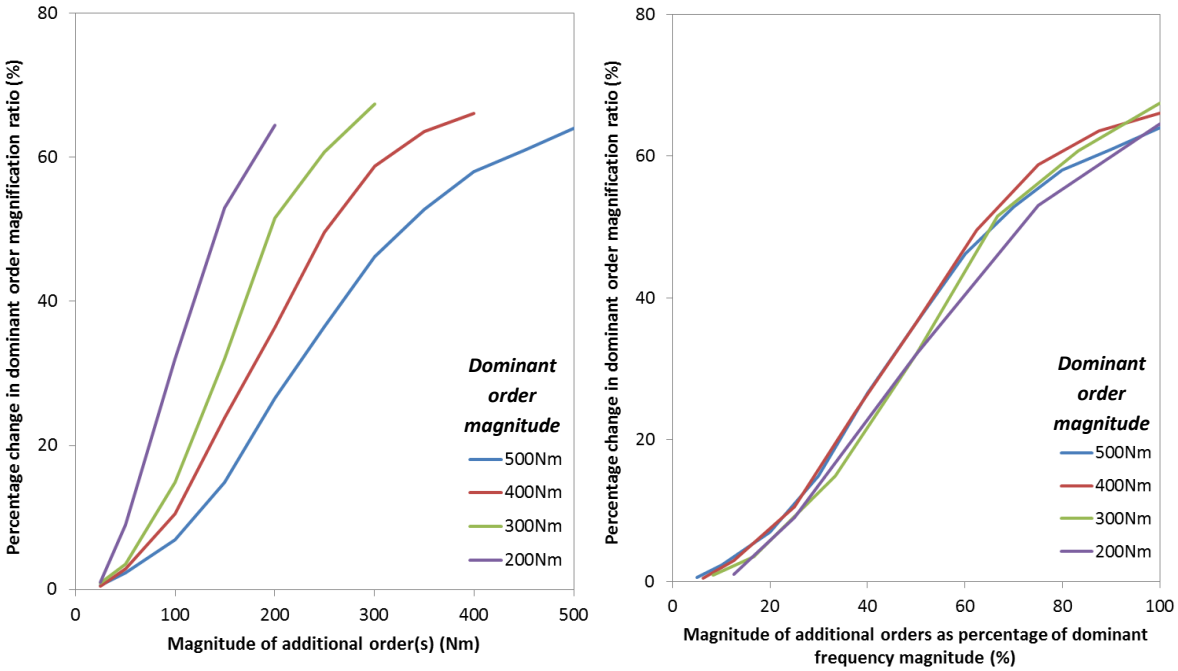

Figure 7.6: Methods for comparing damper attenuation behaviour between different input signals (here when a 4^{th} order frequency is dominant and a 2^{nd} order frequency introduced)

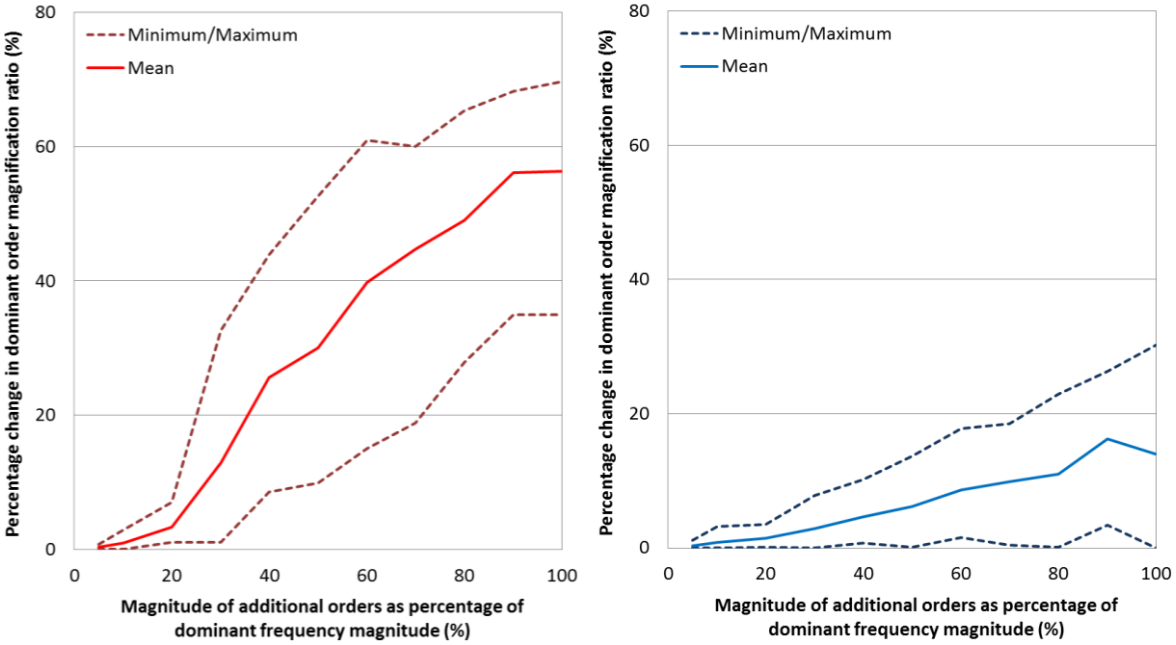

Figure 7.7: Testing below outer spring set knee point: effect of additional order magnitude on dominant order magnification ratio when frequencies of additional orders are lower (Left) and higher (Right) than the dominant order

As can be seen from Figures 7.7 and 7.8, the general trend is that additional orders have a greater impact on the attenuation behaviour of the damper if they have a lower frequency than the dominant order. The effect on the attenuation of the dominant order is proportional to the magnitude of the additional order(s); however, as can be seen from Figure 7.6, the extent of the effect is dependent on the relative magnitude of the additional orders (to the dominant order) rather than the absolute values of the additional orders.

The impact on dominant order attenuation is most pronounced when both springs sets are active in the damper (maximum observed change of ~70% – see Figure 7.7). When the mean torque of the input signal is higher than the outer spring set knee point limit (inner spring set only active – Figure 7.8), the maximum observed change in magnification ratio is more than halved (~30%).

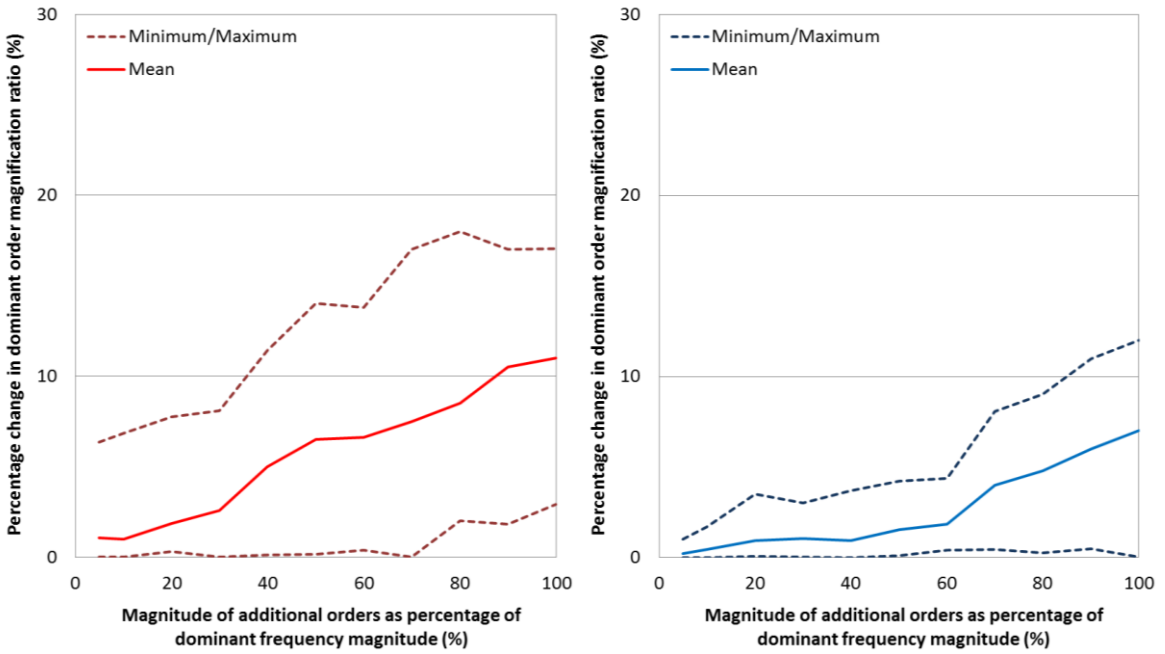

Figure 7.8: Testing above outer spring set knee point: effect of additional order magnitude on dominant order magnification ratio when frequencies of additional orders are lower (Left) and higher (Right) than the dominant order

Below the knee point (Figure 7.7), if the additional orders have a higher frequency, their magnitude can be up to ~40% of that of the dominant frequency before a significant change (e.g. 5%) in attenuation of the dominant order is observed. However, if the frequencies of the additional orders are lower than that of the dominant, the additional order magnitude threshold is reduced to ~20%. This means that when testing the damper at lower mean torques, an engine signal where the 4^{th} order is dominant (e.g. 500Nm) and the sum of the magnitudes of the additional orders is less than 40% of the dominant magnitude (e.g. 200Nm), a sinusoidal signal that approximates the magnitude and frequency of the dominant order only should excite the damper in a representative manner.

If testing at mean torques above the knee point (Figure 7.8) – where only the inner spring set is active – the allowable magnitude of the additional orders is substantially increased. If the additional orders are at a lower frequency, they can have magnitudes of up to ~40% of that of the dominant order before eliciting a substantial reaction (5% magnification ratio change). If the additional orders occur at a higher frequency, on average the effect on dominant order attenuation only exceeds 5% when the total magnitude of the additional orders is ~80% of the dominant magnitude.

It should be noted that (as can be seen from Figures 7.7 and 7.8) these allowable thresholds have been calculated using the mean effect on magnification ratio observed from the simulation data. They are therefore given as a guide to help determine what form of sinusoidal signal is required, rather than absolute values. The difference in allowable threshold between lower and higher frequency signals ties in with the theory that the dominant order in terms of spring behaviour is the lowest frequency order; additional orders with lower frequencies than the dominant order have a much greater impact on attenuation behaviour.

The general rule of thumb is that if a sinusoidal signal approximates the 3 most dominant frequencies in a real signal, the damper will behave in a representative manner. However, in signals where the 2^{nd} and 3^{rd} dominant orders have a higher frequency and a lower magnitude (less than 60% of dominant magnitude when above the knee point, less than 20% when below – using maximum observed values) a simpler signal may be acceptable.

7.1.2 Sufficient excitement

In order to be able to assess the suitability of excitation methods for parameterisation, the ideal type(s) of torsional vibration signal required to sufficiently excite the damper must be established. Exciting the damper sufficiently to ensure that parameterisation – the adjustment of unknown or approximated parameters – can be accurately and quickly performed is different from exciting the damper in a way representative of a real engine. A real engine may in fact not excite the damper sufficiently in some areas; the aim here is to define some boundaries for what is classed as sufficient excitement.

The first few criteria for a parameterisation input signal set are fairly simple to specify; tests need to be done both above and below the knee point (if a two stage damper is being assessed) and across a range of speeds, ideally up to at least 3000rpm – a 6^{th} order frequency can reach 300Hz at 3000rpm, the recommended smallest maximum frequency (see section 7.1.3). In order to accurately detect the location of any knee points – the mean torque at which a spring set becomes inactive – tests at small (~2-5Nm) intervals should be performed in the range approximated using hysteresis loops (see section 6.1).

Sufficient excitement is defined here as a set of input signals that excite the damper in a manner that allows the parameterisation process to be completed as quickly and as accurately as possible. Ideally, any parameter changes should have a significant effect on damper performance; if a substantial parameter change can be made with minimal impact (on the level of torque oscillation outputted from the damper) then it will be harder to narrow down the range in which the value should fall.

Essentially, the aim of this section is to identify the minimum frequency and torque fluctuation magnitude the damper must be excited with in order to produce a response that is useful when adjusting parameters. This has been done by examining how parameter changes affect the attenuation performance of the damper over a range of frequencies, and by comparing how the magnitude of the torsional vibration signal used to excite the damper affects the impact these parameter changes have.

The parameters to be adjusted are those that fall into the estimated category and are typically fine-tuned during the parameterisation process; spring stiffness, inertia values and frictional tuning factors. The values selected using the parameterisation process (see section 6.1) were used as the baseline test. Parameters were then adjusted by a set percentage (e.g. ±20%) and the effect this change had – the change in torque magnitude outputted from the damper – used as measure of the impact a parameter change could have. The parameter changes were tested over approximately the same speed range the damper was tested at (800-3000rpm); by using 2nd and 4th order torsional vibrations this allows the changes to be tested from 27-200Hz. The magnitude of the signal used to excite the damper was adjusted between 40-600Nm. To ensure a complete picture, tests were performed both above and below the knee points; parameters that would have little to no effect on damper behaviour above the knee point – e.g. outer spring friction tuning factor – were not included in the above knee mean torque tests. For each parameter set and input order torque magnitude, an average value for torque output change across the speed range was calculated to allow efficient comparison between the sets.

As can be seen from Figures 7.9 and 7.10, the magnitude of the torque oscillations used to excite the damper does have an effect on parameter adjustment impact. This effect can be seen both above and below the damper knee point. Parameters that appear to have minimal effect on the behaviour of the damper (tertiary inertia) or cannot be altered by a significant percentage (outer spring stiffness) are less strongly affected by the increase in excitation magnitude, but an increase is still present. However, this increase is not linear for all parameters; the impact each increase in excitation magnitude has appears to reduce or stagnate at around 300Nm for certain parameter types – most prominently the friction tuning factors. This suggests that the minimum excitation level (torque oscillation magnitude) should be around 300Nm; while higher magnitudes can increase the impact of some parameter changes further, the extra power the system would require (e.g. if using electric dynamometers) is not considered necessary.

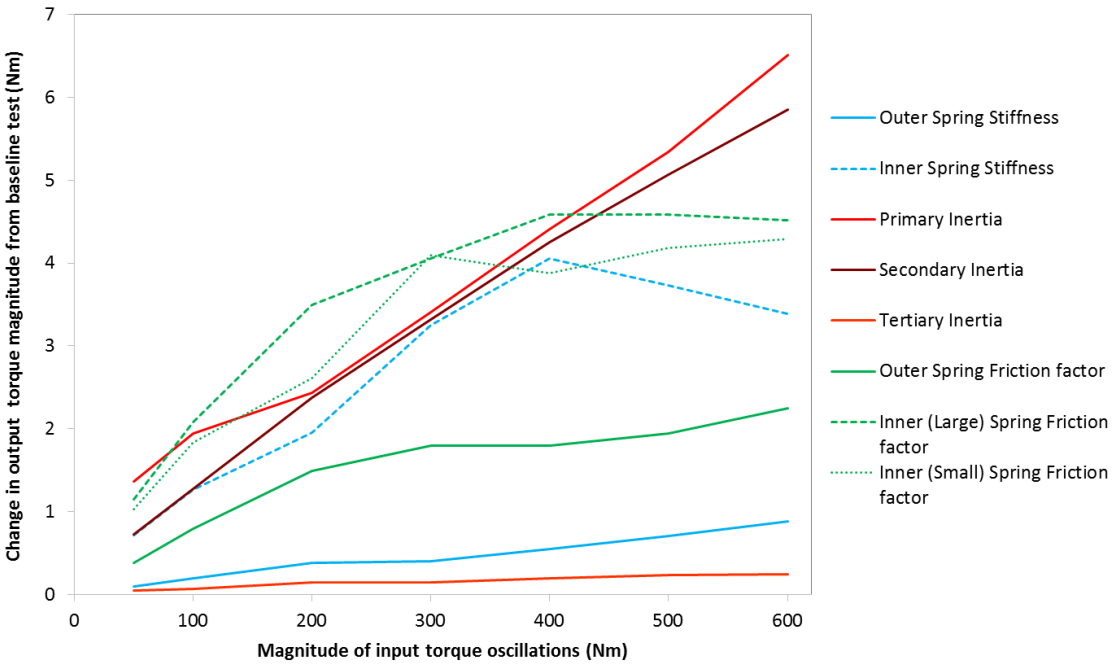

Figure 7.9: Effect of torque excitation signal magnitude on parameter change impact (below knee point)

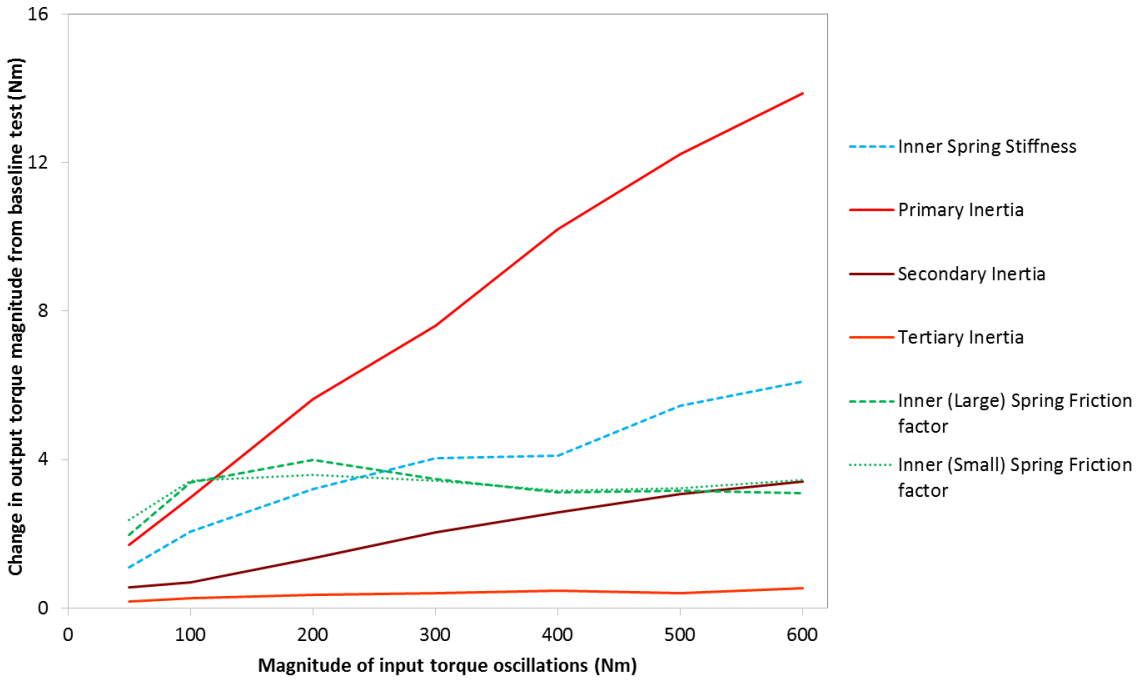

Figure 7.10: Effect of torque excitation signal magnitude on parameter change impact (above knee point)

The impact oscillation magnitude has on damper performance can vary depending on the frequency of the signal and parameter type; as can be seen from Figure 7.11, spring stiffness and inertia parameters are more sensitive to excitation magnitude at lower frequencies (<70Hz). However, friction tuning factors are impacted more by magnitude changes at higher frequencies – above 150Hz. At lower frequencies, higher fluctuation magnitudes have a significant impact on the amount of movement in the damper spring sets (the range over which the springs oscillate – the difference between the maximum and minimum windup angle); at higher frequencies there is far less damper movement (see Figure 7.12). This means that parameters such as spring stiffness and plate inertias are more likely to have a substantial impact on damper performance when spring movement is high; when spring movement is at reduced levels, changes in frictional tuning factors will be more effective at altering damper behaviour.

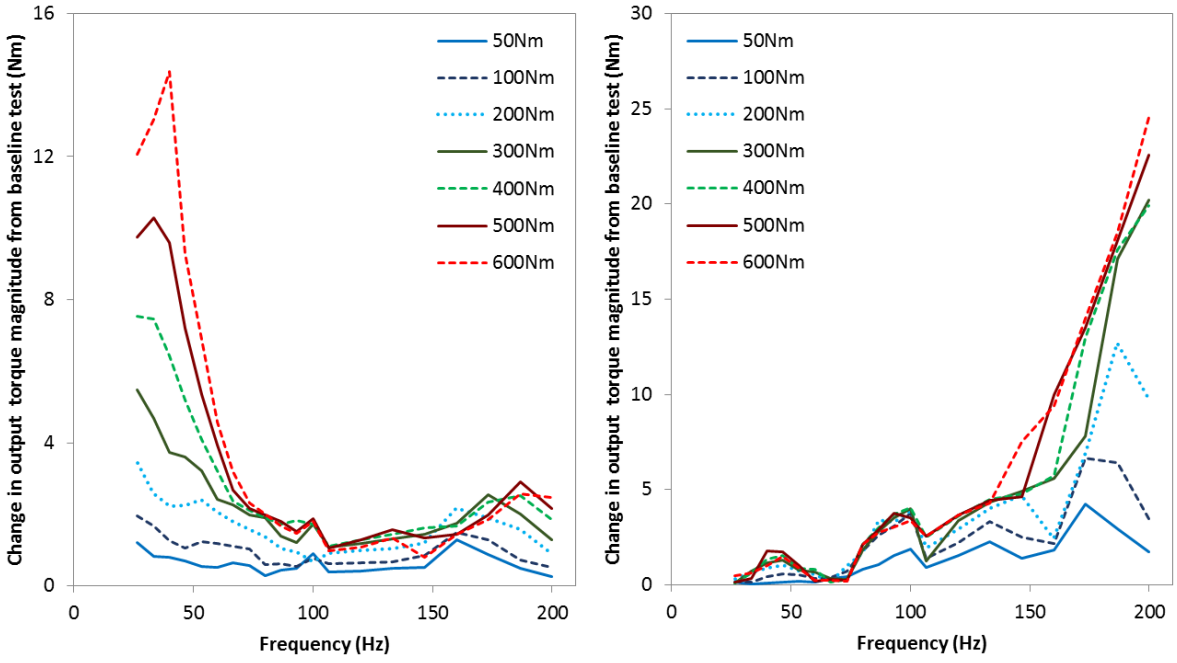

Figure 7.11: Effect of excitation signal frequency on torque oscillation magnitude impact: spring stiffness and inertia parameter changes (Left) and friction tuning factor alterations (Right)

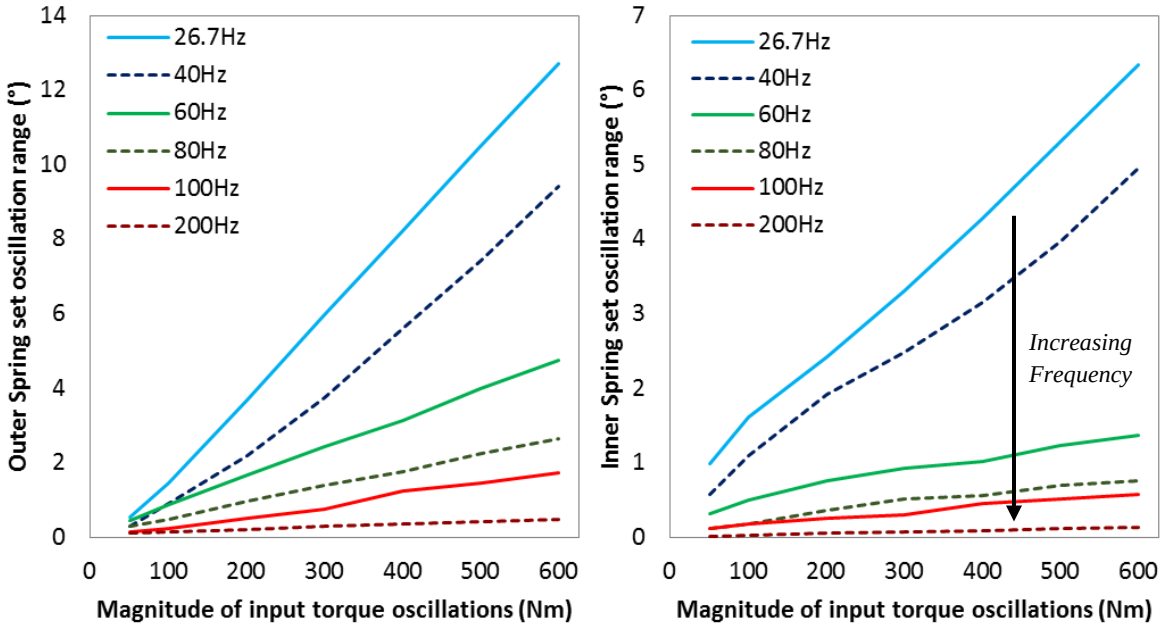

Figure 7.12: Relationship between input torque magnitude and spring set movement (Outer – Left, Inner – Right)

The results shown in Figure 7.11 concur with the conclusion that 300Nm is the optimum excitation magnitude for parameterisation; if oscillations are kept to 300Nm or above then a close to maximum impact on damper attenuation performance is assured across the frequency range. The effect of excitation frequency on parameter changes also suggests that 200Hz is an optimum maximum frequency to aim for when exciting the damper. Below 100-150Hz changes to frictional tuning factors have less of an impact on damper performance and therefore it would be harder to fine-tune these parameters at these lower frequencies.

7.1.3 Efficient mapping procedure

The procedure of mapping any mechanical system (e.g. engine, transmission) can be an extended process. When dealing with experimental rigs the time taken to run a test is very important, as there are only a finite number of rig hours available; if the rig is in use for one project, work cannot be being done on another, potentially delaying results. Delayed results can have financial penalties in both industry and research; thus procedures should be as efficient as possible. When mapping experimentally, this equates to performing as small a number of test points as possible, without compromising on the quality of the data.

In order to test the effectiveness of the following proposed mapping test set, the damper model has been used to predict the results that it would produce; the resultant maps can then be compared to those produced from the far more comprehensive experimental data. The simulated maps, produced using the proposed mapping method, can then be used to predict the behaviour of the damper when excited with a typical mean engine torque profile (the same profile used to excite the damper with the pulsation generator).

The main aim of any mapping procedure is to produce a data set that is able to predict the performance or behaviour of a component in a wide range of situations – e.g. with different engine configurations. The first step is to establish the general range over which damper response needs to be examined; the minimum and maximum frequencies, speeds and mean torques. As the dynamometers used for this project are limited to 3000rpm, this speed was chosen as the maximum. By using 1st, 2nd, 4th and 6th frequency orders, a minimum speed of 1200rpm gives a frequency range of 20 to 300Hz; the test points can be seen in Table 7.1. These test points can be run at range of mean torques; in order to fully capture damper behaviour, it is recommended that the mean torques chosen are no further than 50Nm apart.

The upper and lower torques will depend on the torque range being targeted (e.g. the engine being used); here, the range is set to 100-500Nm with 25Nm steps. In section 7.1.2, it was established that the optimum excitation magnitude for examining damper behaviour is around 300Nm; for completeness, test sets at both 100Nm and 300Nm fluctuation magnitude were performed. Mapping damper performance in this way relies on one key assumption; that the damper behaves in a set way at a frequency, irrespective of the (engine) speed. It has already been established that there is a clear relationship between frequency and magnification ratio (see section 6.3.1); however, the effect that speed may have on this relationship needs further investigation.

To examine whether the performance of the damper at a frequency set point is consistent, independent from engine speed, the simulation was run with input signals formed of two different frequency orders. Each order was run in a different speed range in order to produces two sets with the same frequency range. The 4th and 6th frequency orders were selected; as can be seen from Table 7.2, these orders give a frequency range of 20-200Hz when run at 1200-3000rpm and 800-2000rpm respectively. The use of 2nd order frequencies was considered; however, to reach the same frequency range, speeds of 2400-6000rpm would be required. The simulation has not been tested – or validated – above 3000rpm, thus it was decided that this would be the upper limit of the speed range (this excludes the use of the 2nd order torsionals). The simulation was run at two mean torque levels; 200Nm (below the knee point) and 400Nm (above the knee point).

Table 7.1: Proposed mapping test points

	Order			
Frequency (Hz)	1st	2nd	4th	6th
	Speed (rpm)			
20	1200			
30	1800			
40		1200		
50		1500		
60		1800		
70		2100		
80			1200	
90			1350	
100			1500	
110			1650	
120			1800	
130			1950	
140			2100	
150			2250	
160			2400	
170			2550	
180			2700	
190			2850	
200			3000	
210				2100
220				2200
230				2300
240				2400
250				2500
260				2600
270				2700
280				2800
290				2900
300				3000

As can be seen from Figure 7.13, the mean torque of the test (whether or not both spring sets are active) does alter the effect that speed has on damper performance at a set frequency. Above the knee point – when only the inner spring set is active – correlation between the 4th and 6th frequency orders is stronger, implying that speed has less impact on damper behaviour. Figure 7.13 also demonstrates that fluctuation magnitudes of 300Nm and above are optimum for damper testing; as suggested in section 7.1.2, fluctuation magnitudes over 300Nm (e.g. 500Nm – see Figure 7.13) do not appear to further alter damper behaviour significantly.

From this graph set (and section 7.1.2) it can be concluded that when attempting to map a damper (with the minimum possible test points) the optimum fluctuation magnitude is 300Nm; fluctuations below 100Nm may not produce a map representative of real-world damper behaviour, while higher fluctuations will not produce much improvement in accuracy. Figure 7.13 also suggests that the accuracy of the map – its ability to predict damper behaviour – will be greater when the mean torque is above the outer spring set knee point. However, the correlation between the 4th and 6th orders when exciting both damper spring sets is still strong; these graphs suggest that a damper can indeed be mapped with the minimum number of test points, without compromising results.

Table 7.2: Demonstrating speed differences for different orders at the same frequency

		Frequency (Hz)												
	Order	80	90	100	110	120	130	140	150	160	170	180	190	200
Speed (RPM)	4th	1200	1350	1500	1650	1800	1950	2100	2250	2400	2550	2700	2850	3000
	6th	800	900	1000	1100	1200	1300	1400	1500	1600	1700	1800	1900	2000

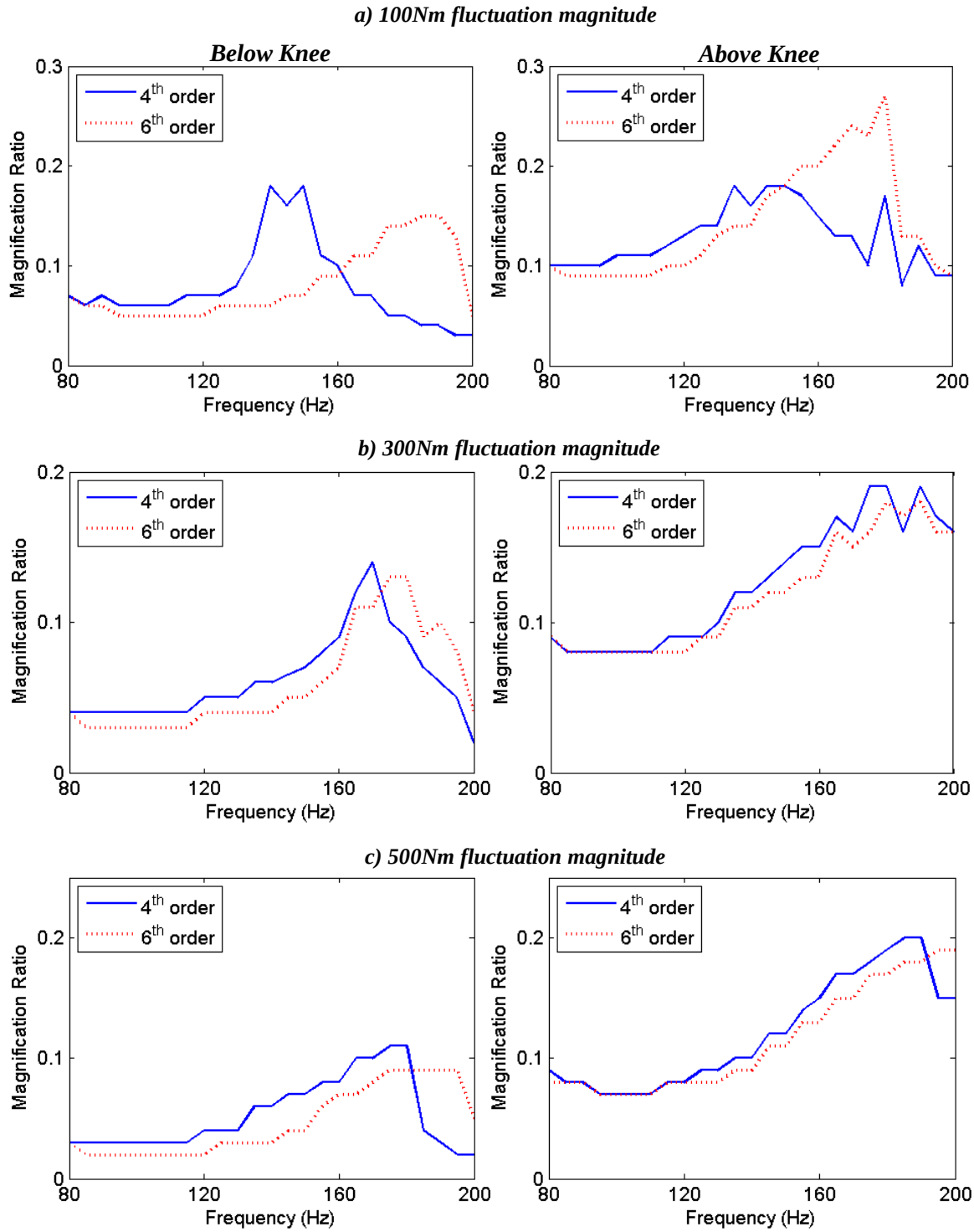

Figure 7.13: Effect of speed on attenuation performance; comparing 4th and 6th order torsional behaviour below (Left) and above (Right) the knee point.

Having confirmed that (in theory) the proposed set of test points would produce a damper map representative of real-world behaviour, the simulation was then used to test the mapping method. The test points proposed in Table 7.1 were performed at mean torques in the range 100-500Nm (25Nm steps); in order to demonstrate that fluctuation magnitudes of 300Nm or greater would be optimum, maps were performed at both 100Nm and 300Nm fluctuation magnitudes. In order to clearly present these maps, data interpolation was required; this was performed using the built-in MATLAB function. The resultant damper attenuation performance maps can be seen in Figure 7.14.

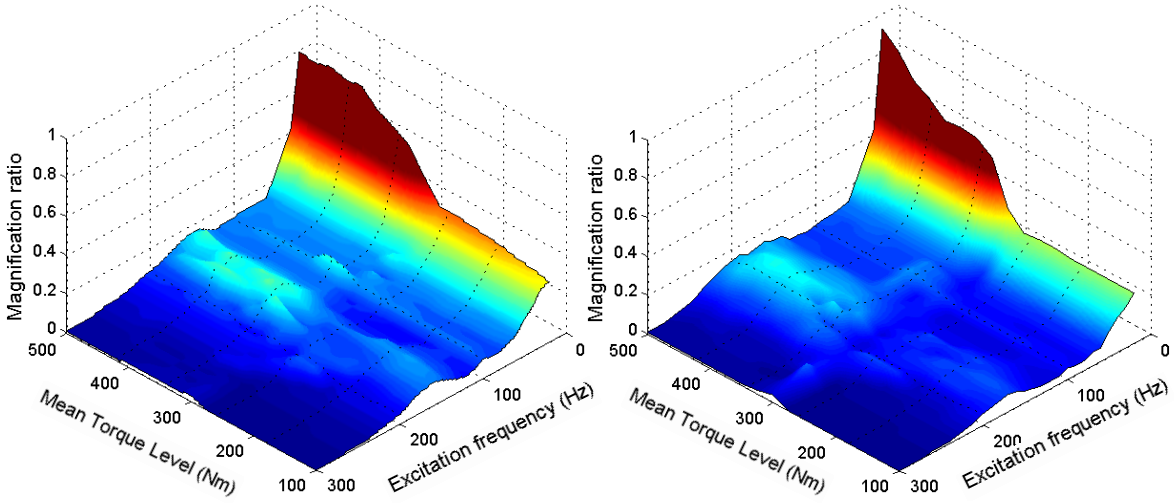

Figure 7.14: Simulated damper attenuation performance when mapped using the proposed method with 100Nm (Left) and 300Nm (Right) magnitude fluctuations

As predicted by examining the effect of speed on frequency behaviour (Figure 7.13), there are significant differences between the 100 & 300Nm fluctuation magnitude maps. At lower frequencies the maps are quite similar, though attenuation is slightly higher (magnification ratio reduced) when 300Nm magnitude fluctuations are used. Once the frequency increases above ~100Hz the differences become more obvious; the crest that appears above 300Nm (between 150-250Hz) is shifted downwards in the frequency range when 100Nm fluctuations are used.

In order to confirm that the mapping procedure (with 300Nm fluctuations) has produced a map that is representative of real-world damper behaviour, it has been compared to the experimental map produced in section 6.3.1. In Figure 7.15, it can be seen that this efficient mapping data set captures the general trends in the data; below the knee point (~300Nm – when both spring sets are active) damper attenuation is high and the area of poor damper performance at low frequencies and high mean torque is also captured. However there are some differences, potentially caused by the lower effective sampling rate; while damper performance is shown to be poorer at high mean torques and frequencies, the peak in this region is substantially lower. While these maps offer a good visual representation of the performance of the proposed mapping method, an alternative method is to examine the prediction capability of the mapped data set.

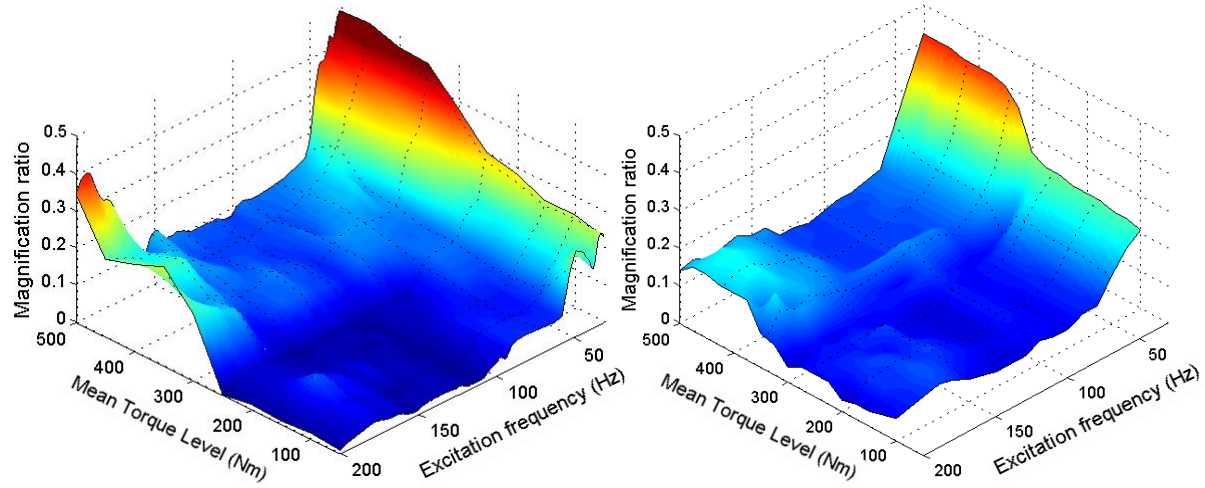

Figure 7.15: Comparing experimental (Left) damper attenuation performance (substantially larger number of data points) with the simulated proposed mapping methodology (Right – 300Nm fluctuations)

In the following graphs (Figure 7.16) the simulated maps produced using the proposed method (for both 100 and 300Nm fluctuation magnitudes) have been used to predict damper attenuation performance when subjected to a typical engine torque curve.

The same torque curve (mean torque and speed points) was used to excite the damper with the pulsation generator experimentally; this gives a baseline that the predicted performance curves can be compared to. It should be noted that the only similarities between the experimental curve and the predicted curves extracted from the simulated map is the mean torque and frequency of the test point; the speeds and fluctuation magnitudes inputted to the damper at each test point may vary significantly due to the nature of the mapping procedure.

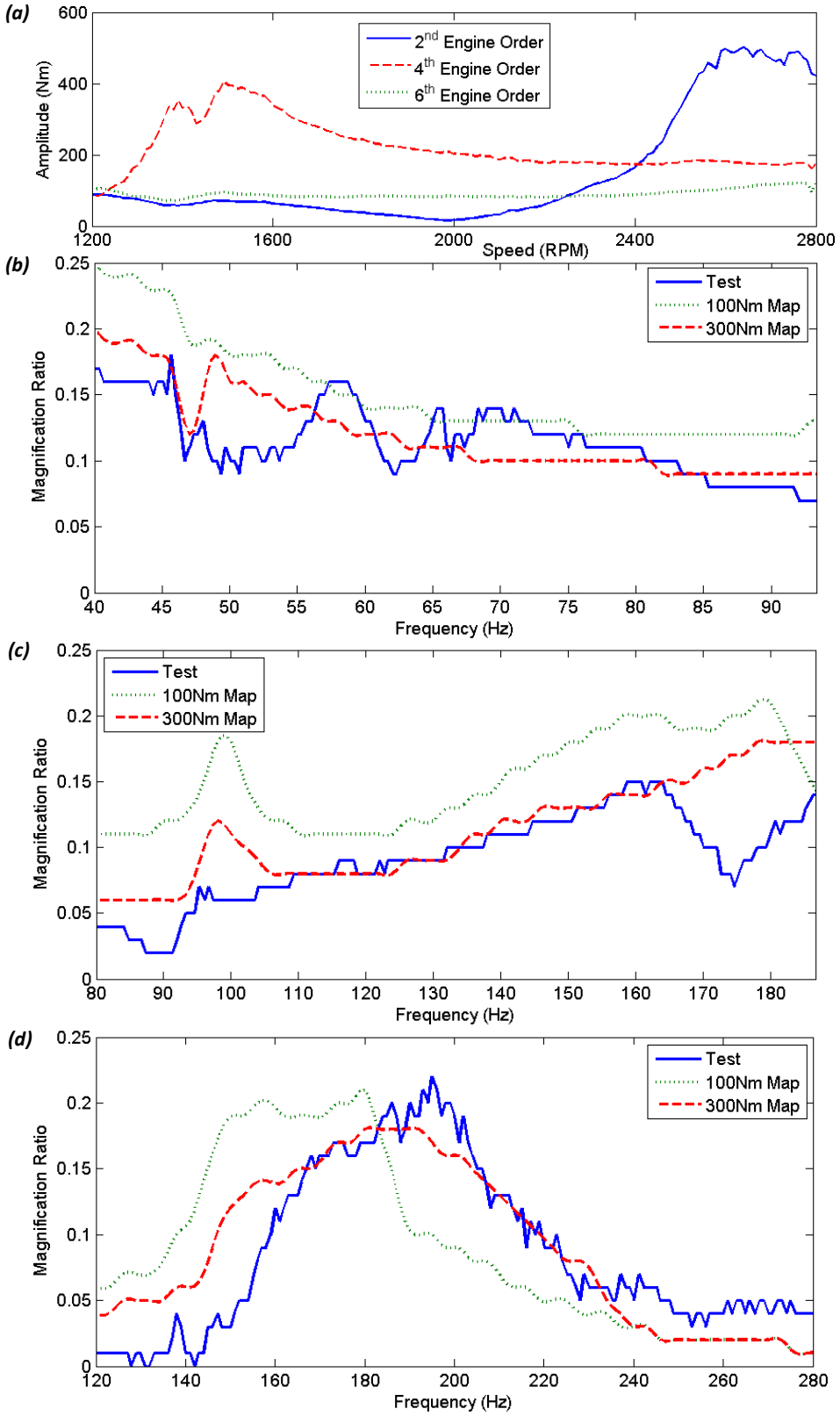

Figure 7.16: a) Order dominance in experimental data (2.5 bar torque converter damper testing) and predictive capabilities of proposed mapping method at b) 2nd, c) 4th and d) 6th frequency orders

As can be seen from Figure 7.16, the mapping procedure (with 300Nm fluctuations) appears to be an effective way of predicting damper behaviour using just mean torque and frequency set points (though these graphs again demonstrate that 100Nm is not a suitable fluctuation magnitude for mapping). It would appear that neither engine speed nor precise excitation magnitude must be replicated in order to predict approximate performance. There are some areas where the accuracy of the prediction is reduced; for example, around 1300-1400rpm (orders 4 and 6) and above 160Hz (order 4 – 2400rpm). The reduced prediction performance at the lower end of the speed range may be due to the large steps between torque set points (25Nm); this may result in the map not accurately capturing damper behaviour around the knee point.

The lack of the expected trough in the 4th order curve above ~165Hz may be due to only using a singular frequency sinusoidal excitation signal at each test point. As can be seen from Figure 7.16 (a), this trough occurs when (in the experimental data) the 4th order ceases to be dominant; the magnitude of the 2nd order becomes larger. It has already been demonstrated in section 7.1.2 that in a signal with multiple orders, the order with the lowest frequency tends to have the greatest impact on damper behaviour.

This mapping method does have its limitations; it has only been tested with the damper fully locked, in 6th gear. While it is capable of indicating regions where the system may benefit from some TC clutch slip or the damper being un-locked, it is unknown whether this mapping method could be applied to situations where the TC clutch or hydraulic circuit is active (i.e. during start-up). General trends are captured, leading to the conclusion that this method has potential; at minimum it may highlight areas of poor performance that should be investigated further, without requiring excessive experimental (rig) testing. The proposed set of 380 test points (reduced to 285 if the minimum mean torque is raised to 200Nm) would require ~13hrs of testing time.

7.2 Areas of poor damper performance

Producing damper attenuation performance maps (see section 6.3.1) revealed three main areas of reduced performance: lower frequencies (below ~60Hz), low torque fluctuation magnitudes (less than ~20Nm) and at higher frequencies (>160Hz) with mean torque levels above the knee point (only the inner spring set being active). The first area of poor performance – low frequencies – was already known from literature (see section 2.1); it is this poor performance at lower frequencies that can prevent the lock-up clutch being engaged earlier in the engine speed range (a torque converter is at its most efficient when it is locked). In this section, the aim is to explore the performance of the damper in these regions with more detail.

For the low frequency tests, the mean torque was kept below the outer spring set knee point level, as in a real world situation the outer spring set will almost certainly be active at such low frequencies. The magnitude of the fluctuations used to excite the damper were varied from 50-500Nm; by testing at a range of fluctuation magnitudes it is ensured that any conclusions on low frequency behaviour are being drawn independent of the effect fluctuation magnitudes may have. The engine speed was varied between 500-1200rpm; by using 1st, 2nd and 4th order frequencies a frequency range of 8-80Hz could be examined.

When examining the impact of lower torque fluctuation magnitudes (2-30Nm), simulation tests were performed both above and below the knee point mean torque level; this allows any behaviour changes that occur when the outer spring set is no longer active to be observed. By testing in the 800-2000rpm speed range and using 1st, 2nd, 4th and 6th engine orders, frequencies in the range of 13-200Hz could be examined. Reduced damper performance at high frequencies is only seen when the outer spring set is inactive (see section 6.3.1); therefore for the high frequency tests, the mean torques examined ranged from 400-500Nm. The same magnitude range was used as for the low frequency tests; however the frequency range was shifted to 140-400Hz (2100-4000rpm using 4th and 6th orders).

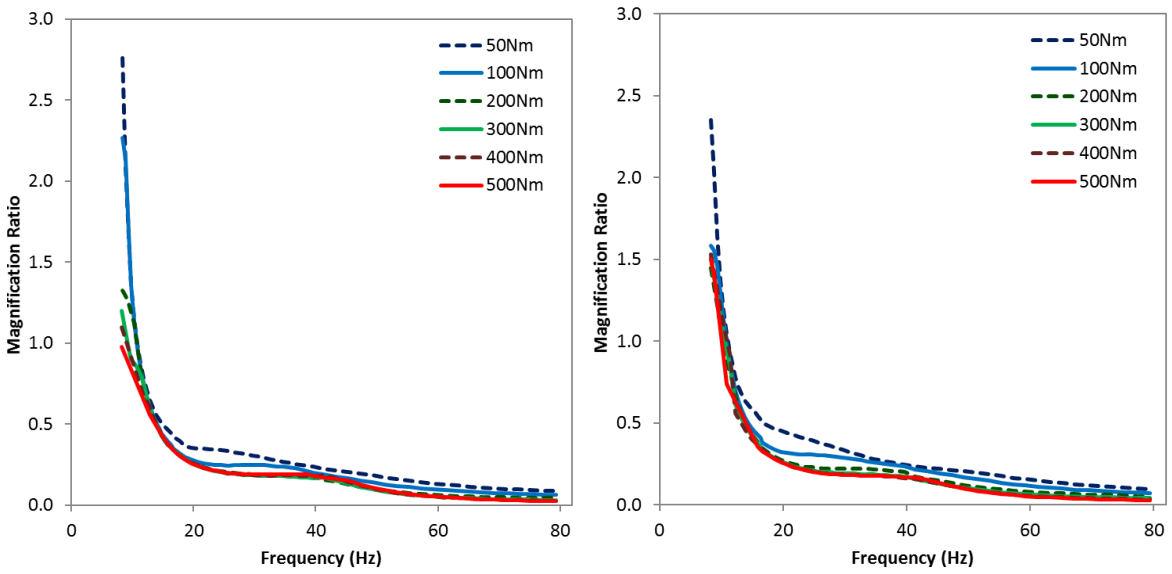

Figure 7.17: Impact of low frequency excitation on damper magnification ratio at different fluctuation magnitudes – at 100Nm mean torque (Left) and 200Nm mean torque (Right)

While the test data demonstrated that at lower frequencies (<80Hz) the magnification ratio increases – damper attenuation performance is reduced – fluctuations of significant magnitude (>20Hz) below 30Hz were not able to be tested, so it was unknown to what extent this effect occurs. Thus the simulation was used to test further down the frequency range – down to 8.3Hz (500rpm using 1st order fluctuations). As can be seen from Figure 7.17, the simulation data agrees with the test data in the overlap range (30-80Hz); the trend of increasing magnification ratio with lower frequencies then continues, with a significant spike below 20Hz.

Simulation testing also allows the effect torque fluctuation magnitude has on the changes in magnification ratio to be examined. As can be seen from Figure 7.17, fluctuations with amplitudes of 300Nm and above result in very similar damper behaviour. Lower amplitude fluctuations – 50 & 100Nm – can result in higher magnification ratios, especially at the lowest end of the frequency range. However, even with a magnification ratio of 2.8, a 50Nm fluctuation will only be 138Nm on damper output – substantially less than the 500Nm fluctuation with a magnification ratio of 1.

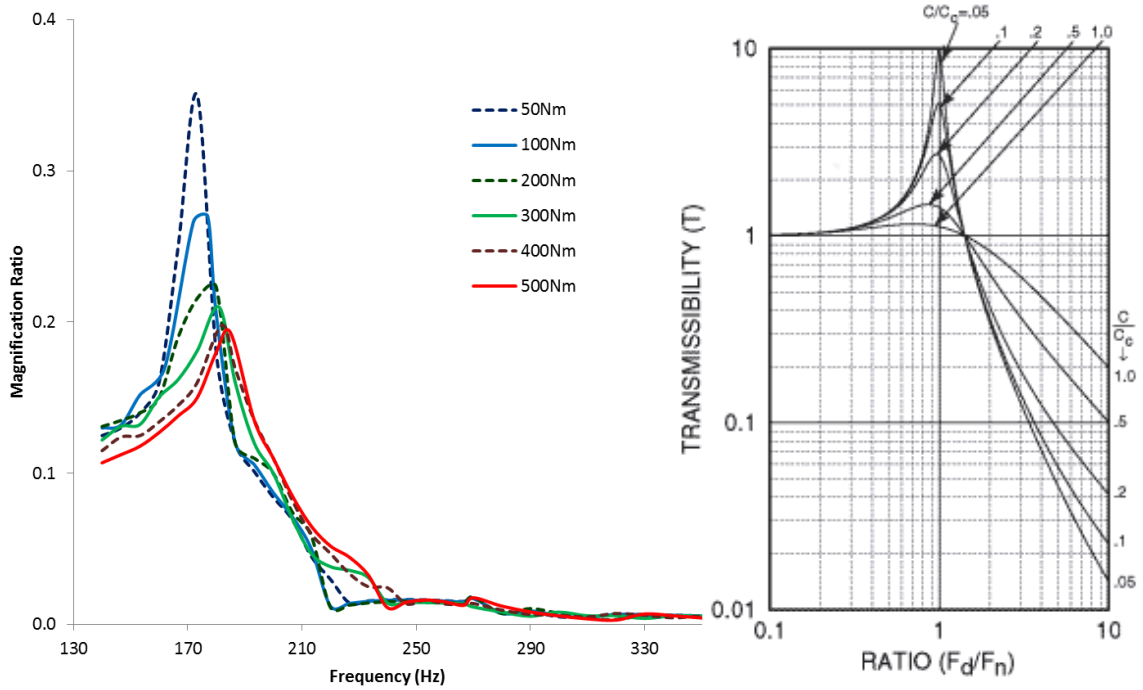

Figure 7.18: Magnification ratio peaks in frequency spectrum at different fluctuation magnitudes (Left) and an example transmissibility curve demonstrating the effect of resonance [100] (Right)

Test data demonstrated that above 140Hz magnification ratio can increase; this effect is primarily seen when the outer spring set is inactive (see Figure 7.15). Simulation testing from 140Hz and beyond, into the range out of reach by rig testing (>300Hz), reveals that while there is a spike in magnification ratio between 140-200Hz (see Figure 7.18), there is not a linear relationship between increased frequency and increased magnification ratio. Once a spike occurs, the magnification ratio is actually reduced to very low levels (after ~210Hz – see Figure 7.14). The location of the spike in magnification ratio is also dependent on the magnitude of the of the torque excitation signal; higher magnitudes move the spike up the frequency range.

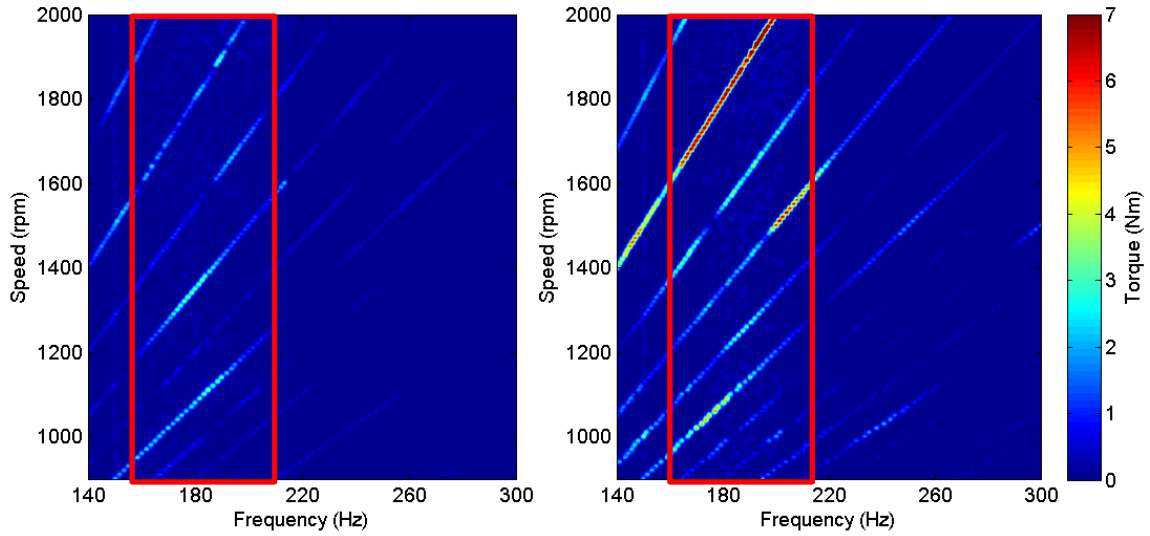

Figure 7.19: Resonance on damper output in test data at higher frequencies – below (Left) and above (Right) the outer spring set knee point

The examination of colourmaps produced from the test data (see Figure 6.20) suggests a cause for spikes in magnification ratio at both low and higher frequencies; resonances. As can be seen from Figures 7.19 & 7.20, resonance bands at ~5-10Hz and 170-210Hz were detected. Resonances are characteristics of either the system as a whole (damper or rig) or the excitation of particular components. A resonance occurs at a particular frequency (or range) and when another vibration signal – i.e. an engine order – crosses the resonance band, its ability to attenuate can be substantially reduced. When compared to a traditional resonance transmissibility curve (see Figure 7.18) a potential cause of the reduction in height (and frequency shift) of the magnification ratio spike with increased torque fluctuation magnitude is seen; damping of the system. Damping is clearly linked to the excitation signal magnitude; in general, as the fluctuation magnitude increases, damping also increases (though it appears to stagnate around 300-400Nm fluctuation magnitude).

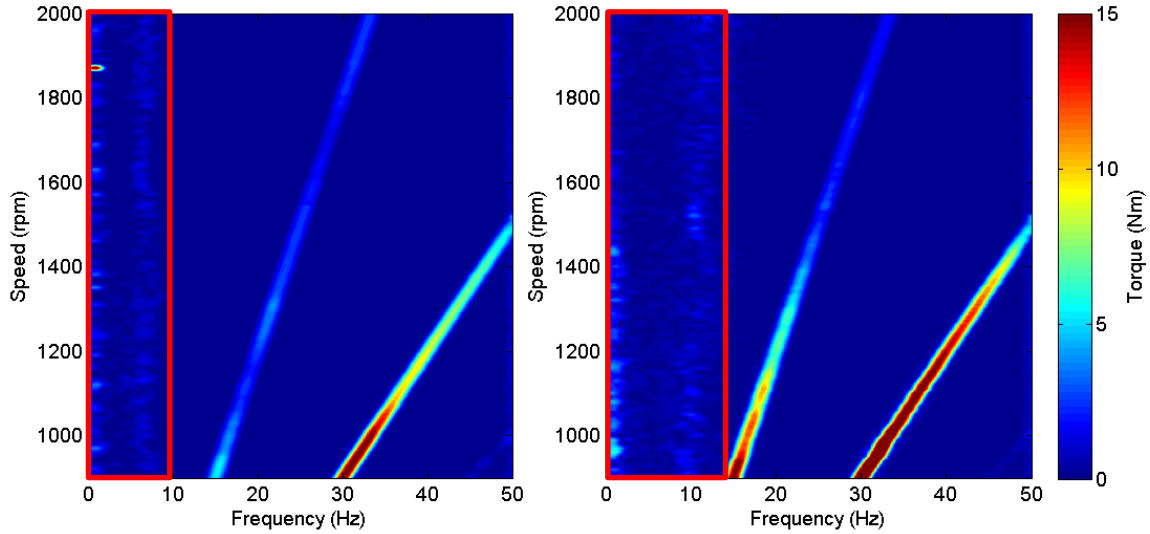

Figure 7.20: Resonance on damper output in test data at low frequencies – below (Left) and above (Right) the outer spring set knee point

The low and high frequency resonance bands have been highlighted in Figure 7.19 and Figure 7.20; the colourbar of these maps has been adjusted to highlight the resonance bands and does not accurately reflect the peak torques in the orders (see Figure 6.12). A resonance occurs when a vibrating signal forces another signal to oscillate with a large amplitude; at the points where the frequency orders cross the resonance band their magnitude is increased. As can be seen from the maps, the damper is more effective at attenuating torsional vibrations at the majority of frequencies when both spring sets are active. Essentially, there is no real change in damper behaviour above the knee point; the effect of the resonance band is just greater.

The increased magnification ratio at low torque fluctuation magnitude seen in the test data (see Figure 6.20) is replicated in the simulation data; these more regimented tests covered a wider (clearer) range of frequencies. As can be seen from Figure 7.21, these tests reveal that the impact of low torque fluctuation magnitudes on magnification ratio is also dependent on frequency. Below the knee point, if the frequency of the excitation signal is more than 22Hz, low torque magnitudes do not appear to affect the attenuation performance of the damper significantly; e.g. the attenuation of a 30Nm signal is the same as a 5Nm signal – see Figure 7.21. However, at lower frequencies (especially below 19Hz) the damper becomes increasingly unable to attenuate the signals, even magnifying some of them (ratio >1).

Interestingly, the frequency range in which low torque fluctuations affect magnification ratio changes when testing above the knee point. At low frequency fluctuations (less than ~23Hz) there is no effect, however once the frequency is larger than 23Hz a very clear trend of low torque magnitude increasing magnification ratio can begin to be seen. The point at which the reduction in magnitude starts to affect the magnification ratio changes as the frequency increases; at 25Hz the effect of torque magnitude on magnification ratio only begins once fluctuation is reduced to ~6Nm, but above 50Hz the effect start point stabilises at around 20Nm.

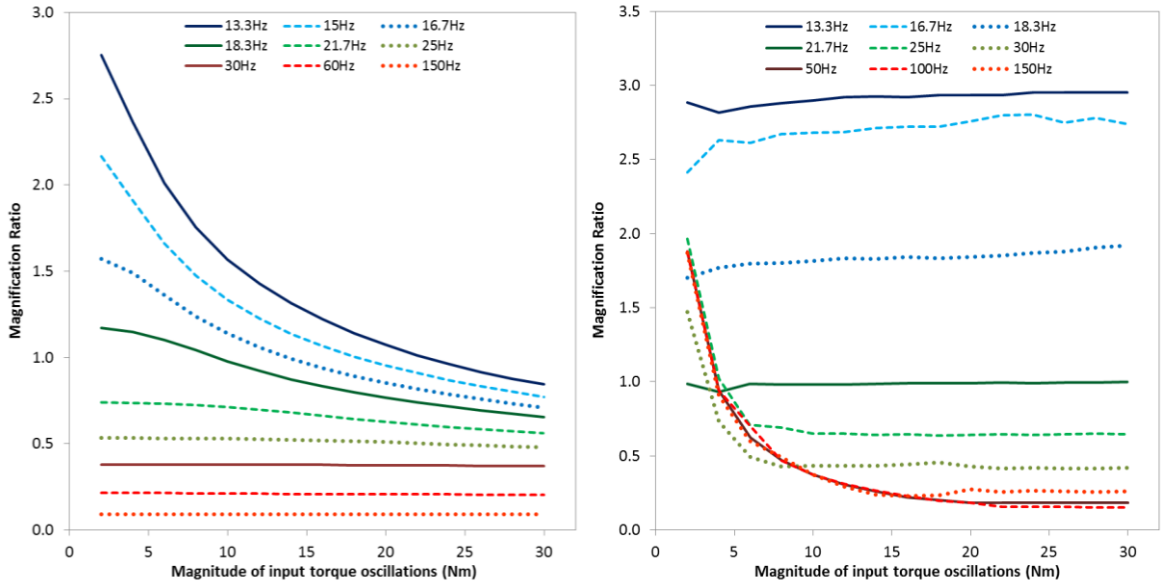

Figure 7.21: Effect of low input torque magnitude on magnification ratio over a range of frequencies – below (Left) and above (Right) the outer spring set knee point

These further investigations into the relationship between fluctuation magnitude, frequency and magnification ratio confirm that while fluctuation magnitude does impact magnification ratio, fluctuation frequency has the most significant (dominant) impact. The frequencies that have been seen to have the greatest impact in Figure 7.21 correlate with the resonance points demonstrated in Figure 7.17 and Figure 7.18. Thus, when investigating damper behaviour, it can be concluded that it is more important to test damper response over a range of frequencies than testing with multiple fluctuation magnitudes.

7.3 Damper behaviour: Speed and Stiffness

The aim of this section is to investigate (and potentially improve understanding of) the causes behind a damper behaviour that is frequently discussed in arc spring damper literature; the effect of (engine) speed on damper stiffness. As seen in section 6.3.2, the stiffness increase caused by increased engine speeds has already been observed in the hysteresis loops. As discussed in literature (section 2.4.2), the general theory is that increased speed increases frictional forces (due to centrifugal effects). These increased frictional forces can cause the spring segments to not compress homogeneously (evenly) and possibly even prevent some segments from moving at all. These inactive segments effectively shorten the length of the spring (without decreasing its torque capacity), thus increasing its stiffness.

While previous studies have used various forms of hysteresis loops (angular movement against torque) to confirm that there is a link between speed and dynamic spring stiffness, very few [62] have more closely examined the movement and behaviour of the individual spring segments. This section examines the behaviour of the springs when subjected to very low frequency torque ramps as well as higher frequency fluctuating torque signals (with reduced spring movement).

7.3.1 Hysteresis loop testing

The effect of increased engine speed can be seen during low frequency torque ramp testing, also known as hysteresis loop production. Hysteresis loop torque ramps were applied at a rate of 50Nm per second; for a full ramp, this is the equivalent of a 0.04Hz fluctuating signal. As can be seen from Figure 7.22, when the engine speed increases, the windup angle (the angle difference between the damper input and gearbox output) at which a torque set point (e.g. 150Nm) occurs is reduced. Thus there is less spring movement for a given torque level; essentially, the stiffness of the damper has increased. This effect can be replicated in the simulation; the simulation allows the movement of each spring set to be examined separately, as well as the movement of individual segments (Figure 7.23).

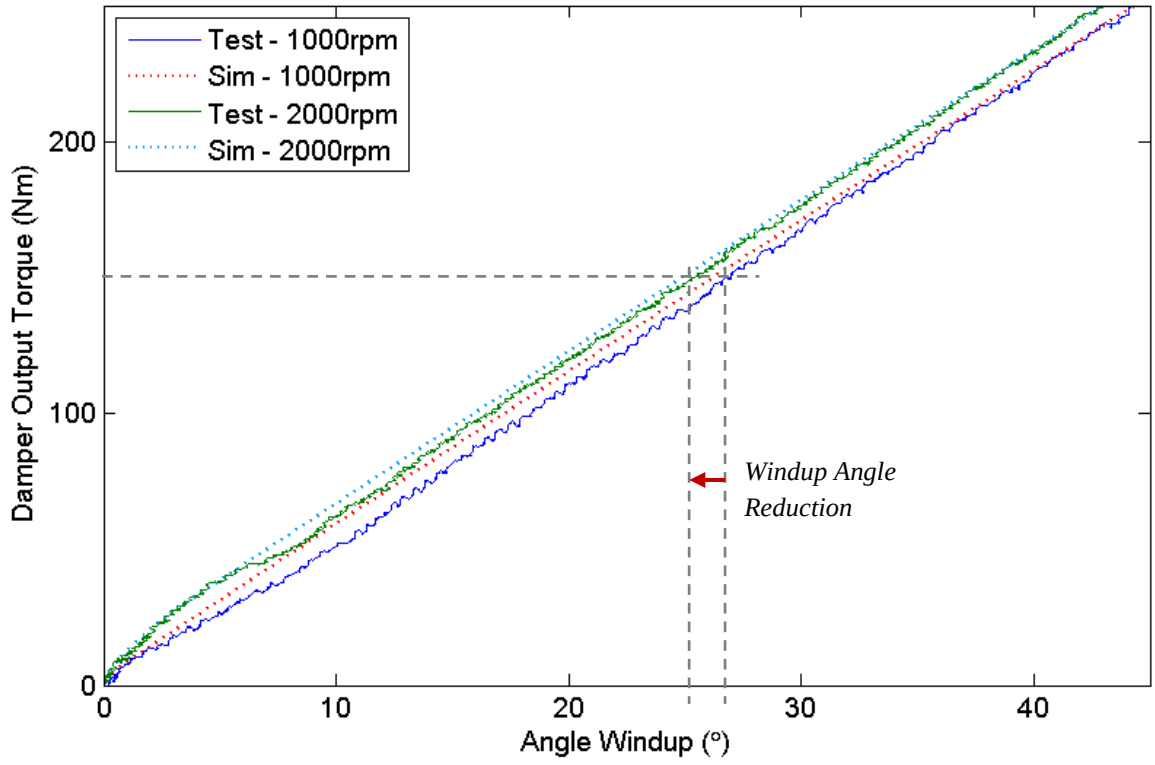

Figure 7.22: Effect of engine speed on damper windup angle (stiffness) in test and simulation data

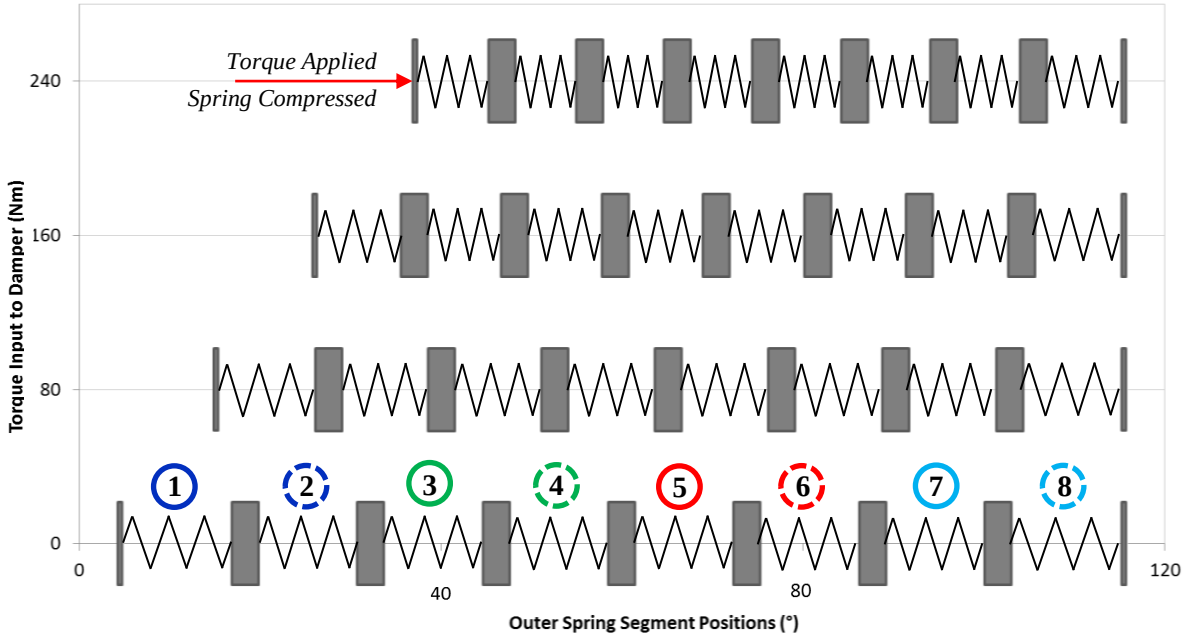

Figure 7.23: Movement of individual outer spring segments as torque is applied to damper and spring compressed

The movement of the individual segments in the outer spring, as a torque is applied to the damper, are demonstrated in Figure 7.23; for ease of display, the number of segments has been reduced to eight (though 16 separate segments were simulated). Torque is applied to the spring by the primary inertia at segment 1, with the last segment (here, number 8) in contact with the secondary inertia. While this graph demonstrates how spring movement and separation of the inertia plates has been simulated, it is difficult to discern the variations in segment compression. This non-homogeneous movement, and the effect of speed on segment compression, can be seen in Figure 7.24 and Figure 7.25.

As can be seen from Figure 7.24, at low engine speeds (500rpm) the spring segments compress at a similar rate as the torque is applied to the spring; there is only a slight difference in the amount the length of each segment is reduced by. However, as the torque applied to the damper increases, the difference in compressed segment lengths between the primary segment and the N^{th} segment does increase.

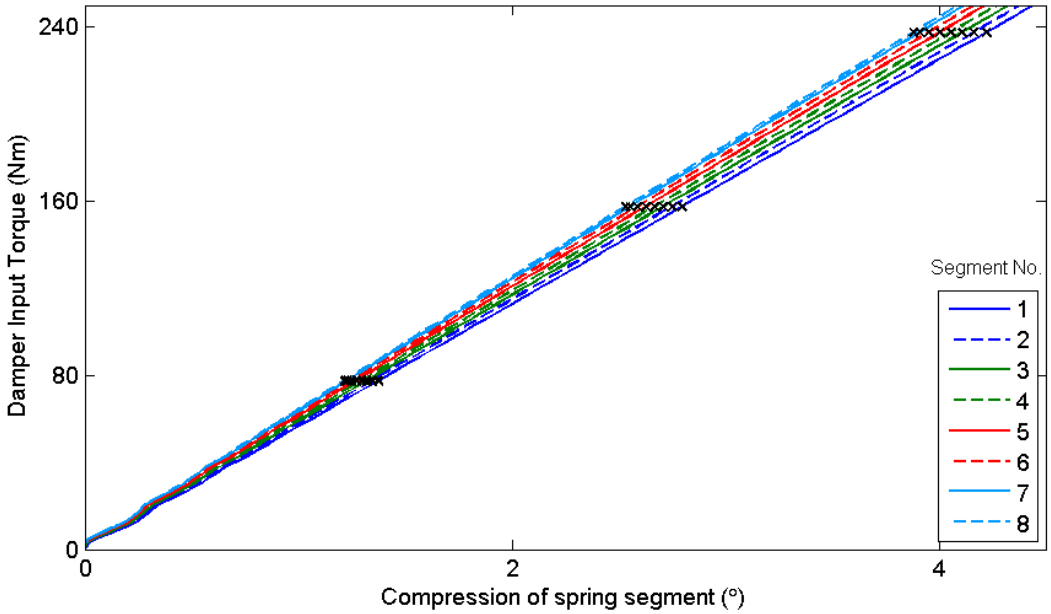

Figure 7.24: Compression of outer spring segments from their static (neutral) lengths as a steady torque ramp is applied at an engine speed of 500rpm. The sampled segment positions shown in Figure 7.23 are represented by 'x' marks.

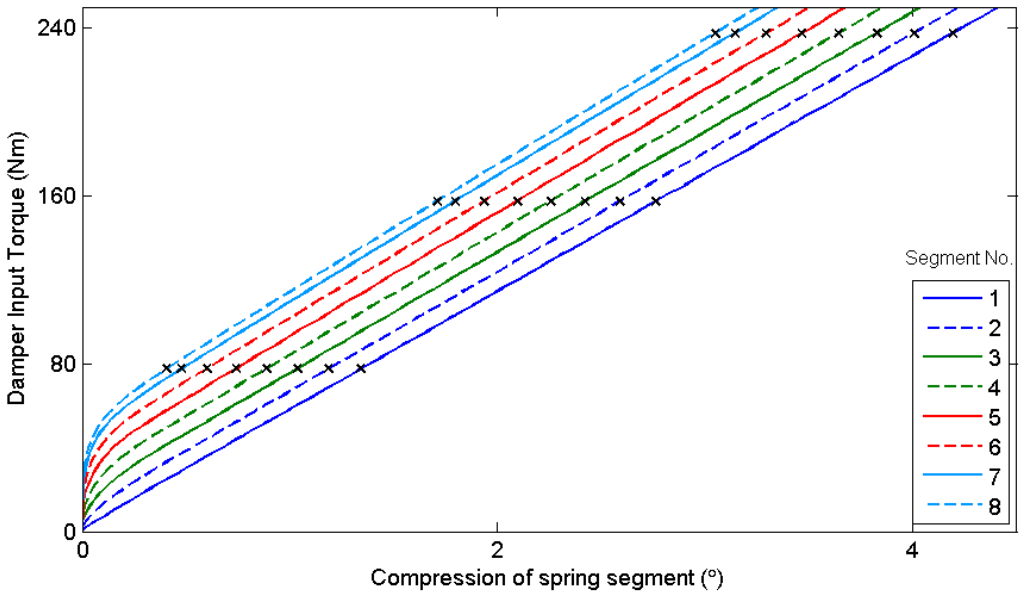

Figure 7.25: Compression of outer spring segments from their static (neutral) lengths as a steady torque ramp is applied at an engine speed of 3000rpm. The sampled segment positions shown in Figure 7.23 are represented by 'x' marks.

As the engine speed of the test is increased (to 3000rpm), a significant change in the distribution of segment lengths is observed (Figure 7.25). It is this non-homogeneous compression of the spring that has been suggested in the literature (see section 2.4.2) to be the cause of the speed dependent spring stiffness characteristic.

These spring movement graphs, combined with closer examination of the dynamic stiffness along the hysteresis curves (Figure 7.26), reveal the cause of the apparent damper stiffness increase. It would appear that the increased engine speed delays the movement of the segments at the (output) end of the spring; at lower speeds, when the torque is first applied, all of the segments begin to move instantaneously. It is this delay in all spring segments starting to move – all segments becoming active – that results in the increased stiffness seen at the beginning of the torque ramp. When spring segments are inactive, the effective length of the spring is shorter; there is less spring movement when a torque is applied, increasing the effective stiffness. However, once all segments are in motion the stiffness of the damper is the same, irrespective of the (engine) speed; this demonstrates why hysteresis curves are not an accurate indicator of spring stiffness or knee point location. If stiffness measurements are taken from a small section of the hysteresis curve, at a higher torque level (e.g. 100-200Nm), the results at both speeds are the same; if stiffness is calculated using the origin (0° of movement at 0Nm) and a fixed point (e.g. angle windup at 200Nm) two different values for damper stiffness will be obtained.

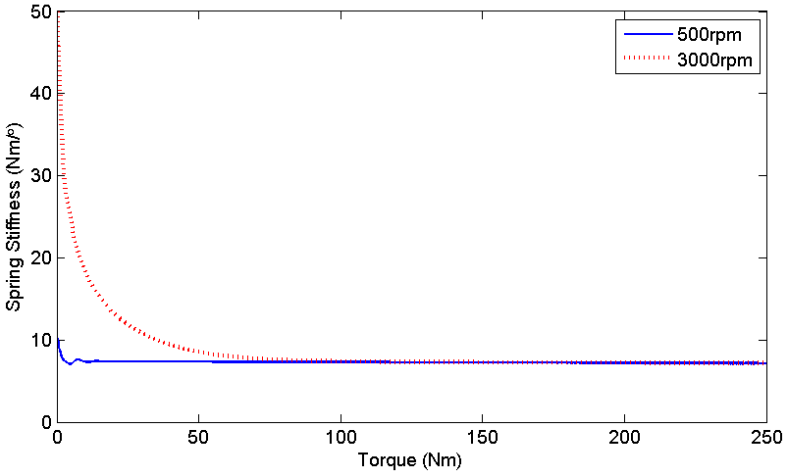

Figure 7.26: Dynamic stiffness of outer spring set at 500 and 3000rpm as the torque ramp is applied

While the cause of hysteresis ramps varying with engine speed has been demonstrated, this form of low frequency ramp does not occur during typical operating conditions; a ramp rate of 50Nm for a short, positive only loop equates to a frequency of just 0.06Hz, far below the typical range. At this low frequency, spring movement is very high; in order to fully understand the effect speed may have on spring behaviour, the movement of the springs at higher frequencies must be examined.

7.3.2 Speed and Spring Vibration Angle

This section investigates speed dependent friction (and therefore spring stiffness) behaviour over a range of spring vibration angles. In section 6.3.1, the alternative potential definitions of vibration angle were discussed; when mapping overall damper performance, vibration angle signifies the mean windup angle at which the damper vibrates at a particular torque level. Here, however, vibration angle signifies the range of motion of the spring; what is the maximum and minimum angle the spring compresses and extends to when subjected to a sinusoidal torque input.

In order to fully understand how the effect of engine speed varies with spring movement, the simulation was run with sinusoidal torque inputs at 1 to 20Hz; 20Hz is the equivalent of 1200rpm 1st order or 600rpm 2nd order excitation. While these frequencies are at the low end of the typical operating regime, these frequencies are substantially faster than the torque ramp application rate used for hysteresis loops and produce a wide range of spring movement amounts (vibration angles). In order to ensure both sets of springs remained active throughout the tests, a mean torque of 150Nm was chosen; tests at both 50 and 100Nm fluctuation magnitudes were performed. A speed range of 500 to 3000rpm (with 250rpm intervals) was utilised; the resultant outer spring stiffness map can be seen in Figure 7.27.

This form of map was previously used to investigate the stiffness of a Dual Mass Flywheel as a function of speed and spring movement [62]. DMFs are typically single stage (have only one spring set), while the simulated torque converter damper has two spring sets. Unlike the test data, the damper simulation allows the movement, torque output and therefore stiffness of the two spring sets to be examined independently. Initial results revealed that speed has a much more significant effect on the outer spring set than the inner springs, thus it was decided that the investigation would focus on the behaviour of the outer springs.

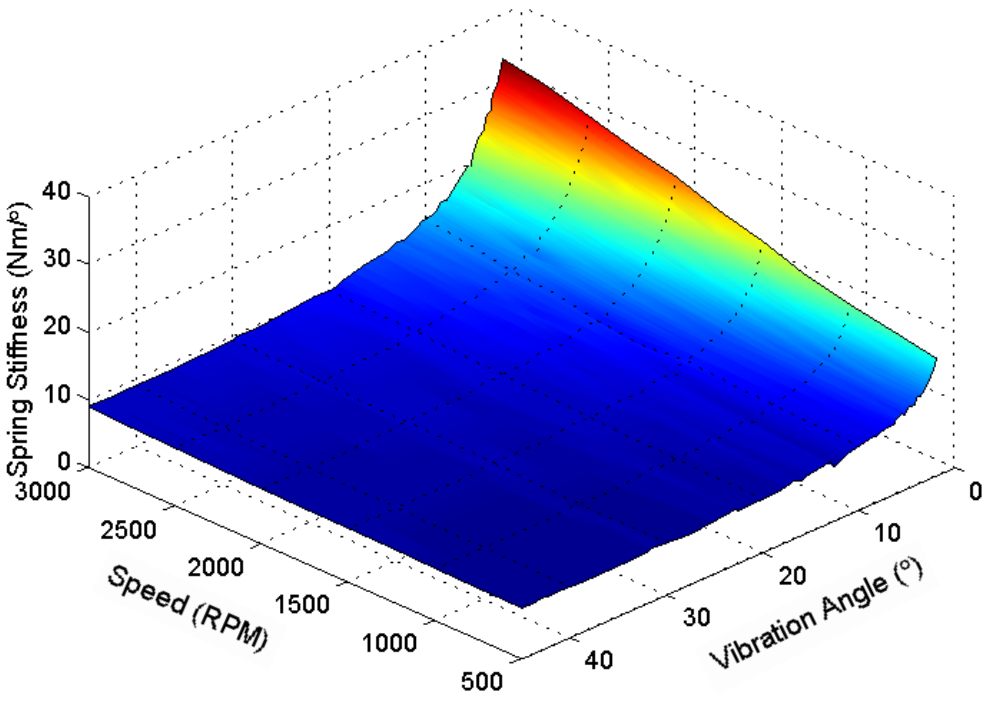

Figure 7.27: Outer spring stiffness variations with engine speed at a range of spring vibration angles

As can be from Figure 7.27, the effect that speed has on outer spring set stiffness is very dependent on vibration angle – i.e. the amount the spring is moving. At low vibration angles – when the spring segments are not moving a substantial amount – stiffness (the relationship between movement and torque) is naturally greater; at these low angles speed has a significant effect on the effectiveness stiffness of the springs. At larger vibration angles – when the spring segments are fluctuating over a much larger arc – speed has a less significant effect; this variation can be more clearly seen in Figure 7.28.

In Figure 7.28, curves demonstrating the movement dependent stiffness behaviour of the outer spring set at three speed points have been extracted from the map. At low vibration angles (e.g. 5° of total spring movement) speed significantly impacts the stiffness of the outer springs; the increasing stiffness can be clearly seen in the changing steepness of the hysteresis loops. At a higher vibration angle (e.g. 30° of spring movement) the impact of speed on hysteresis loop angle (spring stiffness) is far less severe, though speed does appear to have a more significant effect on the energy dissipated by the springs (the area inside the loop) than at smaller vibration angles.

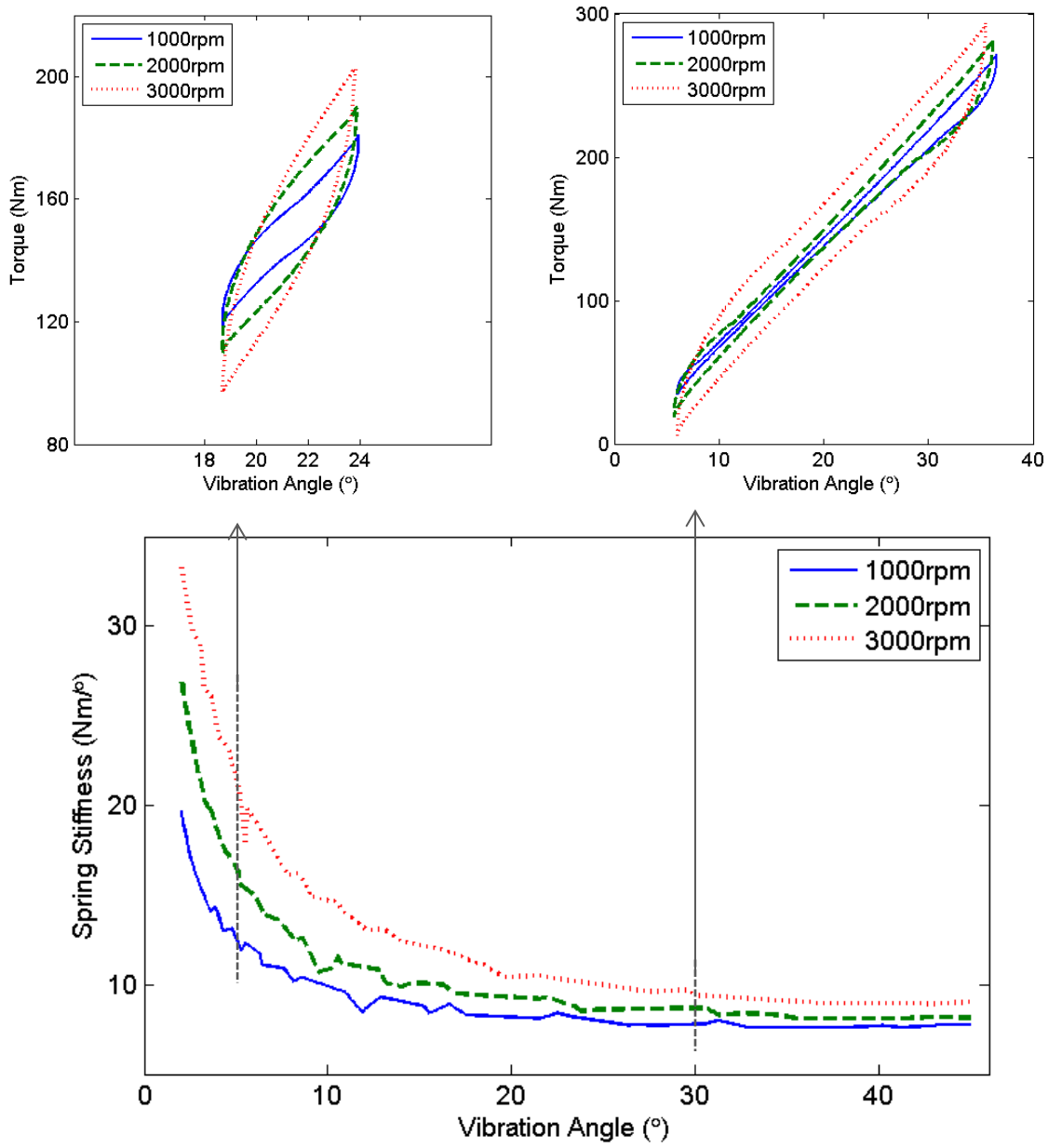

Figure 7.28: The variation of outer spring stiffness and hysteresis behaviour with spring movement at three key speeds

While it has been confirmed that speed can have an effect on dynamic spring stiffness, the cause of this effect – and the reasons why it varies with spring movement – have not yet been established. In order to investigate the cause of this speed dependent characteristic, the movement of individual spring segments should be examined more closely. The following graphs (Figure 7.29 and Figure 7.30) demonstrate why the impact speed can have on spring stiffness is variable and related to spring movement (vibration angle). In these graphs, the compression of a selection of spring segments is displayed; segment compression demonstrates the relative movement of segments more effectively than their absolute locations. For each movement range (using the points selected in Figure 7.28: ~5° and 30° total spring movement) simulations at both 1000 and 3000 rpm have been performed and the movement of the outer spring segments recorded.

The largest increase in spring stiffness is seen when segments become inactive; as can be seen from Figure 7.29, at smaller vibration angles (where the segments are not vibrating as much) an increase in speed results in the end segments of the spring not moving, despite the spring being excited with the same signal. If the same speed increase (2000rpm) is applied when spring movement is much higher (increased vibration angle – Figure 7.30), the spring end segments (which are in contact with the secondary inertia) remain active, though their range of movement is reduced. Thus it can be concluded that the more substantial increases in dynamic spring stiffness observed at smaller vibration angles are due to spring segments becoming inactive, shortening the effective length of the spring; if all sections of the spring remain active the effect of speed is less significant.

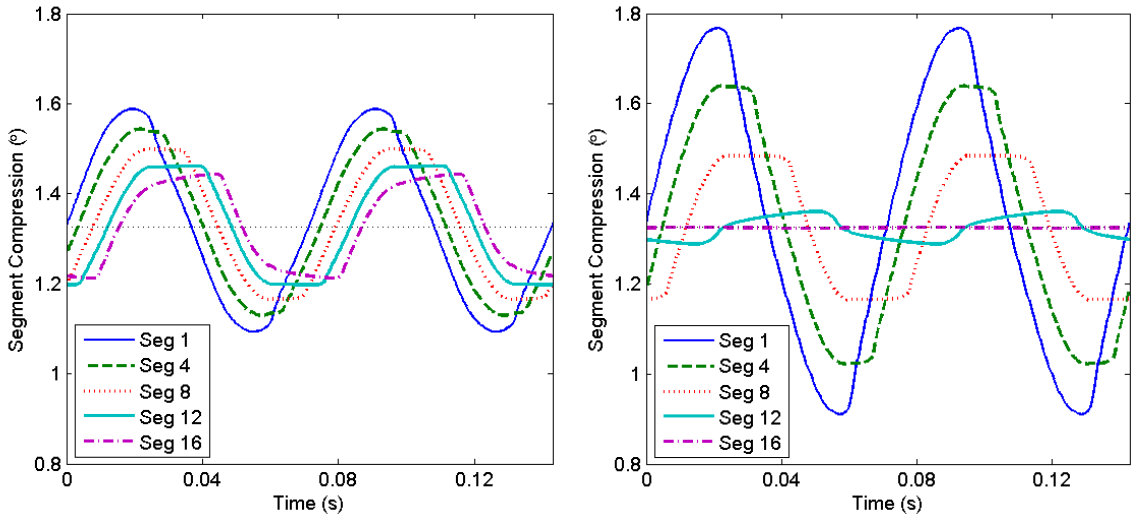

Figure 7.29: Spring segment movement at low vibration angles (5°); at 1000rpm (Left) and 3000rpm (Right)

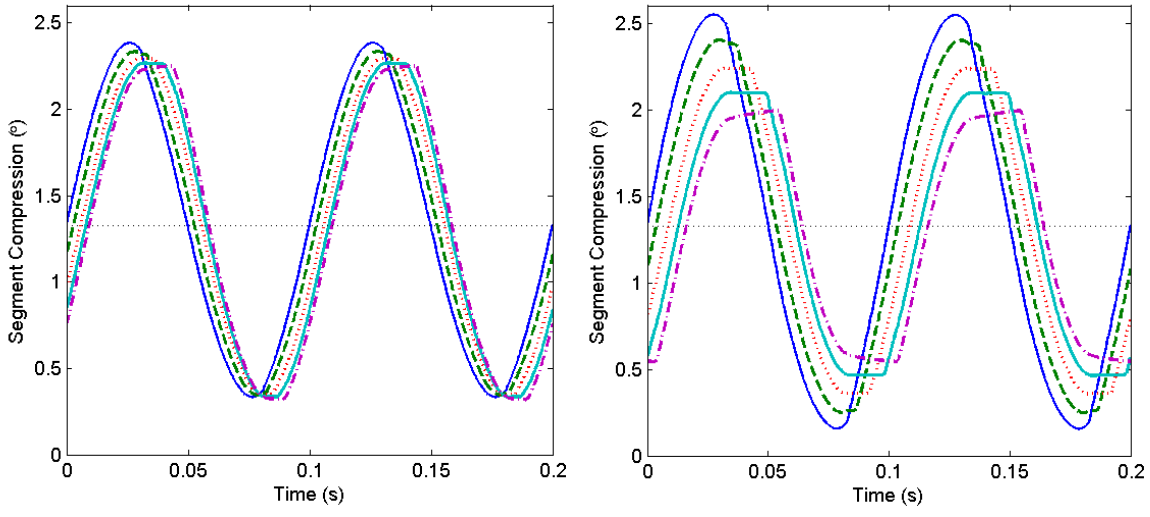

Figure 7.30: Spring segment movement at large vibration angles (30°); at 1000rpm (Left) and 3000rpm (Right)

While Figure 7.29 and Figure 7.30 explain the variation in the impact speed has on stiffness, in order to understand the cause of the speed dependent behaviour the factors that influence spring segment movement must be examined. It is commonly known that the speed at which an object is rotating influences its friction (with its housing) due to centrifugal effects; the spring is forced into its housing, increasing the radial forces (see section 2.4.2). In the following graph set (Figure 7.31) the impact these increased radial forces have on the friction (between the spring and its housing), slip speed and therefore movement of three segments along the length of the spring is demonstrated.

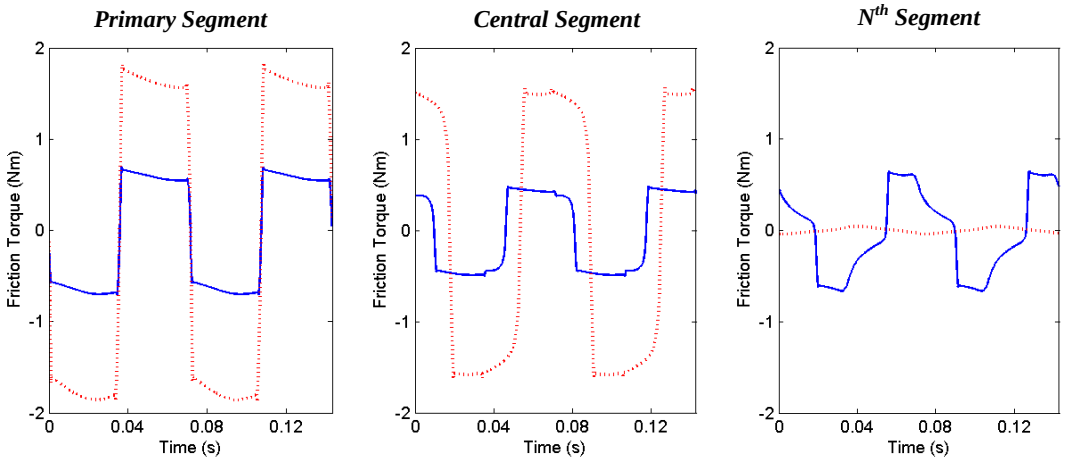

(a) Total frictional force, including radial forces, exerted on segment masses at 1000 and 3000rpm

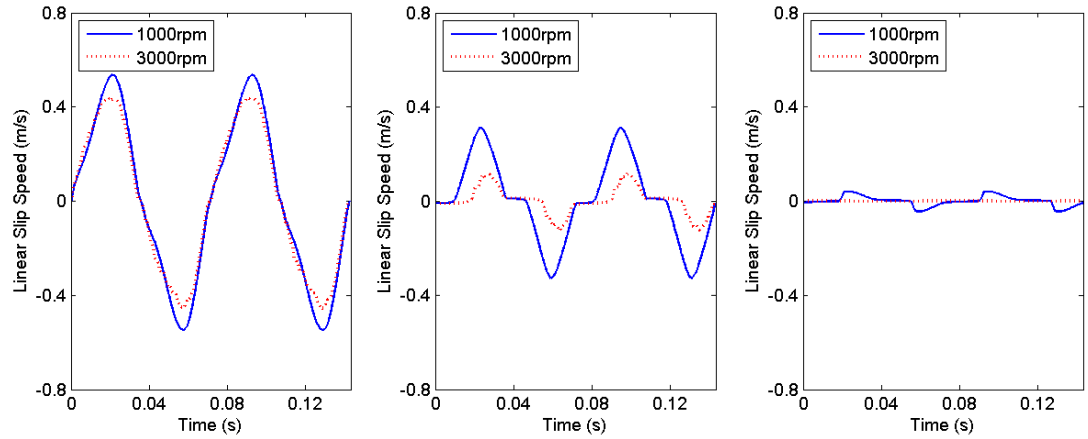

(b) Linear slip speed of masses at 1000 and 3000rpm

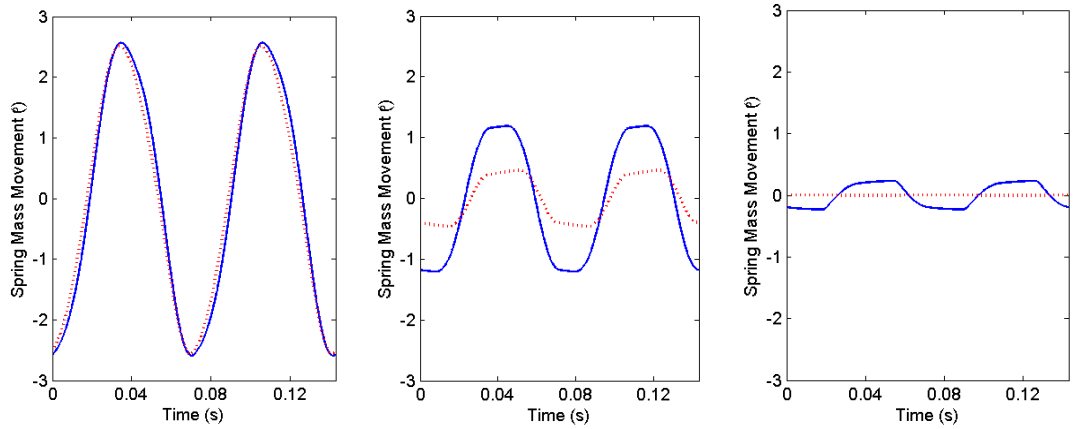

(c) Resultant movement of spring masses at 1000 and 3000rpm

Figure 7.31: The effect of a speed increase on the friction behaviour (a), slip speed (b) and movement (c) of three individual masses along the length of the spring; the 1st (Left), central (Middle) and Nth (Right) segment masses.

Three outer spring segments have been selected; the first segment (in contact with the primary inertia), a central segment and the output end segment (in contact with the secondary inertia). A point at which spring movement was low (5°), and therefore the impact of speed on stiffness high, was selected for analysis; an increase in speed of 2000rpm was used (1000-3000rpm). In Figure 7.31 (c), for ease of comparison, spring segment movement is represented as the movement from its mean, absolute location.

As can be seen from Figure 7.31 (a), the higher radial forces in turn increase the friction torque between the primary and central spring segments. The frictional force exerted on the N^{th} spring segment is substantially smaller when speed is increased as it is essentially inactive. As demonstrated in Figure 7.31 (b), this increased friction slows the spring segments; the slowed segments therefore move (and compress) less, as seen in Figure 7.31 (c). The central figures (those depicting the movement of a central spring segment) also demonstrate another way the increased speed affects spring movement; the response of segment to the inputted torque signal (its movement) is delayed. The graphs in Figure 7.31 provide more context to the theory that speed affects spring stiffness by slowing the coils, due to increased friction. However, it has also been shown that unless some segments are slowed to the point where they become inactive the effect on speed will be minimal.

7.4 Summary

In this chapter the validated simulation has been used to investigate excitation signal, areas of poor damper performance and the link between speed and damper stiffness. The investigation into the impact of the input signal on damper behaviour was divided into three parts; required accuracy of a sinusoidal approximation, quantifying sufficient excitement and optimum excitation for efficient performance mapping.

The key outcomes from this chapter have been summarised below:

Effect of Input Signal on Damper Behaviour

- When using a sinusoidal signal to replicate a torsional vibration input it is recommended that the three primary (dominant) orders are included. If only the dominant frequency is replicated, the magnification ratio performance of the damper can be altered by up to 10%; however, including more than the 3 primary orders does not significantly alter the performance of the damper.

- In general, if an additional (non-dominant) order has a lower frequency it will have a greater impact on the attenuation behaviour of the damper.

- The effect of additional orders on attenuation behaviour is also linked to their magnitude (relative to the dominant order). If both spring sets are active, the magnitude threshold at which additional orders start to have a significant effect is reduced.

- These conclusions lead to the general rule of thumb that if a sinusoidal signal approximates the 3 most dominant frequencies in a real signal, the damper will behave in a representative manner. However, in signals where the 2nd and 3rd dominant orders have a higher frequency and a magnitude below the threshold (60% when above the knee point, 20% when above), a simpler signal may be acceptable.

- When aiming to sufficiently excite a damper for the purposes of simulation validation, some basic criteria must be met; if a multi-stage damper is used, tests need to be done both above and below the knee point (ideally up to at least 3000rpm).

- In order to detect the mean torque (spring compression) at which the knee points occur (a spring set becomes inactive), tests at small (~2-5Nm) intervals should be performed in the range approximated using hysteresis loops.

- The magnitude of the torque oscillations used to excite the damper is linked to parameter adjustment impact, though this relationship is not linear for all parameters; for certain parameter types the improvement in excitation magnitude stagnates at higher torques.

- An approximate level of 300Nm should be used for excitation (torque oscillation magnitude); this torque level ensures that maximum impact on damper attenuation performance is assured across the frequency range.

- Spring stiffness and inertia parameters are more sensitive to excitation magnitude at lower frequencies (<70Hz), while friction tuning factors are impacted more by magnitude changes at higher frequencies – above 150Hz. This means that parameters such as spring stiffness and plate inertias are more likely to have a substantial impact on damper performance when spring movement is high; when spring movement is low, changes in frictional tuning factors will be more effective at altering damper behaviour.

- By using 1^{st}, 2^{nd}, 4^{th} and 6^{th} order torsionals at engine speeds of 1200-2100rpm a mapping frequency range of 20-200Hz is achieved. This frequency map has been applied across a range of mean torques (100-500Nm), with the magnitude of the sinusoidal input signal set to the optimum 300Nm.

- The effect that speed may have on the relationship between frequency and magnification ratio has been investigated. It has been demonstrated that while speed can have an effect, this effect is far less significant at mean torques above the knee point and when sinusoidal input magnitude is kept at or above the recommended 300Nm.

- The damper performance maps produced using the simulation from the suggested mapping test points were used to predict damper attenuation performance when subjected to a typical engine torque curve; these predictions were then compared to pulsation generator test data. It was concluded that neither engine speed nor precise excitation magnitude must be replicated in order to predict approximate performance; prediction capability is weakest at lower mean torques.

- This efficient mapping method does have limitations; it has only been proved with a 1:1 gearbox ratio, with the damper fully locked. However, it is capable of capturing general trends; at minimum it may highlight areas of poor performance that should be investigated further. The proposed mapping set (covering 100-500Nm mean torques) would require ~13hrs of rig testing time to complete.

Areas of Poor Damper Performance

- This section aimed to explore areas of poor damper performance to a greater extent than was possible with rig testing. It was confirmed that the trend of increasing magnification ratio with lower frequencies seen in experimental data continued below 30Hz, with a significant spike seen below 20Hz.

- Simulation testing allows the effect torque fluctuation magnitude has on the changes in magnification ratio at low frequencies to be examined; lower amplitude fluctuations (e.g. 50 & 100Nm) can increase magnification ratio, especially below 10Hz. However, while high magnification ratios (especially those that exceed 1) are undesirable, the most

important factor when attempting to improve damper performance is the absolute value of the torque on damper output.

- Simulation testing from 140Hz and beyond, outside the range obtained during rig testing (>300Hz), revealed that there is not a linear relationship between increased frequency and increased magnification ratio. This effect has also been seen when demonstrating the efficient mapping methodology.

- The location of the spike in magnification ratio seen around 170-200Hz is also dependent on the magnitude of the torque excitation signal; higher magnitudes alter the frequency location of the peak.

- Test data colourmaps suggest that the cause of these magnification ratio spikes is likely to be resonances from the damper or the rig system as a whole.

- Further investigation into the relationship between fluctuation magnitude, frequency and magnification ratio confirms that while fluctuation magnitude does impact magnification ratio, fluctuation frequency has the most significant (dominant) impact. Thus when investigating damper behaviour it is more important to test damper response over a range of frequencies than testing with multiple fluctuation magnitudes.

Damper Behaviour: Speed and Stiffness

- The effect of speed on apparent damper stiffness was investigated for both hysteresis loop testing and across a range of outer spring vibration angles.

- It was confirmed that increasing speed does result in non-homogeneous compression of the springs; the spring segments compress at different rates, by different amounts.

- Different values for damper stiffness will be obtained from different speed hysteresis curves, depending on where (or how) spring stiffness is calculated; this is due to speed effects delaying the movement of spring end segments when a torque is first applied. If a stiffness measurement is taken when all spring segments are in motion, there will be minimal variation in stiffness with speed.

- It was established that while speed can have an effect on spring stiffness, this effect will vary significantly depending on the movement range (vibration angle) of the spring. At low vibration angles (e.g. <10°) the effect of speed is substantially more significant.

- The largest increase in spring stiffness with speed is seen when segments of the spring become inactive (cease to move), hence why the effect of speed is more substantial at low vibration angles.

- It has been demonstrated that the theory posited in literature as to why speed has an effect on spring stiffness is correct; higher speeds result in increased centrifugal forces and therefore increased frictional forces. These increased frictional forces slow the damper segments, resulting in reduced – and sometimes no – movement.

Chapter 8 Conclusions

8.1 Summary

This thesis has focused on the simulation and characterisation of a two-stage torque converter arc spring damper system; this included the development of a novel method for exciting a damper with a high frequency signal. In Chapter 2 a review of current damper technology, simulation methods and testing methodology was carried out. It was established that there was scope for an original contribution to knowledge to be made on the subject of torque converter damper simulation and experimental excitation. In Chapter 3 the available testing facilities were described, and experimental methodologies established; Chapter 4 detailed the novel pulsation generator concept that was developed in order to adequately excite the damper system. The methods used to simulate the damper and rig system were introduced in Chapter 5, with new methodologies for some components proposed. The performance of the damper system was examined in Chapter 6; the experimental data was used to parameterise and validate the simulation. Finally, in Chapter 7, the simulation was used to answer questions on the impact of excitation signals on damper behaviour, as well as examining some observed damper behaviours.

8.2 Conclusions

In the following section, the conclusions from this investigation have been summarised and evaluated against the objectives detailed in Chapter 1.

1.) *Review current torque converter damper technology and literature relating to damper testing and simulation, including high frequency pulsation generation technology.*

The purpose of this objective was to gain a greater understanding of damper technology as well as testing and simulation methodologies; completing this objective allowed areas of potential contribution to knowledge to be identified. To this end, a review of torque converter damper technology as well as simulation and testing methods was presented in Chapter 2. Due to the lack of available literature on torque converter dampers, the review was expanded to include testing and simulation methodologies for Dual Mass Flywheels (DMFs) and other driveline components.

Torque converter dampers are primarily used to reduce the torsional vibrations transmitted from the engine to the driveline when the lock-up clutch is engaged. Coil spring dampers can use both straight and arc springs; a single damper can have multiple spring sets, and these spring sets can also use nested springs. Driveline component testing methodologies can be roughly separated into two categories; those that use electrical dynamometers and those that use fired engines. Electrical dynamometers are typically combined with a mechanical solution or virtual engine controllers in order to produce high frequency fluctuations (similar to a fired engine). The flexibility and accuracy of the controllers can be limited, while the reviewed mechanical solutions can struggle to produce high frequency fluctuations at low speeds. A review of spring damper simulation methodology concluded that a more complex discretised simulation method would be most suitable for this application. In order to accurately simulate the movement of the springs, this discretisation methodology should be combined with a continuous dynamic friction model.

Areas of literature that were identified as having potential for contributions to knowledge:

- The literature is lacking a cheap, adjustable mechanical solution that is capable of exciting the damper over a range of speeds, frequencies and mean torques.
- The simulation of nested springs in a discretised model.
- The simulation of spring-limiting hardstops
- The effect that non-dominant frequencies in the excitation signal may have on damper behaviour – what type of signal is sufficient to excite a TC damper.
- The occurrence and cause of speed-dependent damper behaviour - in the majority of cases investigations into centrifugal effects do not cover the full operating range of the damper.

2.) *Develop a methodology for, and implement, an experimental programme to produce a results set that can be used to characterise and validate a damper simulation.*

The purpose of this objective was two-fold; firstly, to identify if the experimental facilities available were capable of exciting the torque converter damper, and secondly, to devise and plan an experimental programme that excited the damper in a range of different ways. To meet this objective, in Chapter 3 the experimental facilities available were outlined, as well as the upgrades that were undertaken to enhance performance. It was during this methodology development process that it was discovered that an additional pulsation generator unit would be required to allow the rig to perform high frequency excitation experiments.

The experimental setup was designed to allow multiple forms of tests to take place, including hysteresis loop testing (transmission only) and high frequency excitation (with the pulsation generator). It was determined that the transmission would be used in a gear that gave 1:1 ratio (6^{th}) and the damper over-locked (to minimise clutch slip). It was found that in order to achieve torques below ~20Nm (including negative torques), a false torque level signal was required to be sent to the gearbox ECU.

3.) *Develop a prototype pulsation generator concept for damper excitation.*

During the initial assessment of the capabilities of the available experimental facilities (as part of the second objective) it was discovered that the electric dynamometers were not suitable for high frequency damper excitation. Thus, a pulsation generator was required; the development of a novel pulsation generator concept is detailed in Chapter 4. This objective required the concept to be cheap, simple to develop and maintain, while providing a good level of controllability over its outputted signal. The purpose of the pulsation generator is not to perfectly mimic a fired engine, but to be able to adequately excite a damper.

To meet this objective, a pulsation generator was developed from a 4-cylinder motored diesel engine; the cylinders are filled with compressed air through dummy injectors and the crankshaft driven using the input electric dynamometer. The input dynamometer provides the mean torque level, while the compression of the pressurised air in the cylinders creates the fluctuations.

As part of this objective, the performance of the pulsation generator was assessed using simulation and experimental data. A non-linear crank-angle based simulation was developed of the pulsation generator using MATLAB Simulink®; this simulation could be used in the future to investigate improvements to the pulsation generator concept. Simulation and experimental data demonstrated that the basic functions of the pulsation generator perform as expected, though the frequency of the output pulsations does vary from a fired engine; this is due to reactions between the pulsation generator and the stiffness and inertias of other components on the rig. The pulsation generator concept is capable of exciting the damper in the manner required for simulation characterisation.

As part of assessing the suitability of the novel pulsation generation concept, a review of its performance against other damper excitation methods (including electrical dynamometers and fired engines) was conducted. It was determined that fired engines and electric motors are more suitable for durability testing due to their reliability and ability to produce a real-world torque signal; the flexibility of the electric motors and the low running costs of the pulsation generator suit damper performance tests.

Contribution to knowledge:

- A methodology for developing a cheap pulsation generator from a (spare) fired engine has been developed, implemented and assessed.

4.) *Develop a simulation of a two-stage arc spring torque converter damper.*

This objective required a simulation to be developed utilising the discretised spring method identified from literature. In order to complete this objective, an examination of the selected damper hardware was required; this process, along with the methods used to simulate the two-stage damper system, has been presented in Chapter 5. MATLAB Simulink® was chosen as the simulation environment, as its flexible block-based simulation method allows subsystems and library components to be constructed and parameters easily adjusted.

While examining the hardware, it was found that this damper is constructed from three inertias (primary, secondary and tertiary) that are separated by two spring sets; the outer spring set has 3 individual arc springs, while the inner set has 5 nested spring pairs. In the simulation, the principle of conservation of angular momentum is applied to each of the three inertias in order to calculate their individual accelerations and relative movement. As all the springs in a set are identical, it is only necessary to model the full movement and forces of one spring from each set. The arc springs have been discretised into mass and (massless) spring segments; the acceleration of each of the segment masses is calculated in the same way as the inertias. Centrifugal and tangential forces are used to calculate the radial component of the frictional force (calculated using the Makkar continuously differentiable friction model) exerted on the segments and the housing. The rig components were also simulated by assuming they function as short, very stiff, mechanical shafts; this method allowed torsional feedback between components to be implemented.

As found when completing the first objective, no literature was available on potential methods for simulating nested spring pairs or physical hardstops. In this study, the nested springs were simulated as a pair of parallel springs (rather than as a single stiffer arc spring) due to the friction that occurs between the springs; the torque loading is shared across both springs. During the hardware deconstruction completed as part of this objective, it was found that the movement range of both the outer and inner spring sets is limited by physical hardstops. As part of this damper simulation objective, it was determined that the optimum simulation method was to directly transfer the torque from the input to the output inertia once hardstop contact is made. Another feature not discussed in the reviewed literature was spring segment movement limitations; this feature was included in the damper simulation in order to prevent spring segments in the simulation compressing further than physically possible in a real spring. The spring segment movement limitations were implemented by comparing the positions of neighbouring segments.

Contributions to knowledge:

- It has been demonstrated that a discretised spring methodology previously used to simulate DMFs can be adapted for a torque converter damper.
- A methodology for simulating nested spring pairs as parallel, discretised springs with friction between them.
- A method for simulating physical hardstops has been detailed; once contact is made, torque is directly transferred to the next inertia.
- A technique has been proposed for implementing spring segment movement limitations by comparing the positions of neighbouring segments.

5.) *Characterise the torque converter damper through simulation parameterisation and experimental validation.*

The primary purpose of this objective was to ensure the damper simulation accurately represented real-world damper behaviour. In order to meet this objective, the simulation was parameterised by tuning a set of variables; the performance of the tuned simulation was then compared to the experimental damper. The methodology used for simulation parameterisation has been presented in Chapter 6; the resultant simulation has excellent correlation with experimental data.

Simulation parameters were divided into three categories: observed, calculated and estimated. It is the estimated category that requires parameterisation – tuning by comparing simulation and experimental damper performance. In order to simulate the surface area contact between the spring coils and their housing, friction tuning factors were used; values were calculated by examining the contact area on the hardware. Initial estimates for inertia values of the mass assemblies were calculated using the rotational inertia for a hollow cylinder equation; spring stiffness approximations were obtained from hysteresis loop testing. While rough approximations of knee point locations can also be obtained from hysteresis loops, high frequency excitation tests are able to provide more reliable estimations.

In order to parameterise the simulation, it must be excited using sampled experimental data. To maximise parameterisation process efficiency, each time a parameter change was made a set of key test points were selected in order to assess simulation performance change. It is not recommended that single test points be examined individually; parameter changes may improve simulation performance at one test point but have an adverse reaction at another. It was found that when investigating knee point location, test points with small steps in mean torque are required; the location of the knee points can be signified by a sudden change in the attenuation ability of the damper. The developed parameterisation methodology has been presented in flow chart form. Parameterisation initially focuses on test points where only the inner spring set is active; once inner spring behaviour has reached a satisfactory performance level, below the knee test points are used.

The second part of this objective required the performance of the damper simulation to be assessed against the experimental results; for the 2.5 bar torque curve experimental data set the simulation performs excellently, with on average less than 5% error. Overall torque error is less than 10% across the speed range, with mean torque differences between simulated and tested order magnitudes of less than 5Nm. A variety of methods for analysing damper (and simulation) performance have been presented; magnification factor maps (previously used to investigate the effective speed range of a DMF arc spring damper) have been used to demonstrate the variation in magnification ratio with speed and mean torque level.

6.) *Use the validated simulation to establish excitation signal requirements and investigate some aspects of damper behaviour.*

The purpose of this objective was to use the simulation to investigate the effect of excitation signals on damper behaviour; if knowledge on damper behaviour is improved, experimental excitation procedures can potentially be made more efficient or effective. This objective has been met in Chapter 7; here, the validated simulation has been used to investigate excitation signal, areas of poor damper performance and the link between speed and damper stiffness.

The excitation signal investigation was divided into three parts; required accuracy of a sinusoidal approximation, quantifying sufficient excitement and optimum excitation for efficient performance mapping. In order to establish the required accuracy of a sinusoidal signal approximation, the simulation was subjected to a variety of sinusoidal input signals; the behaviour of the damper was then compared to its performance when excited with real-world high-frequency signals. When attempting to sufficiently excite a damper for the purposes of simulation characterisation, the key aim is to produce a dataset that will minimise the length of the parameterisation process while capturing key damper behaviours (such as knee points). Therefore, tests should be performed both above and below the knee point (in a two-stage damper); in the approximate mean torque range where the knee points occur, tests at small (~2-5Nm) intervals should be performed. Ideally, the magnitude of the oscillations should maximise parameter adjustment impact; this will help ensure parameterisation process efficiency. In order to examine the most efficient damper mapping method, the simulated response to the proposed mapping procedure was used to predict damper attenuation when subjected to a typical engine torque curve. The effect of speed on the relationship between frequency and magnification ratio was also investigated.

During the investigation into areas of poor damper performance, it was confirmed that the trend of increasing magnification ratio with lower frequencies seen in test data continued below the tested frequency range. Simulation testing above the experimental frequency range, in combination with results from the efficient mapping procedure tests, revealed that there is not a linear relationship between increased frequency and increased magnification ratio. The location of the spike in magnification ratio seen at higher frequencies is dependent on the magnitude of the excitation signal; test data colourmaps suggest that the cause of these magnification ratio spikes is likely to be damper or rig system resonances. It has been confirmed that while fluctuation magnitude does impact magnification ratio, fluctuation frequency has the most significant (dominant) impact.

In the final part of this study, the effect of speed on apparent damper stiffness was investigated for both hysteresis loop testing and across a range of outer spring vibration angles; it was confirmed that increasing speed does result in non-homogeneous compression of the springs.

Contributions to knowledge:

- Accuracy of sinusoidal approximation:
    - If a signal approximates the 3 most dominant frequencies in a real signal, the damper will behave in a representative manner.
    - Additional orders that have lower frequencies than the dominant order will have a greater impact on the attenuation behaviour of the damper
    - The effect of additional orders on attenuation behaviour is also linked to their magnitude (relative to the dominant order).
- Sufficient excitement (for simulation characterisation):
    - The magnitude of the torque oscillations used to excite the damper is linked to parameter adjustment impact, though this relationship is not linear for all parameters; an approximate level of 300Nm should be used for excitation.
    - Parameters such as spring stiffness and plate inertias are more likely to have a substantial impact on damper performance when spring movement is high (lower frequencies)
    - When spring movement is low, changes in frictional tuning factors will be more effective at altering damper behaviour.
- Excitation for performance mapping:
    - While speed can have an effect on the relationship between frequency and magnification ratio, this effect is far less significant at mean torques above the knee point and when sinusoidal input magnitude is kept at or above 300Nm.
    - Neither engine speed nor precise excitation magnitude must be replicated in order to predict approximate performance.
- Link between speed and stiffness:
    - Speed can have an effect on spring stiffness, but the effect varies significantly depending on the movement range (vibration angle) of the spring.
    - The largest increase in spring stiffness with speed is seen when segments of the spring become inactive (cease to move), hence why the effect of speed is more substantial at low vibration angles.
    - The theories linking speed and stiffness found in the literature have been confirmed; higher speeds increase frictional forces, slowing damper segments, resulting in reduced movement.

8.3 Limitations and Further Work

The work conducted in this thesis can be divided into two categories; the development of the pulsation generator (which was used for characterisation) and the simulation of the torque converter damper. The limitations of the novel pulsation generator unit were discussed in Chapter 4; its primary limitations are the strength of the crankshaft and its below desired flexibility (controllability). Two potential solutions to mitigate or prevent crankshaft failure have been proposed; a modification of the existing crankshaft (may still fail at high cylinder pressures) and a custom designed replacement crankshaft (expensive). The failure of the crankshaft, while disappointing, was expected; the location of the failure had been identified earlier in the development process. To improve controllability, ideally the cylinder air charging system would be controlled remotely from the control desk (outside the test cell); a control system linked to in-cylinder pressure transducers could also be implemented to ensure the minimum pressure in the cylinder is maintained at the required level. While this novel concept has some limitations, it is a cheap prototype that was able to effectively excite a damper for characterisation; it has potential for further work that may be able open up new avenues of testing.

The main limitation of the characterisation, simulation and parameterisation methodologies is that they have only been tested with a single design of damper. Ideally the proposed methods would be tested with a simpler, single stage damper design as well as a slightly more complex damper (e.g. two-stage nested springs); this is an avenue of potential further work. In the future, further investigation of areas of poor damper performance could be performed. The suggested focus is the impact of resonances on damper behaviour; while the areas of poor damper performance have been highlighted in this thesis, there is potential for examining what could be done to reduce resonance impact. The simulation could also be used to investigate potential damper design improvements, for example changes to spring design. It would also be beneficial to investigate if the proposed parameterisation and characterisation methods can be applied to other forms of damper; for example centrifugal pendulum absorbers.

The findings of this thesis are relevant to damper simulation and testing engineers; by expanding knowledge of damper behavioural responses to high frequency excitation signals, as well as demonstrating an effective method for producing validated damper simulations, it is hoped that the vehicle design process will be more efficient and damper modifications more effective.

References

[1] ZF Friedrichshafen AG. *"8-Speed Automatic Transmission*" [online]. Available: http://www.zf.com/corporate/en_de/products/product_range/cars/cars_8_speed_automatic_transmission.shtml#tabs1-1

[2] Nice, K., 2000. *"How Torque converters work"* [online]. Available: www.howstuffworks.com

[3] Hrovat, D., Tobler, W. E., "Bond Graph Modeling and Computer Simulation of Automotive Torque Converters". *Journal of the Franklin Institute*, 1985, 319(1/2): 93-114, 0016-0032/85

[4] Bai, S., Maguire, J., Peng, H., *"Dynamic Analysis and Control System Design of Automatic Transmissions"*. Warrendale, PA: SAE International, 2013

[5] Fischer, R., Otto, D., 2008. *"Torque converter clutch systems"*. LuK Schaeffler

[6] Robinette, D., Grimmer, M., Horgan, J., Kennell, J. et al., "Torque Converter Clutch Optimization: Improving Fuel Economy and Reducing Noise and Vibration," *SAE Int. J. Engines* 4(1):94-105, 2011, doi:10.4271/2011-01-0146

[7] Lindemann, P., Krause, T., Swank, M., et al, "Torque Converters – Launching over new challenges", *Schaeffler symposium*, Chapter 8 pp 124-137, 2010.

[8] Schwab, M., "Electronic Control of a 4-Speed Automatic Transmission with Lock-Up Clutch," *SAE Technical Paper* 840448, 1984, doi:10.4271/840448

[9] Hiramatsu, T., Akagi, T., and Yoneda, H., "Control Technology off Minimal Slip-Type Torque Converter Clutch," *SAE Technical Paper* 850460, 1985, doi:10.4271/850460

[10] Crowther, A., Zhang, N., Liu, D. K., Jeyakumaran, J. K., "Analysis and simulation of clutch engagement judder and stick-slip in automotive powertrain systems", *Proceedings of the Institution of Mechanical Engineers, Part D: Journal of Automobile Engineering*, December 15, 2005, vol. 218, Issue 12: 1427-1446, doi: 10.1243/ 0954407042707731

[11] Ogawa, H., Hayashi, E., Yoshida, O., Hayakawa, Y. et al., "Mechanism of Shudder Phenomena in Torque Converter and System Simulation Model," *SAE Technical Paper* 2007-01-0243, 2007, doi:10.4271/2007-01-0243

[12] Ryu, T., Matsuzaki, K., Nakae, T., Sueoka, A. et al., "A Study on Shudder in Automatic Transmission Lock-up Clutch Systems and Its Countermeasures," *SAE Technical Paper* 2011-01-1509, 2011, doi:10.4271/2011-01-1509

[13] Tohyama, M., Ohmori, T., and Ueda, F., "Anti-Shudder Mechanism of ATF Additives at Slip-Controlled Lock-Up Clutch," SAE Technical Paper 1999-01-3616, 1999, doi:10.4271/1999-01-3616

[14] Lam, R., Chavdar, B., and Newcomb, T., "New Generation Friction Materials and Technologies," SAE Technical Paper 2006-01-0150, 2006, doi:10.4271/2006-01-0150

[15] Hebbale, K., Lee, C., Samie, F., Kao, C. et al., "Model Based Torque Converter Clutch Slip Control," *SAE Technical Paper* 2011-01-0396, 2011, doi:10.4271/2011-01-0396

[16] Prasanth, B.,, Wagh, S. and Raghuvanshi, J., "Body Induced Boom Noise Control by Hybrid Integrated Approach for a Passenger Car," *SAE Int. J. Passeng. Cars - Mech. Syst.* 6(2):2013, doi:10.4271/2013-01-1920.

[17] Steinel, K. and Tebbe, G., "New Torsional Damper Concept to Reduce Idle Rattle in Truck Transmissions," *SAE Technical Paper* 2004-01-2722, 2004, doi:10.4271/2004-01-2722

[18] Kugimiya, T., Mitsui, J., Yoshimura, N., Kaneko, H. et al., "Development of Automatic Transmission Fluid for Slip-Controlled Lock-Up Clutch Systems," *SAE Technical Paper* 952348, 1995, doi:10.4271/952348

[19] Tariku, F., Rogers, R., "Improved Dynamic Friction Models for Simulation of One-Dimensional and Two-Dimensional Stick-Slip Motion". *ASME Journal of Tribology*, 123, 661-669 (2000) (9 pages); doi:10.1115/1.1331057.

[20] Cameron, T., Tersigni, S., McCombs, T., and Jao, T., "ATF Effects on Friction Stability in Slip-Controlled Torque Converter Clutches," *SAE Technical Paper* 2003-01-3255, 2003, doi:10.4271/2003-01-3255

[21] Wang, X., *Vehicle Noise and Vibration Refinement*. Cambridge: Woodhead Publishing Ltd, 2010
[22] Yamaguchi, T. and Tanaka, K., "Transient Flow Field Analysis Around a Lockup Clutch Inside a Torque Converter," *SAE Technical Paper* 2012-01-2001, 2012, doi:10.4271/2012-01-2001
[23] Stahl, K., Pflaum, H., Meingassner, G. J., Lohmann, B. et al., "Testing the performance of innovative torsional vibration reduction systems". *Innovative Automotive Transmissions*, Hybrid & Electric Drives, 2012
[24] Reik, W., *"Torsional Vibrations and Transmission Noise",* LuK, 1986, 0006/5/01.86/S+S
[25] Hage, A., Szatkowski, A., and Li, Z., "Improving Low Frequency Torsional Vibrations NVH Performance through Analysis and Test," *SAE Technical Paper* 2007-01-2242, 2007, doi:10.4271/2007-01-2242
[26] Banks power. *"Banks Billet torque converter"* [online]. Available: http://bankspower.com/techarticles/show/8-The-Banks-Billet-Torque-Converter-is-Diesel-Tough
[27] Faust, H., "Powertrain Systems of the Future", *Schaeffler symposium*, Chapter 2 pp 24-141, 2014.
[28] Szadkowski, A. and Morford, R., "LTD - Long Travel Damper," *SAE Technical Paper* 2001-01-2806, 2001, doi:10.4271/2001-01-2806
[29] Li, Z. and Sandhu, J., "Transmission Torque Converter Arc Spring Damper Dynamic Characteristics for Driveline Torsional Vibration Evaluation," *SAE Int. J. Passeng. Cars - Mech. Syst.* 6(1):477-482, 2013, doi:10.4271/2013-01-1483
[30] Biggs, S., "Torque Converter Damper Attenuation Performance using Multi-Body Systems Analysis", *NAFEMS World Congress*, Salzburg, 2013
[31] Swank, M. and Lindemann, P., "Dynamic Absorbers for Modern Powertrains," *SAE Technical Paper* 2011-01-1554, 2011, doi:10.4271/2011-01-1554
[32] Engelmann, D., Werner, M., Maienschein, S. and Dinger, C., "Hydrodynamic torque converter", US. US20100269497 A1, Oct 28th 2010.
[33] Maienschein, S., Droll, P., Kombowski, E., "Vibration Damper", Schaeffler Technologies, U.S. Patent 8 382 597 B2, February 26, 2013
[34] Folkson, R., *"Alternative Fuels and Advanced Vehicle Technologies for Improved Environmental Performance"*. Cambridge: Woodhead Publishing Ltd, 2014
[35] Robinette, D., Grimmer, M., and Beikmann, R., "Dynamic Torque Characteristics of the Hydrodynamic Torque Converter," *SAE Int. J. Passeng. Cars – Mech. Syst.* 4(2):1023-1032, 2011, doi:10.4271/2011-01-1540
[36] Abe, T., Obourn, L., Cheng, M., Maskill, M. et al., "The Ford Motor Company Spin-Torsional NVH Test Facility," *SAE Technical Paper* 1999-01-1837, 1999, doi:10.4271/1999-01-1837
[37] Kodama, T., Wakabayashi, K., Honda, Y., and Iwamoto, S., "Dynamic Characteristics of Viscous-Friction Dampers by Simultaneous Vibration Displacement Measurement at Two Points," *SAE Technical Paper* 2001-01-0281, 2001, doi:10.4271/2001-01-0281
[38] Browne, M., "Practical Considerations of Driveline Vibration and Acoustic Test Cell with Case Study of McLaren's Driveline Dynamometers," *SAE Technical Paper* 2011-01-1645, 2011, doi:10.4271/2011-01-1645
[39] Galvagno, E., Velardocchia, M., Vigliani, A., and Tota, A., "Experimental Analysis and Model Validation of a Dual Mass Flywheel for Passenger Cars," *SAE Technical Paper* 2015-01-1121, 2015, doi:10.4271/2015-01-1121.
[40] Pohl, B., "Transient Torque Converter Performance, Testing, Simulation and Reverse Engineering," *SAE Technical Paper* 2003-01-0249, 2003, doi:10.4271/2003-01-0249
[41] Mockeridge, T., Dohman, H., and Phiilips, D., "HIL Driveline Dyno," *SAE Technical Paper* 2014-01-1738, 2014, doi:10.4271/2014-01-1738
[42] Otanez, P., Samie, F., Lee, C., and Kao, C., "Aggressive Torque Converter Clutch Slip Control and Driveline Torsional Velocity Measurements," *SAE Int. J. Fuels Lubr.* 1(1):883-892, 2009, doi:10.4271/2008-01-1584

[43] Plint, M.A., Martyr, A.J., Technical Note: “Some limitations of the chassis dynamometer in vehicle simulation”, *Proceedings of the Institution of Mechanical Engineers, Part D: Journal of Automobile Engineering*, March 1, 2001, vol. 215: 431-437, doi: 10.1243/ 0954407011525647
[44] Webster, F., Thomas, J., “Transmission and Driveline Rig NVH Measurements”, Jaguar Land Rover NVH overview, 2012
[45] Yoo, J., Pfeiffer, K., and Kang, K., "Front Loading NVH Test on the Highly Dynamic Powertrain Test Bed," *SAE Technical Paper* 2011-01-1512, 2011, doi:10.4271/2011-01-1512
[46] AVL, *“Full Vehicle, Powertrain or Drivetrain durability test”* [online]. Available: https://www.avl.com/-/on-site-vsm-dyno-installations
[47] Wurst, R., "Engine Torque Measurement Using Telemetry," *SAE Technical Paper* 2004-01-2679, 2004, doi:10.4271/2004-01-2679
[48] Otanez, P., Samie, F., Lee, C., and Kao, C., "Aggressive Torque Converter Clutch Slip Control and Driveline Torsional Velocity Measurements," *SAE Int. J. Fuels Lubr.* 1(1):883-892, 2009, doi:10.4271/2008-01-1584
[49] Castellini, P., Martarelli, M., Tomasini, E.P., “Laser Doppler Vibrometry: Development of advanced solutions answering to technology's needs”, *Mechanical Systems and Signal Processing*, August 2006, vol. 20, 6: 1265-1285, doi:10.1016/ j.ymssp.2005.11.015
[50] Albers, A., Zingel, C., Zehetner, J., and Meitz, K., "Influence of Low-Frequency Powertrain-Vibrations on Driveability-Assessments," *SAE Technical Paper* 2010-01-1419, 2010, doi:10.4271/2010-01-1419
[51] Laderaranch, 2008. *“LDV Schematic”* [online]. San Francisco: Wikimedia Foundation. Available from: http://commons.wikimedia.org/wiki/File:LDV_Schematic.png
[52] Jung, J., Ryu, D., Jeong, K., and Chang, K., "Development of a Clutch Disk Torque Sensor for An Automobile," *SAE Technical Paper* 2001-01-0869, 2001, doi:10.4271/2001-01-0869
[53] Kang, T-S., Kauh, S.K. and Ha, K-P., “Development of the displacement measuring system for a dual mass flywheel in a vehicle”, *Proceedings of the Institution of Mechanical Engineers, Part D: Journal of Automobile Engineering*, October 1, 2009, vol. 223: 1273-1281, doi:10.1243/ 09544070JAUTO1066
[54] Lee, J.Y., Kauh, S.K. and Ha, K-P., “Development of a disc-type torque meter for an automatic transmission vehicle”, *Proceedings of the Institution of Mechanical Engineers, Part D: Journal of Automobile Engineering*, December 1, 2005, vol. 219: 1443-1449, doi:10.1243/ 095440705X35107
[55] Li, W., Shi, X., Guo, D., and Yi, P., "A Test Technology of a Vehicle Driveline Test Bench with Electric Drive Dynamometer for Dynamic Emulation," SAE Technical Paper 2015-01-1303, 2015, doi:10.4271/2015-01-1303
[56] Newberger, N., Nevius, T., Lasota, P., Lethbridge, M. et al., "Virtual Engine Dynamometer in Service Life Testing of Transmissions: A Comparison Between Real Engine and Electric Dynamometers as Prime Movers in Validation Test Rigs," *SAE Technical Paper* 2010-01-0919, 2010, doi:10.4271/2010-01-0919
[57] Lahti, J. and Moskwa, J., "A Transient Hydrostatic Dynamometer for Testing Single-Cylinder Prototypes of Multi-Cylinder Engines," *SAE Technical Paper* 2002-01-0616, 2002, doi:10.4271/2002-01-0616
[58] Rao, M., Frank, J., and Raghavendran, P., "Experimental Investigation of Effect of Driveline Torsional Fluctuations on Overall NVH Performance of the Vehicle," SAE Technical Paper 2015-01-2192, 2015, doi:10.4271/2015-01-2192
[59] Reitz, A., Biermann, J., Kelly, P., “Special test bench to investigate NVH phenomena of the clutch system”, *The new role of experimentation in the modern automotive product development process, Proceedings, 1999 6th international Florence ATA conference*, Firenze, 17-19 November 1999.
[60] Girstmair, J., Albertini, P., Meitz, K., Klinger, S. et al., "Improved Comfort Analysis and Drivability Assessment by the Use of an Extended Power Train Model for Automatic

Transmissions," *SAE Int. J. Passeng. Cars - Mech. Syst.* 5*(*3):1073-1083, 2012, doi:10.4271/2012-01-1529
[61] Schaper, U., Sawodny, O., Mahl, T., Blessing, U., "Modeling and torque estimation of an automotive Dual Mass Flywheel," *American Control Conference*, 2009. ACC '09, vol. 16, issue 6, pp.1207,1212, 10-12 June 2009, doi: 10.1109/ACC.2009.5160136
[62] Albers, A., Albrecht, M., Krüger, A., and Lux, R., "New Methodology for Power Train Development in the Automotive Engineering - Integration of Simulation, Design and Testing," *SAE Technical Paper* 2001-01-3303, 2001, doi:10.4271/2001-01-3303
[63] Metsenaere, C., *"Fracture Analysis of Dual Mass Flywheel Arc Springs"*. LuK GmbH & Co., 2002
[64] Ahn, K., Lee, J.M., Lim, W., Parks, Y., "Analysis of a Clutch Damper Using a Discrete Model". *KSME International Journal*, Vol. 18 No. 11, pp. 1883 ~ 1890, 2004
[65] Albers, A., "Advanced Development of Dual Mass Flywheel (DMFW) Design – Noise Control for Today's Automobiles", *5th LuK Kolloquium*,pp 5-41, 1994
[66] Armstrong-Hélouvry, B., *Control of Machines with Friction*, Boston, Kluwer, 1991.
[67] Armstrong-Hélouvry, B., Dupont, P., and Canudas De Wit, C., "A Survey of Models, Analysis Tools and Compensation Methods for the Control of Machines with Friction," *Automatica*, vol. 30, no. 7, pp. 1083-1138, July 1994.
[68] Dahl, P., *"A Solid Friction Model"*, The Aerospace Corporation, El Segundo, CA, Tech. Rep. TOR-0158(3107-18), 1968.
[69] Canudas De Wit, C., Olsson, H., Astrom, K.J., and Lischinsky, P., "A New Model for Control of Systems with Friction," *IEEE Transactions Automatic Control*, vol. 40, pp. 419-425, Mar. 1995
[70] Swevers, J., Al-Bender, F., Ganseman, C. G., and Prajogo,T., " An Integrated Friction Model Structure with Improved Presliding Behavior for Accurate Friction Compensation," *IEEE Transactions Automatic Control*, vol. 45, pp. 675-686, Apr. 2000
[71] Guenther, R., Perondi, E., DePieri, E. and Valdiero, A.,"Cascade Controlled Pneumatic Positioning System with LuGre Model Based Friction Compensation". *Journal of the Brazilian Society of Mechanical Sciences & Engineering*, Vol 28, no 1, pp.48-57, 2006.
[72] Sobczyk, M., Perondi, E. and Cunha, M., "A continuous approximation of the LuGre friction model", in *20th International Congress of Mechanical Engineering*, Brazil, 2009
[73] Makkar, C., Dixon, W.E., Sawyer, W. G., Hu, G., "A new continuously differentiable friction model for control systems design," *Advanced Intelligent Mechatronics. Proceedings, 2005 IEEE/ASME International Conference*, Monterey, CA, 24-28 July 2005, pp.600,605, doi: 10.1109/AIM.2005.1511048
[74] Makkar, C., "Nonlinear modelling, identification, and compensation for frictional disturbances", Master's thesis, University of Florida, Gainesville, FL, 2006
[75] Winterbone, D., Thiruarooran, C., and Wellstead, P., "A Wholly Dynamic Model of a Turbocharged Diesel Engine for Transfer Function Evaluation," *SAE Technical Paper* 770124, 1977, doi:10.4271/770124
[76] Ledger, J. and Walmsley, S., "Computer Simulation of a Turbocharged Diesel Engine Operating Under Transient Load Conditions," *SAE Technical Paper* 710177, 1971, doi:10.4271/710177
[77] Rakopoulos, C. and Giakoumis, E., "Review of Thermodynamic Diesel Engine Simulations under Transient Operating Conditions," *SAE Technical Paper* 2006-01-0884, 2006, doi:10.4271/2006-01-0884
[78] Rizzoni, G., "Estimate of indicated torque from crankshaft speed fluctuations: a model for the dynamics of the IC engine," *IEEE Transactions on Vehicular Technology*, vol.38, no.3, pp.168,179, Aug 1989 doi: 10.1109/25.45470
[79] Zweiri, Y.H., "Diesel Engine Indicated Torque Estimation Based on Artificial Neural Networks". *International Journal of Intelligent Technology* 1(1) 2006. ISSN 1305-6417

[80] Liu, Q., Chalhoub, N.G., Henein, N., "Simulation of a Single Cylinder Diesel Engine Under Cold Start Conditions Using Simulink" *J. Eng. Gas Turbines Power* 123, 117-124 (2000) (8 pages); doi:10.1115/1.1290148
[81] Filipi, Z. S. and Assanis, D. N. "A non-linear, transient, single-cylinder diesel engine simulation for predictions of instantaneous engine speed and torque". *Proceedings of Technical Conference of ASME ICE*, Colorado, 1997. Paper 97-ICE-8, pp. 61–70. DOI: 10.1115/1.1365122
[82] Rizzoni, G., Zhang, Y., "Identification of a non-linear internal combustion engine model for on-line indicated torque estimation". *Mechanical Systems and Signal Processing*, 8(3):275–287, 1994.
[83] Zhang, Y., Rizzoni, G., "An on-line indicated torque estimator for IC engine diagnosis and control". *ASME J. Advanced Automotive Tech.*,52:147–162, 1993
[84] Ricardo, *"Wave: 1D engine performance and NVH" [online].* Available: https://www.software.ricardo.com/Products/WAVE
[85] Zweiri, Y.H., Whidborne, J.F. and Seneviratne, L.D., "Detailed analytical model of a single-cylinder diesel engine in the crank angle domain". *Proceedings of the Institution of Mechanical Engineers, Part D: Journal of Automobile Engineering* 215(11): 1197-1216, 2001. DOI: 0.1243/0954407011528734
[86] Zweiri, Y.H., Whidborne, J.F. and Seneviratne, L.D., "Instantaneous friction components model for transient engine operation". *Proceedings of the Institution of Mechanical Engineers, Part D: Journal of Automobile Engineering* 214(7): 809-824, 2000. DOI: 10.1243/0954407001527664
[87] Wang, P., "Causal Tracking Control of a Non-Minimum Phase HIL Transmission Test System", Ph.D. dissertation, Department of Mechanical Engineering, University of Bath, Bath, 2009
[88] Scherer, H., Bek, M., and Kilian, S., "ZF New 8-speed Automatic Transmission 8HP70 - Basic Design and Hybridization-," *SAE Int. J. Engines* 2(1):314-326, 2009, doi:10.4271/2009-01-0510
[89] Schicker, R., Wegener, G*., "Measuring Torque Correctly"*. HBM-Publication.
[90] Dewetron. *"DEWE-43 data sheet"* [online]. Available from: http://download.dewetron.com/catalogue/pdf-email-version/DEWE-43_DE-D080901e.pdf
[91] HBM. *"T40B Torque Flange"* [online]. Darmstadt, Hottinger Baldwin Messtechnik GmbH. Available from: http://www.hbm.com/fileadmin/mediapool/hbmdoc/technical/b3406.pdf
[92] Wellmann, T., Govindswamy, K., Braun, E., and Wolff, K., "Aspects of Driveline Integration for Optimized Vehicle NVH Characteristics," *SAE Technical Paper* 2007-01-2246, 2007, doi:10.4271/2007-01-2246.
[93] Chen Y., Ishibashi A., "Investigation of the Noise and Vibration of Planetary Gear Drives", *9th ASME International Power Transmission and Gearing Conference, Parts A and B*. Vol. 4, pp.507-513, 2-6 September 2003, doi:10.1115/DETC2003/PTG-48065.
[94] National Instruments, 2015. *"Understanding FFTs and Windowing"* [online]. Available: http://www.ni.com/white-paper/4844/en/#toc2
[95] Heywood, J. B., *Internal Combustion Engine Fundamentals*. New York: McGraw-Hill, 1998
[96] Bengtsson, F., *"Estimation of Indicated and Load Torque from Engine Speed Variations",* Master's thesis, Linköping University, 2006
[97] Sudau, J., Strumer, A., Rudiger, L., et al, "Torque transmission assembly, in particular hydrodynamic torque converter, fluid coupling or wet-running clutch", ZF Friedrichshafen AG, U.S. Patent 0205944 A1, August 15, 2013
[98] MathWorks, *"Mechanical Shaft"* [online]. Available from: http://uk.mathworks.com/help/physmod/sps/powersys/ref/mechanicalshaft.html
[99] du Bois, J. L., Lieven, N. A. J., Adhikari, S. (2009), "Error Analysis in Trifilar Inertia Measurements". *Experimental Mechanics*, 49(4), 533 - 540. 10.1007/s11340-008-9142-4
[100] Hutchinson Aerospace & Industry, "*Isolators Selection"* [online]. Available from: http://www.hutchinsonai.com/userfiles/file/Product_Catalog/specialty/IsolatorsSelection.pdf

Appendix

Table 9.1: Typical value ranges for flexible crankshaft simulation parameters

	Inertia damping	***Stiffness***	***Stiffness damping***
	N.m.s/rad	*N.m/rad*	*N.m.s/rad*
Cylinder 1	0.001-0.003	580000-595000	50-150
Cylinder 2	0.001-0.003	580000-595000	50-150
Cylinder 3	0.001-0.003	600000-700000	50-150
Cylinder 4	0.001-0.003	1000000-1100000	50-150

Table 9.2: Typical value ranges for rig component simulation parameters

	Inertia	***Inertia damping***	***Stiffness***	***Stiffness damping***
	kg.m²	*N.m.s/rad*	*N.m/rad*	*N.m.s/rad*
Gearbox	0.100-0.130	0.005-0.015	9000-12500	50-100
T40B Transducer	0.014-0.015	0.005-0.015	2500000-2550000	50-100
ROBA Coupling	0.057-0.058	0.005-0.015	1720000-1750000	50-100
Flange group 1	0.025-0.035	0.005-0.015	1400000-1600000	50-100
Flange group 2	0.015-0.025	0.005-0.015	1400000-1600000	50-100
Output motor	1.00-1.15	0.005-0.015		